Impact of glycine transporter 1 knockout on inhibitory neurotransmission in the lateral superior olive

vom Fachbereich Biologie der Universität Kaiserslautern

zur Verleihung des akademischen Grades

„Doktor der Naturwissenschaften“

genehmigte

Dissertation

M. Sc. Julia Hammerich

Kaiserslautern 2019

- D 386 -

Datum der Disputation:	22.11.2019	
Promotionskommission	Vorsitz:	Prof. Dr. Stefan Kins
	1. Gutachter:	Prof. Dr. Eckhard Friauf
	2. Gutachter:	PD. Dr. Volker Eulenburg

Hiermit erkläre ich, dass ich diese Arbeit selbst verfasst und keine anderen als die angegebenen Quellen und Hilfsmittel verwendet habe.

Kaiserslautern, August 2019

_____

Julia Hammerich

“A scientist in his laboratory is not a mere technician: he is also a child confronting natural phenomena that impress him as though they were fairy tales.”

Marie Curie

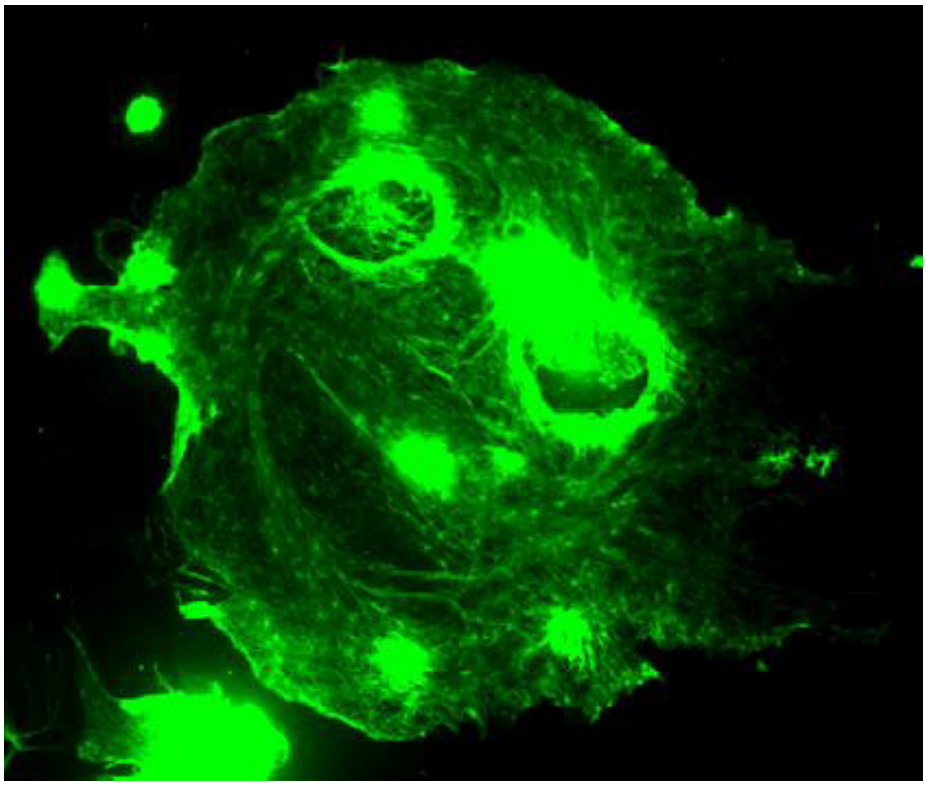

Astrocytes are funny…

TABLE OF CONTENTS

INDEX OF FIGURES ..... **IV**

INDEX OF TABLES ..... **VI**

SUMMARY **1**

1. INTRODUCTION **2**

1.1. The auditory brainstem – the first station of sound source localization 2

1.2. The MNTB-LSO synapse 5

1.3. GlyT1 and its relevance for the MNTB-LSO synapse 8

1.4. Aims of study 14

2. MATERIAL AND METHODS **15**

2.1. GlyT1b/c KO mouse line 15

2.1.1. Ethical approval, housing and breeding *15*

2.1.2. Generation *15*

2.1.3. Genotyping *16*

2.1.4. Survival analysis *17*

2.2. Western blotting 18

2.2.1. Sample preparation *18*

2.2.2. SDS-PAGE *18*

2.2.3. Western blotting *19*

2.2.4. Total protein staining *19*

2.2.5. Immunodetection *20*

2.2.6. Evaluation *20*

2.3. Electrophysiology 21

2.3.1. Preparation of acute brainstem slices *21*

2.3.2. Recording from LSO principal neurons *21*

2.3.3. sIPSC properties *23*

2.3.4. Electrical stimulation of MNTB-LSO synapses *24*

2.3.5. eIPSC properties *24*

2.3.6. FDD and recovery *26*

2.3.7. Fidelity *27*

2.3.8. Synapse properties *27*

2.3.9. Challenge-induced changes of synapse properties *29*

2.4. Data presentation and statistics 30

3. RESULTS 32

3.1. GlyT1b/c KO mouse model 32

3.1.1. Normal birth rate of KO mice, but impaired gain in weight 32

3.1.2. KO mice do not suffer from reduced survival rate 33

3.2. GlyT1 content in KO brainstems is severely reduced and not compensated by GlyT2 34

3.3. Spontaneous transmission to LSO principal neurons 35

3.3.1. GlyT1 loss does not change sIPSC occurrence 36

3.3.2. GlyT1 loss does not affect sIPSC properties and q 36

3.4. WT and KO MNTB-LSO synapses exhibit similar basic synaptic strength at 1 Hz stimulation . 38

3.5. FDD and recovery of the MNTB-LSO synapse 40

3.5.1. Depression at 200 Hz is more pronounced in KO 42

3.6. Fidelity of the MNTB-LSO synapse 45

3.6.1. Fidelity is negatively correlated to stimulation frequency in WT and KO 45

3.6.2. Fidelity at 200 Hz is more severely reduced in KO 50

3.7. MNTB-LSO synapse properties during challenges 52

3.7.1. WT and KO have a similar RRP and P_r 52

3.7.2. q during the last 10 s of challenges is stronger reduced in KO as in WT 56

3.7.3. No higher m in KO to compensate the decrease in q 58

3.8. Precision at the MNTB-LSO synapse during sustained transmission 60

3.8.1. Latencies increase in a time- and frequency-dependent manner in WT and KO 63

3.8.2. $SD_{Latency}$ augments during challenges in WT and KO 64

3.8.3. Latencies during challenges and recoveries are significantly longer in KO 67

3.9. eIPSC decay times during sustained transmission at the MNTB-LSO synapse 72

3.9.1. Challenges induce decay time prolongations in both genotypes 72

3.9.2. 50 Hz stimulation leads to irreversibly increased decay times in KO 74

3.10. Summary of principal findings 77

4. DISCUSSION 79

4.1. General aspects of the GlyT1b/c mouse 80

4.2. GlyT1 at the MNTB-LSO synapse is dispensable for glycine clearance under resting conditions 80

4.3. Basic synaptic properties and performance of the MNTB-LSO synapse during 1 Hz stimulation are not affected by the loss of GlyT1 83

4.4. GlyT1 loss leads to impairment of the MNTB-LSO synapse during high activity 85

4.4.1. Mechanism I - postsynaptic GlyR desensitization 92

4.4.2. Mechanism II - enhanced presynaptic GlyR activation 93

4.4.3. Mechanism III - disturbed glycine shuttle 96

4.5. Conclusion 101

4.6. Outlook 102

5. REFERENCES 105

6. INDEX OF ABBREVIATIONS 122

7. SUPPLEMENTARY FIGURES AND TABLES 124

8. CURRICULUM VITAE 133

9. ACKNOWLEDGEMENT 135

INDEX OF FIGURES

Figure 1: Auditory pathway in the lower brainstem and extraordinary synapses 3
Figure 2: Cues for sound localization in the horizontal plane 4
Figure 3: Mechanisms underlying STD and attenuation 7
Figure 4: GlyT1 – gene, expression, and stoichiometry 9
Figure 5: GlyT1 and GlyT2 at the somata of MNTB- and LSO neurons 12
Figure 6: Glycine cycle at the MNTB-LSO tripartite synapse 13
Figure 7: Generation and genotyping of GlyT1b/c KO mice 16
Figure 8: Characterization and properties of LSO principal neurons 22
Figure 9: Experimental setup, stimulation protocol, and analysis of IPSC parameters 25
Figure 10: RRP calculation 28
Figure 11: Determination of q 28
Figure 12: Adjustment of bin size for q determination 29
Figure 13: KO mice have a reduced gain of weight, but show a normal birth- and survival rate 33
Figure 14: GlyT1 content in KO brainstems is severely reduced, and not compensated by increased GlyT2 expression 34
Figure 15: Loss of GlyT1 does not change sIPSC properties 37
Figure 16: Similar basic synaptic strength in WT and KO 39
Figure 17: FDD and recovery of example cells 41
Figure 18: FDD during 200 Hz challenge is more pronounced in KO 44
Figure 19: Fidelity in both genotypes is negatively correlated to the stimulation frequency. 48
Figure 20: Fidelity during 200 Hz is stronger reduced in KO 51
Figure 21: Initial synaptic properties in KO are similar to WT. 54
Figure 22: q in KO is reduced in the last 10 s of challenges. 57
Figure 23: m during the last 10 s is similar in WT and KO 59
Figure 24: Synaptic precision during 1 Hz and challenges of two example recordings of WT and KO 61
Figure 25: Synaptic precision during recoveries of two example recordings of WT and KO ... 62
Figure 26: Challenge-induced latency prolongation and $SD_{Latency}$ increase in WT and KO 65
Figure 27: Latency prolongation during challenges and recoveries is more severe in KO 68

Figure 28: Frequency-dependent change of decay times in WT and KO 73
Figure 29: Decay times during challenges and recoveries are stronger prolonged as in WT .. 75
Figure 30: Graphical summary of principal findings 78
Figure 31: Hypothetical mechanisms that could be causative for the observed differences between WT and KO 100

Figure S.1: FDD and recovery of WT and KO (absolute values) 126
Figure S.2: Latency and $SD_{Latency}$ of the first and last 10 events 128
Figure S.3: Decay time of the first and last 10 events 130

INDEX OF TABLES

Table 1: Significance levels 31
Table 2: GlyT1 and GlyT2 contents in brainstem 35
Table 3: sIPSC properties and q 38
Table 4: Basic synaptic strength 40
Table 5: FDD and recovery of example cells 42
Table 6: Comparison of FDD and recovery 46
Table 7: Fidelity during the last 10 s 50
Table 8: Initial synapse properties 55
Table 9: Initial synapse properties - p values and significances for frequency-dependent changes 55
Table 10: $q_{Last\ 10\ s}$ compared to initial q 58
Table 11: Absolute amplitudes and m during the last 10 s 59
Table 12: Latency change 66
Table 13: $SD_{Latency}$ change 66
Table 14: Latency comparison between WT and KO 70
Table 15: $SD_{Latency}$ comparison between WT and KO 71
Table 16: Decay time change 73
Table 17: Decay time comparison between WT and KO 76

Table S.1: Cells used for eIPSC analysis with color code and membrane properties 124
Table S.2: Survival probability 125
Table S.3: GlyT1 and GlyT2 content in brainstem - arbitrary units 125
Table S.4: Failures and fidelity of WT and KO example cells 125
Table S.5: FDD and recovery of WT and KO (absolute values) 127
Table S.6: $q_{Last\ 10\ s}$ compared to initial q (absolute values) 127
Table S.7: Latency comparison between first 10 events and last 10 events 129
Table S.8: $SD_{Latency}$ comparison between first 10 events and last 10 events 129
Table S.9: Decay time comparison between first 10 events and last 10 events 131
Table S.10: Decay time ratios of the last and first 10 events 131
Table S.11: Comparative study 132

SUMMARY

Glycine constitutes the major neurotransmitter at inhibitory synapses of lower brain regions. A rapid removal of glycine from the synaptic cleft and consequent recycling is crucial for synaptic transmission in systems with high effort on temporal precision. This is mainly achieved by glycine translocation via two glycine transporters (GlyTs), namely GlyT1 and GlyT2. At inhibitory synapses, GlyT2 was found to be specifically expressed by neurons, supplying the presynapse with glycine needed for vesicle filling. In contrast, GlyT1 is attributed to astrocytes and primarily mediates the termination of synaptic transmission by glycine removal from the synaptic cleft. Employing patch-clamp recordings from principal neurons of the lateral superior olive (LSO) in acute brainstem slices of GlyT1b/c knockout (KO) mice and wildtype (WT) littermates at postnatal day 20, I analyzed how postsynaptic responses are changed in a GlyT1-depleted environment. During spontaneous vesicle release I found no change of postsynaptic responses, contradicting my initial hypothesis of prolonged decay times. Electrical stimulation of fibers of the medial nucleus of the trapezoid body (MNTB), which are known to form fast, reliable and highly precise synapses with LSO principal neurons, revealed that GlyT1 is involved in proper synaptic function during sustained, high frequent synaptic transmission. Stimulation with 50 Hz led to a stronger decay time and latency prolongation in GlyT1b/c KO, accelerating to 60% longer decay times and 30% longer latencies. Additionally, a more pronounced frequency-dependent depression and fidelity decrease was observed during stimulation with 200 Hz in GlyT1b/c KO, resulting in 67% smaller amplitudes and only 25% of WT fidelity at the end of the challenge. Basic properties like readily releasable pool, release probability, and quantal size (q) were not altered in GlyT1b/c KO, but interestingly q decreased during 50 Hz and 100 Hz challenges to about 84%, which was not observed in WT. I conclude that stronger accumulation of extracellular glycine due to GlyT1 loss leads to prolonged activation of postsynaptic glycine receptors (GlyRs). As a further consequence, activation of presynaptic GlyRs in the vicinity of the synaptic cleft might be enhanced, accompanied by a stronger occurrence of shunting inhibition. Furthermore, I assume a GlyT1-dependent glycine shuttle, which is absent at GlyT1b/c KO synapses. This could result in a diminished glycine supply to GlyT2 located at more distant sites, causing a disturbed replenishment during periods with excess release of glycine. Conclusively, my study reveals a contribution of astrocytes in fast and reliable synaptic transmission at the MNTB-LSO synapse, which in turn is crucial for proper sound source localization.

1. INTRODUCTION

We humans are known to be “visual creatures”, but situations in daily life let us consistently become aware that hearing, or more specifically spatial hearing, is also of importance. Such situations can occur when we notice an approaching car while crossing the street lost in thoughts, when we search for an annoying noise source, or when we have to localize a person in a crowd that calls our name. If one ear is clogged or deaf, these tasks are nearly unsolvable as spatial hearing requires the sound perception at both ears. To constitute a correct sound source localization, synapses in the auditory system evolved a markedly fast and precise signal transmission. In this study, I provide evidence that astrocytes at a special auditory synapse are involved in proper synapse function and are therefore presumably needed for accurate spatial hearing.

1.1. The auditory brainstem – the first station of sound source localization

Whereas sound frequency is encoded in the cochlea, sound source localization must be computed at more central levels in the auditory pathway (Figure 1) (Grothe et al., 2010). However, the frequency cue of the sound source is maintained by the tonotopic organization of the cochlea and auditory nuclei, meaning that all projections throughout the auditory brainstem are organized topographically and hence the frequency representation is preserved in all of these nuclei (Kandler et al., 2009). While vertical localization is achieved via monaural spectral analysis, horizontal localization depends on binaural cues (Grothe et al., 2010). To enable the convergence of binaural signals, inner hair cells (IHCs) in the cochlea excite spiral ganglion neurons with glutamate, which further transmit the information via the auditory nerve to spherical and globular bushy cells (SBCs, GBCs) in the cochlear nucleus (CN). SBCs project to neurons of the ipsi- and contralateral medial superior olive (MSO) (Warr, 1966), whose neurons determine the time differences of glutamatergic signals arriving from ipsi- and contralateral SBCs. These interaural time differences (ITDs) result from the temporal delay of the sound arrival at the more distant ear, and provide the main cue for source localization of low-frequency sounds (Figure 2A_1; Jeffress, 1948; Ashida and Carr, 2011). As another pathway, GBCs send glutamatergic projections to principal neurons of the contralateral medial nucleus of the trapezoid body (MNTB) (Warr, 1966; Spirou et al., 1990). This nucleus provides glycinergic inhibitory inputs to principal neurons in the lateral superior olive (LSO) on the same side (Spangler et al., 1985). In combination with excitatory inputs from SBCs of the ipsilateral

CN (Cant and Casseday, 1986), the LSO determines level differences of signals from the ipsi- and contralateral ear (Boudreau and Tsuchitani, 1968; Caird and Klinke, 1983). These interaural level differences (ILDs) are used for source localization of high-frequency sounds (Figure 2A$_2$), and result from the so-called "shadowing" effect of the head for sounds with a smaller wavelength as the head diameter (Tollin, 2003). Together with MNTB and MSO, the LSO belongs to the superior olivary complex (SOC; Warr, 1966; Jenkins and Masterton, 1982; Helfert et al., 1989; Sanes, 1990). To calculate the ILD, the inhibitory input from the contralateral ear and the excitatory input from the ipsilateral ear are compared (Figure 2B)

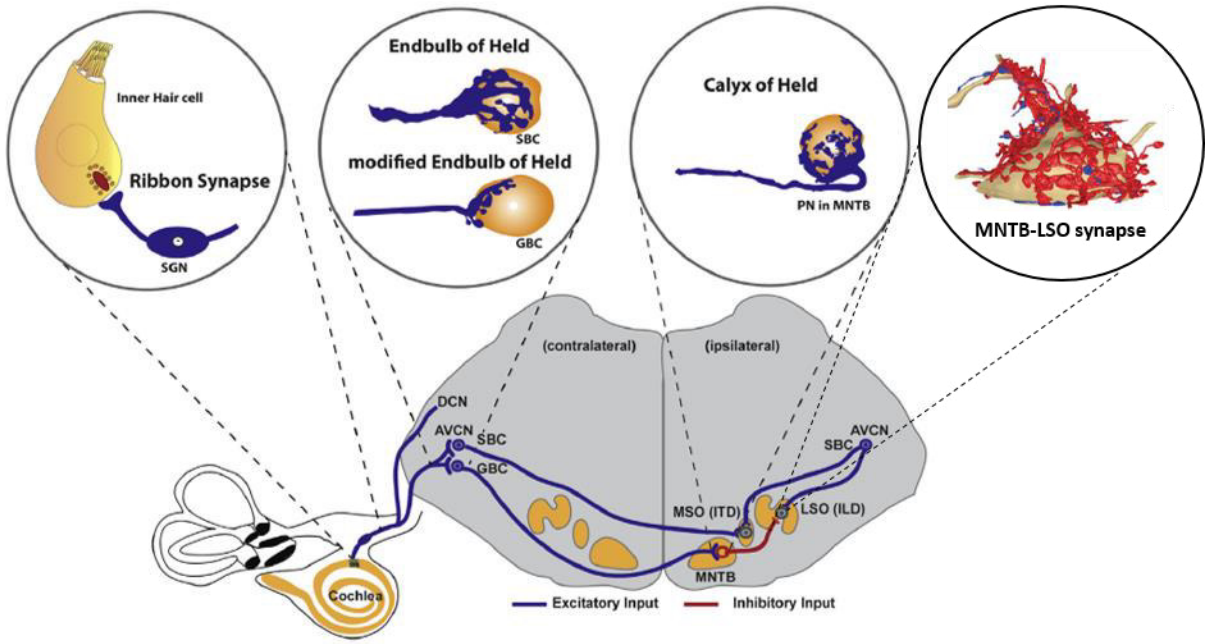

Figure 1: Auditory pathway in the lower brainstem and extraordinary synapses
Overview of signal transmission and specialized synapses along the auditory pathway in the lower brainstem. Inner hair cells in the cochlea are activated by sounds of a distinct frequency and transmit glutamatergic signals to SGNs via the ribbon synapse. SGNs extend their axons to the DCN and AVCN. In the AVCN they form glutamatergic endbulbs of Held with SBCs and smaller modified endbulbs of Held with GBCs. SBCs send bilateral projections to the ipsi- and contralateral MSO, forming a pathway crucial for determining ITDs. Axons of GBCs form glutamatergic synaptic contacts known as the calyces of Held with principal cells of the contralateral MNTB. MNTB provides glycinergic inhibitory input to principal cells of the ipsilateral LSO, receiving also excitatory, glutamatergic inputs from SBCs of the ipsilateral AVCN. In the LSO, the inhibitory signals originating from the contralateral ear and the excitatory signals from the ipsilateral ear are used to compute ILDs. ITDs and ILDs are the cue for binaural sound localization of low or high frequency sound sources, respectively. The large size of the synapses or numerous synaptic contacts accompanied with efficient release and replenishment mechanisms enable a fast and high fidelity neurotransmission. Inset of the MNTB-LSO synapse modified from Gjoni et al. (2018b) the other parts modified from Yu and Goodrich (2014). SGN = spiral ganglion neuron, DCN/AVCN = dorsal/anteroventral cochlear nucleus, SBC = spherical bushy cell, GBC = globular bushy cell, MSO = medial superior olive, ILD/ITD = interaural level/time difference, MNTB = medial nucleus of the trapezoid body, LSO = lateral superior olive

(Boudreau and Tsuchitani, 1968; Moore and Caspary, 1983; Tollin et al., 2008; Beiderbeck et al., 2018), and the rather simple one-to-one subtraction determines the spike probability (Figure 2C). With sound sources in the ipsilateral hemifield, spike rates are high, but the more it is positioned contralaterally, spike rates become lower (Caird and Klinke, 1983; Joris and Yin, 1995; Park et al., 1996). For calculation of ITDs the temporal delay of the contralateral inputs in regard to the ipsilateral input is compared (Grothe et al., 2010). The responses of the LSO are conveyed to higher auditory stations like the inferior colliculus or nuclei of the lateral lemnisci, and further on to the medial geniculate nucleus and the auditory cortex. Aside from the simplistic view of a straight forward model of signal transmission, the nuclei modulate

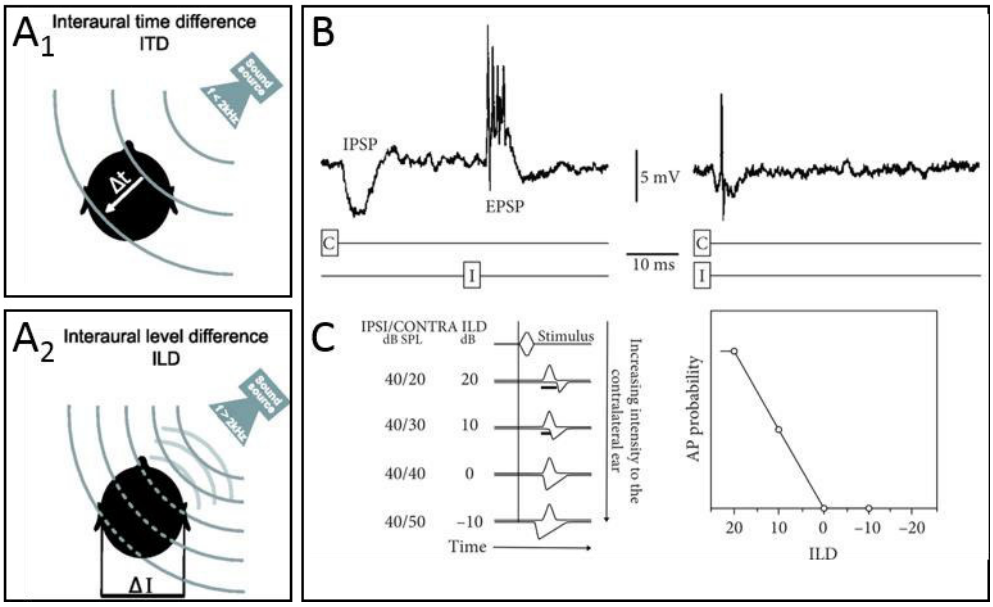

Figure 2: Cues for sound localization in the horizontal plane
A_1, ITD: the difference in the arrival time (Δt) of a sound wave (gray lines) at the two ears is used to localize low-frequency sound sources (<2 kHz). **A_2**, ILD: For high-frequency sound sources (>2 kHz) that generate only small Δt, intensity differences (ΔI) are the cue for sound source localization. They are caused by the shadowing effect of the head, resulting in a decreased sound intensity at the opposed ear. **B**, Intracellular recording from an LSO neuron. Contralateral (C) stimulation with 55 dB evokes an IPSP, whereas ipsilateral (I) stimulation evokes an EPSP (same sound pressure). When stimuli are simultaneously presented (≙ sound source in the front), the PSPs nearly completely attenuate each other. **C**, Hypothetical EPSPs and IPSPs from a LSO neuron (left) and corresponding ILD function (right). ILDs are generated by increasing the sound level to the contralateral ear, reflecting a sound source that changes its position circularly from one side (ipsilateral) to the other side (contralateral). Bars below PSPs indicate the time window during which APs can be evoked. In this example, ILDs ≤ 0 evoke no AP. A_1 and A_2 modified from Grothe et al. (2010), B and C modified from Friauf et al. (2019) with original publications in Finlayson and Caspary (1989) and Park et al. (1996), respectively. ILD/ITD = interaural level/time difference, PSP = postsynaptic potential, EPSP/IPSP = excitatory/inhibitory PSP, LSO = lateral superior olive, AP = action potential

synaptic transmission among themselves in a very sophisticated and yet not completely analyzed manner (Friauf et al., 2019). For example, MNTB neurons are not the only glycinergic input to LSO, as terminals positive for glycine transporter 2 (GlyT2, a marker for glycinergic terminals) were detected in the LSO of mice lacking the MNTB (Altieri et al., 2014). Possibly, these inputs originate from small multipolar neurons of the lateral nucleus of the trapezoid body (LNTB; Spirou and Berrebi, 1997) or from the ipsilateral CN (Wu and Kelly, 1994).

The prerequisite for correct calculation of ITD and ILD is the exact timing of the binaural signals (Beiderbeck et al., 2018). Therefore, synapses and axons of the lower auditory system are anatomically and functionally specialized to permit sustained and reliable signal transmission (Yu and Goodrich, 2014; Wichmann, 2015; Lujan and von Gersdorff, 2017). For example, GBC axons converging to the MNTB have one of the largest known diameter in the central nervous system (CNS) of about 5.5 µm (Spangler et al., 1985), ensuring fast signal transmission to the contralateral side (Spirou et al., 1990; Joris and Yin, 1998; Ford et al., 2015). Regarding synaptic specializations, they are markedly represented at the so called glutamatergic "giant synapses" in the auditory system (Felmy and Künzel, 2014): the ribbon synapse between IHCs and SGNs, the endbulb of Held between SGN terminals and SBCs, and the calyx of Held between GBC terminals and MNTB neurons (Figure 1; Schneggenburger et al., 2002; Neher, 2010; Manis et al., 2012; Yu and Goodrich, 2014; Wichmann, 2015; Joris and Trussell, 2018). They have multiple active zones with several docked vesicles, summing up into large readily releasable pools (RRPs; Kaeser and Regehr, 2017) with 600, 1,000 and >1,500 vesicles, respectively (Khimich et al., 2005; Lorteije et al., 2009; Lin et al., 2011; Lauer et al., 2013; Chen et al., 2015). In comparison to these synapses with their ribbon or calyceal structure, the MNTB-LSO synapse looks strikingly different with its numerous abundance at one LSO neuron and their small bouton-like shape (Blaesse et al., 2006; Weisz et al., 2016). Nevertheless, by using distinct strategies, the transmission at this synapse was shown to be similarly able to mediate fast and reliable transmission (see next chapter).

1.2. The MNTB-LSO synapse

In contrast to the giant synapses, bouton-type synapses like the hippocampal CA3-CA1 synapse or the synapse between entorhinal cortex and dentate granule cells (EC-DG) often exhibit only a weak performance during sustained activation, indicated by a strong short-term depression (STD), and a deterioration of fidelity and synaptic precision (Dobrunz and Stevens,

1997; Krachan et al., 2017). This is based on a relatively low number of released vesicles (quantal content, m) at CA3-CA1 synapses with an RRP of 65-228 vesicles, but a release probability (P_r) of only 1%, or a fast depletion of a small RRP at the EC-DG synapse, comprising only 40 readily releasable vesicles with a 25% probability to be released. However, the MNTB-LSO synapse in contrast to the CA3-CA1 and EC-DG synapses depicts a distinctly better performance with high fidelity and exquisite temporal precision during sustained stimulation (Krachan et al., 2017). These distinctions are achieved by the formation of numerous synaptic contacts (Figure 1) of 2-10 MNTB neurons with one LSO neuron (Sanes, 1990; Kim and Kandler, 2003, 2010; Noh et al., 2010; Hirtz et al., 2012; Krachan et al., 2017; Gjoni et al., 2018a; Muller, 2019), summing up into a large RRP with a high P_r of 16% (Krachan et al., 2017). As one MNTB neuron forms ~150 presynaptic boutons (Hirtz et al., 2012) and innervates presumably 3-5 LSO neurons, it is estimated that one LSO neuron receives about 30-50 synaptic contacts of one individual MNTB-fiber (Krachan et al., 2017). With about two vesicles in the RRP at each synapse, the MNTB-LSO connection therefore provides a large RRP almost identical as in giant synapses (Krachan et al., 2017; Weingarten, 2018).

A further important feature of the mature MNTB-LSO synapse is the ability of the synapse to maintain signaling even during extended periods of synaptic activity and does reach a steady-state level after a few seconds instead of collapsing completely (Kramer et al., 2014; Friauf et al., 2015; Krachan et al., 2017). This is due to highly efficient replenishment of the RRP, which would be completely emptied in a tens of seconds range during sustained high frequency stimulation (Sakaba and Neher, 2001; Lipstein et al., 2013). The glycine-containing vesicles therefore are derived from upstream vesicle pools, namely the recycling and reserve pool (Figure 3A; Rizzoli and Betz, 2005; Kavalali, 2006; Denker and Rizzoli, 2010), or directly by newly formed and filled vesicles. However, until now it is still not fully elucidated if and how these vesicle pools are separated and how exactly they differentiate, as an assignment of a vesicle to a distinct pool is up to now very difficult (Rizzoli and Betz, 2005). Furthermore, the three-pool model has been extended by further pools, e.g. a spontaneously releasing pool, a stranded vesicle pool, and a super-pool (Denker and Rizzoli, 2010). Also *de novo* formation of vesicles is still under question. Nevertheless, it is suggested that they primarily derive from endocytic membrane retrieval (Rizzoli and Betz, 2005).

Summarizing, these outstanding features of the MNTB-LSO synapse determine its behavior during sustained synaptic precision. In general, the way a synapse behaves as response to a millisecond to seconds-lasting activity period is a matter of short-term plasticity (STP), and depends on its ability to adapt and modify the signal transmission (Zucker and Regehr, 2002; Citri and Malenka, 2008; Regehr, 2012; Friauf et al., 2015; Friauf et al., 2019). STP describes the enhancement or decrease of postsynaptic responses in a ms-s range, which allows critical computational functions in neural circuits (Abbott and Regehr, 2004). An increase is called short-term facilitation (STF), caused by transient accumulation of Ca^{2+} in the presynapse. The latter positively affects P_r, leading to exocytosis of a higher number of vesicles at the next action potential (AP). If the increased m is maintained for seconds or minutes, STF is called augmentation. Negative STP, named short-term depression (STD; Figure 3B) is caused by a

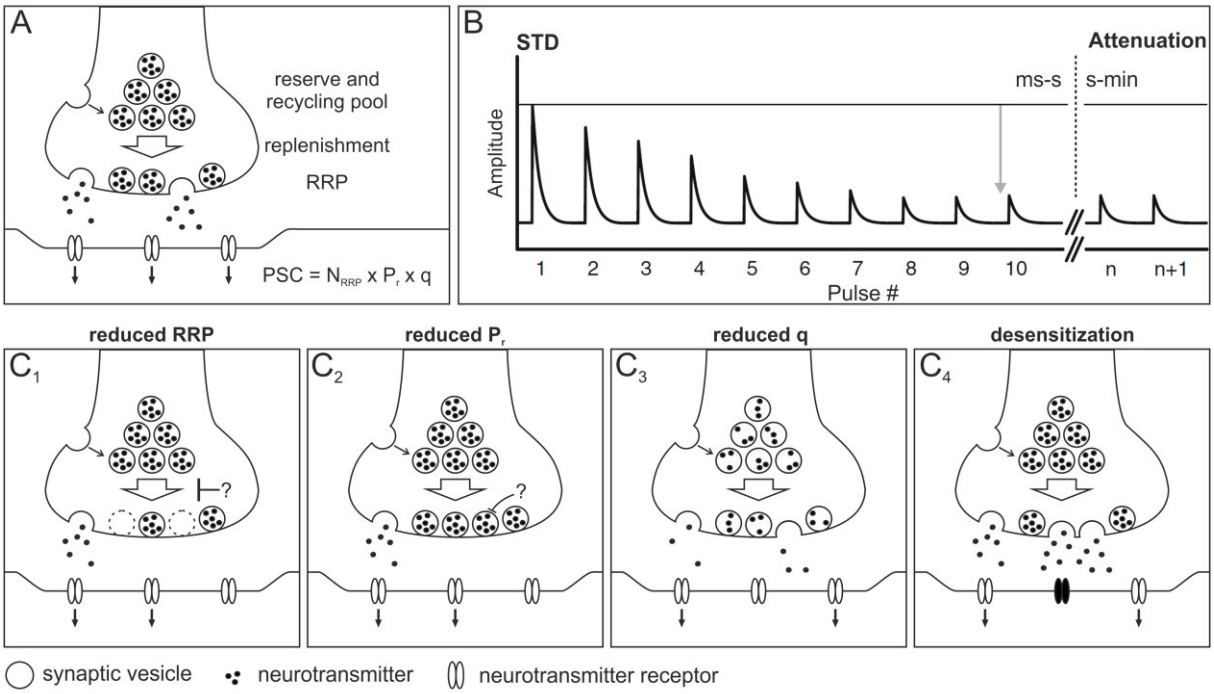

Figure 3: Mechanisms underlying STD and attenuation
A, Binding of neurotransmitter to postsynaptic receptors lead to ion influx through intrinsic channels, which can be measured as a PSC. The elicited PSC is described as the product of three parameters, namely the number of vesicles in the readily releasable pool (N_{RRP}), the release probability (P_r) of a vesicle, and the quantal size (q). The complete depletion of the RRP during sustained activity is prevented by replenishment from the reserve or recycling pool. New vesicles derive from upstream pools like the super pool (not shown) or by membrane retrieval. **B**, STD describes the reduction of amplitudes during sustained activity in a ms-s range. In the s-min range, STD is called attenuation. **C**, Several mechanisms that contribute to STD and attenuation as they result in reduced PSCs. **C_{1-3}**, Consequences of the reduction of the parameters shown in A. **C_4**, Desensitization as a postsynaptic cue that can also be involved in STD. Modified from Friauf et al., 2015. STD = short-term depression, PSC = postsynaptic current

decrease of postsynaptic currents (PSCs). If the postsynaptic responses stay depressed for seconds to minutes, STD is called attenuation. One causative mechanism is a transient depletion of the RRP, possibly due to an insufficient replenishment, which results in a lower m (Figure $3C_1$; Lipstein et al., 2013). Another scenario is the inhibition of the presynaptic release machinery, including a decrease of P_r, (Figure $3C_2$), and can be elicited by modulatory substances of the presynapse, postsynapse, or neighboring cells (Betz, 1970). Also a reduced quantal size (q) can be causative for smaller PSCs, as a lower amount of neurotransmitter per vesicle is exocytosed (Figure $3C_3$; Edwards, 2007). Furthermore, desensitization of postsynaptic receptors are known to contribute to STD/attenuation, as they can achieve a decreased sensitivity during prolonged agonist exposure (Figure $3C_4$; Jones and Westbrook, 1996). However, synaptic plasticity appears not to be only determined by pre- and postsynaptic cues. Astrocytes, the most abundant cell type in the brain (Volterra and Meldolesi, 2005; Herculano-Houzel, 2014; Verkhratsky and Nedergaard, 2018), were found to influence, to some extent, the behavior of synapses (Allen and Barres, 2005; Perea and Araque, 2007; Theodosis et al., 2008; Ben Achour and Pascual, 2010; Pannasch et al., 2011; De Pitta et al., 2016; Kim et al., 2017). This contribution of astrocytes to signal transmission has led to the development of the tripartite synapse model (Araque et al., 1999), assigning an active participation of astrocytes in proper synaptic functioning.

1.3. GlyT1 and its relevance for the MNTB-LSO synapse

Such an active participation of astrocytes in synapse function was found to occur via the glycine transporter 1 (GlyT1) (Supplisson and Bergman, 1997; Gomeza et al., 2003a; Lim et al., 2004; Whitehead et al., 2004; Beato, 2008; Aroeira et al., 2014). In the early 90s, GlyT1 was identified by Liu et al. (1992), Smith et al. (1992), and Guastella et al. (1992), and was detected throughout most regions of the CNS (Guastella et al., 1992; Zafra et al., 1995; Jursky and Nelson, 1996; Eulenburg et al., 2018). A former hypothesis which suggested that GlyT1 is specifically expressed by astrocytes (Adams et al., 1995) was disproved as several studies revealed its abundance also in neurons (Pow and Hendrickson, 1999; Cubelos et al., 2005a; Yee et al., 2006; Eulenburg and Gomeza, 2010; Raiteri and Raiteri, 2010). However, in lower brain regions like the brainstem, marked by a high ratio of glycinergic transmission, GlyT1 was found to be strongly expressed by astrocytes (Figure 5; Adams et al., 1995; Zafra et al., 1995; Szoke et al., 2006; Stephan and Friauf, 2014), enriched in their fine processes (Zafra et al.,

1995; Aroeira et al., 2014). In contrast, neurons express mainly the isoform GlyT2 (Friauf et al., 1999; Zeilhofer et al., 2005), which is highly abundant in the cytoplasm. At presynaptic terminals, it is inserted in the membrane in direct opposition to GlyRs, but stays beyond active zones (Jursky and Nelson, 1995; Poyatos et al., 1997; Spike et al., 1997; Gomeza et al., 2003b). This cell type restriction of the two GlyTs at inhibitory synapses was not observed at glutamatergic synapses as GlyT1 was found in neurons as well as in astrocytes (Cubelos et al., 2005a). Furthermore, genetic analyses have revealed that GlyT1 and GlyT2 share ~50% amino acid homology, although they are expressed from different genes (Liu et al., 1993; Jursky et al., 1994). They both belong to the solute carrier family 6 (Slc6), which depict a common transmembrane topology with 12 transmembrane domains, and function via cotransport of Na^+ and Cl^- (Nelson, 1998; Kristensen et al., 2011; Pramod et al., 2013). In case of GlyT1, different promoter usage or splicing leads to the expression of several isoforms in a development- and species-dependent manner, that differ in their intracellular N- and

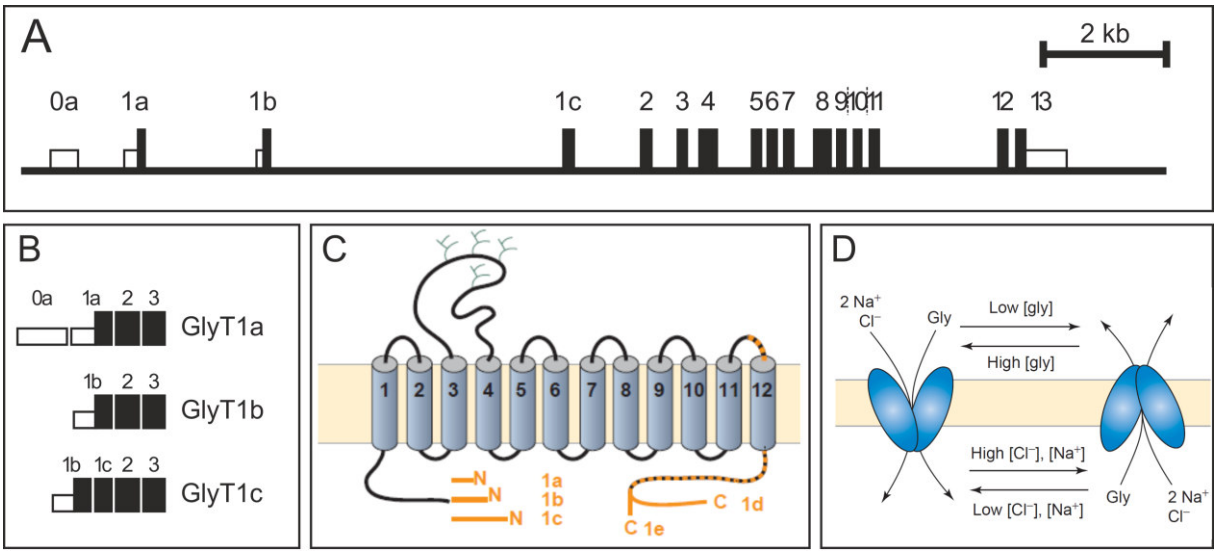

Figure 4: GlyT1 – gene, expression, and stoichiometry
A, Schematic representation of the genomic sequence of the murine GlyT1. Exons are represented as boxes, with coding regions in black and noncoding regions in white. Numbering of exons is provisional because additional exons might exist. **B**, Representation of 5'-exonic mRNA sequences of GlyT1a, b, and c. GlyT1a and GlyT1b/c are expressed by different promoters, GlyT1b and c are splice variants. **C**, GlyT1 protein contains 12 putative TMDs with intracellular N- and C-termini. Different isoforms (orange) are generated by alternative promoter usage or splicing. In mice, isoforms a, b, and c were identified with d as C-terminus. C-terminus e, a splice variant of d, was up to now only found in bovine, whose TMD12 (dotted line) might cross the membrane not as an α helix. **D**, GlyT1 catalyzes the co-transport of glycine with two Na^+ and one Cl^- ion. GlyT1 works close to equilibrium and is able to work in reverse mode depending on ion gradients and membrane potential. A and B modified from Adams et al. (1995), C and D modified from Eulenburg et al. (2005). GlyT1 = glycine transporter 1, TMD = transmembrane domain, gly = glycine

C-termini (Figure 4A-C; Borowsky et al., 1993; Liu et al., 1993; Kim et al., 1994; Olivares et al., 1994; Adams et al., 1995; Olivares et al., 1997; Borowsky and Hoffman, 1998; Hanley et al., 2000; Supplisson and Roux, 2002). In mice, the isoforms GlyT1a and GlyT1b with different N-termini but with the same C-terminus (1d) were identified, whose expression is controlled by different promoters. The expression of GlyT1c in mice as a GlyT1b splice variant is discussed (Borowsky and Hoffman, 1998), as its expression was so far only verified in human substantia nigra (Kim et al., 1994). The discrimination between GlyT1 isoforms on protein level is difficult, as no isoform specific antibodies are available. However, by using a GlyT1b/c knockout (KO) mouse, Schuster (2015) found an age-dependent reduction of GlyT1 signal in KO in spinal cord, brainstem, and midbrain, which was not observed in wildtype (WT). This indicates a developmental shift from GlyT1a to GlyT1b/c expression in these brain regions, which can only occur as their expression is controlled by different promoters. From this developmental shift it was concluded that it could be critical for cells to differentially regulate the expression levels of these transporters, implying different functions for GlyT1 and GlyT1b/c during development. Nevertheless, it is supposed that all GlyT1 isoforms have the same transport properties as they only differ in their N- and C-termini (Kristensen et al., 2011).

Regarding the transport mechanisms of GlyT1 and GlyT2, glycine uptake is coupled to the transmembrane Na^+ gradient, serving as the electrochemical driving force. However, the stoichiometry of the two transporters is different with $2Na^+$:$1Cl^-$:1glycine for GlyT1 (Figure 4D), and $3Na^+$:$1Cl^-$:1glycine for GlyT2 (Supplisson and Roux, 2002). GlyT1 is working close to resting membrane potential (V_{Rest}) and therefore can function in a reverse mode after cell depolarization, intracellular increase in Na^+, or at low extracellular glycine concentrations, thus releasing glycine in the extracellular space (Roux and Supplisson, 2000; Aragon and Lopez-Corcuera, 2003; Richerson and Wu, 2003; Aubrey et al., 2005; Beebe et al., 2016; Shibasaki et al., 2017). However, it can only establish an intracellular glycine concentration of ~4-11 mM (Zafra et al., 2017). GlyT2 in contrast to GlyT1 has a 2-fold stronger driving force under physiological conditions because of its higher Na^+ transport stoichiometry and a very positive reversal potential, preventing reverse transport activity (Roux and Supplisson, 2000). Therefore, GlyT2 is able to establish and maintain a presynaptic glycine concentration of ~20-40 mM (Supplisson and Roux, 2002; Verkhratsky and Nedergaard, 2018). This property is important for the main role of neuronal GlyT2, which was shown to be glycine reuptake into the presynapse, establishing an intracellular glycine concentration needed for vesicle refilling

(Spike et al., 1997; Gomeza et al., 2003b). In contrast, the main task of GlyT1 was shown to be the fast removal of glycine from the synaptic cleft, mediating the termination of inhibitory neurotransmission and preventing spillover of glycine (Adams et al., 1995; Roux and Supplisson, 2000; Gomeza et al., 2003a; Zafra and Gimenez, 2008; Eulenburg and Gomeza, 2010; Kurolap et al., 2016; Verkhratsky and Nedergaard, 2018). GlyT2, also contributes to glycine clearance (Logan and Snyder, 1972; Fedele and Foster, 1992; Bradaia et al., 2004), but its main function was shown to be the supply of glycine to the presynapse, as its loss or inhibition causes a decrease of glycinergic transmission (Raiteri et al., 2001; Gomeza et al., 2003b; Raiteri et al., 2005; Harvey et al., 2008; Rousseau et al., 2008; Latal et al., 2010). At glutamatergic synapses, neuronal and astrocytic GlyT1 tightly control glycine concentration via glycine uptake and release. As glycine is also a N-methyl-D-aspartate receptor (NMDAR) co-agonist (Johnson and Ascher, 1987; Traynelis et al., 2010; Harsing and Matyus, 2013; Hansen et al., 2018), GlyT1 activity can regulate NMDAR function, suggestively being the main function in this scenario (Supplisson and Bergman, 1997; Igartua et al., 2007). In general, a loss of GlyT1 in mice was shown to cause a high lethality (Gomeza et al., 2003a; Tsai et al., 2004), and induced a subtype of the human disease glycine encephalopathy, which is marked by elevated glycine in the cerebrospinal fluid (Applegarth and Toone, 2001; Kurolap et al., 2016). In contrast, the loss or inhibition of GlyT2 induces a phenotype that resembles the human disease hyperekplexia, caused by overexcitation (Gomeza et al., 2003b; Harvey et al., 2008; Harvey and Yee, 2013).

The functional discrepancy of both transporters at glycinergic synapses like the MNTB-LSO synapse in combination with their close proximity (Figure 5) leads to the assumption that they operate in concert (Figure 6). Upon an incoming AP in the presynaptic MNTB terminal, voltage-gated Ca^{2+} channels (VGCCs) open and the concomitant Ca^{2+} influx initiates exocytosis of vesicles in the RRP. The released glycine diffuses through the synaptic cleft and binds to densely packed glycine receptors (GlyRs) in the postsynaptic membrane (Betz et al., 1999; Legendre, 2001; Laube et al., 2002). The postsynaptic receptors are heteropentamers, composed of the subunits α1 and β (Becker et al., 1988; Takahashi et al., 1992; Friauf et al., 1997; Kungel and Friauf, 1997; Singer et al., 1998; Laube et al., 2002; Altieri et al., 2014). Subunit α thereby is responsible for ligand detection and the subunit β mediates the anchoring to postsynaptic sides via binding to gephyrin, a neuronal assembly protein (Meyer et al., 1995; Betz et al., 1999; Legendre, 2001). The activation of GlyRs leads to the

opening of intrinsic Cl^- channels, enabling Cl^- influx. This influx can be measured as an inhibitory PSC (IPSC) in patch-clamp recordings. The increase of intracellular Cl^- concentration hyperpolarizes and therefore inhibits the postsynaptic cell (Lynch, 2004; Dutertre et al., 2012). The action of glycine is terminated by its dissociation from the receptor, induced by a decline of its concentration in the synaptic cleft due to diffusion (Titmus et al., 1996) or due to uptake by GlyT1 (Roux and Supplisson, 2000; Gomeza et al., 2003a; Kurolap et al., 2016). To what extent astrocytes in general contribute to neurotransmitter removal at a synapse, depends on the degree of astrocytic synapse enwrapping (Danbolt, 2001; Xu-Friedman et al., 2001; Witcher et al., 2010; Chung et al., 2015; Tso and Herzog, 2015). Beyond active zones, GlyT2 transports glycine into the presynapse. Intracellularly, the glycine is filled into newly formed vesicles (Rizzoli and Betz, 2005) via the vesicular inhibitory amino acid transporter (VIAAT; Dumoulin et al., 1999). Outside of the synapse, GlyT1 can act in reverse mode due to the low extracellular glycine concentration (Roux and Supplisson, 2000; Aragon and Lopez-Corcuera, 2003; Aubrey et al., 2005; Beebe et al., 2016; Shibasaki et al., 2017), and therefore constitutes an additional glycine source for GlyT2. Besides uptake from the extracellular space, glycine can be derived also by *de novo* synthesis. *De novo* synthesis is mediated by cytoplasmic and

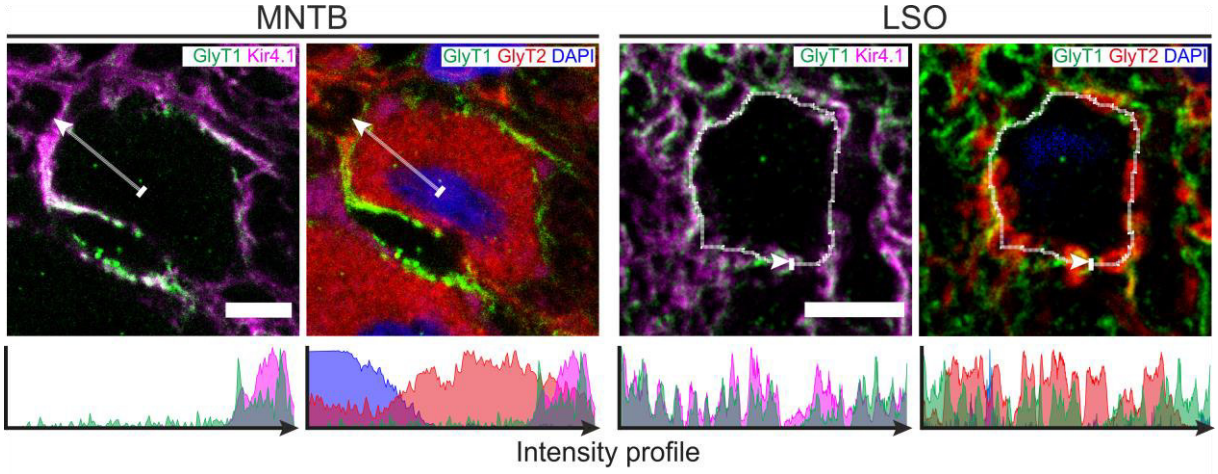

Figure 5: GlyT1 and GlyT2 at the somata of MNTB- and LSO neurons
At the somata of MNTB neurons (left), GlyT2 is highly abundant in the cytoplasm. GlyT1 appears to be present in close association with the cell membrane. Intensity profile reveals a stronger co-localization of GlyT1 with the astrocytic marker Kir4.1 as with the neuronal marker GlyT2. At the somata of LSO neurons (right), GlyT2 signal most likely derives from glycinergic MNTB-terminals, providing an impression of the bouton-like synapse architecture. As in the MNTB, GlyT1 is strongly co-localized with Kir4.1 (see intensity profile) and shows a weaker co-localization with GlyT2. In MNTB and LSO, the strong correlation of GlyT1 and Kir4.1 localization let suspect an astrocyte-restricted GlyT1 expression. Scale bars 5 µm. Arrows indicate origins of the intensity profiles. p. com. Jonathan Stephan. GlyT1/2 = glycine transporter 1/2, Kir4.1 = inwardly rectifying K^+ channel 4.1, MNTB = medial nucleus of the trapezoid body, LSO = lateral superior olive

mitochondrial serine hydroxymethyltransferase (SHMT), which catalyzes the conversion of the metabolic precursor serine into glycine (Shank and Aprison, 1970; Zafra et al., 1997b; Legendre, 2001). However, *de novo* synthesis is suggested to play only a minor role at the MNTB-LSO synapse, as deletion or inhibition of GlyT2 led to reduced vesicle filling and/or reduced presynaptic glycine (Gomeza et al., 2003b; Rousseau et al., 2008; Latal et al., 2010), indicating a high glycine rate. Accordingly, the glycine cleavage system (GCS), which is expressed only in astrocytes, is nearly absent in brainstem (Sato et al., 1991) and hence glycine is rather reused than degraded. Therefore, an efficient glycine recycling probably with contribution of GlyT1 enables the MNTB-LSO synapse to maintain an appropriately sized presynaptic glycine pool, especially during periods with excess release of glycine.

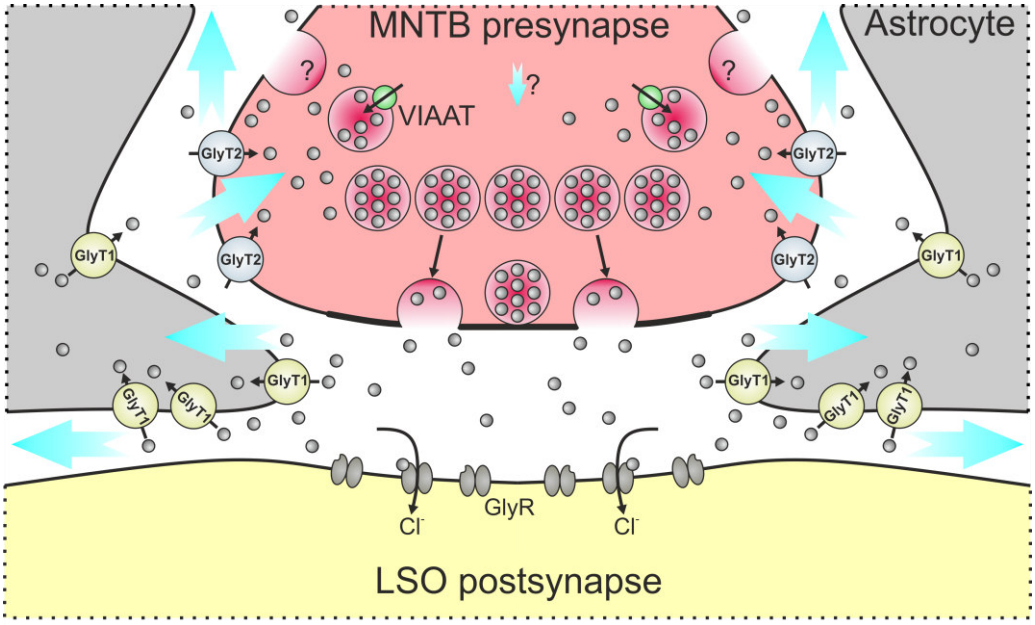

Figure 6: Glycine cycle at the MNTB-LSO tripartite synapse
Inhibitory signaling at MNTB-LSO is mediated by the neurotransmitter glycine. In the MNTB presynapse, glycine-containing vesicles are stored in different vesicle pools (cf. Figure 3A). Upon a stimulus, one or more vesicles are exocytosed, releasing glycine in the synaptic cleft. Glycine molecules diffuse to the postsynapse and activate GlyRs opposed to the active zone. The subsequent Cl^- influx elicits an IPSC, leading to hyperpolarization of the LSO neuron. GlyR activation is terminated by a decrease of glycine concentration via diffusion or uptake (large blue arrows). The main contributor to glycine clearance at glycinergic synapses was shown to be the astrocytic GlyT1, which can also function in reverse mode. GlyT2 is crucial for glycine uptake into the presynapse, providing a sufficient glycine concentration needed for VIAAT activity. VIAAT translocates glycine into new vesicles presumably derived from membrane retrieval. Uptake and therefore recycling of glycine was shown to be the major mechanism in maintenance of presynaptic glycine levels, whereas *de novo* synthesis (small blue arrow) plays a negligible role. The RRP is replenished by newly filled vesicles and by vesicles stored in upstream vesicle pools. MNTB = medial nucleus of the trapezoid body, LSO = lateral superior olive, RRP = readily releasable pool, GlyR = glycine receptor, GlyT1/2 = glycine transporter 1/2, VIAAT = vesicular inhibitory amino acid transporter

1.4. Aims of study

In the last decades, manifold functions of astrocytes were unraveled. In these studies, a lot of attention was paid mostly on glutamatergic synapses like the calyx of Held or the CA3-CA1-synapse. However, the influence of astrocytes on glycinergic neurotransmission is still ambiguous. To extend the knowledge about this aspect, the ambition of this study was to elucidate the contribution of astrocytic GlyT1 to the fast and highly precise glycinergic signaling at the MNTB-LSO synapse in the auditory brainstem. By using the GlyT1b/c KO mouse model that does not suffer from the high lethality of other GlyT1 KO mouse models, the consequences of GlyT1 loss for the mature MNTB-LSO circuit was analyzed by using the patch-clamp technique. In this study, the following questions were addressed to elucidate the associated hypotheses:

Questions	*Hypotheses*
Does GlyT1 loss at the MNTB-LSO synapse lead to decay time prolongation of spontaneous inhibitory postsynaptic currents (sIPSCs) as it was observed at other glycinergic synapses? (4.2)	*Due to glycine accumulation, GlyRs are longer activated, resulting in prolonged sIPSC decay times.*
Is there a change in basic synaptic properties due to the lack of GlyT1 activity? (4.3)	*As GlyT1 is expressed only in astrocytes at inhibitory synapses, a loss does not impair presynaptic glycine uptake and therefore no change in basic synaptic properties is expected.*
How does GlyT1 loss affect proper signal transmission during sustained stimulation with high frequency? (4.4)	*The accumulation of excess glycine during sustained synaptic activation leads to longer decay times of eIPSCs, but fidelity and temporal precision are not impaired.*

2. MATERIAL AND METHODS

2.1. GlyT1b/c KO mouse line

2.1.1. Ethical approval, housing and breeding

Animal breeding, housing and experiments were approved by the regional council according to the German animal protection law (TSchG §4, Absatz 3) and followed the NIH guide for care and use of laboratory animals. Animals were housed on a 12/12 h light-dark cycle with *ad libitum* access to food and water in the local animal facility of the University of Kaiserslautern. The day of birth was designated as postnatal day (P) 0. At P56 (male) or P70 (female) heterozygous (HT) animals were used for breeding and were kept 1/1 (male/female) in one cage. At P20 ± 1, KO animals of both sexes were used for experiments, with wildtype (WT) littermates serving as controls. The experimenter remained blind for the genotype during electrophysiological data acquisition and its analysis. After the completion of analysis, the genotypes of the animals were revealed and the data were accordingly grouped and compared.

2.1.2. Generation

All chemicals listed in this and subsequent chapters were purchased from Sigma-Aldrich or AppliChem, if not stated otherwise. GlyT1b/c KO mice (official nomenclature: B6.129/Sv129-Slc6a9$^{tm5(LucR)veul5}$) were generated and kindly provided by PD. Dr. Volker Eulenburg (Eulenburg et al., 2018) with the genetic concept illustrated in Figure 7A. A targeting construct containing DNA encoding for a fusion protein (renilla luciferase, LucR) of luciferase (*Lampyridae*, Promega) and FP635 (*Entacmaea quadricolor*, Origene) in exon 1b of the GlyT1 gene 15 nucleotides downstream of the GlyT1b start codon was generated. Additionally, a neomycin resistance cassette (NEO) flanked by two Flp (flippase) recombinase targeting sequence (Frt) sites for positive selection was inserted about 400 bp downstream of exon 1b. For negative selection, a gene encoding for the herpes simplex virus thymidine kinase (HSV-TK) was introduced at the 3' end of the targeting construct. For homologous recombination, mouse genomic fragments were retrieved from a bacterial artificial chromosome (BAC) clone including two homologous regions with 15 kB upstream and 1.5 kB downstream the LucR-NEO construct. For insertion into the WT allele, the targeting construct was introduced in Sv129/OlaHasd (E14TG2A) mouse embryonic stem cells. With 1-[2-deoxy,2-

fluoro-8-D-arabinofuranosyl]-5-iodouracil (FIAU) treatment, cells with random insertion of the targeting construct were eliminated as HSV-TK phosphorylates FIAU, which consecutively acts as a competitive inhibitor of the DNA polymerase. With geneticin (G418), cells with homologous recombination and therefore G418-resistance due to NEO were selected. Positive clones were injected into C57BL/6J blastocysts and obtained male chimeras were mated with C57BL/6J females. Offsprings carrying the modified allele were mated to Flipper mice (Farley et al., 2000; Eulenburg et al., 2018) leading to the excision of NEO via action of the Flp recombinase. Homozygous GlyT1b/c knockin (KI) mice were generated by mating HT mice. As the KI in exon 1b leads to a functional KO of isoforms GlyT1b and c, the mouse line was named GlyT1b/c KO. For more detailed generation of this mouse line see Schuster (2015).

2.1.3. Genotyping

Mouse biopsies were taken around P4 and additionally at the day of experiment for *post hoc* genotyping, and stored at -20°C until further use. After adding 200 µl digesting solution (25 mM NaOH, 0.2 mM ethylenediaminetetraacetic acid (EDTA, Roth), pH12) the samples were vortexed and centrifuged for 1 min at 16,060 x g (Biofuge fresco, Hereaus) and incubated

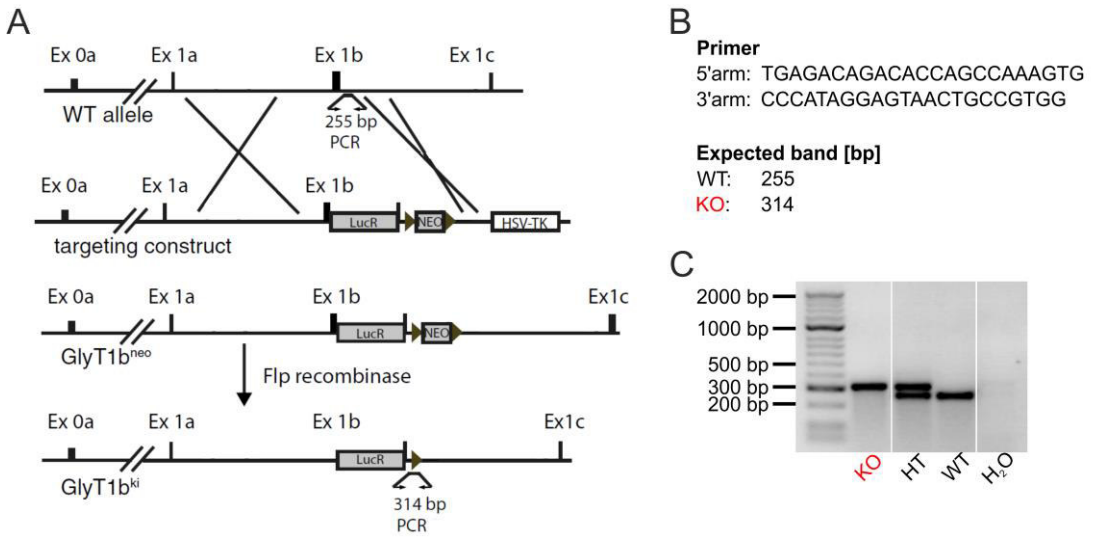

Figure 7: Generation and genotyping of GlyT1b/c KO mice
A, Schematic drawing of the gene targeting strategy for the generation of a GlyT1b-LucR knockin, leading to a functional GlyT1b/c knockout. LucR reporter and NEO are indicated as grey boxes, HSV-TK cassette is indicated as a white box. Frt recognition sites are displayed as triangles, and primer binding sites used for genotyping (small arrows, cf. 2.1.3) are indicated. **B**, Sequences of used primers with the expected band sizes of amplicons. **C**, Example PCR analysis of genomic DNA isolated from biopsies from a GlyT1b/c wildtype (WT), heterozygous (HT) and knockout (KO) mouse, respectively, derived from the same gel. The WT allele is indicated by an amplicon of 255 bp, the targeted allele by an amplicon of 314 bp. Panel A modified from Eulenburg et al., 2018. Ex = exon, NEO = neomycin resistance cassette, HSV-TK = herpes simplex virus thymidine kinase, Flp = flippase, Frt = Flp recombinase targeting sequence, LucR = renilla luciferase

at 95°C for 1 h in a gently shaking incubator (Thriller, Peqlab). Afterwards, the samples were vortexed and neutralized with 200 µl tris(hydroxymethyl)aminomethane (Tris)-HCl (Tris buffer). After vortexing, they were centrifuged for 10 min at 16,060 x g, and 200 µl of the supernatants (containing the DNA) were transferred into new Eppendorf tubes and used for genotyping. The polymerase chain reaction (PCR) contained 8 µl of this DNA solution, 5 µl sterile distilled H_2O, 4.0 µl 5x PCR buffer (Bioline), 1.0 µl of each primer (Screen Neo Frt for/rev, for primer sequences see Figure 7B) with 10 pmol/µl and 0.3 µl Taq polymerase (self-made). Initial denaturation was performed for 3 min at 94°C, followed by 30 cycles of 30 s denaturation at 94°C, 30 s primer annealing at 60°C, and 30 s elongation (FlexCycler 2, Analytic Jena). Final elongation was carried out for 3 min at 72°C. Afterwards, 5 µl sample buffer (40 mM Tris buffer, 20 mM acetic acid, 1 mM EDTA (TAE buffer), 40% glycerol, hint of xylencyanol) was added to the samples and the solution was mixed by pipetting it up and down for several times. 11 µl of the samples as well as 5 µl DNA ladder (HyperLadder™ 50bp, Bioline) were loaded onto a 1.5% agarose gel (1.5% agarose (Axon) in TAE buffer with 0.001% ethidium bromide (Merck), heated in a microwave until the agarose was dissolved) and run for 50 min at 100 V in TAE buffer. The PCR products were visualized by exciting ethidium bromide with UV light and detecting the emission at 590 nm (Biometra TI1, LTF Labortechnik). As the primers anneal to regions left- and right-sided to the remaining Frt (Figure 7A), an amplicon of 314 bp signifies the GlyT1b/c KO, whereas an amplicon of 255 bp indicates GlyT1b/c WT (Figure 7C). Genotyping was assisted by Kornelia Ociepka and Ralph Reiss.

2.1.4. Survival analysis

To assess the occurrence of increased prenatal death due to the reporter KI, the Mendelian distribution of the different genotypes was analyzed. For postnatal impairment, a survival analysis via the Kaplan-Meier plot (Kaplan and Meier, 1958) was performed in Winstat.

Formula of Kaplan-Meier estimate (Klein and Moeschberger, 2003):

$$\hat{S}(t) = \begin{cases} 1, & t < t_1 \\ \prod_{t_i \le t} (1 - \frac{d_i}{n_i}), & t_1 \le t \end{cases}$$

$\hat{S}$ = Survivalrate

i = timepoint with natural death(s)

n_i = number of natural deaths at timepoint i

d_i = number of animals at timepoint i

2.2. Western blotting

2.2.1. Sample preparation

Mice were anesthetized with an intraperitoneal injection of about 150 µl ketamine hydrochloride (50 mg/ml, Inresa Arzneimittel). After loss of pain reactions, mice were decapitated and the brains extracted into 4°C artificial cerebrospinal fluid (ACSF; 12.5 mM NaCl, 2.5 mM KCl, 1.25 mM NaH_2PO_4, 2 mM Na-pyruvate, 3 mM myo-inositol, 0.44 mM L-ascorbic acid, 25 mM $NaHCO_3$. 10 mM D-glucose, 1 mM $MgCl_2$, 2 mM $CaCl_2$, 290 ± 10 mOsmol). The brainstems were separated and immediately frozen in liquid nitrogen. Afterwards, the samples were stored at -80°C until further use. The samples were weighted and fractionated following a protocol established by Marz (2018). Subsequently, the samples were homogenized in 3-fold amount of homogenization buffer (HB; 50 mM Tris, 150 mM NaCl, 5 mM $MgCl_2$, 1 mM phenylmethane sulfonyl fluoride (PMSF), in deionized H_2O, pH 7.4) by performing ten strokes with 360 rpm (drill machine, Metabo) with a glass-teflon-homogenizer (conical polytetrafluoroethylene pestle, Buddeberg Laboratory Technology). For lysis, the homogenates were mixed with 1% (v/v) triton-X-100 diluted in HB, and incubated for 30 min at 4°C. This was followed by centrifugation with 150,000 x g (Optima L-80XP, Type70.1Ti rotor, Beckman Coulter) at 4°C for 45 min. The supernatant, containing membrane and cytosolic proteins, was transferred into a new Eppendorf tube and taken for total protein amount estimation using the Direct Detect infrared spectrometer (Merck Millipore), already described by Marz, 2018; 2.10.6). 40 µg protein were taken and added to HB with a final volume of 10 µl. After mixing with 2.5 µl 5 x sample buffer (SB; 312.5 mM Tris pH 6.8, 500 mM dithiothreitol (DTT), 10% sodium dodecyl sulfate (SDS), 0.05% bromphenol blue, 50% glycerol), proteins were denaturized by heating them at 40°C for 20 min (Julabo U3, Julabo) and frozen until further use. To get technical replicates, two samples of each animal were prepared.

2.2.2. SDS-PAGE

For separating the proteins, SDS-polyacrylamide gel electrophoresis (PAGE) (Lottspeich and Engels, 2006) with 10 or 15 wells was performed. Gels had a size of 7.5 x 8 cm^2, a thickness of 1 mm and were self-casted by using a gel casting module (MiniGelapparatur, Bio-Rad Laboratories). The acrylamide concentration of the stacking gel was 5% (125 mM Tris pH 6.8, 5% acrylamide-mix (29.2% acrylamide, 0.8% N,N'-methylenebisacrylamide), 0.075% ammonium persulfate (APS), 0.125% N,N,N',N'-tetramethylethylenediamine (TEMED) in

deionized H_2O), and of the separating gel 10% (390 mM Tris pH 8.8, 10% acrylamide-mix, 0.1% SDS, 0.1% APS, 0.2% TEMED in deionized H_2O. The gel cassette was placed into the electrode assembly and put into the gel electrophoresis chamber (Mini PROTEAN Tetra Cell, Bio-Rad Laboratories), which was filled completely with running buffer (Laemmli buffer; 25 mM Tris, 192 mM glycine, 0.1% SDS in deionized H_2O). The samples and 4 µl PageRuler Plus Prestained Protein Ladder (Thermo Fisher Scientific) as marker were loaded onto the gel and SDS-PAGE was performed at 4°C with 15 mA/gel (PowerPac 300/1,000, Bio-Rad Laboratories) until the samples had reached the separating gel. Subsequently, 25 mA/gel were applied until proteins were sufficiently separated. Afterwards, the gel was removed from the glass plates and incubated for 5 min in blotting buffer (BB; 20% MeOH (Fisher Scientific), 1x Laemmli buffer in distilled H_2O).

2.2.3. Western blotting

For western blotting (cf. Marz (2018), chapter 2.4.5), a polyvinylidine fluoride (PVDF)-membrane (Immobilon-Fl PVDF-membrane, Merck Millipore) was activated for 30 s in MeOH, washed in BB and immediately put onto the gel. The membrane and the gel were placed between two filter papers and a sponge on each site, which were soaked with BB. This construct was placed into a module (Mini Trans-Blot Cell, Bio-Rad Laboratories) which was subsequently put into a tank blotting chamber (Mini Trans-Blot Cell, Bio-Rad, Bio-Rad Laboratories) and filled with BB. By applying 350 mA for 1 h at 4°C, proteins were transferred from the gel onto the membrane.

2.2.4. Total protein staining

At first, the total protein content was visualized with the Revert Total Protein Stain Kit (926-11010, LI-COR Bioscience; cf. Marz (2018), chapter 2.7). To do so, the membrane was activated in MeOH and washed for 2 min with deionized H_2O. Afterwards, it was incubated for 5 min in 5 ml Revert total protein staining solution (LI-COR Bioscience) on a CAT RM5 agitator (Labortechnik Fröbel) and washed twice for 30 s with 5 ml Revert wash solution (LI-COR Bioscience), respectively. This was followed by an additional washing step for 1 min with deionized H_2O. The total protein staining was imaged for 2 min at 700 nm with the FC-Odyssey and the Image Studio Software version 2.0.38 (LI-COR Bioscience). After acquisition, the membrane was rinsed briefly with water and blocked with StartingBlock Tris-buffered saline (TBS) blocking buffer (TBS-BB; Thermo Fisher Scientific) for 30 min on the agitator.

2.2.5. Immunodetection

For immunodetection, a polyclonal rabbit antibody against GlyT1 (α-GlyT1, Synaptic Systems 272103) was diluted 1:1000 in TBS-BB and incubated with the membrane for 2 h at room temperature (RT) and subsequently overnight at 4°C on the agitator. Afterwards, the membrane was washed four times for 2.5 min, respectively, with TBS (150 mM NaCl, 20 mM Tris pH 7.5) containing 1% Tween20 (T-TBS). For 1 h at RT, the membrane was incubated light protected with the secondary donkey antibody against rabbit (IRDye 800 CW), diluted 1:10.000 in TBS-BB on the agitator. Afterwards, the membrane was washed four times for 2.5 min, respectively, with T-TBS and once for 3 min with TBS. The antibody signal was measured for 3 min at 800 nm as described in 2.2.4. For GlyT2 signal detection, the membrane was shortly incubated in MeOH and washed twice with distilled H_2O. Then the membrane was incubated with the polyclonal mouse antibody against GlyT2 (α-GlyT2, Synaptic Systems 272003) and the secondary donkey antibody against mouse (IRDye 800 CW) in the same dilutions and with the same procedure as described above. Antibody signals were obtained at the expected molecular weights of ~70 kDa for GlyT1 and ~87 kDa for GlyT2. Steps 2.2.2-2.2.5 were assisted by Ralph Reiss.

2.2.6. Evaluation

With Image Studio Software version 2.0.38 (LI-COR Bioscience), the intensities of GlyT1 and GlyT2 bands were measured. The following steps were done separately for each blot: a rectangle for the respective band (GlyT1 or GlyT2) was adjusted in size and height and used for each lane of the blot. Afterwards, the same rectangle was set on a suitable position to measure the background, which was subtracted from the obtained grey values. The background-subtracted values where normalized to the corresponding total protein value, obtained by measuring the grey value of one lane on the total protein blot with a square over the entire length. The rectangle stayed the same for each lane on one blot. After this correction, which prevents imprecisions for example due to pipetting errors, the mean value of the WT signals was calculated and set as 100%. After this normalization, the mean of technical replicates (repetition of the same blot) was calculated to have one single value for each sample. Finally, the data of the different blots were pooled and statistically analyzed as described in 2.4.

2.3. Electrophysiology

2.3.1. Preparation of acute brainstem slices

Mice were lethally injected with ketamine hydrochloride (cf. 2.2.1), and acute coronal brainstem slices containing the SOC were retrieved as described earlier (Hirtz et al., 2012). After loss of pain reactions, mice were decapitated and the brains quickly extracted into an ice-cold preparation solution adopted from Ting et al. (2014) (93 mM N-methyl-D-glucamine (NMDG), 2.5 mM KCl, 1.2 mM NaH_2PO_4, 30 mM $NaHCO_3$, 20 mM N-(2-hydroxyethyl)piperazine-N'-2-ethanesulfonic acid (HEPES), 25 mM D-glucose, 5 mM L-ascorbic acid, 3 mM myo-inositol, 3 mM Na-pyruvate, 10 mM $MgCl_2$, 0.5 mM $CaCl_2$, adjusted to pH 7.4 with 37% HCl, 300 ± 10 mOsmol). The solution was bubbled with carbogen (95% O_2, 5% CO_2) during preparation to keep the pH. The brains were carefully freed from meninges and subsequently brainstems were isolated by removing the forebrain and cerebellum with a razor blade. A planar razor blade cut at the caudal side of the brainstem created a surface for gluing the brainstem onto a magnetic plate with cyanoacrylate adhesive (UHU 45545, UHU). The magnetic plate was transferred into a slicing chamber filled with ice-cold, bubbled preparation solution and cut into 270 µm thick coronal slices with a vibratome (VT1200 S, Leica). Slices containing the LSO were incubated for 7 min at 37°C in preparation solution and subsequently kept for at least 1 h at RT in ACSF, bubbled with carbogen to sustain the pH at 7.4. Slices were maximally stored 8 h before they were used for experiments.

2.3.2. Recording from LSO principal neurons

One slice at a time (Figure $8A_1$) was transferred to the bath chamber and weighted down with a U-shaped platinum iridium wire with a grid of nylon threads (Edwards et al., 1989). The chamber was mounted under an upright microscope (Eclipse FN1, Nikon), equipped with infrared-differential interference contrast (DIC) optics (60x water immersion objective N.A. 1.0) and an infrared video camera (XC-ST70CE, Hamamatsu). Slices were continuously supplied with carbogen-bubbled ACSF by using a circular pump-driven tube system (Ismatec ISM796B, Cole-Parmer), and heated to physiological temperature (36 ± 1 °C, temperature controller VII, Luigs&Neumann). To pharmacologically isolate inhibitory inputs to the LSO, excitatory synaptic transmission was prevented by adding 20 µM 6-cyano-7-nitroquinoxaline-2,3-dione (cyanquixaline (CNQX), Abcam), a competitive α-amino-3-hydroxy-5-methyl-4-isoxazolepropionic acid receptor (AMPAR)/kainate receptor antagonist, to the ACSF. Patch

pipettes were pulled from borosilicate glass capillaries (GB150(F)28P, Science Products) using a horizontal puller (P-87, Sutter Instruments) and were filled with a pipette solution (10 mM HEPES, 5 mM ethylene glycol-bis(2-aminoethylether)-N,N‘,N‘,N‘-tetraacetic acid (EGTA), 1 mM $MgCl_2$, 2 mM Na_2ATP, 0.3 mM Na_2GTP, adjusted to pH 7.2 with 2 M KOH, ~290 mOsmol). Pipette resistances ranged from 3.5-8.8 MΩ. The liquid junction potential of 15.4 mV was corrected online. After identifying LSO principal neurons optically by their

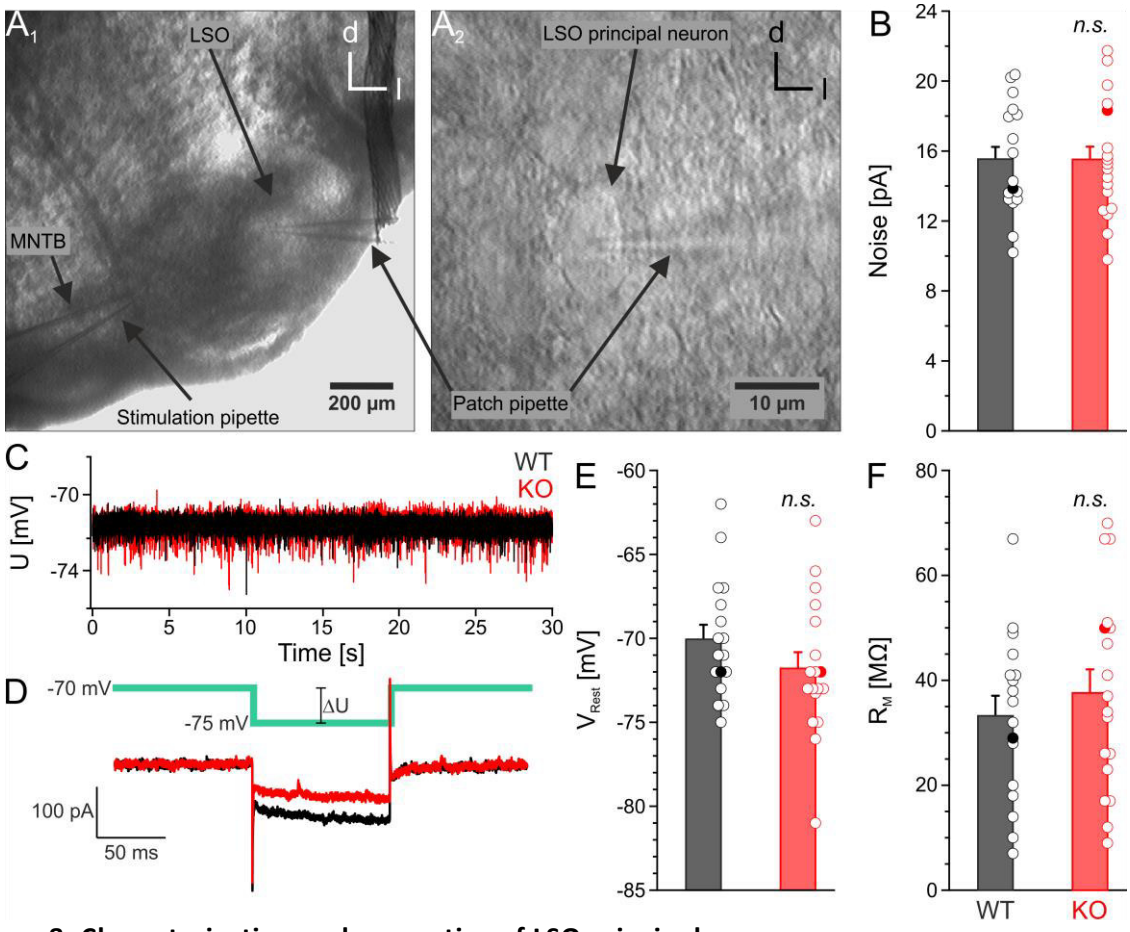

Figure 8: Characterization and properties of LSO principal neurons

A, DIC images of a P20 brainstem slice containing the MNTB and LSO (**A_1**) and of a patched LSO principal neuron (**A_2**). The stimulation pipette was placed at the lateral corner of the ipsilateral MNTB and a LSO principal neuron was patched after visual identification by its typical spindle shape. **B**, Noise of voltage-clamp recordings in WT and KO, which was used to calculate a threshold for failures (2-fold noise criteria; cf. 2.3.5). **C**, Example voltage recordings of a WT and a KO cell used for determining V_{Rest}. **D**, Example current traces during a voltage clamp (green) of -70 mV with a -5 mV step (ΔU) for determining R_M. **E,F**, V_{Rest} and R_M of WT and KO. Filled circles indicate the data of the two example cells shown in C and D. These example cells were used for all example traces in eIPSC figures (WT§, KO§). Details in Table S.1. For significance levels see Table 1. n(cells) = 17(WT) / 18(KO). MNTB = medial nucleus of the trapezoid body, LSO = lateral superior olive, d = dorsal, l = lateral, eIPSC = inhibitory postsynaptic current, *n.s.* = not significant, V_{Rest} = resting membrane potential, R_M = membrane resistance

fusiform somata (Sterenborg et al., 2010; Figure 8A$_2$), whole-cell configuration was established (Hamill et al., 1981). Current or voltage traces were recorded with an EPC10 amplifier and visualized with "PatchMaster 2.40" software (HEKA Elektronik). All recordings were sampled at 20 kHz and low-pass filtered at 7.2 kHz. Series resistances (R_S) ranged from 11-33 MΩ and were compensated by 11-39%. Measurements were rejected if the R_S exceeded 33 MΩ to ensure sufficient electrical and diffusional access to the patched cell (Pusch and Neher, 1988). Voltage-clamp (VC) recordings were performed at a holding potential of -70 mV, which is close to the V_{Rest} of LSO principal neurons (Sterenborg et al., 2010). By executing a set of standard protocols with recordings in VC and current-clamp (CC), basic electrical membrane properties were determined and used for further confirmation of cell identity (Sterenborg et al., 2010) as well as for quality assurance of gathered data. Data were analyzed using "IGOR Pro 6.37" software (WaveMetrics). The noise level was determined in the current recordings during 1 Hz stimulation (cf. 2.3.4) as described in Fischer (2016), chapter 5.5.1), and was the same for WT and KO cells (WT: 15.5 ± 0.8 pA (17), KO: 15.5 ± 0.8 pA (18), p = 0.98748 (*n.s.*)) (Figure 8B), so recordings of WT and KO were not differently impaired. With a voltage recording for 30 s at 0 pA (Figure 8C), V_{Rest} was estimated and was not different between WT and KO (WT: -70.1 ± 0.9 mV (17), KO: -71.8 ± 1.0 mV (18), p = 0.19274; Figure 8E). To determine the membrane resistance (R_M), the R_S was subtracted from the input resistance (R_{In}). R_S and R_{In} were derived from pipette capacitance compensated current traces with a 5-mV hyperpolarizing step for 100 ms (Figure 8D). With 33.2 ± 3.9 MΩ (17) for WT and 37.6 ± 4.5 MΩ (18) for KO, R_M in both genotypes was not different (p = 0.46773, *n.s.*; Figure 8F).

2.3.3. sIPSC properties

For sIPSC analysis, 36 WT and 24 KO cells were patched (Figure 9A$_1$) and used after check of quality criteria (cf. 2.3.2). sIPSCs in a 60 s-lasting VC recording at -70 mV (part of the standard protocols, Figure 9A$_2$) were analyzed for their frequencies, amplitudes and kinetics (10-90% rise time, 100-37% decay time) using Mini Analysis (Synaptosoft; Figure 9B). For kinetics, sIPSCs with correct decay time estimation were chronologically collected until a sufficiently high number for analysis was obtained (WT: n(sIPSCs) = 101 ± 3 (36), KO: n(sIPSCs) = 106 ± 5 (24)). For frequency and amplitude, all sIPSCs of this time segment were analyzed (WT: n(sIPSCs) = 286 ± 25 (36), KO: n(sIPSCs) = 308 ± 31 (24)). The following number of sIPSCs was

analyzed: WT (36): 3630 for kinetics, + 6671 for amplitude/frequency, KO (24): 2551 for kinetics, +4849 for amplitude/frequency. For estimation of the interevent-intervals (IEIs), the time between the peaks of two consecutive sIPSCs was calculated. IEIs of all cells were pooled and grouped in 5-ms bins.

2.3.4. Electrical stimulation of MNTB-LSO synapses

A bipolar stimulation electrode (glass capillary; pulled as described for patch pipettes) with ~20 µm tip diameter was filled with ACSF and connected to a stimulus isolator (STG 4002, Multi-Channel Systems). Using low magnification (4x objective), the electrode was placed at the lateral edge of the ipsilateral MNTB (Figure 8A$_1$, Figure 9A$_1$). Bipolar rectangular current pulses of 200 µs duration and 40-1000 µA intensity were adjusted to yield a maximal but stable postsynaptic response. To obtain the basic synaptic strength, MNTB axons were stimulated with 1 Hz for 60 s. The mean amplitude of the evoked inhibitory postsynaptic currents (eIPSCs) was used for subsequent normalization of eIPSCs, as at 1 Hz no frequency-dependent depression (FDD) is expected (Galarreta and Hestrin, 1998; Kramer et al., 2014; Friauf et al., 2015). To probe for differences between WT and KO to sustain reliable synaptic transmission at high frequencies, 60-s lasting challenges with stimulation at 50, 100 and 200 Hz were performed. Each challenge was followed by a recovery phase at 1 Hz for 60 s, designated as rec50, rec100 or rec200 (Figure 9A$_2$). At the end of each recovery phase, a test pulse with a hyperpolarizing 5 mV step was applied for 100 ms to monitor R_{In}. As R_M is thought to stay stable, a change of R_{In} is counted as an indicator for changes in R_S and hence for the quality of the patch. If R_{In} changed >35% during prolonged recordings, measurements were discarded and consequently the number of analyzed cells is getting less with increasing stimulation frequency (n(cells) at 1/50/100/200 Hz: 17/14/11/10 (WT), 18/18/15/10 (KO)). For an overview of all analyzed cells and their R_{In} changes see Table S.1.

2.3.5. eIPSC properties

Analyzed parameters

eIPSC properties and stimulus artifacts were analyzed with custom-written routines (Dr. Alexander Fischer, Technical University of Kaiserslautern) for IGOR Pro (WaveMetrics) running Patcher's Power Tools (Max Planck-Institute for Membrane Biophysics) as described in Fischer (2016) (Figure 9C). Using this tool, the artifact timing was determined by detecting its local minimum or maximum. Five data points before the onset of the artifact were averaged to

calculate the baseline, also designated as foot of the eIPSC. Additionally, the peak of the eIPSC was determined. With these data points, eIPSC amplitude (ΔY from foot to peak) and latency (ΔX from artifact to peak) were calculated. By dividing the amplitude of an eIPSC by the cell specific q, m for this eIPSC was determined and resembles the number of vesicles released at this event.

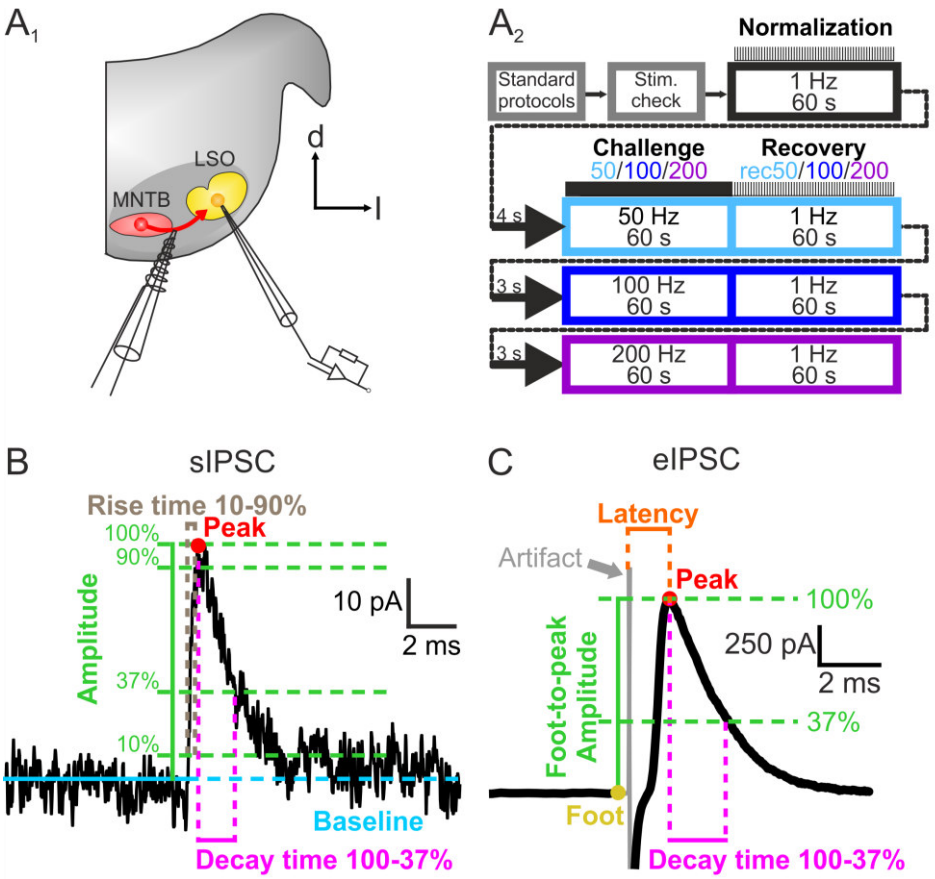

Figure 9: Experimental setup, stimulation protocol, and analysis of IPSC parameters
A, Illustration of experimental setup (**A₁**) and protocol sequence with stimulation protocol (**A₂**). Prior to stimulation, different standard protocols were performed to identify LSO principal neurons and to determine basic membrane properties. Afterwards, MNTB-fibers were stimulated with 1 Hz to check for synaptic connection in a section called stimulation check (Stim. check). Stimulation intensity was adjusted in respect to obtain maximal and stable responses. For normalization of amplitudes, a 1 Hz/60 s stimulation was applied before challenges and recoveries. Consecutively, the challenges with stimulation frequencies of 50 Hz, 100 Hz and 200 Hz for 60 s, respectively, were performed, each of them followed by a 1Hz/60 s recovery phase (rec50, rec100, rec200). **B**, Analyzed parameters of sIPSCs derived from a 60-s current recording included in the standard protocols (A), illustrated at an example sIPSC. The baseline (blue) was calculated by a linear fit through the current trace preceding the sIPSC and the peak (red) was set at its maximum. The ΔY of these two parameters was used to calculate the amplitude (green). ΔX between 10% and 90% amplitude defines the 10-90% rise time (grey), ΔX between peak and 37% amplitude the 100-37% decay time. **C**, Analyzed parameters of eIPSCs. In contrast to sIPSCs, the amplitude was calculated as ΔY between foot and peak ("Foot-to-peak amplitude"). The foot was defined as the average of five data points preceding the stimulus artifact. Latency (orange) describes the ΔX between the stimulus artifact and the peak. IPSC = inhibitory postsynaptic current, sIPSC = spontaneous IPSC, eIPSC = evoked IPSC

Decay time and failure criteria

The eIPSC 100-37% decay time was assessed as described in Fischer (2016). If the eIPSC amplitude was smaller than the 2-fold noise (cf. 2.3.2), the eIPSC was considered as failure and was excluded from decay time analysis. As a further quality criteria for decay time analysis, events with $R^2 \leq 0.8$ of the decay fit were excluded. The term "event" is further on used for the designation of eIPSCs that fulfill all quality criteria. For decay time changes within a genotype, the first ten events were compared with the last ten events of each condition, whereby the last ten events had to be in the last 10 s. This was the case for each cell, so none had to be excluded from analysis. Regarding the comparison between WT and KO, all events were grouped in 5-s bins for 1 Hz conditions (1 Hz, rec50/100/200) and in 1-s bins for higher frequency stimulation (50/100/200 Hz). As a consequence, the comparison between WT and KO could be performed in more detail as it was done for the comparison of the genotypes separately. Regarding decay time analysis of the 200 Hz condition, the superposition of eIPSCs in most cells was so strong that the 37% amplitude was not reached until the next stimulus. Consequently, 200 Hz had to be excluded from decay time analysis.

Latency and $SD_{Latency}$

Latency and its standard deviation ($SD_{Latency}$, also referred to as "latency jitter") was assessed as an indicator of synaptic precision. All eIPSCs with amplitudes above the failure criteria (termed as "events", see above) were taken for analysis. This was performed as described for decay time, but with inclusion of the 200 Hz condition. Regarding the grouping into 1-s or 5-s bins, this means for $SD_{Latency}$ that it is the SD of all latencies in the respective bin. It should be noted that the number of events is higher as for decay time analysis, because eIPSCs used for analysis are not subject to the additional criteria of a good decay time fit. Thus, in some cases the last ten events in latency and $SD_{Latency}$ analysis differ from those in decay time analysis.

2.3.6. FDD and recovery

For analyzing the impact of stimulation frequencies on amplitude depression, the temporal courses of amplitudes were illustrated and the average of the last ten amplitudes were compared between the different challenges with paired *t*-test for WT and KO separately. For the comparison between the genotypes, the amplitudes were normalized to the mean amplitude of the 1 Hz situation. This avoids falsification of data analysis due to a possible

GlyT1-loss-driven impairment of synapse development. The recovery of amplitudes was also analyzed to get a further impression of the synapse robustness. For better visibility, the courses were smoothed with 5% of the data points (data points/5%: 60/3 (1 Hz, rec50/100/200), 3000/150 (50 Hz), 6000/300 (100 Hz), 12000/600 (200 Hz)). Smoothed data were used only for illustration but not for statistics.

2.3.7. Fidelity

Fidelity was analyzed as another parameter indicative for reliable synaptic transmission. eIPSCs with amplitudes above the 2-fold noise level were counted as events (= responded stimuli) with a fidelity of 100%. Below this threshold, eIPSCs were designated as failures (cf. 2.3.5) with 0% fidelity. For illustration, fidelity courses were smoothed with 5% of the data points as described in 2.3.6. To calculate potential differences between the different stimulation frequencies or genotypes, the fidelity of the eIPSCs in the last 10 s was assessed.

2.3.8. Synapse properties

To analyze synapse specific properties, several parameters were analyzed. However, it must be noted that this analysis refers to the complete synaptic input and not to a single synapse.

Basic synaptic strength

One parameter analyzed was the basic synaptic strength, determined by the total amplitudes during 1 Hz stimulation. As no FDD occurs at this stimulation frequency, the mean of these amplitudes were considered as the 100% amplitude and were used for subsequent normalization.

Quantal size (q)

q describes the postsynaptic current elicited by the transmitter release of one vesicle (Katz, 1971). For determination, sIPSC amplitudes (n(sIPSCs) ≥ 100; cf. 2.3.3) were grouped into 5-pA bins and plotted in a histogram (Figure 11). A Gaussian fit was performed on the distribution ranging from the first bin without sIPSCs to the bin after the first maximum (Krachan et al., 2017) and with the condition Y(0) = 0. The X-value of the Gaussian curves peak indicates q. sIPSCs with an amplitude similar to q are also designated as miniature IPSC (mISPC; for example see Figure 15D_1).

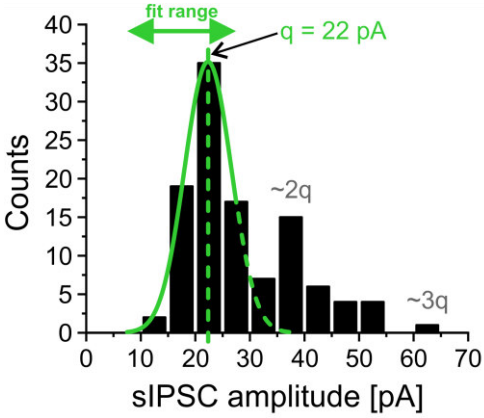

Figure 11: Determination of q
For each cell, q was determined by performing a Gaussian fit (solid green line) in a sIPSC amplitude histogram (bin size 5 pA), shown here for an example cell. The borders for the fit were set before the first bin and after the first local maximum. The X-value of the peak was used as q value. The second maximum in the amplitude histogram is caused by the simultaneous release of two vesicles (2q) and the third by three vesicles (3q). The probability for such events decreases with higher number of simultaneously released vesicles. sIPSC = spontaneous inhibitory postsynaptic current, q = quantal size

Readily releasable pool (RRP), quantal content (m), and release probability (P_r)

Further important synapse properties are the RRP and P_r. The RRP is used as a term for all vesicles of a synaptic input that can fuse upon a stimulus with the plasma membrane and release neurotransmitter, leading to a current in the postsynapse (I_{RRP}; for review see Kaeser and Regehr, 2017). However, not all vesicles of the RRP are released at once, as their release depends on several parameters involved in vesicle fusion leading to a certain P_r. This parameter is calculated by the ratio of the first eIPSC ($eIPSC_1$) amplitude and the I_{RRP}. To determine the I_{RRP}, a method described by Elmqvist and Quastel (1965) (EQ method) was used (Figure 10). This method hypothesizes that the first PSC amplitudes during a stimulation with a sufficiently high frequency can be used to determine the RRP before the beginning of stimulation. The hypothesis is based on studies showing that the refilling of the presynaptic vesicle pool via replenishment occurs only after a delay of several milliseconds (for review see

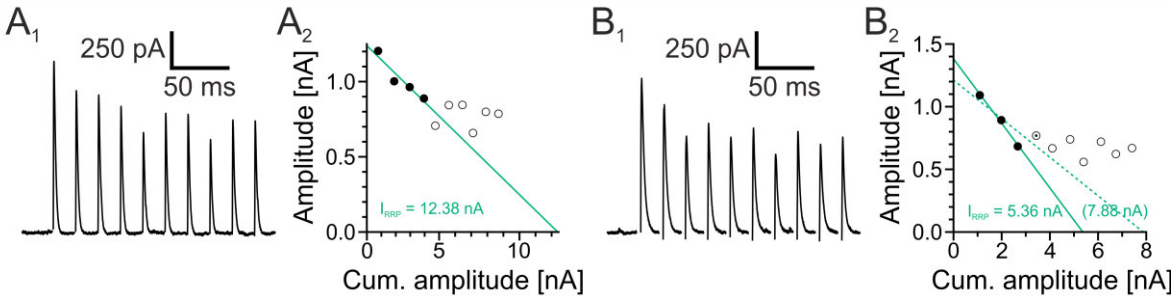

Figure 10: RRP calculation
Illustration of RRP calculation with the Elmqvist and Quastel method by the example of two example recordings at 50 Hz stimulation. **A,** eIPSCs (**A_1**) were plotted with their absolute (Y-axis) and cumulative amplitude (X-axis) (**A_2**). A linear fit was drawn through the first four data points. The intersection of the X-axis was taken as I_{RRP} value. **B,** If the 4th eIPSC had a higher amplitude than the 3rd (**B_1**), this could indicate a contribution of newly replenished vesicles to the 4th response. To isolate the initial RRP, the fit was therefore drawn only through the first three data points (**B_2**). eIPSC = evoked inhibitory postsynaptic current, RRP = readily releasable pool

Kaeser and Regehr, 2017). Accordingly, in my study the first four eIPSCs of 50, 100 and 200 Hz were used for RRP determination. To do so, eIPSC amplitudes (Figure 10A$_1$) were plotted with their absolute (Y-axis) and cumulative amplitudes (X-axis). A linear fit (green line) through the first four data points was calculated and the X-axis intersection was taken as I_{RRP} value (Figure 10A$_2$). To avoid overestimation of I_{RRP} due to an early onset of vesicle replenishment (dotted green line, I_{RRP} value in brackets), the fit was drawn through the first three eIPSC data points only if the 4th had a higher amplitude than the 3rd eIPSC (Figure 10B). Amplitudes and I_{RRP} can be converted into vesicle units by dividing them by q, so eIPSC$_1$ amplitude can be expressed as m of eIPSC$_1$ (m_1) and I_{RRP} as N_{RRP}. Hence, m_1 resembles the vesicle number released upon the first stimulus, and N_{RRP} the number of vesicles stored in the RRP. As I_{RRP} could not be defined in some rare cases, also P_r and N_{RRP} could not be determined for these cells.

2.3.9. Challenge-induced changes of synapse properties

A reduction in amplitudes can result from a lower amount of released transmitter, but also from an impaired vesicle refilling as it appears to be the case in GlyT2 KO mice (Gomeza et al., 2003b). To check this, q was determined *de novo* with sIPSCs occurring in the last 10 s of a condition ($q_{Last\ 10\ s}$; for example see Figure 22). As the minimal number of sIPSCs to estimate q was set to n(sIPSC) ≥ 30, some KO cells had to be excluded from analysis as n(sIPSC) was too small (number of excluded cells: 50 Hz: 1, rec50: 1, 100 Hz: 3, rec100: 1). In WT cells, the critical sIPSC number was always reached or exceeded. For rec50, in two WT cells bin size had to be halved, as otherwise no converging fit could be calculated (Figure 12). This was because the fit range (cf. 2.3.8) only included two 5-pA bins with sIPSCs and therefore insufficient data for fit calculation. Because of the superposition of eIPSCs during 200 Hz stimulation, no sIPSCs

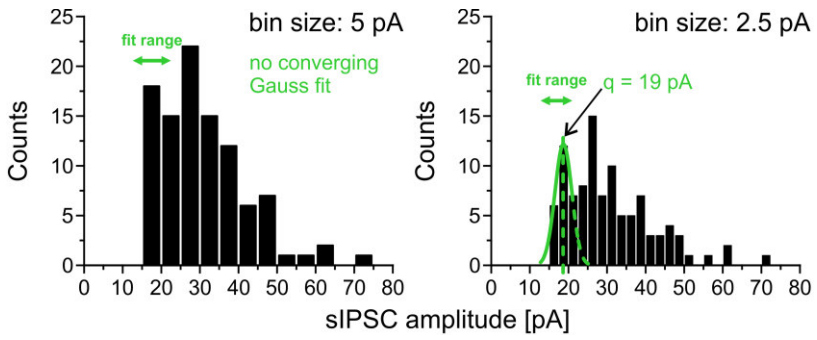

Figure 12: Adjustment of bin size for q determination
In two cases, bin size for q determination had to be halved from 5 to 2.5 pA, because a Gaussian fit needs a minimum of three bins for convergence. q = quantal size

could be analyzed and therefore no $q_{Last\ 10\ s}$ could be determined for this condition. As data were compared with the preceding condition to find changes, $q_{Last\ 10\ s}$ for rec200 was also not analyzed. $q_{Last\ 10\ s}$ was normalized to q of the standard protocols (cf. 2.3.8) and compared to this basic value. Additionally, data were compared to the preceding $q_{Last\ 10\ s}$. To check if the m is reduced, amplitudes of the last 10 s were averaged and via division with $q_{Last\ 10\ s}$ converted into m (cf. 2.3.8).

2.4. Data presentation and statistics

WT and KO data are presented in black and red, respectively, if not stated otherwise. Depending on kind of analysis, n resembles the number of animals, tissue samples or number of cells, and is indicated in figure legends and tables. Mean is always calculated as arithmetic mean and is illustrated as bars + standard error of the mean (SEM) or bold lines/symbols ± SEM. If the overlap of SEMs was too strong to distinguish between WT and KO, only + SEM or - SEM is depicted (Figure 15B$_2$). Single cell values are presented as circles or thin lines. For better visibility, temporal courses of amplitudes and fidelity were smoothed in Origin 2017G with 5% of the data points (cf. 2.3.6), but were not used for statistical analysis.

As example cells for sIPSC properties, the cells with the ID 15073201_S1-C2 for WT and 15053304_ki_S3-C2 for KO were chosen because of their accordance to mean values. In figures with population data, their single values are presented as filled circles. For eIPSC figures, the cells 15063105_S2-C3 for WT and 15061101_S1-C3 for KO were chosen as example cells based on their participation in all analyses of all applied frequencies and their proximity to mean values in analyses of normalized amplitudes. As these cells were kept as example cells for all eIPSC figures, they do not represent the mean in all analyses. But to give a good overview of the behavior of a single cell and therefore enable the traceability of this cell throughout all eIPSC figures, I decided to keep them as example cells. These example cells are indicated in some eIPSC figures with the symbol character “WT§“ or “KO§“. Additionally, the connection of different properties to a distinct cell was enabled by using continuous color coding throughout all eIPSC figures with single cell data (Increment list Q11 Candy, Origin 2017G) (for color code and the corresponding cell ID see Table S.1).

Statistical analyses were performed on original data with Excel 2013 except for outlier detection, normal distribution testing, Wilcoxon-test and Mann-Whitney *U*-test, which were done with the Excel plugin Winstat 2012.1 (R. Fitch Software). Outliers were defined as data

points located beyond the 95% confidence interval of the total population. Subsequently, they were excluded from mean calculation and statistics, but were indicated in figures as cross-marked circles. In tables, the reduced sample size is depicted separately. Remaining data were checked for normal distribution (Kolmogorov-Smirnov). With a Kolmogorov-Smirnov p value ≥ 0.05, distribution was considered as normal and a paired or unpaired *t*-test was performed. For GlyT1 content and decay time analysis, one-tailed *t*-test was applied, for all other analyses the two-tailed *t*-test. If unpaired, F-test was applied to check for variance. For F-test p values ≥ 0.05, variance was considered as equal (homoscedastic), for values < 0.05 as unequal (heteroscedastic). If testing for normal distribution was negative (Kolmogorov-Smirnov p value < 0.05), Wilcoxon-test for paired and Mann-Whitney *U*-test for unpaired data was performed. If not stated otherwise in table legends, Student's *t*-test was used. In case of multiple comparisons, *post hoc* Šidák correction was applied (Abdi, 2007), whereby horizontal (within a genotype) and vertical (between WT and KO) comparisons were analyzed independently from each other. The significance levels are shown in Table 1 and are indicated in figures with *n.s.* (not significant) or no labeling, * (no Šidák correction), or # (Šidák corrected). In cases of insufficient data amount for statistical analyses (n < 7) or missing values because of a failed fit/analysis (e.g. RRP or q determination), this is indicated in figures and tables with n.d. (not determined).

Table 1: Significance levels

number of comparisons	1		2	3	4	5	6	
Significance levels	<0.05000	*	<0.02532	<0.01695	<0.01274	<0.01021	<0.00851	#
	<0.01000	**	<0.00501	<0.00334	<0.00251	<0.00201	<0.00167	##
	<0.00100	***	<0.00050	<0.00033	<0.00025	<0.00020	<0.00017	###

Significance levels are indicated with asterisks. In case of multiple comparisons, significance levels were *post hoc* Šidák corrected and indicated with hash tags.

3. RESULTS

3.1. GlyT1b/c KO mouse model

Some aspects regarding the characterization of the GlyT1b/c mouse model were described by Schuster (2015). But it is important to be aware that diverse environmental influences, such as different housing and breeding conditions, can affect birth rate, gain in weight, and survival. For example, mice employed in the Schuster study were kept 1:2 (male:female) in one cage for breeding, enhancing survival probability due to better nursing and caring of pubs. In my study, mice were kept 1:1 (cf. 2.1.1). Hence, I performed the most basic characterization like birth rate, body weight increase and survival rate separately for my study.

3.1.1. Normal birth rate of KO mice, but impaired gain in weight

The Mendelian distribution predicts a proportion of 25%:50%:25% of WT, HT and KO, respectively. I found a non-significant shift from KO towards WT and HT (26%:53%:21%, n = 504, p = 0.65051 (χ^2 test); Figure 13A). At P7, KO mice were indistinguishable from WT regarding body size and weight. This changed with increasing age. At P20, KO mice were smaller and appeared weaker (Figure 13B). To analyze possible developmental impairments due to GlyT1b/c KO, the body weight was measured at P7 and P20 (Figure 13C). The reason to choose these two ages is due to the fact that at P7 mainly the isoform GlyT1a is expressed and so no impairment should be observed at this age. In contrast, KO mice at P20 were expected to suffer from a systemic GlyT1 KO as the expression of GlyT1a shifts to GlyT1b/c until this age (Schuster, 2015). At P7, there was no difference in bodyweight (in [g]: WT: 4.17 ± 0.24, 7 mice; KO: 3.76 ± 0.22, 9 mice; p = 0.22931). In contrast to this, KO mice at P20 had significantly less body weight compared to their WT littermates (in [g]: WT: 8.53 ± 0.18, 50 mice; KO: 5.91 ± 0.15, 48 mice; $p = 8.9 \times 10^{-19}$). Thus, KO mice gained only half the weight as WT mice from P7 to P20 (WT: +101%, KO: +52%).

Taken together, KO mice appeared to have a normal prenatal development, but suffer from impairments during postnatal development.

3.1.2. KO mice do not suffer from reduced survival rate

The survival rate of WT, HT and KO mice was analyzed via Kaplan-Meyer estimation. KO mice revealed a slightly decreased survival probability (Figure 13D$_1$). Until P2, KO exhibited a 5% lower probability to survive. Until P30, the highest age analyzed in KO, the survival probability remained reduced by 3% compared to WT. Nevertheless, the Mantel-Cox logrank test revealed no significant difference between WT and KO ($p = 0.30290$). Regarding HT mice, they had a higher survival rate compared to KO for nearly the complete observation period, but during P11-38 it was also even higher compared to WT. Nevertheless, it has to be considered

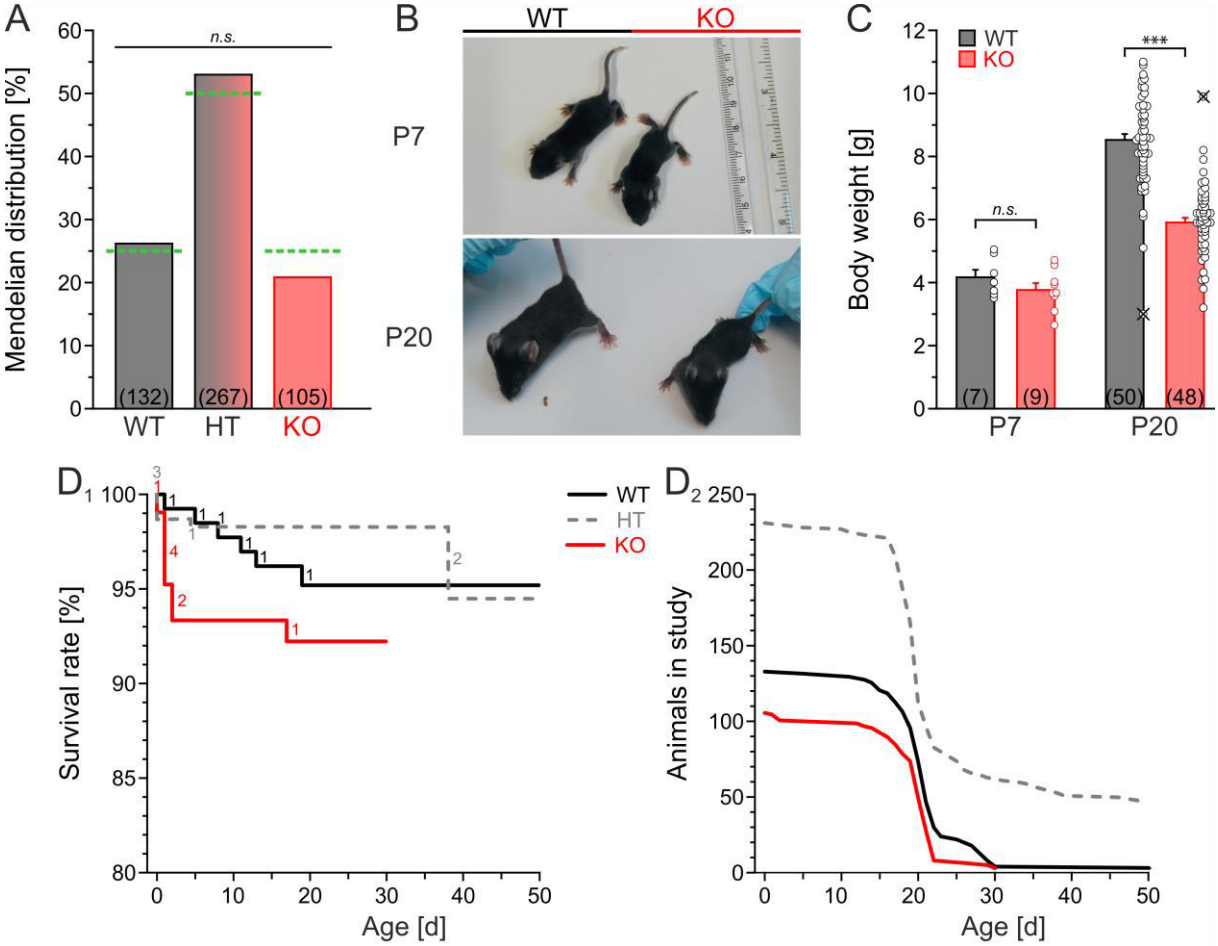

Figure 13: KO mice have a reduced gain of weight, but show a normal birth- and survival rate
A, Mendelian distribution of the genotypes. Green dashed lines indicate the expected distribution. Numbers in brackets depict sample sizes (animals). χ^2 test revealed no significant difference. **B**, WT (left) and KO (right) mice at P7 and P20. **C**, Body weight of WT and KO mice at P7 and P20. Cross-marked circles indicate outliers, numbers in brackets depict sample sizes (animals), outliers excluded. **D**, Survival analysis (cf. 2.1.4). **D$_1$**, Kaplan-Meier plot indicating the survival rate of the different genotypes. Numbers at curves depict the absolute number of events (natural deaths), consequently leading to a decrease of survival rate. **D$_2$**, Decreasing number of animals over time due to experiments, killings or natural deaths. For significance levels see Table 1. WT = wildtype, HT = heterozygous, KO = knockout, *n.s.* = not significant

that the WT and KO cohorts were very small after P21 due to their use for electrophysiological experiments and western blotting (Figure 13D$_2$). So WT and KO survival rates are not reliable beyond this age. For numbers see Table S.2.

In summary, natural death occurred more often in KO as in WT or HT during the first two days after birth. Afterwards, this effect appeared to be reversed, resulting in a WT-like progression of survival rate.

3.2. GlyT1 content in KO brainstems is severely reduced and not compensated by GlyT2

To verify the KO, brainstem tissue samples were tested with respect to the GlyT1 protein levels. Additionally, GlyT2 content was analyzed as an enhanced expression could compensate the lack of GlyT1. GlyT1 and GlyT2 were detected at the expected band sizes of ~70 kDa (Guastella et al., 1992; Zafra et al., 1995; Figure 14A), and ~75 kDa (Zafra et al., 1995; Aroeira et al., 2014), respectively. As both transporters tend to form oligomers (Horiuchi et al., 2001; Bartholomaus et al., 2008), bands appearing above these sizes are caused by homodimers

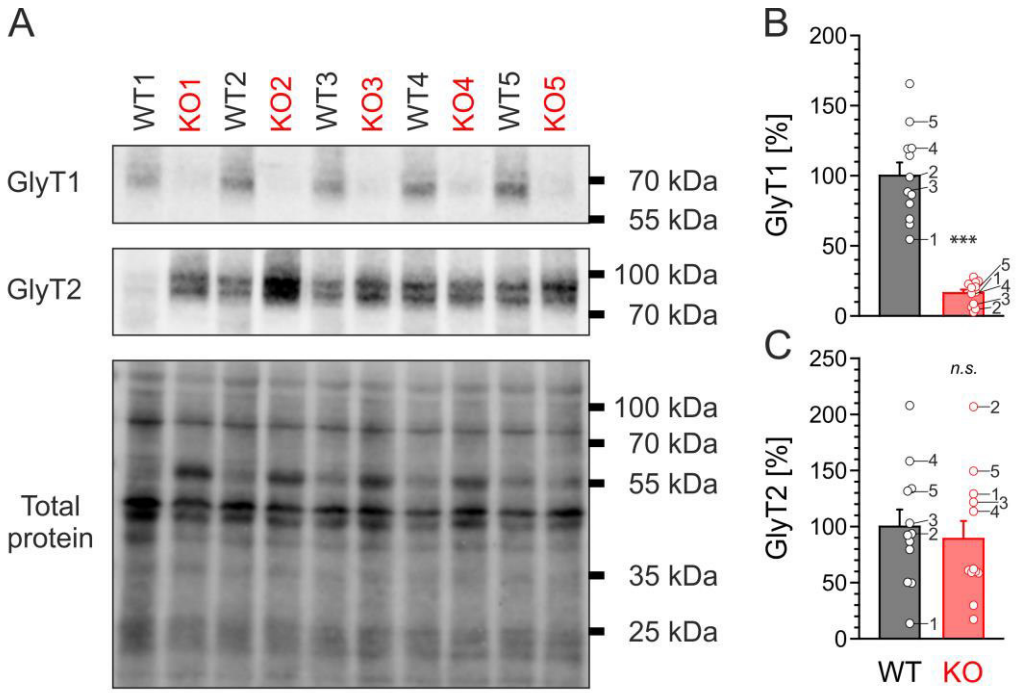

Figure 14: GlyT1 content in KO brainstems is severely reduced, and not compensated by increased GlyT2 expression

A, Example western blot of GlyT1 and GlyT2 of five WT and five KO brainstem samples. GlyT1 and GlyT2 signals were detected at their expected molecular weight of ~70 kDa and ~87 kDa, respectively. Total protein staining was used as loading control (cf. 2.2.6). **B**,**C**, GlyT1 and GlyT2 content, respectively. Single cell data derived from blot shown in A are marked with respective numbers. In total, three blots were analyzed with two technical replicates for each blot. n(tissue samples) = 12(WT) / 12(KO). Details in Table 2. For significance levels see Table 1 and for absolute values Table S.3. *n.s.* = not significant

or -oligomers. Total protein staining for normalization resulted in a quite similar pattern for WT and KO, except for one band at 55 kDa. GlyT1 antibody signals were background subtracted and normalized to the total protein staining. The mean intensity of WT was set to 100%. This revealed a highly significant GlyT1 reduction of 84% in KO ($p = 6.5 \times 10^{-7}$; Figure 14B, Table 2). In contrast, GlyT2 expression was very heterogeneous with the same extent of minimal and maximal values in WT and KO. Thus, the assumption that GlyT2 is overexpressed as a compensatory mechanism was not confirmed. Actually, the expression was reduced by 11%, but this decline was not significant due to similar standard errors of the mean (Figure 14C, Table 2; for absolute values see Table S.3).

Based on the findings for GlyT1 and GlyT2 content, a tremendous decrease of GlyT1 was observed with no concomitant increase in GlyT2, confirming the functionality of the KO for my experiments.

Table 2: GlyT1 and GlyT2 contents in brainstem

Genotype:	WT (12)	KO (12)	p value	significance
GlyT1 [%]	100 ± 33	16 ± 9	6.5×10^{-7}	***
GlyT2 [%]	100 ± 53	89 ± 55	0.62433	*n.s.*

Data are presented as normalized mean ± SEM of the GlyT1 and GlyT2 antibody signal, respectively, obtained from western blotting (cf. Figure 14). Data were normalized to the mean absolute value of WT (cf. 2.2.6). Numbers in brackets depict sample sizes (number of tissues). For significance levels see Table 1. *n.s.* = not significant

3.3. Spontaneous transmission to LSO principal neurons

Former studies revealed that loss of GlyT2 leads to decreased amplitudes and a reduced occurrence of sIPSCs at hypoglossal motoneurons and dissociated spinal neurons (Gomeza et al., 2003b; Latal et al., 2010). In contrast, a study which examined the effects of GlyT1 loss at hypoglossal motoneurons revealed no changes in sIPSC amplitudes but a prolonged decay time (Gomeza et al., 2003a), underlining the importance of GlyT1 for lowering glycine concentrations at inhibitory synapses. Regarding this, I wanted to find out if there are also changes in spontaneous inhibitory neurotransmission to the LSO, mediated by synapses with high requirements on fast and reliable transmission.

3.3.1. GlyT1 loss does not change sIPSC occurrence

In contrast to Gomeza et al. (2003a), synaptic noise was not increased in KO recordings (Figure 8B, Figure 15A$_{1,2}$). For sIPSC frequency, all sIPSCs were analyzed and revealed a tendential decrease in KO (KO/WT: 69%, p = 0.25776; Figure 15A$_3$, Table 3). To gain insight into the frequency of any analyzed parameter, the occurrence per time interval is a very imprecise measurement. Periods with a high and a low frequency within the observed time interval would result in the same value as a mean frequency during the complete time interval. Thus, a more detailed analysis was performed consisting in the calculation of sIPSC IEIs. This revealed the 5-10 ms IEI as the mainly occurring interval in WT and KO (WT: 15 ± 2% (36), KO: 12 ± 2% (24), p = 0.30152; Figure 15B$_1$). In total, the IEI distribution was quite similar except for a slightly higher percentage of longer IEIs in KO as indicated by the stronger slope of the cumulative IEI plot, particularly for IEIs >250 ms (Figure 15B$_2$).

Concluding from these observations, only a slight decrease in sIPSC frequency was observed in KO, which was not significantly different.

3.3.2. GlyT1 loss does not affect sIPSC properties and q

To analyze further differences in sIPSC properties, amplitudes, rise times, and decay times were compared (Figure 15C, Table 3). Regarding sIPSC amplitudes, no significant difference could be detected (KO/WT: 93%; p = 0.25027; Figure 15C$_{1,2}$). For rise time and decay time analysis, sIPSCs of which kinetics could not be determined (due to overlapping with other sIPSCs) were excluded (Figure 15A$_2$, open arrows). KO sIPSCs appeared to have prolonged kinetics (KO/WT: 112% rise time, 117% decay time), but were not significantly different (rise time: p = 0.06849, decay time: p = 0.06047; Figure 15C$_{3,4}$). Furthermore, q was estimated (Figure 15D$_1$). This parameter resembles the approximate sIPSC amplitude elicited by the release of one vesicle (cf. 2.3.8). Amplitude distribution was quite similar for WT and KO, exemplarily shown in Figure 15D$_2$. Consequently, q was not significantly different (KO/WT: 97%, p = 0.52345).

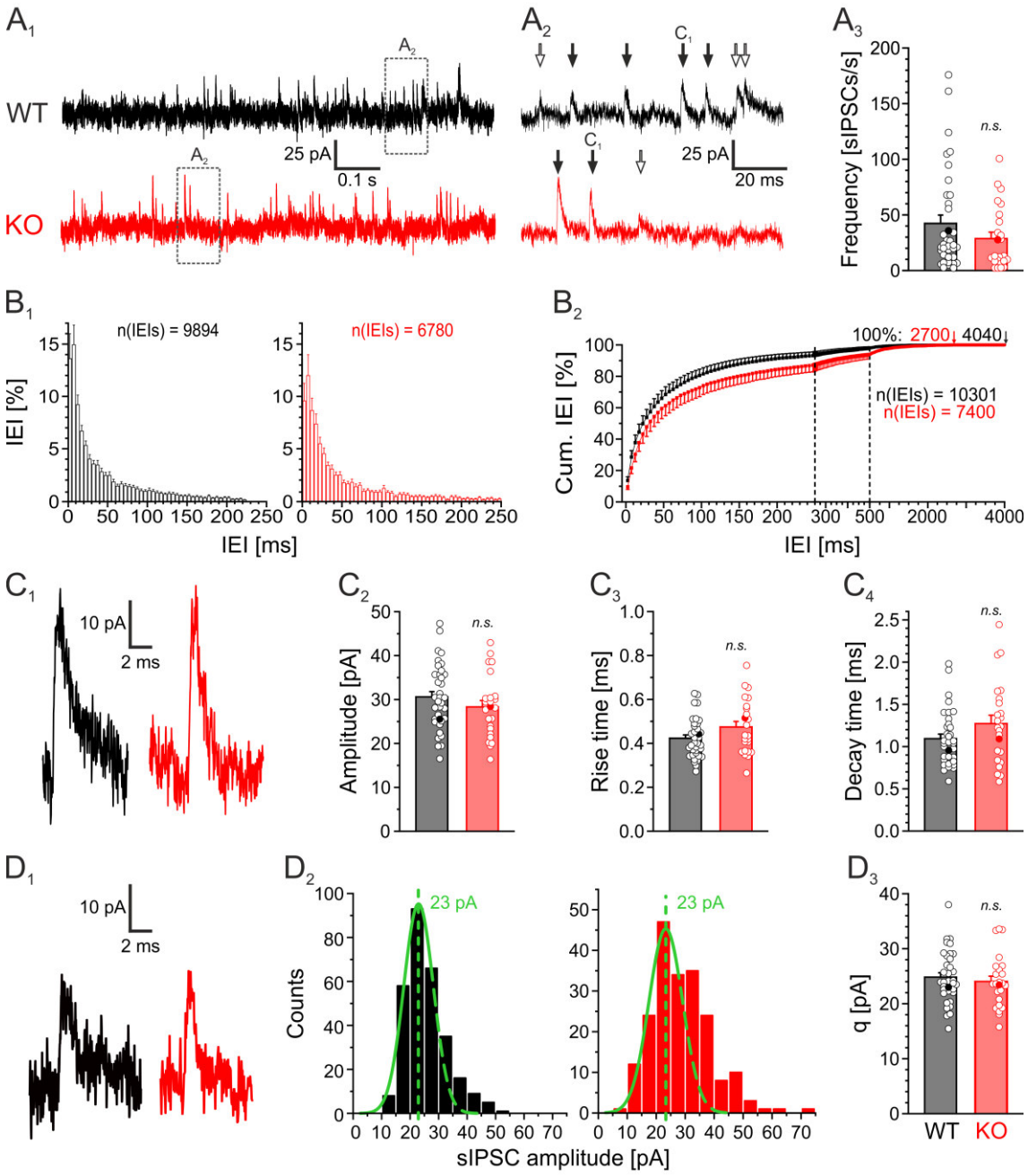

Figure 15: Loss of GlyT1 does not change sIPSC properties

A, sIPSC frequency. **A_1**, 1 s section of a voltage-clamp recording of two example cells. Boxes mark 100 ms-time frames enlarged in A_2. **A_2**, Arrows indicate events used for analysis; only events tagged with filled arrows were also used for rise time and decay time analysis due to quality criteria (cf. 2.3.3). **A_3**, sIPSC frequency of WT and KO. **B**, Fraction of IEIs grouped in 5-ms bins in a range of 5-250 ms (**B_1**) and as a cumulative plot of all IEIs (**B_2**). Dashed lines in B_2 mark segments of the X-axis with different time scales. The total amount of analyzed IEIs is indicated in the figures (n(IEIs)) as well as the maximal IEI (100%). **C**, sIPSC properties. **C_1**, Two example sIPSCs originating from the traces in A_2. **C_2-C_4**, Property analysis comprised amplitude, 10-90% rise time, and 100-37% decay time. **D**, Analysis of q. **D_1**, Two example sIPSCs with an amplitude elicited by the transmitter release of a single vesicle. **D_2**, Illustration of q determination for the two example cells (cf. 2.3.8). **D_3**, q of WT and KO. Filled circles indicate the values obtained from the two example cells, which were the same for all analyses shown in this figure. For details see Table 3. For significance levels see Table 1. n(cells) = 36(WT) / 24(KO). *n.s.* = not significant, IEI = interevent-interval, q = quantal size

Table 3: sIPSC properties and q

Genotype:		WT (36)	KO (24)	p value	significance
Frequency	[s^{-1}]	42 ± 8	29 ± 6	0.25776[a]	*n.s.*
Amplitude	[pA]	31 ± 1	28 ± 1	0.25027	*n.s.*
Rise time	[ms]	0.42 ± 0.02	0.47 ± 0.03	0.06849	*n.s.*
Decay time	[ms]	1.09 ± 0.05	1.27 ± 0.10	0.06047	*n.s.*
Quantal size (q)	[pA]	25 ± 1	24 ± 1	0.52345	*n.s.*

Data are presented as mean ± SEM (cf. Figure 15). Numbers in brackets depict sample sizes (number of cells). [a]: Mann-Whitney *U*-test. For significance levels see Table 1. *n.s.* = not significant, q = quantal size

Summing this up, sIPSCs occurrence in KO was not significantly different from WT, and q as well as amplitudes were similar. Nevertheless, the kinetics were tendentially increased (rise time: +12%, decay time: +17%), but not to the same extent as described in the study of Gomeza et al. (2003a). To examine if an enhanced amount of released glycine leads to different synaptic behavior, I performed maximal electrical stimulation, resulting in multiple vesicle release.

3.4. WT and KO MNTB-LSO synapses exhibit similar basic synaptic strength at 1 Hz stimulation

Synaptic strength is considered as an indicator of synaptic robustness to withstand stress caused by ongoing stimulation (Friauf et al., 2015). As a basal strength value of WT synapses, the amplitudes during stimulation with 1 Hz were examined as no synaptic depression is expected for this frequency at the MNTB-LSO synapse (Kramer et al., 2014). In Figure 16A$_1$, current recordings of two example cells (WT§, KO§) are depicted, exhibiting robust responses to each stimulus. As no depression was observed, the means of the 1 Hz amplitudes were set to 100% (WT§: 971 pA, KO§: 930 pA; Figure 16A$_2$) and were used for normalization of the amplitudes at higher stimulation frequencies. Like the example cells, all other cells showed no depression during 1 Hz stimulation (Figure 16B) and responded to each stimulus. Accordingly, responses during 1 Hz stimulation were considered as basic synaptic strength in both genotypes and the mean amplitudes were set to 100%. Even though every excitation was executed with the highest possible current (cf. 2.3.4), WT and KO responses had a very broad amplitude range. Remarkably, the majority of cells exhibited a so-called “manic” first pulse, i.e. the first eIPSC (eIPSC$_1$) overshoots to abnormally high values at the beginning of a stimulus

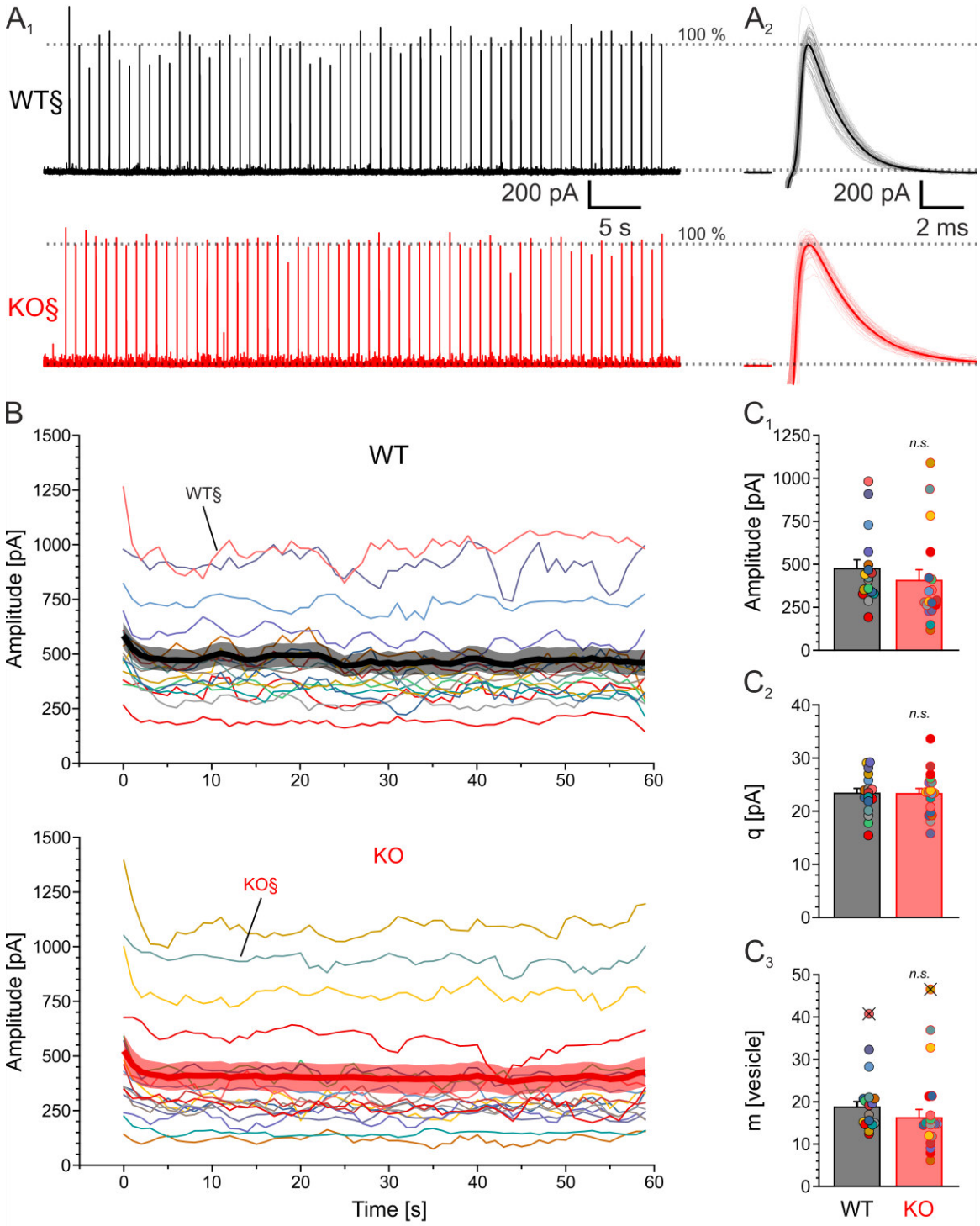

Figure 16: Similar basic synaptic strength in WT and KO

A, eIPSCs of two example cells (WT§, KO§) with blanked stimulus artifacts during 1 Hz stimulation. **A_1**, Voltage-clamp recordings for 60 s. **A_2**, Overlay of the 60 eIPSCs with the mean highlighted with a thick line. **B**, Amplitude courses of WT (upper panel) and KO (lower panel) with the mean highlighted with a bold line ± SEM. For clarity, the courses were smoothed with a moving average of three data points. The courses of the example cells shown in A are indicated. **C**, Analysis of basic synaptic strength: mean amplitudes during 1 Hz stimulation (**C_1**), q (**C_2**), and m (**C_3**). m indicates the mean amount of vesicles released at one response during 1 Hz stimulation (cf. 2.3.8). q of cells not used for eIPSC analysis were omitted (cf. Figure 15D_3). Outliers are indicated with cross-marked circles. For details see Table 4 and for significance levels Table 1. n (cells) = 17(WT) / 18(KO), outliers included. eIPSC = evoked inhibitory postsynaptic current, *n.s.* = not significant, q = quantal size, m = quantal content

train after a silent episode (cf. Figure 9A$_2$), presumably because of a transiently overfilling of the RRP and/or high P_r (Friauf et al., 2015). This behavior was not changed due to loss of GlyT1 as the ratio of eIPSC$_1$ to eIPSC$_2$ was similar (eIPSC$_1$/eIPSC$_2$ in %: WT 114 ± 5 (17), KO 118 ± 6 (18), p = 0.54162). The mean amplitude of KO reached only 85% of WT, but was not significantly different (p = 0.40589; Figure 16C$_1$, Table 4), indicating a similar basic synaptic strength with a similar SEM. By dividing amplitude by q (Figure 16C$_2$), m was calculated (Figure 16C$_3$). With a range from 12 to 32 vesicles in WT synapses (n = 16) and 6 to 37 vesicles in KO synapses (n = 17) as well as one outlier, respectively (WT: 41 vesicles, KO: 47 vesicles), the mean was not significantly different (p = 0.23707; Table 4).

To sum this up, a similar broad variance in amplitudes elicited by 1 Hz stimulation was observed. Converted into vesicles, one stimulus led to the release of ~19 vesicles in WT and ~16 vesicles in KO. With this it can be stated that WT and KO had the same starting conditions for the ensuing challenges.

Table 4: Basic synaptic strength

Genotype:		WT (17)	KO (18)	p value	significance
1 Hz amplitude	[pA]	475 ± 52	405 ± 64	0.40589	*n.s.*
quantal size (q)	[pA]	23 ± 1	23 ± 1	0.95026	*n.s.*
quantal content (m)	[vesicle]	19 ± 1 (16)	16 ± 2 (17)	0.23707	*n.s.*

Data are presented as mean ± SEM (cf. Figure 16). Numbers in brackets depict sample size (number of cells). Reduced sample sizes due to outliers are indicated in brackets at the affected datasets. For significance levels see Table 1. *n.s.* = not significant

3.5. FDD and recovery of the MNTB-LSO synapse

As a lack of GlyT1 could have a strong effect on postsynaptic responses and therefore on synaptic efficacy due to its function in glycine removal, the extent of amplitude depression depending on frequency was examined. Additionally, the recovery was analyzed as a further important feature in determining synapse efficacy. To enable a comparison between cells, values were normalized to the mean value of 1 Hz amplitudes shown in Figure 16A (cf. 2.3.4). Regarding the example cells (Figure 17), stimulation at 50 Hz (3000 stimuli; Figure 17A) resulted in a less fast and milder depression in WT§ as in KO§, and was followed by a faster but finally weaker recovery. In both cells, all stimuli during 50 Hz and rec50 were responded.

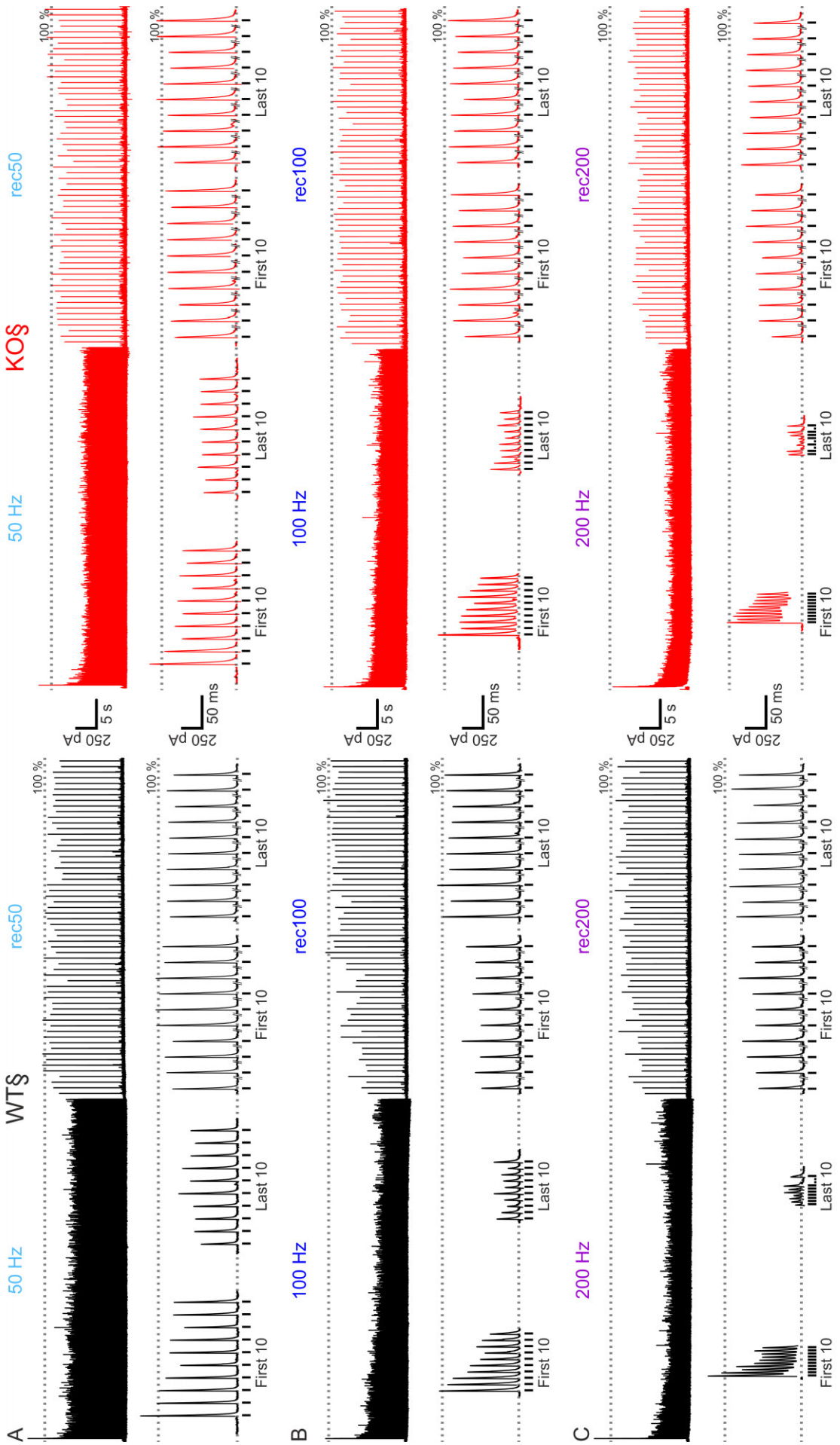

Figure 17: FDD and recovery of example cells
For legend see next page.

Figure 17: (continued) FDD and recovery of example cells
FDD of the two example cells for WT and KO (WT§, left; KO§, right) during stimulation with 50 Hz (**A**), 100 Hz (**B**), and 200 Hz (**C**) with subsequent 1 Hz recovery (rec50, rec100 and rec200). Dashed lines mark the 100% values determined by the mean amplitude during the preceding 1 Hz stimulation (Figure 16C$_1$). Below each trace the first and last ten eIPSCs are magnified. Black bars indicate responded stimuli, dots indicate non-responded stimuli (= failures). For better visibility artifacts were blanked. eIPSC = evoked inhibitory postsynaptic current

Table 5: FDD and recovery of example cells

Condition		Amplitude			
	eIPSCs	WT§		KO§	
		[pA]	[%]	[pA]	[%]
50 Hz	first 10	870 ± 50	89 ± 5	741 ± 48	79 ± 5
	last 10	575 ± 25	59 ± 3	454 ± 14	48 ± 1
rec50	first 10	923 ± 26	94 ± 3	828 ± 17	88 ± 2
	last 10	833 ± 11	85 ± 1	909 ± 28	97 ± 3
100 Hz	first 10	628 ± 68	64 ± 7	662 ± 49	71 ± 5
	last 10	224 ± 20	23 ± 2	253 ± 20	27 ± 2
rec100	first 10	561 ± 26	57 ± 3	775 ± 20	83 ± 2
	last 10	907 ± 20	92 ± 2	800 ± 20	85 ± 2
200 Hz	first 10	598 ± 76	61 ± 8	547 ± 51	58 ± 5
	last 10	121 ± 23	12 ± 2	112 ± 26	12 ± 3
rec200	first 10	643 ± 25	66 ± 3	558 ± 28	60 ± 3
	last 10	816 ± 27	83 ± 3	663 ± 15	71 ± 2

Data are presented as mean amplitudes ± SEM of the first and last 10 eIPSCs as absolute and normalized values of the example cells for WT and KO (WT§/KO§, cf. Figure 17).

At 100 Hz (6000 stimuli; Figure 17B) depression in WT§ was stronger and more stimuli were not responded (failures: WT§ = 22, KO§ = 1). Additionally, WT§ needed longer for recovery, but at the end, the amplitudes were closer to 100% as in KO§. In both cells, all stimuli at rec100 were responded. Regarding 200 Hz (12000 stimuli; Figure 17C), the depression was quite similar with more failures in KO§ (WT§ = 1757, KO§ = 2333). During recovery of 200 Hz, WT§ synapses performed stronger than KO§, but in both cells all stimuli were responded. Number of failures and the fidelity are additionally depicted in Table S.4.

3.5.1. Depression at 200 Hz is more pronounced in KO

In several studies, it was shown that postsynaptic responses at the MNTB-LSO synapse are more depressed with increasing stimulation frequency (Galarreta and Hestrin, 1998; Kramer et al., 2014; Krachan et al., 2017). This could be observed also in this study, with an increasing depression at higher frequencies (Figure S.1, Table S.5). For comparison of WT and KO, normalized data were analyzed. The smoothed amplitude courses give a visual impression about the different behavior of WT and KO at the applied stimulation frequencies (Figure 18A).

At 1 Hz, the courses appeared quite similar. When stimulating with 50 Hz, WT and KO amplitudes depressed comparably in the beginning, but after about 5 s the courses diverged and KO cells exhibited smaller amplitudes. From this point on, the amplitudes appeared to depress in a mostly linear manner and resulted in amplitudes at 35% (WT) and 30% (KO). At 100 Hz, the two courses diverged already after 2.5 s with the KO amplitudes being smaller than WT. However, the courses appeared not to be linear as they converged after 30 s and ended together at ~14%. When stimulating with 200 Hz, the different depression at the beginning was further pronounced compared to the other frequencies. Almost instantaneously, KO amplitudes exhibited a stronger depression compared to WT and declined after 5 s below the 2-fold noise level (10%). In contrast, WT amplitudes depressed in a less severe manner and fell below the 2-fold noise level (7%) just after 15 s. In the end, amplitudes reached 6% in WT and only 2% in KO. Regarding recoveries, WT and KO behaved quite similar after 50 Hz (rec50) and 100 Hz (rec100). Both did not reach 100% but only ~90%. After 200 Hz (rec200), KO amplitudes appeared to have more difficulties getting back to 100% values. Approximately from second 30 to 45, KO recovery showed a stagnation, but then went on and reached 87%, 4% less compared to WT.

For statistics, not only the last ten eIPSCs or last ten seconds were examined as it is often done in other studies (Galarreta and Hestrin, 1998; Krachan et al., 2017). As KO amplitudes appeared to depress stronger already from the beginning on, FDD was analyzed in a higher temporal resolution to gain insight in differences nearly throughout the complete courses and not only at the end (Figure 18B, Table 6). Therefore, every second during the first 10 s of challenges and every ten seconds during the ensuing part of challenges and during 1 Hz conditions (Figure 18C), the average of ten consecutive eIPSC amplitudes was calculated and compared. For 1 Hz until rec100, the courses were quite similar with overlapping SEMs, so no significant differences were detected. In contrast, after 1 s at 200 Hz stimulation KO synapses exhibited a significantly stronger depression almost continuously until 7 s (second 307 at depicted scale). Afterwards, the courses converged until second 20, where the amplitudes of KO again were significantly smaller until the end of the stimulation. The ensuing recovery was comparable in KO and WT, as it was the same for the preceding recoveries. To examine to which extent failures contribute to the observed amplitude depressions, the fidelity as a representative parameter for effective neurotransmission above detection threshold was assessed.

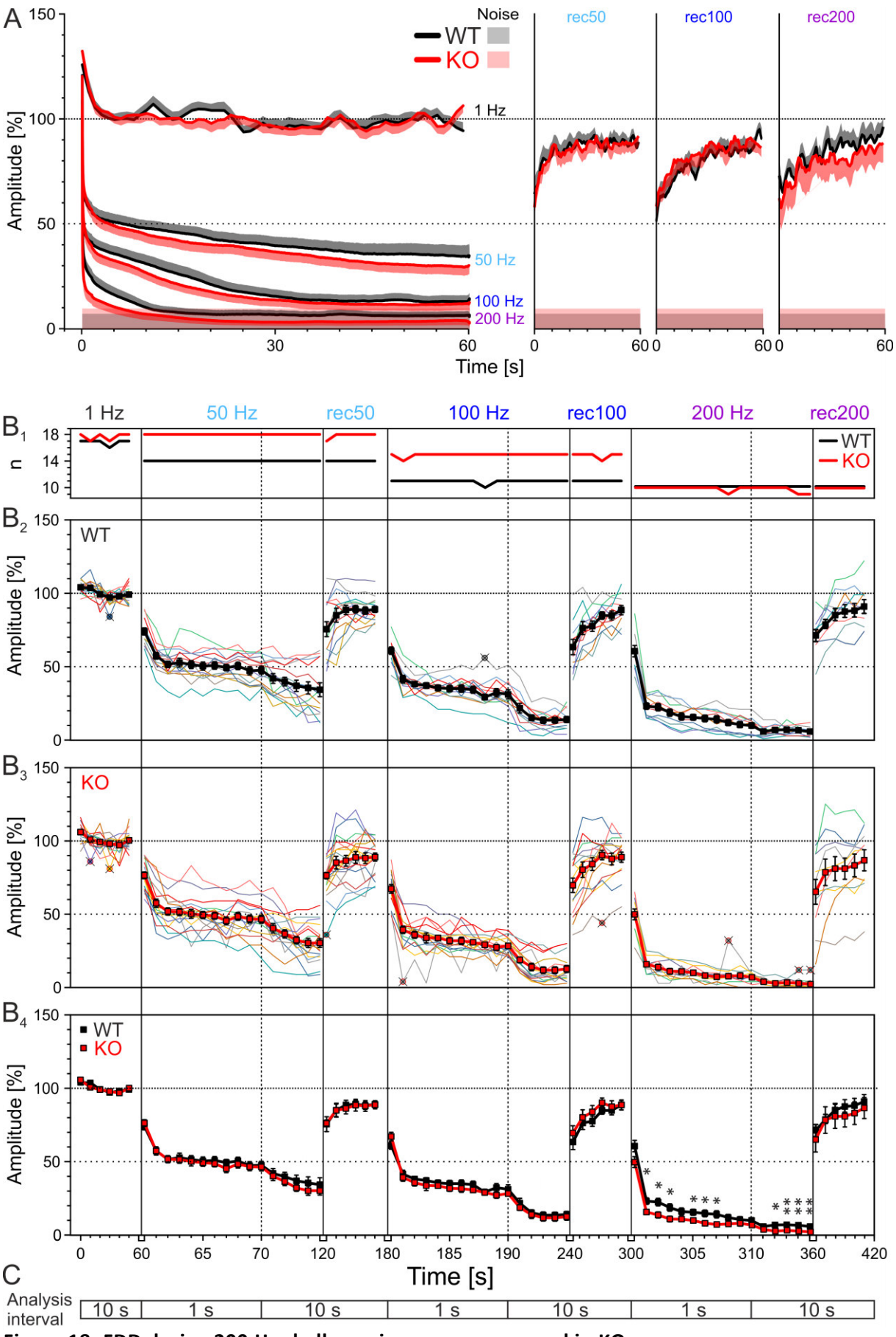

Figure 18: FDD during 200 Hz challenge is more pronounced in KO

For legend see next page.

Figure 18 (continued): FDD during 200 Hz challenge is more pronounced in KO
A, Overlay of the normalized mean amplitude courses of WT and KO in challenge situations (left) and during recovery phases (right) + SEM (WT) or - SEM (KO). Noise level is indicated with a grey and a bright red rectangle for WT and KO, respectively (cf. 2.3.5). For clarity, the courses were smoothed with a moving average of 5% of the data points. n(cells) = 17/14/11/10(WT) / 18/18/15/10(KO). **B**, FDD and recovery. **B_2,B_3**, Normalized mean amplitudes of the first ten eIPSCs after the indicated time points or the last ten eIPSCs at the end of a challenge. Analysis interval was 10-s for 1 Hz conditions and 1-s for challenges (**C**). For better visibility, the single cell data are drawn as lines. **B_1**, Sample sizes (number of cells). Due to outliers, sample sizes are reduced in some datasets, also indicated as cross-marked circles in B_2 and B_3. **B_4**, Overlay and comparison of WT (B_2) and KO (B_3) data. For better visibility, not significant differences are not depicted. For details see Table 6 and for significance levels see Table 1. eIPSC = evoked inhibitory postsynaptic current, n = number of cells

3.6. Fidelity of the MNTB-LSO synapse

MNTB-LSO synapses are able to maintain high fidelity synaptic transmission across a wide range of frequencies and even during activation lasting up to one minute (Kramer et al., 2014; Krachan et al., 2017; Fischer et al., 2019). This high efficiency is due to distinct endocytotic vesicle replenishment with up to 1000 vesicles/s at this synapse (Krachan et al., 2017; Fischer et al., 2019), enabling the constant vesicle release needed for sustained synaptic transmission. As GlyT1 is involved in re-uptake of glycine from the synaptic cleft, I wanted to find out if GlyT1 is also important for maintaining synaptic efficiency during longer periods of synaptic transmission. Therefore, fidelity (cf. 2.3.7) was assessed and the last 10 s of challenges and recoveries were taken into account.

3.6.1. Fidelity is negatively correlated to stimulation frequency in WT and KO

Regarding the example cell WT§ (Figure 19A_1), a fidelity of 100% for 1 Hz and 50 Hz was achieved. Only during the last 15 s at 100 Hz stimulation, some stimuli were not responded leading to a slight intermittent reduction of 2% to 98%. In the last 10 s, the mean fidelity was 99% (for the mean fidelity and total number of failures see Table S.4). At 200 Hz, a more severe reduction was observed. After 8 s, the occurrence of failures was more frequent and led to a decrease in fidelity to a minimum of ~75% after 37 s. This improved to 84% for the last 10 s. During recoveries, all stimuli were responded and therefore 100% fidelity was achieved.

Taken all WT cells together (Figure 19A_2), the fidelity during 1 Hz stimulation was 100%. At 50 Hz, the failure rate slightly increased after 30 s resulting in a decreased fidelity of 96%

Table 6: Comparison of FDD and recovery

condition	timepoint	WT (17/14/11/10) amplitude [%]	KO (18/18/15/10) amplitude [%]	p value	sign.
1 Hz	0	104 ± 1	106 ± 1	0.23611	*n.s.*
	10	104 ± 1	101 ± 1 (17)	0.05821	*n.s.*
	20	99 ± 1 (16)	99 ± 1	0.94759	*n.s.*
	30	97 ± 1	98 ± 1 (17)	0.40021	*n.s.*
	40	98 ± 1	97 ± 1	0.56980	*n.s.*
	50	99 ± 1	101 ± 1	0.47837	*n.s.*
50 Hz	60	74 ± 2	76 ± 2	0.50127	*n.s.*
	61	57 ± 2	57 ± 3	0.99694	*n.s.*
	62	52 ± 2	52 ± 2	0.97037	*n.s.*
	63	53 ± 3	51 ± 2	0.70842	*n.s.*
	64	52 ± 3	50 ± 3	0.76077	*n.s.*
	65	51 ± 3	50 ± 2	0.80483	*n.s.*
	66	51 ± 3	49 ± 2	0.54707	*n.s.*
	67	49 ± 2	45 ± 3	0.27889	*n.s.*
	68	50 ± 3	49 ± 3	0.61482	*n.s.*
	69	47 ± 3	47 ± 3	0.87332	*n.s.*
	70	48 ± 3	47 ± 3	0.75466	*n.s.*
	80	42 ± 3	40 ± 3	0.73141	*n.s.*
	90	40 ± 3	37 ± 3	0.42806	*n.s.*
	100	37 ± 4	32 ± 2	0.29024	*n.s.*
	110	36 ± 4	30 ± 3	0.30916	*n.s.*
	120[a]	34 ± 5	30 ± 3	0.47713	*n.s.*
rec50	120	76 ± 5	76 ± 2 (17)	0.87870	*n.s.*
	130	85 ± 5	85 ± 4	0.97070	*n.s.*
	140	89 ± 3	86 ± 4	0.64298	*n.s.*
	150	89 ± 3	89 ± 4	0.91311	*n.s.*
	160	88 ± 3	88 ± 4	0.98915	*n.s.*
	170	89 ± 2	89 ± 3	0.99960	*n.s.*
100 Hz	180	61 ± 2	67 ± 3	0.12416	*n.s.*
	181	41 ± 3	39 ± 3 (14)	0.57554	*n.s.*
	182	38 ± 2	36 ± 2	0.48765	*n.s.*
	183	37 ± 2	34 ± 3	0.38565	*n.s.*
	184	36 ± 2	34 ± 2	0.53005	*n.s.*
	185	35 ± 2	32 ± 2	0.30815	*n.s.*
	186	35 ± 3	32 ± 3	0.33022	*n.s.*
	187	34 ± 2	31 ± 2	0.24887	*n.s.*

condition	timepoint	WT (17/14/11/10) amplitude [%]	KO (18/18/15/10) amplitude [%]	p value	sign.
100 Hz	188	29 ± 2 (10)	29 ± 1	0.94146	*n.s.*
	189	32 ± 3	27 ± 2	0.15790	*n.s.*
	190	31 ± 3	28 ± 2	0.38963	*n.s.*
	200	22 ± 3	19 ± 2	0.41018	*n.s.*
	210	15 ± 2	14 ± 3	0.69026	*n.s.*
	220	14 ± 2	12 ± 2	0.60341	*n.s.*
	230	14 ± 2	12 ± 2	0.57627	*n.s.*
	240[a]	14 ± 2	13 ± 2	0.64367	*n.s.*
rec100	240	63 ± 5	70 ± 5	0.39291	*n.s.*
	250	76 ± 4	80 ± 5	0.58252	*n.s.*
	260	78 ± 4	84 ± 4	0.28763	*n.s.*
	270	85 ± 3	90 ± 3 (14)	0.21751	*n.s.*
	280	85 ± 3	88 ± 4	0.59956	*n.s.*
	290	89 ± 3	89 ± 3	0.96353	*n.s.*
200 Hz	300	61 ± 4	50 ± 4	0.06458	*n.s.*
	301	23 ± 2	16 ± 2	0.01646	*
	302	23 ± 3	14 ± 2	0.01742	*
	303	19 ± 3	11 ± 2	0.02727	*
	304	16 ± 3	11 ± 2	0.08755	*n.s.*
	305	16 ± 2	10 ± 2	0.04394	*
	306	15 ± 2	8 ± 1	0.02636	*
	307	14 ± 3	7 ± 1	0.02748	*
	308	12 ± 2	8 ± 1 (9)	0.09699	*n.s.*
	309	11 ± 2	8 ± 2	0.38970	*n.s.*
	310	10 ± 2	7 ± 1	0.21624	*n.s.*
	320	6 ± 1	4 ± 1	0.21541	*n.s.*
	330	7 ± 1	3 ± 1	0.01289	*
	340	7 ± 1	3 ± 1	0.00916	**
	350	7 ± 1	3 ± 1 (9)	0.00146	**
	360[a]	6 ± 1	2 ± 1	0.00948	**
rec200	360	71 ± 4	65 ± 9	0.51926	*n.s.*
	370	79 ± 3	79 ± 9	0.97433	*n.s.*
	380	85 ± 4	81 ± 8	0.64773	*n.s.*
	390	88 ± 5	81 ± 7	0.45386	*n.s.*
	400	88 ± 5	83 ± 8	0.57922	*n.s.*
	410	91 ± 5	87 ± 7	0.61563	*n.s.*

For legend see next page.

Table 6: (continued) Comparison of FDD and recovery
Data are presented as mean ± SEM of ten consecutive eIPSCs starting or ending ([a]) at the indicated time (cf. Figure 18). Numbers in brackets depict the sample sizes (number of cells). Reduced sample sizes due to outliers are indicated in brackets at the affected datasets. For significance levels see Table 1. sign. = significance, *n.s.* = not significant

after 40 s. This value was maintained until the end of the challenge. At 100 Hz, the decline in fidelity started earlier (after 5 s) and reached its minimum after 40 s with ~64% staying nearly constant until the end. When applying 200 Hz, the fidelity decreased immediately and reached a steady-state level after 20 s with ~35% fidelity. This value was nearly constant until the end of the challenge. Regarding the recoveries, the cells immediately exhibited a fidelity of 100% throughout the complete courses. To analyze the severity of fidelity decrease depending on stimulation frequency, the means of the last 10 s for challenges (Figure 19B_1) and recoveries (Figure 19B_2) were compared (Table 7). During the last 10 s at 50 Hz, the synaptic transmission remained mostly at 100% (eight cells) as it was in the 1 Hz situation, and only six cells showed a reduction. Therefore no significant difference to 1 Hz was calculated ($p = 0.04068$, *post hoc* Šidák corrected $\alpha = 0.02532$; see Table 1). At the end of 100 Hz stimulation, only five cells stayed at a high fidelity rate (>85%), whereas six cells exhibited a fidelity below the mean (<64%). The reduction was significantly different to 1 Hz and 50 Hz, ($p = 0.00207$, $p = 0.00148$, respectively). At the end of 200 Hz, the fidelity of all cells was even stronger reduced and resulted in significantly lower fidelities compared to 1 Hz and 100 Hz ($p = 0.00002$, $p = 0.00015$, respectively). Regarding the last 10 s of recoveries, no differences were determined as all cells had regained a fidelity of 100%.

Regarding the KO example cell (Figure 19C_1), the fidelities during 1 Hz and 50 Hz were at 100%, as it was already observed in WT§. Also similarly, at the end of the 100 Hz stimulation the first failures occurred (after 54 s; for the mean fidelity and total number of failures see Table S.4), leading to a slight decrease in fidelity around this time point. At 200 Hz, the fidelity already declined after 7 s and reached a minimum of ~70% after 38 s. In the last 10 s, fidelity recovered to 75%.

Taken all KO cells together (Figure 19C_2), the fidelity was 100% during 1 Hz stimulation, as it was observed in WT cells. At 50 Hz, the decrease in fidelity was more severe as in WT as failures occurred immediately after the start. This resulted in a nearly linearly decreasing

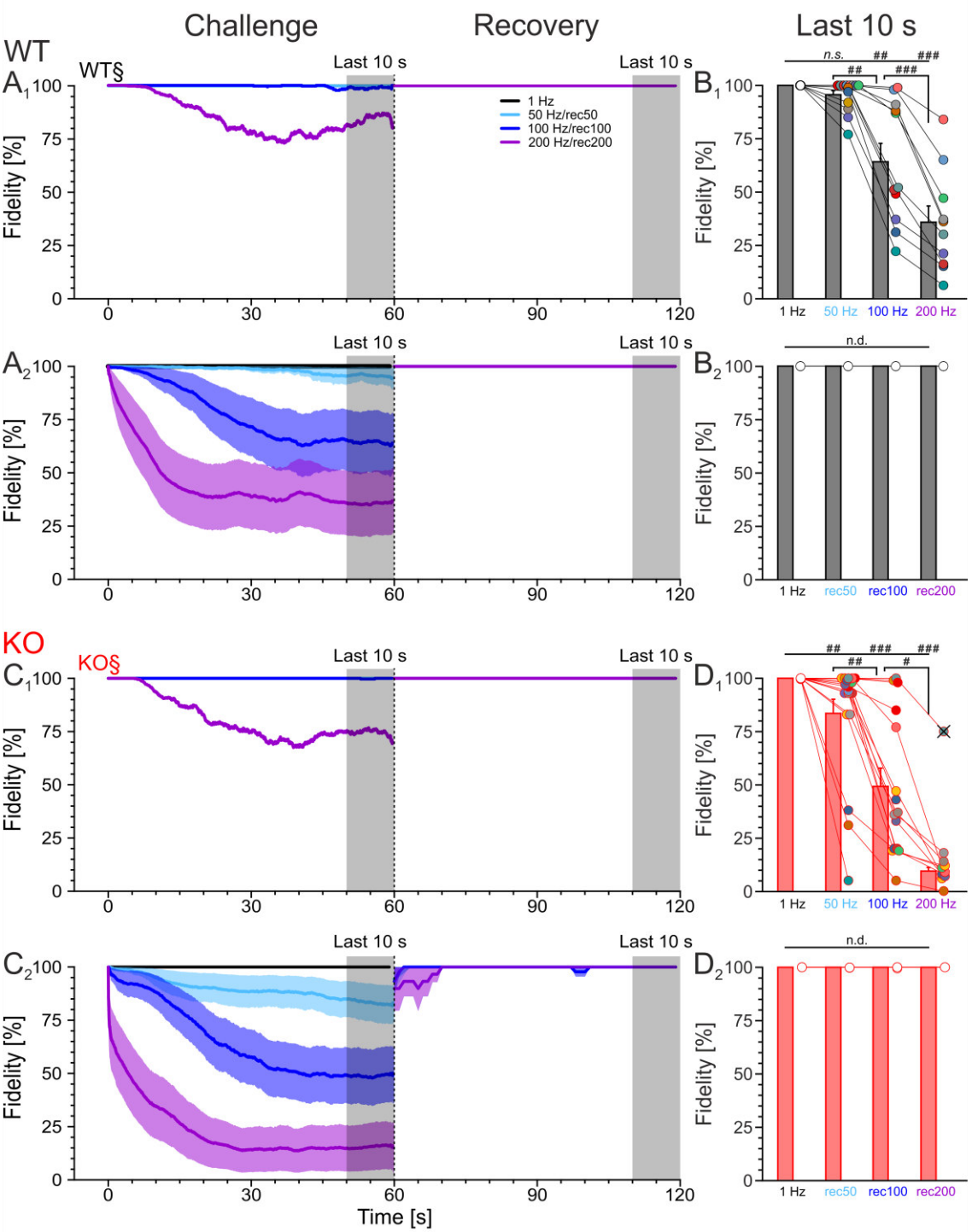

Figure 19: Fidelity in both genotypes is negatively correlated to the stimulation frequency
A,C, Fidelity courses during challenge (left) and recovery periods (right) of the example cells (**A_1,C_1**) and the complete population of WT (**A_2**, WT; **C_2**, KO). For better visibility, courses were smoothed with 5% of the data points. Grey bars mark the period (last 10 s) used for analysis in B and D. **B,D**, Comparison of WT (B) and KO (D) fidelity during the last 10 s of challenges (**B_1,D_1**) and recovery periods (**B_2,D_2**). Outliers are indicated with cross-marked circles. Testing of significance was applied for the challenge data to the 1 Hz situation and additionally to the preceding challenge with *post hoc* Šidák correction. As recovery data were not different, no significance test was performed on these data. For comparison of WT and KO see Figure 20 and for details Table 7. For significance levels see Table 1. n(cells) = 17/14/11/10(WT) / 18/18/15/10(KO), outliers included. *n.s.* = not significant, n.d. = not determined

fidelity down to ~84% during the last 10 s. At 100 Hz, the decline at the beginning was stronger compared to 50 Hz, but stayed at a nearly constant level of about 91% from second 3 to second 7. Afterwards, the fidelity further decreased to a steady-state level of 49% after 35 s. At 200 Hz, an even more severe decline of fidelity occurred starting immediately at the beginning of the stimulation and resulted in a steady-state level of about 16% after 27 s. Regarding recovery situations, KO synapses appeared to have more difficulties to regain 100% fidelity compared to WT. During rec50, the synapses depicted a fidelity of 95% at the beginning and reached 100% after 3 s. The trace is hidden behind rec100, as it showed nearly the same fidelity course (rec100: after 2 s recovery from 95% to 100% fidelity). In contrast to rec50, a transient decline to 98% was observed in rec100 from second 38 to second 40. In rec200, the difficulty to recover to 100% was more pronounced compared to preceding recoveries. The cells started with 90% and required 10 s to respond to every stimulus. As it was done for WT, the mean fidelities of the last 10 s of challenges (Figure 19D$_1$) and recoveries (Figure 19D$_2$) were compared. In contrast to WT, already the 50 Hz fidelity was significantly reduced compared to the 100% of the 1 Hz situation ($p = 0.00147$). For comparison, the Wilcoxon test had to be applied as 50 Hz data were not normally distributed. This is due to an ambivalent behavior: 13 cells had a relatively high fidelity rate above 92%, two exhibited 84% and three cells a severely reduced fidelity below 40%. Stimulation with 100 Hz led to a further decline for nearly all cells, resulting in a significant reduction of fidelity compared to 1 Hz and 50 Hz ($p = 0.00004$, $p = 0.00065$, respectively). Again, Wilcoxon test had to be performed for the comparison with 50 Hz data. Nevertheless, three cells still depicted a high fidelity level of more than 96%. At 200 Hz, the fidelity further declined in all cells with a mean of 9%, leading to a significant difference compared to 1 Hz and 100 Hz ($p = 2.2 \times 10^{-11}$, $p = 0.00931$, respectively). The outlier depicts the example cell with an unusual high fidelity (75%) compared to other KO cells and is responsible for the higher last 10 s-fidelity value in the courses. Regarding the last 10 s of recoveries, no differences were determined as all cells had a fidelity of 100% like in WT cells.

In summary, the extent of decline in fidelity in both genotypes was dependent on stimulation frequency. With increasing frequency, a stronger reduction was observed which appeared to be more pronounced in KO. To analyze this, the direct comparison between WT and KO was qualified in the next chapter.

3.6.2. Fidelity at 200 Hz is more severely reduced in KO

To compare fidelity courses and the fidelity during the last 10 s between WT and KO, data from Figure 19 were directly compared for better illustration of differences (Figure 20). Additionally, unsmoothed mean values are depicted in this figure. For last 10 s fidelity values and significance testing see Table 7. As all WT and KO cells responded to each stimulus during 1 Hz, courses and last 10 s values were identical (Figure 20A$_1$). During 50 Hz, KO fidelity courses exhibited a clearly stronger and earlier decline of fidelity with an onset after ~5 s (WT: 34 s) and ended at a 13% lower value compared to WT (Figure 20A$_2$). However, when comparing the last 10 s-values, there was no detection of significance (p = 0.18088). Regarding the courses at 100 Hz, the fidelity diverged just from the beginning on (Figure 20A$_3$). Already after 3 s, the KO course was ~6% smaller compared to WT and resulted in a 15% lower fidelity during the last 10 s. As the single cell data was quite diverse in both genotypes, no significant difference was detected (p = 0.24002). During 200 Hz, the fidelity diverged just from the beginning as it was observed in 100 Hz, with an approximately 23% lower fidelity in KO for 20 s (Figure 20A$_4$). After this period, WT fidelity course reached a steady-state level of 36%, whereas KO fidelity further declined to a steady-state level of 16% after 27 s. Hence, during steady-state condition, KO fidelity was 20% lower compared to WT. Regarding the last 10 s values for significance testing, the KO mean value (9 ± 2%) is significantly different to WT (p = 0.00777), but differs also from the KO course. This is due to the outlier (75%) which was excluded from mean calculation and significance testing. During recoveries (Figure 20B), the WT and KO courses were quite similar at 100%, except for the beginning. As WT cells

Table 7: Fidelity during the last 10 s

Condition	WT (17/14/11/10)					KO (18/18/15/10)					WT/KO	
	Fidelity [%]	to 1 Hz		to preceding		Fidelity [%]	to 1 Hz		to preceding			
		p value	sign. (k = 3)	p value	sign. (k = 2)		p value	sign. (k = 3)	p value	sign. (k = 2)	p value	sign.
1 Hz	100 ± 0					100 ± 0					n.d.	
50 Hz	96 ± 2	0.04068	*n.s.*			84 ± 7	0.00147[a]	##			0.18088[b]	*n.s.*
100 Hz	64 ± 9	0.00207	##	0.00148	##	49 ± 9	0.00004	###	0.00065[a]	##	0.24002	*n.s.*
200 Hz	36 ± 8	0.00002	###	0.00015	###	9 ± 2 (9)	2.2×10^{-11}	###	0.00931	#	0.00777	**
rec50	100 ± 0	n.d.				100 ± 0	n.d.				n.d.	
rec100	100 ± 0	n.d.		n.d.		100 ± 0	n.d.		n.d.		n.d.	
rec200	100 ± 0	n.d.		n.d.		100 ± 0	n.d.		n.d.		n.d.	

Data are presented as mean of the last 10 s ± SEM (cf. Figure 19). Numbers in brackets depict sample sizes (number of cells). Reduced sample sizes due to outliers indicated in brackets. Due to multiple comparisons, the critical α value was *post hoc* Šidák corrected for comparison with 1 Hz and with preceding challenge/recovery. The number of comparisons (k) is indicated on top. For significance levels see Table 1. [a] = Wilcoxon test, [b] = Mann-Whitney *U*-test, prec. = preceding, sign. = significance, *n.s.* = not significant, n.d. = not determined

responded immediately to each stimulus with an amplitude above the 2-fold noise level, KO synapses started below 100% (rec50 and rec100: 95%, rec200: 90%) and required more time to regain 100% fidelity (rec50: 3 s, rec100: 2 s, rec200: 10 s). Significant differences of recoveries were not determined as data of the last 10 s were identical.

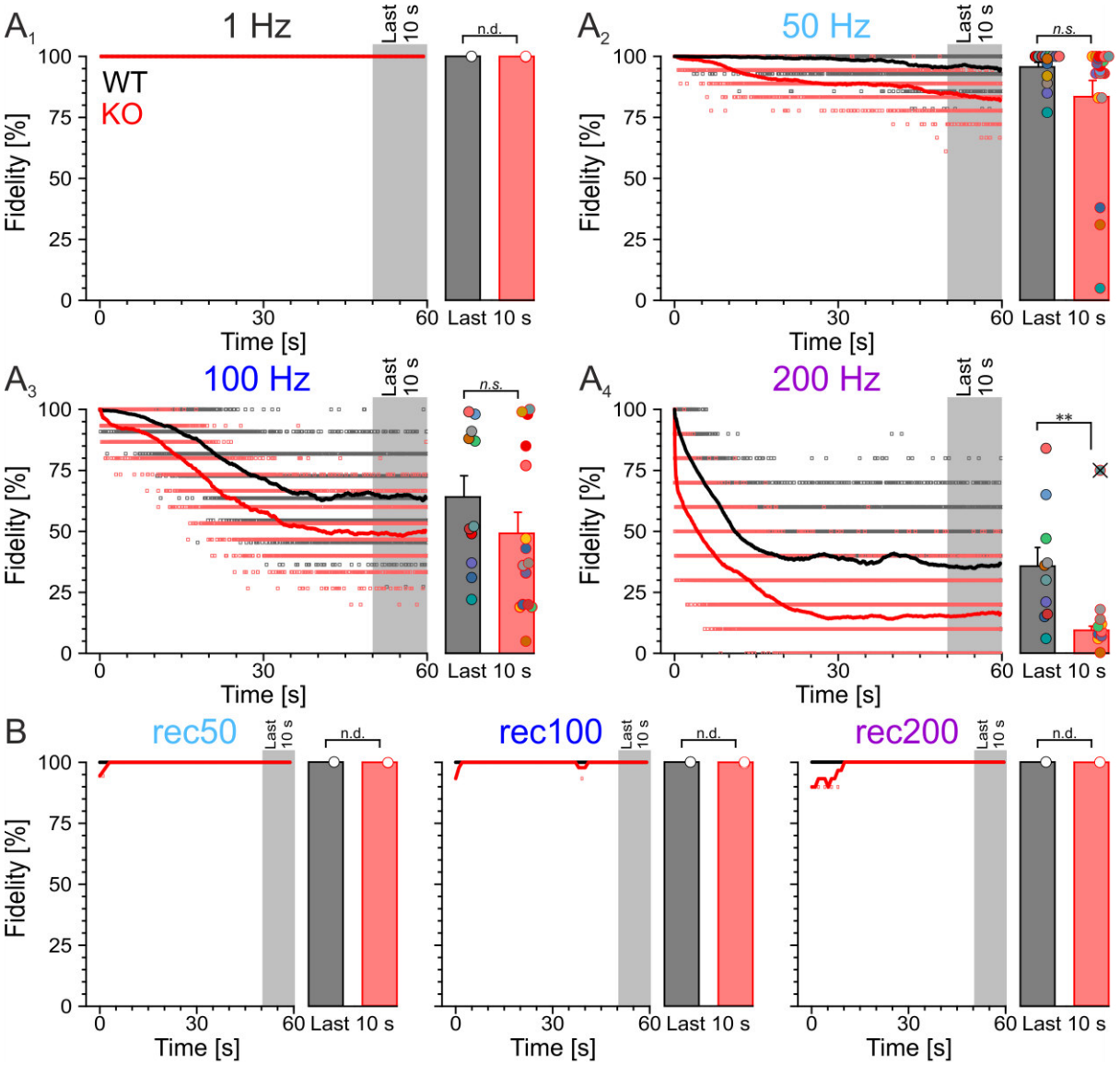

Figure 20: Fidelity during 200 Hz is stronger reduced in KO
Comparison of WT and KO fidelity shown in Figure 19. **A**, Fidelity courses for the different challenge periods (**A_1**, 1 Hz, **A_2**, 50 Hz, **A_3**, 100 Hz, **A_4**, 200 Hz) (left) and analysis of differences between the genotypes in the last 10 s (right). Single data points in the course panels represent the mean values used for the calculation of the 5%-smoothed curves. Outliers are indicated with cross-marked circles. **B**, Fidelity during recovery periods. Same data presentation and analysis as in A. Significances of recovery and 1 Hz data were not determined as data were identical. For details see Table 7 and for significance levels Table 1. n (cells) = 17/14/11/10 (WT) / 18/18/15/10 (KO), outliers included. *n.s.* = not significant, n.d. = not determined

To summarize the comparison, KO had a more severe reduction of fidelity during challenges compared to WT. As the variance in both genotypes was quite extensive in 50 Hz and 100 Hz with some cells exhibiting a high fidelity and some cells with a low fidelity, a significant reduction in fidelity is just visible at 200 Hz, where all KO data depicted a fidelity below 20%. At the beginning of recoveries it is remarkable that KO needed longer to regain 100% fidelity as it was observed in WT. This was most pronounced at rec200, indicative for the higher stress during 200 Hz stimulation leading to a stronger impairment of recovery mechanisms as during 50 Hz and 100 Hz.

3.7. MNTB-LSO synapse properties during challenges

Synaptic strength is determined by synaptic properties including RRP, q and P_r. In former studies, the EQ method (Elmqvist and Quastel, 1965) was found to be appropriate for RRP estimation at the MNTB-LSO synapse (Brill, 2018; Fischer et al., 2019). This method hypothesizes that due to a delay in vesicle replenishment the first four ePSC amplitudes are only elicited by vesicles originating from the RRP. Therefore, these amplitudes remain unbiased by vesicle replenishment from other pools and can be used for RRP estimation. As the extent and velocity of RRP refilling depends on several factors including glycine reuptake (Gomeza et al., 2003b), a loss of GlyT1 as a potential glycine source for the presynapse could impact vesicle refilling. Accordingly, q, RRP size and P_r would be influenced. Therefore, I investigated these aspects and also analyzed their changes elicited by continuous synaptic stress during high frequency stimulation of MNTB-LSO projections.

3.7.1. WT and KO have a similar RRP and P_r

The EQ method proved to be suitable for my RRP analysis of both WT and KO (cf. 2.3.8, example cells WT§ and KO§ in Figure 21A,B), as in most cases there was a constant amplitude depression of the first four eIPSCs.

WT $eIPSC_1$ amplitudes were tendentially higher than KO values at each condition (50 Hz, 100 Hz, 200 Hz; Figure $21C_1$), but no significant difference was detected (Table 8). Regarding the changes during challenges for each genotype independently from each other (Table 9), the mean values stayed nearly the same in WT and KO with one exception: a significant difference between KO $eIPSC_1$ 50 Hz and $eIPSC_1$ 100 Hz was calculated ($p = 0.00785$), caused by a uniform $eIPSC_1$ reduction in most cells.

For I_{RRP} (Figure 21C$_2$), WT and KO comparison again revealed no significant difference throughout all challenges (Table 8). Regarding the changes, the decrease of WT I_{RRP} from 50 Hz to 100 Hz was significant ($p = 0.00635$) as the I_{RRP} in most single cells was reduced. For KO I_{RRP} values, no significant changes were detected (Table 9). Notably, in each data set an outlier was detected marking a great divergence of single cell data. Additionally, the I_{RRP} could not be estimated for one KO cell at 50 Hz and one WT cell at 200 Hz due to quality criteria (cf. 2.3.8).

To calculate P_r (Figure 21C$_3$), $eIPSC_1$ was divided by I_{RRP}. In terms of cells with no I_{RRP} estimation, also P_r could not be calculated. As it was already observed for $eIPSC_1$ and I_{RRP}, WT and KO data were similar throughout all challenges (Table 8). Analyzing the P_r changes for the genotypes separately (Table 9), a stepwise increase occurred in WT, whereas KO exhibited an increased P_r just at 200 Hz. Compared to 50 Hz, this augmentation was significant ($p = 0.00859$).

To express the current values of $eIPSC_1$ and I_{RRP} in vesicles (m_1 and N_{RRP}, respectively), the single cell data were divided by q (for q data see Figure 16 and Table 4). For m_1 (Figure 21C$_4$), the differences between WT and KO were analogous to $eIPSC_1$ with the WT means being higher than KO. But as in $eIPSC_1$ analysis, WT and KO data were similar. When analyzing the changes, a significant decrease in KO m_1 from 50 Hz to 100 Hz was found as it was already the case for $eIPSC_1$ data. Regarding the N_{RRP} (Figure 21C$_5$), WT and KO data were not significantly different, as it was also observed for the I_{RRP}. But compared to 50 Hz, the N_{RRP} of 100 Hz in WT was significantly reduced ($p = 0.00594$). In Figure 21C$_6$, the calculation methods are summarized.

Taken these results together, KO synapses appeared to have a WT-like $eIPSC_1/m_1$, I_{RRP}/N_{RRP} and P_r. Regarding the changes of these parameters for the genotypes separately, m_1 (and also $eIPSC_1$) stayed relatively constant with 23 vesicles in WT and 19 vesicles in KO. However, a high variation was observed for N_{RRP}. In WT, the N_{RRP} at the beginning of 100 Hz was significantly smaller compared to 50 Hz (101 and 199 vesicles, respectively) but was not further changed towards 200 Hz (104 vesicles). In KO, the N_{RRP} increased from 124 vesicles (50 Hz) to 145 vesicles (100 Hz), and was again smaller at 200 Hz (87 vesicles). Consequently, the P_r also changed during the challenges with a tendential increase towards the next challenge. Thus, in both genotypes, P_r at 200 Hz was the highest (WT: 25%, KO: 27%), indicating the need for sufficient vesicle release despite a reduced N_{RRP}.

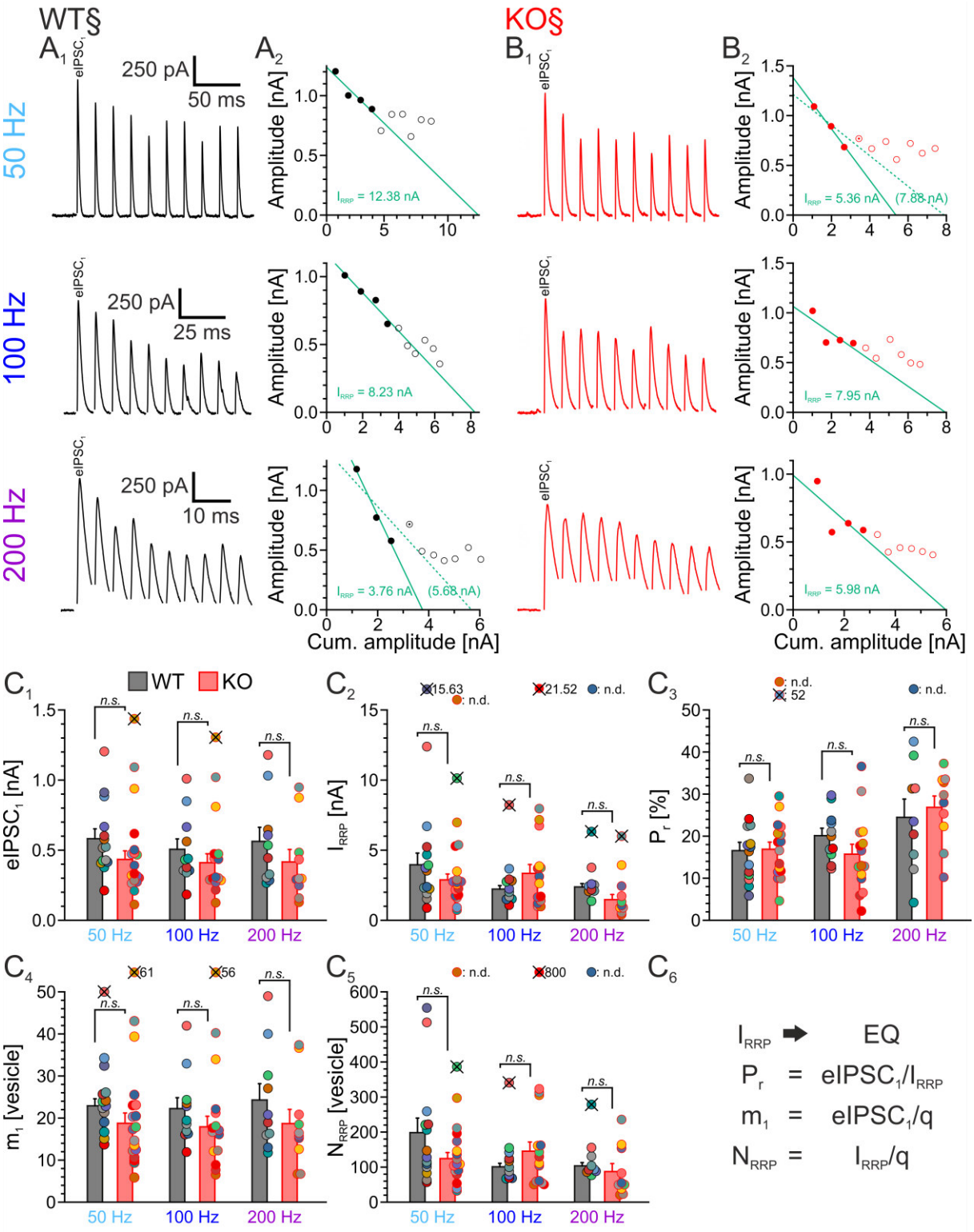

Figure 21: Initial synaptic properties in KO are similar to WT.
A,B, Calculation of RRP. **A_1,B_1**, Illustration of the first ten eIPSCs of the example cells (WT§, KO§) at stimulation with 50 Hz, 100 Hz and 200 Hz. The first eIPSC is indicated with $eIPSC_1$. For better visibility, stimulus artifacts were blanked. **A_2,B_2**, The ten eIPSCs shown in A_1 and B_1 are plotted with their absolute (Y-axis) and cumulative (X-axis) amplitudes. Applying the Elmqvist & Quastel method, I_{RRP} (green value) was determined by a linear fit (green solid line) through the first three or four data points (cf. 2.3.8 and Figure 10). Dotted lines and values in brackets show overestimated I_{RRP}s due to an early onset of vesicle replenishment. (Legend continued on next page.)

Figure 21: (continued) Initial synaptic properties in KO are similar to WT.
C, Comparison of synapse properties: $eIPSC_1$ (**C_1**), I_{RRP} (**C_2**) and P_r (**C_3**) as well as the conversion of $eIPSC_1$ and I_{RRP} into vesicles (m_1, **C_4**; N_{RRP}, **C_5**). If I_{RRP} could not be calculated, the missing data points are indicated at the top ("n.d."). Accordingly, P_r and N_{RRP} could not be calculated for these cells. **C_6**, Formulas for the calculation of the parameters. Outliers are indicated with cross-marked circles. For details see Table 8 and Table 9. For q values used for the calculation of m_1 and N_{RRP} see Figure 16 and Table 4, and or significance levels Table 1.
n (cells) = 17/14/11/10 (WT) / 18/18/15/10 (KO), outliers and n.d. cells included. eIPSC = evoked inhibitory postsynaptic current, RRP = readily releasable pool, P_r = release probability, m = quantal content, n.d. = not determined, *n.s.* = not significant, q = quantal size, EQ = Elmqvist & Quastel (1965) method

Table 8: Initial synapse properties

		50 Hz			100 Hz			200 Hz		
		WT (14) / KO (18)	p value	sign.	WT (11) / KO (15)	p value	sign.	WT (10) / KO (10)	p value	sign.
$eIPSC_1$ [nA]	WT	0.58 ± 0.07	0.11958	*n.s.*	0.51 ± 0.07	0.33611	*n.s.*	0.56 ± 0.10	0.28994	*n.s.*
	KO	0.43 ± 0.06 (17)			0.41 ± 0.06 (14)			0.42 ± 0.09		
I_{RRP} [nA]	WT	3.96 ± 0.83 (13)	0.25606	*n.s.*	2.22 ± 0.26 (10)	0.12411	*n.s.*	2.37 ± 0.24 (8)	0.06177	*n.s.*
	KO	2.86 ± 0.42 (16)			3.33 ± 0.64 (14)			1.45 ± 0.37 (9)		
P_r [%]	WT	17 ± 2	0.90029	*n.s.*	20 ± 2	0.17575	*n.s.*	25 ± 4 (9)	0.63625	*n.s.*
	KO	17 ± 2 (16)			16 ± 2			27 ± 3		
m_1 [vesicle]	WT	23 ± 2 (13)	0.20032	*n.s.*	22 ± 3	0.24894	*n.s.*	24 ± 4	0.29004	*n.s.*
	KO	19 ± 2 (17)			18 ± 3 (14)			19 ± 3		
N_{RRP} [vesicle]	WT	199 ± 42	0.11522	*n.s.*	101 ± 10 (10)	0.14642	*n.s.*	104 ± 9 (8)	0.51138	*n.s.*
	KO	124 ± 17 (16)			145 ± 27 (14)			87 ± 23		

Data are presented as mean ± SEM (cf. Figure 21). Numbers in brackets depict sample sizes (number of cells). For the calculation of the different parameters see Figure 21B_6. Reduced sample sizes due to outliers are indicated in brackets at the affected datasets. For significance levels see Table 1 and for changes of the data within a genotype see Table 9. $eIPSC_1$ = first eIPSC, RRP = readily releasable pool, P_r = release probability, m_1 = quantal content of $eIPSC_1$, N_{RRP} = number of vesicles in RRP, sign. = significance, *n.s.* = not significant

Table 9: Initial synapse properties - p values and significances for frequency-dependent changes

	comparison	*k*	$eIPSC_1$ [nA]		I_{RRP} [nA]		P_r [%]		m_1 [vesicle]		N_{RRP} [vesicle]	
			p value	sign.	p value	sign.	p value	sign.	p value	sign.	p value	sign.
WT	50/100 Hz	2	0.03620	*n.s.*	0.00635	#	0.10436	*n.s.*	0.06954	*n.s.*	0.00594	#
	50/200 Hz	2	0.52670	*n.s.*	0.24312	*n.s.*	0.43140	*n.s.*	0.53774	*n.s.*	0.27324	*n.s.*
	100/200 Hz	2	0.23764	*n.s.*	0.03876	*n.s.*	0.08556	*n.s.*	0.26655	*n.s.*	0.03765	*n.s.*
KO	50/100 Hz	2	0.00785	#	0.37273	*n.s.*	0.87590	*n.s.*	0.01006	#	0.32841	*n.s.*
	50/200 Hz	2	0.35117	*n.s.*	0.05261	*n.s.*	0.00859	#	0.31148	*n.s.*	0.05238	*n.s.*
	100/200 Hz	2	0.04125	*n.s.*	0.05727	*n.s.*	0.05148	*n.s.*	0.04091	*n.s.*	0.07722	*n.s.*

p values and corresponding significances of synapse property data shown in Table 8 (cf. Figure 21). Comparisons were made between the different challenges for WT and KO separately. Due to multiple comparisons the critical α value was *post hoc* Šidák corrected for two comparisons (*k*). For significance levels see Table 1. $eIPSC_1$ = first eIPSC, RRP = readily releasable pool, P_r = release probability, m_1 = quantal content of $eIPSC_1$, N_{RRP} = vesicles in RRP, *k* = number of comparisons, sign. = significance, *n.s.* = not significant

3.7.2. q during the last 10 s of challenges is stronger reduced in KO as in WT

In the previous analyses it was shown that synapse properties like q (WT/KO: 25/24 pA, p = 0.52; cf. 3.3.2) as well as I_{RRP}/N_{RRP} (e.g. at 50 Hz WT/KO: 3.96/2.86 [nA], p = 0.26; 199/124 [vesicles], p = 0.12), $eIPSC_1/m_1$ (e.g. at 50 Hz WT/KO: 0.58 /0.43 [nA], p = 0.12; 23/19 [vesicles], p = 0.20) and P_r (e.g. at 50 Hz WT/KO 17/17 [%], p = 0.90; cf. 3.7.1) of WT and KO were not significantly different. These results indicate the presence of similar basic conditions of WT and KO synapses at the beginning of challenges. Contrarily, effects of GlyT1 loss were observed in the course of challenges, as a stronger extent of FDD (cf. 0) and a reduced fidelity (cf. 3.6.2) occurred. As a consequence, I wanted to find out if q is changed during the challenges. This could provide an explanation for the reduced synapse performance which was present especially at the end of the stimulation courses. Therefore I analyzed q during the last 10 s ($q_{Last\ 10\ s}$) of a stimulation period to find out if a reduction could be an explanation for reduced amplitudes and fidelity. As the time between one eIPSC and the ensuing stimulus artifact gets smaller with increasing stimulation frequency, the detection of sIPSCs was hampered, and in some cells, the number of sIPSCs (≥30) for q calculation was not achieved. At 200 Hz, it even was impossible to detect sIPSCs, as eIPSCs superimposed (for examples see Figure 17C, Figure 21A_1,B_1). Consequently, a change of q was analyzed only up to rec100. In Figure 22A_1,B_1, the detection of sIPSCs at the end of the different challenges/recoveries is illustrated for the two example cells (WT§, KO§) and $q_{Last\ 10\ s}$ was calculated as described in 2.3.8 (Figure 22A_2,B_2).

To enable the comparison of all cells, $q_{Last\ 10\ s}$ was normalized to the initial q (cf. Figure 16). The changes relative to this initial value were analyzed, and the values were compared to the preceding situation (Figure 22C, Table 10). In WT, no significant q changes were detected as the mean stayed nearly constant with the greatest reduction of -8% at 100 Hz (Figure 22C_1). Nevertheless, the single cell data depicted strong variations, as in some cases $q_{Last\ 10\ s}$ was reduced or increased, independently from stimulation frequency. For example, q of two WT inputs was tremendously reduced to ~60% at the end of 1 Hz or rec100, whereas in other cases $q_{Last\ 10\ s}$ increased to ~130%. Regarding the q changes in KO (Figure 22C_2), a more uniform pattern was observed compared to WT: at the end of the challenges, $q_{Last\ 10\ s}$ was significantly reduced compared to the initial q (p values: 0.00006 (50 Hz); 0.00099 (100 Hz)), with a stronger decrease at 100 Hz (-19%) compared to 50 Hz

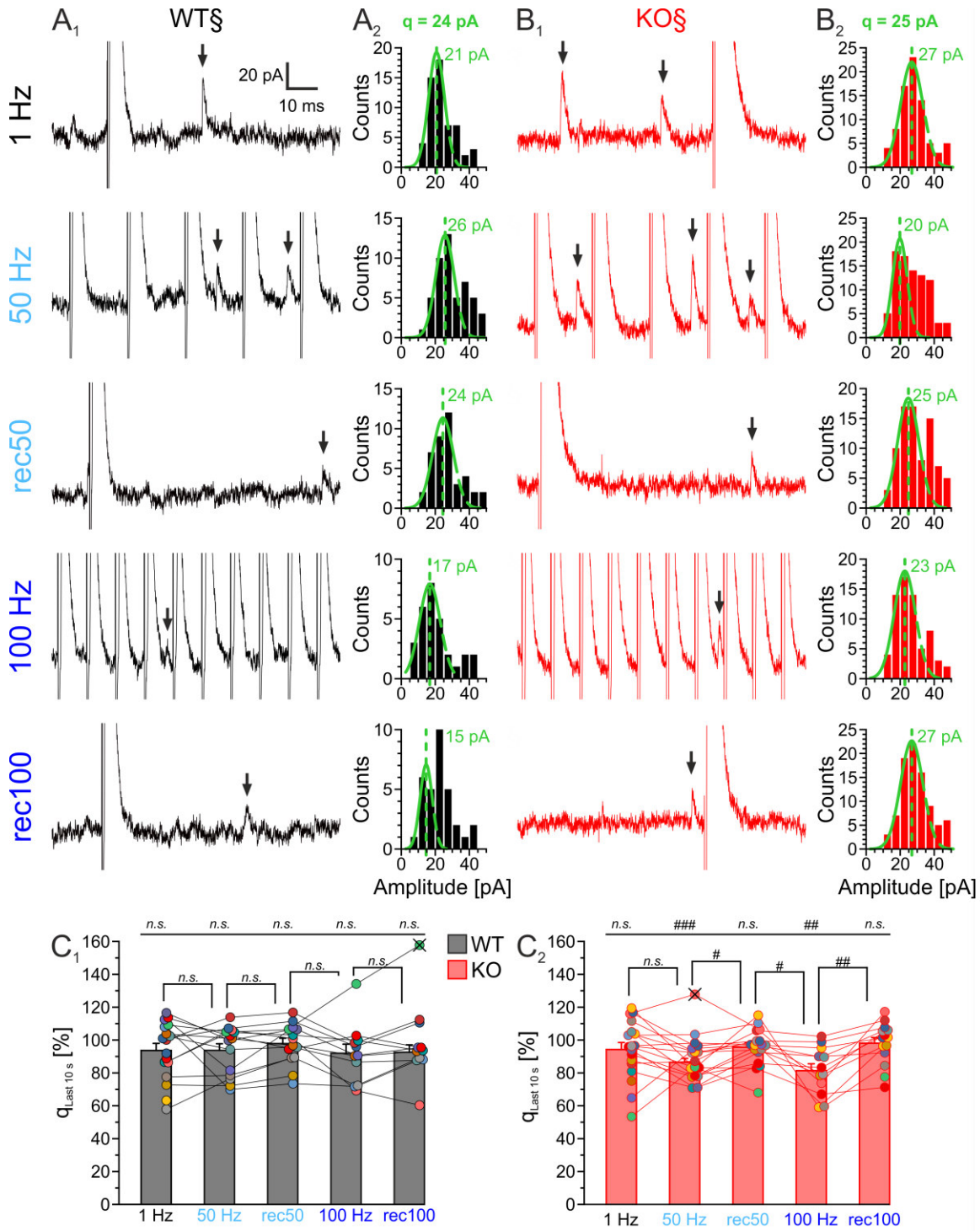

Figure 22: q in KO is reduced in the last 10 s of challenges.

A_1,B_1, Example current traces at the end of 1 Hz, 50 Hz, 100 Hz and of corresponding recoveries (rec50, rec100) of the example cells WT§ (A_1) and KO§ (A_3). sIPSCs (arrows) in the last 10 s of the traces were used for $q_{Last\ 10\ s}$ determination via a Gaussian fit from the sIPSC amplitude histogram (**A_2,B_2**, cf. 2.3.8 and Figure 11). eIPSCs and stimulus artifacts in A_1 and B_1 were cut off for better visibility of sIPSCs. **C,** $q_{Last\ 10\ s}$ of the different conditions in WT (**C_1**) and KO (**C_2**) cells. Data were normalized and compared to the initial q (cf. Figure 16) and to the preceding condition. Due to multiple comparisons, significance levels were *post hoc* Šidák corrected. Note the reduced sample sizes due to outliers, also indicated with cross-marked circles, and due to cells with too few sIPSCs for q estimation. For details see Table 10 and for absolute values Table S.6. For significance levels see Table 1. n (cells) = 17/14/14/11/10 (WT) / 18/16/17/12/14 (KO), outliers excluded. q = quantal size, *n.s.* = not significant, q = quantal size

Table 10: $q_{Last\ 10\ s}$ compared to initial q

Initial q: (100%)	WT (17/14/11/10) 23.4 ± 0.9 [pA]					KO (18/18/15/10) 23.3 ± 1.0 [pA]					WT/KO	
Condition	$q_{Last\ 10\ s}$ [%]	to initial q		to preceding q		$q_{Last\ 10\ s}$ [%]	to initial q		to preceding q		p value	sign.
		p value	sign. (k = 5)	p value	sign. (k = 2)		p value	sign. (k = 5)	p value	sign. (k = 2)		
1 Hz	94 ± 4	0.15940	*n.s.*			94 ± 4	0.18996	*n.s.*			0.92023	*n.s.*
50 Hz	94 ± 4	0.13984	*n.s.*	0.60090	*n.s.*	86 ± 2 (16)	0.00006	###	0.10986	*n.s.*	0.11721	*n.s.*
rec50	98 ± 3	0.52239	*n.s.*	0.10071	*n.s.*	96 ± 3 (17)	0.13142	*n.s.*	0.00842	#	0.61030	*n.s.*
100 Hz	92 ± 6	0.17573	*n.s.*	0.13750	*n.s.*	81 ± 4 (12)	0.00099	##	0.00804	#	0.13738	*n.s.*
rec100	93 ± 5 (10)	0.13370	*n.s.*	0.16746	*n.s.*	98 ± 4 (14)	0.58319	*n.s.*	0.00053	##	0.33757	*n.s.*
200 Hz	n.d.					n.d.					n.d.	
rec200	n.d.					n.d.					n.d.	

Data (cf. Figure 22) were normalized to the initial q (Figure 16) and are presented as normalized mean ± SEM. Numbers in brackets depict sample sizes (number of cells). Due to outliers and due to cells with too few sIPSCs to determine q, the sample sizes are reduced in some conditions, indicated in brackets at the affected datasets. Due to multiple comparisons, the critical α value was *post hoc* Šidák corrected for comparisons with the initial q and with the preceding q. The number of comparisons (k) is indicated on top. For significance levels see Table 1 and for absolute values see Table S.6. q = quantal size, prec. = preceding, sign. = significance, *n.s.* = not significant, n.d. = not determined

(-14%). During recoveries, $q_{Last\ 10\ s}$ recovered back to 96% (rec50) or 98% (rec100), and were significantly higher to the preceding challenge ($p = 0.00842$; $p = 0.00053$; respectively), but not significantly different to the initial q ($p = 0.13142$; $p = 0.58319$; respectively). This uniform behavior of $q_{Last\ 10\ s}$ (decrease during challenges, resurgence during recoveries) was depicted by all cells with three exceptions which exhibited an unusual increase of $q_{Last\ 10\ s}$ from 1 Hz to 50 Hz ensued by a decrease at the end of rec50.

To summarize, q of KO was clearly reduced in the last 10 s of 50 Hz and 100 Hz, but recovered back to values comparable to the initial q. In contrast, no tendency for a q change was observed in WT. Despite this dissimilar behavior, no significant differences between WT and KO were calculated. For absolute values see Table S.6.

3.7.3. No higher m in KO to compensate the decrease in q

As shown in Figure 18, the normalized amplitudes of WT and KO are not significantly different until 200 Hz. If q gets reduced in the course of a challenge, m of each response could be increased to compensate the lack of neurotransmitter and to ensure reliable signal transmission. As q in KO was significantly decreased at the end of the challenges, I wanted to find out if m in KO is higher compared to WT during situations with similar absolute amplitudes but decreased q. Therefore, I analyzed the absolute amplitudes of the last 10 s of challenges and recoveries and converted them into m with the new calculated $q_{Last\ 10\ s}$ values

(cf. Figure 22 and Table 10). The absolute $amplitude_{Last\ 10\ s}$ of WT and KO at 1 Hz was similar (Figure 23A, Table 11) and also $m_{Last\ 10\ s}$ was not significantly different(Figure 23B, Table 11). This was expected as the basic synaptic strength (cf. 3.4) was already found to be not different. At 50 Hz, in both genotypes $amplitude_{Last\ 10\ s}$ was comparably decreased to about 32%. For $m_{Last\ 10\ s}$, WT and KO values were similar, so no higher value for KO was found despite the reduced $q_{Last\ 10\ s}$. The same was observed for 100 Hz: no significantly different $amplitude_{Last\ 10\ s}$, but also no obvious increased $m_{Last\ 10\ s}$ in KO. rec50 and rec100 also exhibited similar $amplitude_{Last\ 10\ s}$ and $m_{Last\ 10\ s}$ values. For 200 Hz, no $m_{Last\ 10\ s}$ was calculated as $q_{Last\ 10\ s}$ could

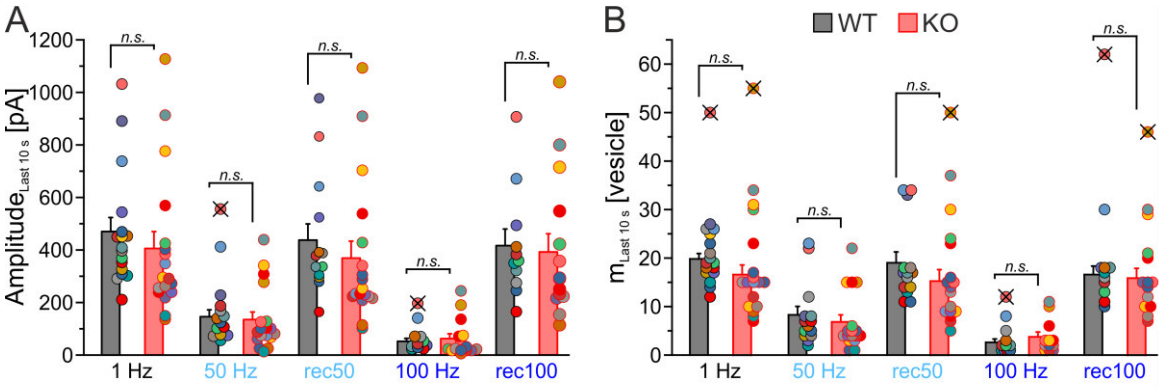

Figure 23: m during the last 10 s is similar in WT and KO
A, eIPSC amplitudes of the last 10 s. **B**, Conversion of eIPSC amplitudes shown in A into m via division of the amplitude by the corresponding $q_{Last\ 10\ s}$ (cf. Figure 22 and Table 10). Outliers are indicated with cross-marked circles. In B, n in some cases is also reduced because of cells with too few sIPSCs for $q_{Last\ 10\ s}$ estimation. For details and for of $amplitude_{Last\ 10\ s}$ at 200 Hz see Table 11. For significance levels see Table 1. n (cells) = 17/14/11 (WT) / 18/18/15 (KO), outliers and cells without $q_{Last\ 10\ s}$ estimation included. q = quantal size, *n.s.* = not significant, m = quantal content

Table 11: Absolute amplitudes and m during the last 10 s

Condition	$Amplitude_{Last\ 10\ s}$ [pA]				$m_{Last\ 10\ s}$ [vesicle]			
	WT (17/14/11/10)	KO (18/18/15/10)	p value	sign.	WT (17/14/11/10)	KO (18/18/15/10)	p value	sign.
1 Hz	470 ± 54	406 ± 64	0.44636	*n.s.*	20 ± 1 (16)	17 ± 2 (17)	0.18545	*n.s.*
50 Hz	146 ± 26 (13)	135 ± 29	0.78841	*n.s.*	8 ± 2	7 ± 1 (17)	0.20401[a]	*n.s.*
rec50	439 ± 62	369 ± 64	0.45412	*n.s.*	19 ± 2	15 ± 2 (16)	0.24897	*n.s.*
100 Hz	52 ± 11 (10)	62 ± 19	0.65063	*n.s.*	3 ± 1 (10)	4 ± 1 (12)	0.44639	*n.s.*
rec100	417 ± 63	392 ± 69	0.80404	*n.s.*	17 ± 2 (10)	16 ± 2 (13)	0.79325	*n.s.*
200 Hz	25 ± 5 (9)	10 ± 2 (9)	0.01308	*	n.d.			
rec200	456 ± 58	339 ± 69	0.21000	*n.s.*	n.d.			

Data are presented as mean ± SEM (cf. Figure 23). Numbers in brackets depict sample sizes (number of cells). Quantal content during the last 10 s ($m_{Last\ 10\ s}$) was calculated by dividing the $amplitude_{Last\ 10\ s}$ by the corresponding $q_{Last\ 10\ s}$. Due to outliers and due to cells with too few sIPSCs to determine $q_{Last\ 10\ s}$, sample sizes were reduced in some conditions, indicated in brackets at the affected datasets. For significance levels see Table 1. [a]= Mann-Whitney *U*-test, sign. = significance, *n.s.* = not significant, n.d. = not determined, m = quantal content

not be determined. Nevertheless, $amplitude_{Last\ 10\ s}$ were significantly different ($p = 0.01308$; not shown in figure but in Table 11).

Conclusively, KO synapses did not release more vesicles at the end of challenges to compensate the decreased q.

3.8. Precision at the MNTB-LSO synapse during sustained transmission

High temporal precision at the MNTB-LSO synapse is essential for the LSO to calculate exact ILDs and further convey this information to higher brain regions (Beiderbeck et al., 2018). To investigate impairments of temporal precision after loss of GlyT1, I analyzed eIPSC peak latencies (cf. 2.3.5) and the corresponding jitter ($SD_{Latency}$).

Color plots illustrating the latencies during challenges are exemplarily depicted for WT§ and KO§ in Figure 24A,C. In WT§, the latencies during 1 Hz were nearly constantly ~1.30 ms. However, with higher stimulation frequency, a time- and frequency-dependent increase was observed up to 2.00 ms at the end of 200 Hz (Figure $24B_1$). Additionally, the $SD_{Latency}$ also increased in the same time- and frequency-dependent manner from ~0.02 ms at 1 Hz to ~0.17 ms at the end of 200 Hz (Figure $24B_2$). In KO§, latency and $SD_{Latency}$ values at 1 Hz (~1.50 ms, ~0.05 ms, respectively) were already higher compared to WT§, but similarly depicted a time- and frequency-dependent increase up to 2.00 ms long latencies with a $SD_{Latency}$ of ~0.23 ms at the end of 200 Hz (Figure $24D_{1,2}$, respectively).

But how did the latencies behave during the recovery periods? In Figure 25, the latency courses of WT§ (Figure 25A,B) and KO§ (Figure 25C,D) during recoveries are illustrated with a reprint of the 1 Hz data shown in Figure 24. In WT§, the latencies recover to a constant value of ~1.50 ms, which is 0.20 ms higher compared to 1 Hz (Figure $25B_1$). Except for rec200, this latency shortening is achieved nearly immediately after the beginning of the recovery period. In rec200, however, latencies needed ~10 s to decrease to the constant value. This could be due to the higher synaptic stress during 200 Hz stimulation, resulting in more severely increased latencies compared to the other challenges (200 Hz: ~2.00 ms; 50 Hz/100 Hz: ~1.5 ms/1.7 ms), which needs longer to be reversed during the ensuing recovery. Comparably, the $SD_{Latency}$ remained at a relatively low level (<0.05 ms), except for rec100 showing phases with a relatively high $SD_{Latency}$ of up to ~0.12 ms (Figure $25B_2$). In KO§, latency mean courses

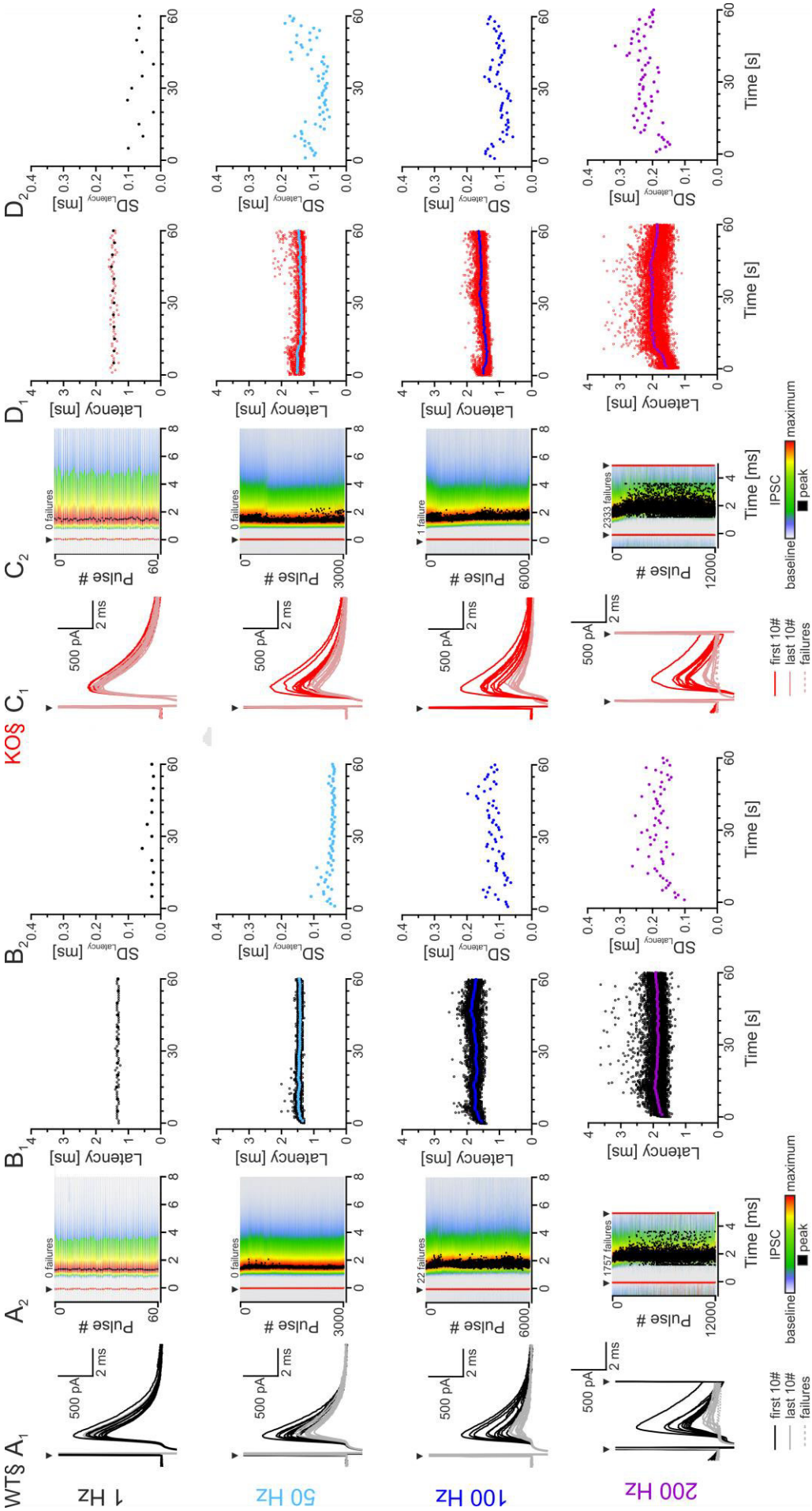

Figure 24: Synaptic precision during 1 Hz and challenges of two example recordings of WT and KO
For legend see page 63.

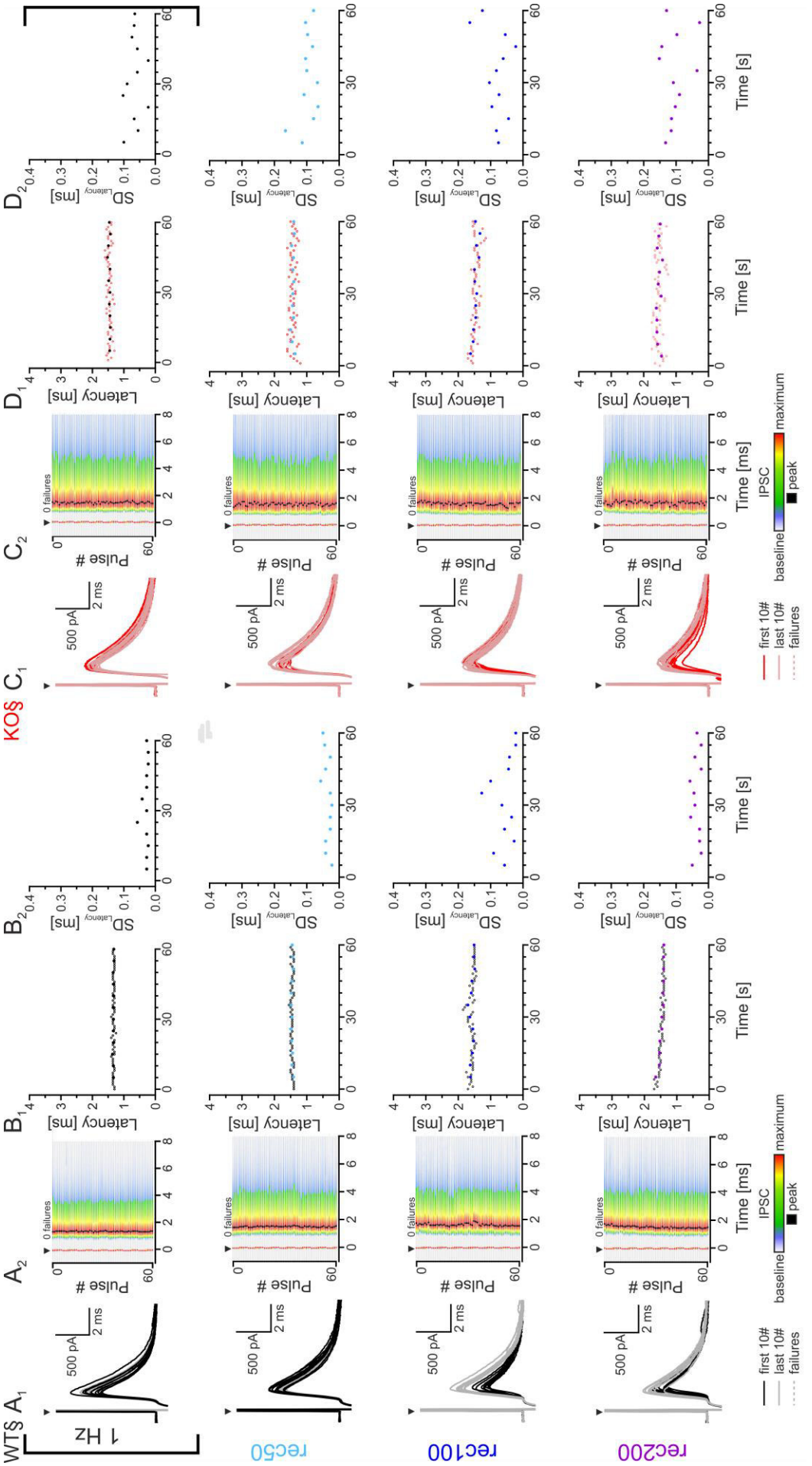

Figure 25: Synaptic precision during recoveries of two example recordings of WT and KO
For legend see next page.

Figure 24: (continued) Synaptic precision during 1 Hz and challenges of two example recordings of WT and KO
Latencies and corresponding standard deviations ($SD_{Latency}$) of the example cells WT§ (A,B) and KO§ (C,D) during 1 Hz, 50 Hz, 100 Hz and 200 Hz. **A_1,C_1**, Overlay of the first (black) and last (grey) 10 eIPSCs (artifact aligned) with failures indicated by dashed lines. Triangles mark the artifacts. **A_2,C_2**, Synaptic precision during the complete stimulation periods illustrated as color-coded time series. Each line represents a single eIPSC with its peak marked by a black square. Color-coding indicates the increase and decrease of eIPSC amplitudes with grey to red illustrating the baseline and the maximum, respectively. Lines with failures are blanked and their counts are indicated at the top of the corresponding panel. Triangles mark the stimulus events, also shown as red spots. **B_1,D_1**, Temporal courses of the latencies shown in A_2 and C_2. Small dots illustrate the latency of each eIPSC (failures excluded), big dots (coloring corresponding to the stimulation frequency) show the binned mean of latencies (5-s bins for 1 Hz, 1-s bins for challenges). **B_2,D_2**, $SD_{Latency}$ of the binned latencies shown in B_1 and D_1, respectively, illustrating the temporal courses of the latency jitter.

Figure 25: (continued) Synaptic precision during recoveries of two example recordings of WT and KO
Latencies and corresponding standard deviations ($SD_{Latency}$) of the example cells WT§ (A,B) and KO§ (C,D) during 1 Hz (cf. Figure 24), rec50, rec100 and rec200. **A_1,C_1**, Overlay of the first (black) and last (grey) 10 eIPSCs (artifact aligned). Triangles mark the artifacts. Failures would be indicated by dashed lines but did not occur in these example cells for the shown conditions. **A_2,C_2**, Synaptic precision during the complete stimulation periods illustrated as color-coded time series as shown in Figure 24. **B_1,D_1**, Temporal courses of the latencies shown in A_2 and C_2. Small dots illustrate the latency of each eIPSC, big dots (coloring corresponding to the recovery period) show the binned mean of latencies (5-s bins). **B_2,D_2**, $SD_{Latency}$ of the binned latencies shown in B_1 and D_1, respectively, illustrating the temporal courses of the latency jitter.

were similar to WT§ (Figure $25D_1$), but in contrast, the $SD_{Latency}$ was higher in all recovery periods with values of up to ~0.17 ms (Figure $25D_2$).

3.8.1. Latencies increase in a time- and frequency-dependent manner in WT and KO

As already observed in the example cells, latency durations of all cells changed in a time- and frequency-dependent manner (Figure 26A). To get an impression about the extent of latency changes, I compared the latencies of the first and the last bin (Table 12). Additionally, I calculated the percentage of the last bin in relation to the mean of 1 Hz. As due to the binning it could have happened that number of compared events was different, I additionally performed the same analysis on the first and last 10 events (Figure S.2A, Table S.7), but the overall outcome was similar to bin analysis.

In WT, latencies at 1 Hz stayed nearly constant ($p = 0.17461$) at 1.46 ms in average (100%) with one cell depicting relatively high latencies (Figure $26A_1$). During 50 Hz, the latencies showed only a slight but no significant increase (103%; $p = 0.16726$). (It has to be mentioned that in the comparison of the first and last 10 events, a significant increase was

detected (Figure S.2A, Table S.7)). This increase was reversed during rec50, resulting in significantly shorter latencies (93%; p = 0.02454), which were even below the initial value. During 100 Hz and 200 Hz latencies were severely prolonged (p = 0.00108; p = 0.00154, respectively) resulting in 21% and 31% longer latencies compared to 1 Hz. However, this increase was clearly reversed during rec100 and rec200 (p = 0.00108; p = 0.00154, respectively) and were at the end even faster compared to 1 Hz (97% and 91%, respectively). In KO (Figure 26A$_2$), the mean latencies during 1 Hz stayed constant (p = 0.73816) at 1.59 ms in average (100%). In contrast to WT, latencies were significantly prolonged in all challenges (p ≤ 0.00144 for all comparisons) and were 21% (50 Hz), 48% (100 Hz), and 55% (200 Hz) longer compared to 1 Hz. During recoveries, these increases were reversed, illustrated by a significant decline of latencies (p ≤ 0.01871 for all comparisons). However, these reversals were not as complete as observed in WT and were longer compared to 1 Hz (rec50: 103%; rec100: 105%; rec200: 113%). For individual p values see Table 12.

Concluding from these observations, stimulation at a distinct high frequency led to latency prolongation. In KO, this effect was more pronounced compared to WT. During recoveries, the increases were reversed in both genotypes. However, in KO the reversal was not as complete as in WT.

3.8.2. $SD_{Latency}$ augments during challenges in WT and KO

Comparable to latencies, also $SD_{Latency}$ changed in a time- and frequency-dependent manner with higher values indicating a weaker synaptic precision (Figure 26). For analyzing changes, I employed the same analysis strategy as for latency data and compared the $SD_{Latency}$ of the first and the last bin (Table 13). As before, I additionally calculated the percentage of the last bin compared to the mean of 1 Hz. As supplementary data, the comparison of the first and last 10 events are shown due to the reasons mentioned before (Figure S.2B, Table S.8).

In WT, $SD_{Latency}$ during 1 Hz stimulation stayed nearly constant at 0.08 ms (100%) in average (Figure 26B$_1$). During the challenges, $SD_{Latency}$ significantly increased (p ≤ 0.02641 for all comparisons) with 175%, 450%, and 413% $SD_{Latency}$ compared to 1 Hz at the end of the challenges of 50 Hz, 100 Hz, and 200 Hz, respectively. (It has to be mentioned that in the comparison of the first and last 10 events, no significant increase was detected during 50 Hz (Figure S.2B, Table S.8)). Nevertheless, already at the beginning of recovery periods, $SD_{Latency}$

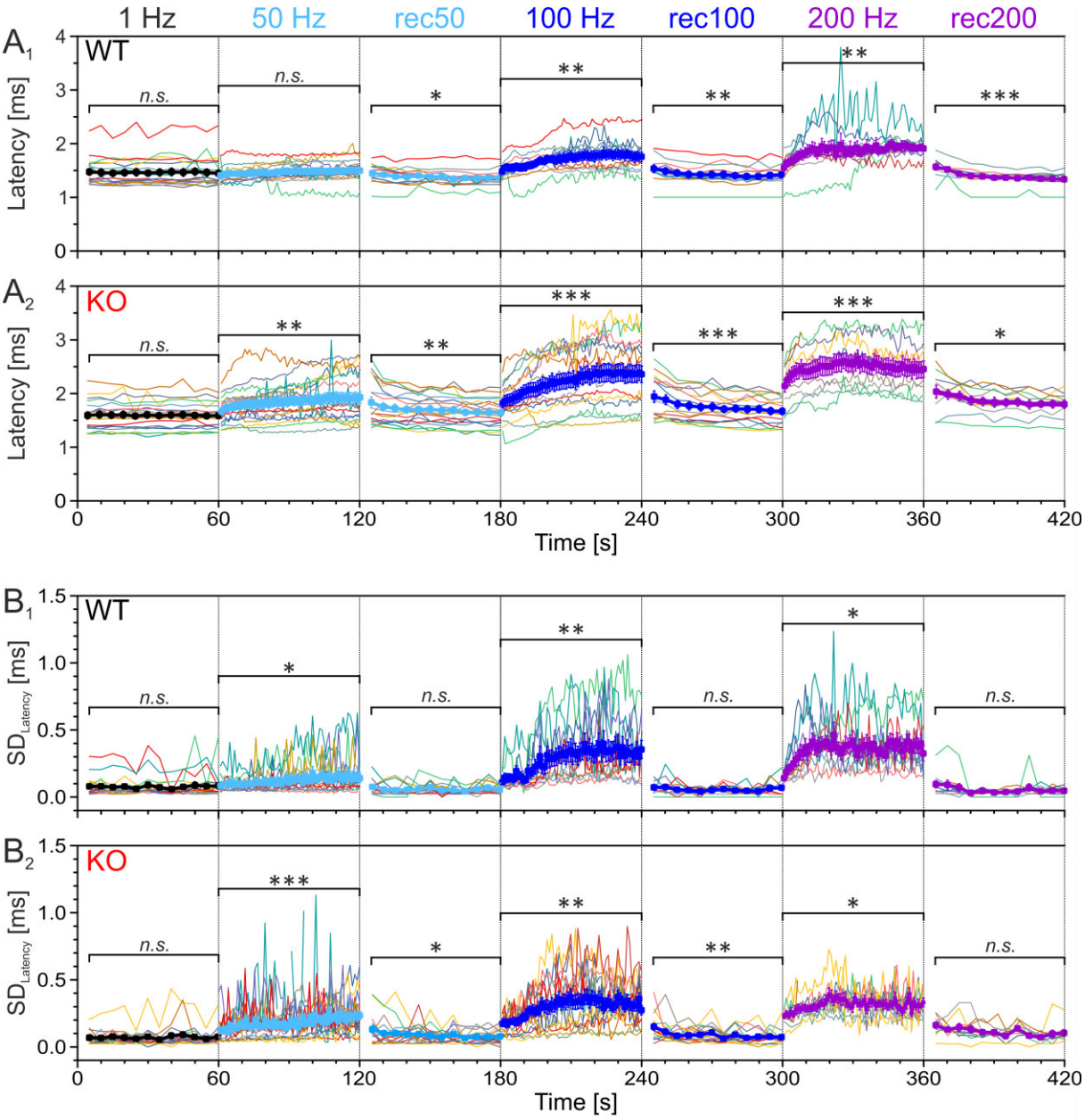

Figure 26: Challenge-induced latency prolongation and $SD_{Latency}$ increase in WT and KO
A, Latency courses in WT (**A_1**) and KO (**A_2**). Latencies of 5-s bins (1 Hz and recoveries) or 1-s bins (challenges) are illustrated for single cell data (thin lines) or as mean values (bold lines with data points). Note that only in KO, 50 Hz challenge already induces prolongation of latencies. **B,** $SD_{Latency}$ over time in WT (**B_1**) and KO (**B_2**). Values were calculated as the SD of the binned latencies. Illustration corresponds to A. Only events with eIPSCs amplitudes above threshold (= responded stimuli/events; cf. 2.3.5) were used for analysis. Significant differences were analyzed between the first and the last bins. For details see Table 12 (latency) and Table 13 ($SD_{Latency}$). For comparison between WT and KO see Figure 27, Table 14 and Table 15. For significance levels see Table 1. n (cells) = 17/14/11/10 (WT) / 18/18/15/10 (KO), no testing for outliers or normal distribution was performed; SD = standard deviation, *n.s.* = not significant

Table 12: Latency change

Condition		WT (17/14/11/10)			KO (18/18/15/10)		
		Latency [ms]	p value	sign.	Latency [ms]	p value	sign.
1 Hz	first bin	1.48 ± 0.06	0.17461	*n.s.*	1.59 ± 0.07	0.73816	*n.s.*
	last bin	1.44 ± 0.07			1.59 ± 0.06		
50 Hz	first bin	1.41 ± 0.05	0.16726	*n.s.*	1.66 ± 0.06	0.00144	**
	last bin	1.50 ± 0.05			1.93 ± 0.11		
rec50	first bin	1.44 ± 0.05	0.02454	*	1.83 ± 0.10	0.00209	**
	last bin	1.36 ± 0.04			1.64 ± 0.06		
100 Hz	first bin	1.48 ± 0.05	0.00108	**	1.82 ± 0.08	8.2×10^{-5}	***
	last bin	1.76 ± 0.09			2.36 ± 0.15		
rec100	first bin	1.53 ± 0.07	0.00321	**	1.94 ± 0.11	9.6×10^{-5}	***
	last bin	1.42 ± 0.06			1.67 ± 0.06		
200 Hz	first bin	1.55 ± 0.07	0.00154	**	2.14 ± 0.12	0.00081	***
	last bin	1.91 ± 0.04			2.46 ± 0.16		
rec200	first bin	1.56 ± 0.06	1.3×10^{-6}	***	2.03 ± 0.12	0.01871	*
	last bin	1.33 ± 0.05			1.80 ± 0.07		

Data are presented as mean latency in the first and the last bin ± SEM (cf. Figure 26A). Latencies were binned in 5-s (1 Hz and recoveries) or 1-s (challenges) intervals. Numbers in brackets depict sample sizes (number of cells). Only events with eIPSCs amplitudes above threshold (= responded stimuli/events; cf. 2.3.5) were used for analysis. Testing for outlier and normal distribution was not performed. For significance levels see Table 1. sign. = significance, *n.s.* = not significant

Table 13: $SD_{Latency}$ change

Condition		WT (17/14/11/10)			KO (18/18/15/10)		
		$SD_{Latency}$ [ms]	p value	sign.	$SD_{Latency}$ [ms]	p value	sign.
1 Hz	first bin	0.08 ± 0.02	0.85334	*n.s.*	0.07 ± 0.01	0.56602	*n.s.*
	last bin	0.08 ± 0.02			0.08 ± 0.02		
50 Hz	first bin	0.08 ± 0.01	0.02641	*	0.12 ± 0.02	0.00089	***
	last bin	0.14 ± 0.03			0.23 ± 0.03 (17)		
rec50	first bin	0.08 ± 0.02	0.17937	*n.s.*	0.13 ± 0.03	0.01099	*
	last bin	0.06 ± 0.01			0.08 ± 0.01		
100 Hz	first bin	0.11 ± 0.01	0.00177	**	0.17 ± 0.02	0.00491	**
	last bin	0.36 ± 0.07			0.27 ± 0.03		
rec100	first bin	0.07 ± 0.01	0.92219	*n.s.*	0.15 ± 0.03	0.00799	**
	last bin	0.07 ± 0.02			0.07 ± 0.01		
200 Hz	first bin	0.14 ± 0.01	0.01831	*	0.23 ± 0.02	0.02532	*
	last bin	0.33 ± 0.06			0.33 ± 0.03 (9)		
rec200	first bin	0.10 ± 0.03	0.17333	*n.s.*	0.16 ± 0.02	0.12935	*n.s.*
	last bin	0.05 ± 0.01			0.10 ± 0.02		

Data are presented as mean of the $SD_{Latency}$ in the first and the last bin ± SEM (cf. Figure 26B). Latencies were binned in 5-s (1 Hz and recoveries) or 1-s (challenges) intervals. Numbers in brackets depict sample sizes (number of cells). Only events with eIPSCs amplitudes above threshold (= responded stimuli/events; cf. 2.3.5) were used for analysis. Testing for outliers and normal distribution was not performed. For significance levels see Table 1. SD = standard deviation, sign. = significance, *n.s.* = not significant

values were comparable to the 1 Hz situation and declined towards the end to values even below the 1 Hz $SD_{Latency}$ (75%, 88%, and 63% for rec50, rec100, and rec200, respectively). For individual p values see Table 13. In KO, $SD_{Latency}$ during 1 Hz (mean ~0.08 ms, 100%) was comparable to WT and remained also nearly constant (Figure $26B_2$). During the challenges, $SD_{Latency}$ significantly increased ($p \leq 0.02532$ for all comparisons) to values being 288%, 338%, and 413% compared to the 1 Hz situation at the end of the challenges of 50 Hz, 100 Hz, and 200 Hz, respectively. This decline in synaptic precision was reversed during the ensuing recoveries as it was observed in WT. However, this reversal was not as strong as in WT (100%, 88%, and 125% for rec50, rec100 and rec200, respectively). Additionally, $SD_{Latency}$ needed longer for the reversal as in WT, indicated by the distinct higher values at the beginning of recoveries. In rec50 and rec100, the last $SD_{Latency}$ value was significantly lower compared to the first ($p \leq 0.01099$ for all comparisons). In rec200 no significant difference was calculated despite the 0.06 ms higher $SD_{Latency}$ at the beginning. However, when comparing the first and the last 10 events, the decrease was significantly different (Figure S.2B, Table S.8). For individual p values see Table 13.

Taken together, $SD_{Latency}$ increased during challenges in both genotypes and was reduced during recoveries. However, $SD_{Latency}$ during 50 Hz increased more severely in KO compared to WT. Additionally, $SD_{Latency}$ reversals during recoveries in KO show a delay which was not observed in WT.

3.8.3. Latencies during challenges and recoveries are significantly longer in KO

In both genotypes latency and $SD_{Latency}$ increased in a time- and frequency-dependent manner. When directly comparing WT and KO latencies (Figure 27A, Table 14), values of KO were significantly higher throughout all conditions (100% significance) except for 1 Hz (0% significance). Already at the beginning of 50 Hz, latencies were 18% longer in comparison to WT ($p = 0.00254$) and resulted in a difference of 29% ($p = 0.00178$) at the end. The same was observed for 100 Hz and 200 Hz with finally 34% ($p = 0.00290$) and 29% ($p = 0.00768$) longer latencies, respectively. Remarkably, the difference at the beginning of 200 Hz with 38% ($p = 0.00043$) was more pronounced compared to the end, indicating a faster latency increase in contrast to a relatively mild slope in WT. During recoveries, latency increases were reversed in both genotypes, whereas this reversal was only partial in KO. Consequently, KO latencies

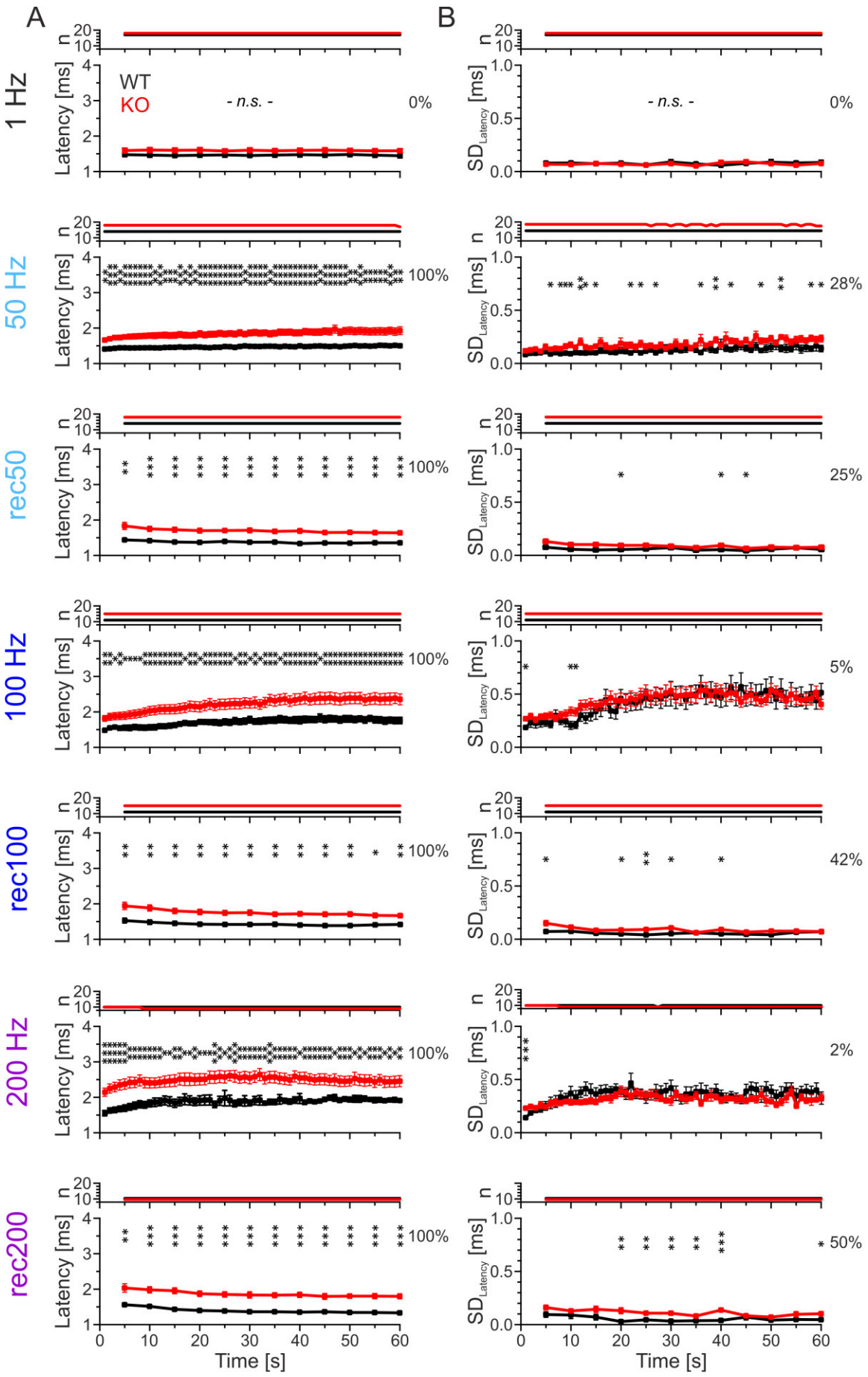

Figure 27: Latency prolongation during challenges and recoveries is more severe in KO
For legend see next page.

Figure 27: (continued) Latency prolongation during challenges and recoveries is more severe in KO
A, Overlays of KO and WT mean latencies illustrated in Figure 26A. Latencies were calculated in 5-s bins (1 Hz and recoveries) or 1-s bins (challenges). Only events with eIPSCs amplitudes above threshold (= responded stimuli; cf. 2.3.5) were used for analysis. Testing for outliers and normal distribution was not applied. Numbers on the right indicate percentage of significantly different bins. For significance levels see Table 1. The sample sizes are indicated on top. For better visibility, not significant differences are not depicted in challenges and recoveries. **B,** Overlays of KO and WT mean $SD_{Latency}$ illustrated in Figure 26B with the corresponding sample sizes. $SD_{Latency}$ was only calculated when number of events in one bin was ≥2. Data presentation is equal to A. For details see Table 14 (Latency) and Table 15 ($SD_{Latency}$). For significance levels see Table 1. n (cells) at start = 17/14/11/10 (WT) / 18/18/15/10 (KO). SD = standard deviation, *n.s.* = not significant

remained at significantly higher values compared to WT with 21%, 35%, and 35% (rec50, rec100, and rec200, respectively) longer latencies at the end of recoveries. Regarding $SD_{Latency}$, (Figure 27B, Table 15), differences were not as pronounced as for latency and mostly the values were not significantly different. During 1 Hz, no significant difference at all was detected. Remarkably, KO at 50 Hz appeared to have more difficulties in maintaining synaptic precision in comparison to WT, indicated by significantly higher values in 28% of comparisons. During 100 Hz and 200 Hz, $SD_{Latency}$ courses nearly coincided (5%, 2% significant different comparisons, respectively), with the significant differences detected during the first 11 s. For example, KO $SD_{Latency}$ during the first second at 100 Hz and 200 Hz was 55% and 64% higher compared to WT, respectively. Regarding recoveries, $SD_{Latency}$ in both genotypes declined and differed significantly in 25% or 42% of comparisons in rec50 and rec100, respectively. Remarkably, during rec200 a more distinct difference (50% significantly different comparisons) was observed, for example +250% in KO during 35-40 s.

Taken together, KO cells started with only mildly higher latencies, but their prolongation during challenges was more pronounced and the decrease during recoveries occurred to only a minor extent compared to WT. Therefore, latencies were significantly longer throughout all challenges and recoveries. Regarding $SD_{Latency}$, differences between KO and WT were not as pronounced as observed for latencies with significant differences in less than 50% of comparisons. The most striking differences occurred during 50 Hz and rec200, indicating a better maintenance of synaptic precision during 50 Hz and a more effective reversal during rec200 in WT.

Table 14: Latency comparison between WT and KO

time	Latency [ms]																									
	1 Hz				50 Hz				rec50				100 Hz				rec100				200 Hz				rec200			
	WT (17)	KO (18)	p value	sign.	WT (14)	KO (18)	p value	sign.	WT (14)	KO (18)	p value	sign.	WT (11)	KO (15)	p value	sign.	WT (11)	KO (15)	p value	sign.	WT (10)	KO (10)	p value	sign.	WT (10)	KO (10)	p value	sign.
1					1.41 ± 0.05	1.66 ± 0.06	0.00254	**					1.48 ± 0.05	1.82 ± 0.08	0.00170	**					1.55 ± 0.07	2.14 ± 0.12	0.00043	***				
2					1.42 ± 0.04	1.70 ± 0.06	0.00043	***					1.55 ± 0.04	1.86 ± 0.10	0.00980	**					1.63 ± 0.07	2.25 ± 0.13	0.00052	***				
3					1.43 ± 0.04	1.73 ± 0.06	0.00041	***					1.57 ± 0.05	1.88 ± 0.10	0.01314	*					1.65 ± 0.08	2.29 ± 0.13	0.00053	***				
4					1.44 ± 0.04	1.73 ± 0.07	0.00119	**					1.54 ± 0.06	1.89 ± 0.10	0.00894	**					1.67 ± 0.08	2.35 ± 0.15	0.00067	***				
5	1.48 ± 0.06	1.59 ± 0.07	0.21632	*n.s.*	1.44 ± 0.04	1.75 ± 0.07	0.00041	***	1.44 ± 0.05	1.83 ± 0.10	0.00188	**	1.55 ± 0.07	1.90 ± 0.11	0.02151	*	1.53 ± 0.07	1.94 ± 0.11	0.00692	**	1.70 ± 0.09	2.37 ± 0.15	0.00093	***	1.56 ± 0.06	2.03 ± 0.12	0.00250	**
6					1.44 ± 0.04	1.76 ± 0.07	0.00082	***					1.55 ± 0.08	1.92 ± 0.11	0.01744	*					1.73 ± 0.09	2.42 ± 0.15	0.00121	**				
7					1.44 ± 0.04	1.77 ± 0.08	0.00080	***					1.57 ± 0.07	1.94 ± 0.11	0.02010	*					1.77 ± 0.10	2.42 ± 0.15	0.00158	**				
8					1.44 ± 0.04	1.77 ± 0.07	0.00066	***					1.56 ± 0.07	1.96 ± 0.12	0.01344	*					1.80 ± 0.10	2.48 ± 0.16	0.00189	**				
9					1.44 ± 0.04	1.78 ± 0.07	0.00054	***					1.56 ± 0.07	2.00 ± 0.12	0.00437	**					1.79 ± 0.09	2.41 ± 0.15 (9)	0.00188	**				
10	1.46 ± 0.07	1.61 ± 0.07	0.14600	*n.s.*	1.44 ± 0.04	1.79 ± 0.08	0.00058	***	1.42 ± 0.05	1.75 ± 0.08	0.00087	***	1.56 ± 0.07	2.03 ± 0.12	0.00388	**	1.48 ± 0.07	1.88 ± 0.09	0.00268	**	1.83 ± 0.10	2.41 ± 0.14 (9)	0.00330	**	1.51 ± 0.03	1.98 ± 0.09	0.00044	***
11					1.44 ± 0.04	1.79 ± 0.08	0.00108	**					1.57 ± 0.07	2.04 ± 0.12	0.00347	**					1.86 ± 0.12	2.41 ± 0.14 (9)	0.00792	**				
12					1.44 ± 0.04	1.80 ± 0.08	0.00050	***					1.60 ± 0.07	2.07 ± 0.13	0.00340	**					1.87 ± 0.11	2.42 ± 0.15 (9)	0.00650	**				
13					1.45 ± 0.04	1.80 ± 0.09	0.00110	**					1.59 ± 0.07	2.07 ± 0.13	0.00342	**					1.91 ± 0.12	2.45 ± 0.16 (9)	0.01508	*				
14					1.45 ± 0.04	1.79 ± 0.08	0.00120	**					1.61 ± 0.07	2.07 ± 0.13	0.00489	**					1.89 ± 0.13	2.46 ± 0.16 (9)	0.01262	*				
15	1.45 ± 0.06	1.60 ± 0.06	0.10306	*n.s.*	1.46 ± 0.04	1.80 ± 0.08	0.00106	**	1.38 ± 0.04	1.73 ± 0.07	0.00042	***	1.63 ± 0.07	2.08 ± 0.13	0.00570	**	1.45 ± 0.07	1.80 ± 0.08	0.00341	**	1.83 ± 0.12	2.47 ± 0.16 (9)	0.00481	**	1.43 ± 0.05	1.96 ± 0.08	0.00004	***
16					1.47 ± 0.04	1.82 ± 0.08	0.00083	***					1.66 ± 0.06	2.10 ± 0.14	0.00860	**					1.88 ± 0.12	2.51 ± 0.17 (9)	0.00603	**				
17					1.46 ± 0.04	1.80 ± 0.08	0.00100	**					1.69 ± 0.07	2.12 ± 0.14	0.01064	*					1.94 ± 0.15	2.51 ± 0.18 (9)	0.02683	*				
18					1.46 ± 0.04	1.79 ± 0.08	0.00097	***					1.67 ± 0.06	2.16 ± 0.14	0.00551	**					1.91 ± 0.13	2.51 ± 0.18 (9)	0.01330	*				
19					1.47 ± 0.04	1.80 ± 0.08	0.00132	**					1.68 ± 0.06	2.15 ± 0.14	0.00643	**					1.88 ± 0.11	2.50 ± 0.16 (9)	0.00460	**				
20	1.46 ± 0.06	1.60 ± 0.07	0.13327	*n.s.*	1.46 ± 0.04	1.84 ± 0.09	0.00088	***	1.37 ± 0.05	1.70 ± 0.07	0.00054	***	1.72 ± 0.07	2.14 ± 0.14	0.01401	*	1.42 ± 0.06	1.77 ± 0.08	0.00364	**	1.91 ± 0.13	2.51 ± 0.16 (9)	0.01007	*	1.40 ± 0.05	1.87 ± 0.08	0.00010	***
21					1.45 ± 0.04	1.81 ± 0.08	0.00077	***					1.72 ± 0.07	2.18 ± 0.14	0.00857	**					1.92 ± 0.14	2.51 ± 0.16 (9)	0.01226	*				
22					1.44 ± 0.05	1.82 ± 0.09	0.00060	***					1.71 ± 0.07	2.22 ± 0.15	0.00680	**					1.93 ± 0.14	2.57 ± 0.17 (9)	0.01025	*				
23					1.46 ± 0.05	1.83 ± 0.08	0.00073	***					1.71 ± 0.08	2.18 ± 0.14	0.00774	**					1.80 ± 0.09	2.56 ± 0.17 (9)	0.00081	***				
24					1.46 ± 0.04	1.85 ± 0.08	0.00036	***					1.69 ± 0.08	2.21 ± 0.14	0.00464	**					1.90 ± 0.13	2.59 ± 0.17 (9)	0.00487	**				
25	1.47 ± 0.07	1.58 ± 0.06	0.23051	*n.s.*	1.48 ± 0.04	1.83 ± 0.08	0.00075	***	1.40 ± 0.04	1.70 ± 0.06	0.00020	***	1.72 ± 0.08	2.21 ± 0.14	0.00753	**	1.42 ± 0.06	1.75 ± 0.07	0.00329	**	1.98 ± 0.22	2.57 ± 0.17 (9)	0.04995	*	1.38 ± 0.05	1.85 ± 0.08	0.00008	***
26					1.47 ± 0.04	1.85 ± 0.08	0.00041	***					1.71 ± 0.08	2.23 ± 0.15	0.00510	**					1.91 ± 0.15	2.61 ± 0.14 (9)	0.00381	**				
27					1.47 ± 0.05	1.83 ± 0.08	0.00085	***					1.75 ± 0.09	2.23 ± 0.15	0.01034	*					1.82 ± 0.09	2.59 ± 0.17 (9)	0.00065	***				
28					1.48 ± 0.05	1.87 ± 0.09	0.00070	***					1.72 ± 0.08	2.23 ± 0.14	0.00583	**					1.86 ± 0.09	2.55 ± 0.16 (9)	0.00107	**				
29					1.50 ± 0.05	1.83 ± 0.08	0.00133	**					1.74 ± 0.09	2.26 ± 0.14	0.00532	**					1.90 ± 0.15	2.57 ± 0.16 (9)	0.00648	**				
30	1.45 ± 0.06	1.60 ± 0.06	0.09919	*n.s.*	1.49 ± 0.05	1.86 ± 0.08	0.00071	***	1.37 ± 0.04	1.71 ± 0.07	0.00031	***	1.78 ± 0.09	2.24 ± 0.14	0.01684	*	1.42 ± 0.06	1.75 ± 0.08	0.00471	**	1.84 ± 0.08	2.55 ± 0.16 (9)	0.00102	**	1.36 ± 0.05	1.84 ± 0.09	0.00042	***
31					1.48 ± 0.05	1.87 ± 0.08	0.00045	***					1.73 ± 0.08	2.27 ± 0.15	0.00547	**					1.91 ± 0.12	2.58 ± 0.16 (9)	0.00332	**				
32					1.48 ± 0.05	1.86 ± 0.09	0.00076	***					1.74 ± 0.09	2.21 ± 0.14	0.01234	*					1.92 ± 0.13	2.64 ± 0.17 (9)	0.00391	**				
33					1.49 ± 0.05	1.87 ± 0.08	0.00049	***					1.76 ± 0.09	2.27 ± 0.14	0.00921	**					1.84 ± 0.06	2.54 ± 0.16 (9)	0.00219	**				
34					1.49 ± 0.05	1.84 ± 0.09	0.00177	**					1.77 ± 0.08	2.34 ± 0.15	0.00381	**					1.87 ± 0.08	2.57 ± 0.16 (9)	0.00081	***				
35	1.46 ± 0.07	1.59 ± 0.06	0.18061	*n.s.*	1.49 ± 0.05	1.86 ± 0.08	0.00084	***	1.38 ± 0.04	1.68 ± 0.07	0.00058	***	1.77 ± 0.09	2.31 ± 0.15	0.00530	**	1.42 ± 0.07	1.71 ± 0.07	0.00686	**	1.87 ± 0.08	2.57 ± 0.17 (9)	0.00265	**	1.36 ± 0.04	1.83 ± 0.07	0.00004	***
36					1.47 ± 0.05	1.88 ± 0.09	0.00041	***					1.80 ± 0.10	2.34 ± 0.15	0.01010	*					1.94 ± 0.13	2.54 ± 0.16 (9)	0.00987	**				
37					1.49 ± 0.05	1.88 ± 0.09	0.00045	***					1.78 ± 0.09	2.36 ± 0.16	0.00377	**					1.90 ± 0.07	2.52 ± 0.16 (9)	0.00442	**				
38					1.48 ± 0.05	1.89 ± 0.09	0.00034	***					1.76 ± 0.08	2.31 ± 0.15	0.00415	**					1.88 ± 0.07	2.49 ± 0.14 (9)	0.00122	**				
39					1.47 ± 0.05	1.86 ± 0.09	0.00053	***					1.77 ± 0.09	2.35 ± 0.16	0.00490	**					1.92 ± 0.09	2.59 ± 0.16 (9)	0.00145	**				
40	1.47 ± 0.07	1.60 ± 0.06	0.21142	*n.s.*	1.50 ± 0.05	1.87 ± 0.09	0.00088	***	1.34 ± 0.04	1.69 ± 0.07	0.00018	***	1.77 ± 0.10	2.36 ± 0.15	0.00634	**	1.40 ± 0.06	1.72 ± 0.07	0.00322	**	1.97 ± 0.14	2.55 ± 0.16 (9)	0.01352	*	1.35 ± 0.04	1.84 ± 0.08	0.00002	***
41					1.47 ± 0.05	1.90 ± 0.09	0.00037	***					1.79 ± 0.09	2.39 ± 0.17	0.00475	**					1.86 ± 0.06	2.55 ± 0.16 (9)	0.00241	**				
42					1.48 ± 0.05	1.89 ± 0.09	0.00036	***					1.79 ± 0.08	2.35 ± 0.15	0.00411	**					1.90 ± 0.06	2.52 ± 0.15 (9)	0.00283	**				
43					1.49 ± 0.05	1.89 ± 0.09	0.00080	***					1.78 ± 0.08	2.37 ± 0.16	0.00335	**					1.87 ± 0.06	2.49 ± 0.14 (9)	0.00217	**				
44					1.49 ± 0.05	1.89 ± 0.09	0.00103	**					1.83 ± 0.11	2.39 ± 0.17	0.02028	*					1.90 ± 0.05	2.51 ± 0.16 (9)	0.00398	**				
45	1.46 ± 0.07	1.60 ± 0.06	0.15951	*n.s.*	1.49 ± 0.05	1.91 ± 0.09	0.00049	***	1.35 ± 0.04	1.65 ± 0.06	0.00082	***	1.79 ± 0.10	2.38 ± 0.16	0.00523	**	1.39 ± 0.06	1.71 ± 0.07	0.00312	**	1.94 ± 0.06	2.51 ± 0.16 (9)	0.00656	**	1.36 ± 0.03	1.80 ± 0.08	0.00044	***
46					1.48 ± 0.05	1.90 ± 0.10	0.00082	***					1.81 ± 0.09	2.39 ± 0.17	0.00560	**					1.99 ± 0.07	2.48 ± 0.14 (9)	0.00522	**				
47					1.49 ± 0.05	1.97 ± 0.11	0.00079	***					1.80 ± 0.09	2.37 ± 0.17	0.00633	**					1.99 ± 0.09	2.50 ± 0.17 (9)	0.01410	*				
48					1.47 ± 0.05	1.89 ± 0.09	0.00063	***					1.78 ± 0.09	2.35 ± 0.16	0.00508	**					1.92 ± 0.07	2.46 ± 0.15 (9)	0.00757	**				
49					1.49 ± 0.06	1.92 ± 0.10	0.00063	***					1.80 ± 0.09	2.38 ± 0.16	0.00526	**					1.95 ± 0.06	2.45 ± 0.14 (9)	0.00803	**				
50	1.48 ± 0.07	1.59 ± 0.06	0.21489	*n.s.*	1.50 ± 0.05	1.93 ± 0.10	0.00111	**	1.35 ± 0.04	1.65 ± 0.06	0.00015	***	1.80 ± 0.09	2.39 ± 0.16	0.00471	**	1.39 ± 0.06	1.71 ± 0.07	0.00267	**	1.94 ± 0.07	2.46 ± 0.14 (9)	0.00336	**	1.34 ± 0.05	1.80 ± 0.06	0.00002	***
51					1.51 ± 0.05	1.91 ± 0.10	0.00143	**					1.79 ± 0.09	2.39 ± 0.16	0.00296	**					1.96 ± 0.10	2.53 ± 0.18 (9)	0.01018	*				
52					1.49 ± 0.05	1.92 ± 0.10	0.00088	***					1.81 ± 0.08	2.39 ± 0.16	0.00422	**					1.96 ± 0.10	2.49 ± 0.16 (9)	0.00891	**				
53					1.50 ± 0.06	1.91 ± 0.10	0.00142	**					1.77 ± 0.09	2.34 ± 0.15	0.00399	**					1.96 ± 0.07	2.47 ± 0.16 (9)	0.01464	*				
54					1.49 ± 0.05	1.90 ± 0.10	0.00103	**					1.82 ± 0.08	2.36 ± 0.15	0.00508	**					1.94 ± 0.05	2.48 ± 0.15 (9)	0.00724	**				
55	1.46 ± 0.07	1.58 ± 0.06	0.18674	*n.s.*	1.50 ± 0.05	1.91 ± 0.10	0.00146	**	1.36 ± 0.04	1.64 ± 0.06	0.00070	***	1.78 ± 0.09	2.38 ± 0.16	0.00409	**	1.41 ± 0.06	1.67 ± 0.07	0.01064	*	1.92 ± 0.07	2.43 ± 0.16 (9)	0.00700	**	1.34 ± 0.04	1.80 ± 0.08	0.00004	***
56					1.51 ± 0.06	1.91 ± 0.11	0.00283	**					1.77 ± 0.09	2.36 ± 0.15	0.00368	**					1.93 ± 0.07	2.49 ± 0.15 (9)	0.00560	**				
57					1.51 ± 0.06	1.90 ± 0.10	0.00272	**					1.75 ± 0.09	2.36 ± 0.16	0.00295	**					1.91 ± 0.05	2.44 ± 0.16 (9)	0.01101	*				
58					1.50 ± 0.06	1.93 ± 0.10	0.00093	***					1.77 ± 0.08	2.37 ± 0.17	0.00418	**					1.92 ± 0.05	2.44 ± 0.15 (9)	0.00776	**				
59					1.51 ± 0.05	1.90 ± 0.11	0.00329	**					1.76 ± 0.09	2.39 ± 0.15	0.00142	**					1.93 ± 0.07	2.44 ± 0.16 (9)	0.01178	*				
60	1.44 ± 0.07	1.59 ± 0.06	0.12009	*n.s.*	1.50 ± 0.05	1.93 ± 0.11 (17)	0.00178	**	1.36 ± 0.04	1.64 ± 0.06	0.00074	***	1.76 ± 0.09	2.36 ± 0.15	0.00290	**	1.42 ± 0.06	1.67 ± 0.06	0.00999	**	1.91 ± 0.04	2.46 ± 0.16 (9)	0.00768	**	1.33 ± 0.05	1.80 ± 0.07	0.00004	***

Data are presented as mean latencies ± SEM of events (cf. 2.3.5) in 5-s (1 Hz and recoveries) or 1-s (challenges) bins (cf. Figure 27A). Numbers in brackets depict sample sizes (number of cells). Only events with eIPSCs amplitudes above threshold (= responded stimuli; cf. 2.3.5) were used for analysis. Sample sizes in KO 50 Hz at 60 s and KO 200 Hz after 9 s are reduced due to cells with too few events in these bins. The reduced sample size is indicated in brackets at the affected datasets. Testing for outlier and normal distribution was not performed. For significance levels see Table 1. sign. = significance, *n.s.* = not significant

Table 15: $SD_{Latency}$ comparison between WT and KO

time	$SD_{Latency}$ [ms]																									
	1 Hz				50 Hz				rec50				100 Hz				rec100				200 Hz				rec200			
	WT (17)	KO (18)	p value	sign.	WT (14)	KO (18)	p value	sign.	WT (14)	KO (18)	p value	sign.	WT (11)	KO (15)	p value	sign.	WT (11)	KO (15)	p value	sign.	WT (10)	KO (10)	p value	sign.	WT (10)	KO (10)	p value	sign.
1					0.08 ± 0.01	0.12 ± 0.02	0.18781	*n.s.*					0.11 ± 0.01	0.17 ± 0.02	0.01215	*					0.14 ± 0.01	0.23 ± 0.02	0.00082	***				
2					0.10 ± 0.01	0.13 ± 0.02	0.28026	*n.s.*					0.14 ± 0.03	0.19 ± 0.02	0.26225	*n.s.*					0.19 ± 0.02	0.25 ± 0.02	0.06714	*n.s.*				
3					0.10 ± 0.01	0.14 ± 0.02	0.09627	*n.s.*					0.14 ± 0.03	0.17 ± 0.02	0.51292	*n.s.*					0.21 ± 0.03	0.23 ± 0.02	0.60534	*n.s.*				
4					0.10 ± 0.01	0.11 ± 0.01	0.44350	*n.s.*					0.14 ± 0.03	0.19 ± 0.02	0.23548	*n.s.*					0.23 ± 0.03	0.26 ± 0.03	0.44656	*n.s.*				
5	0.08 ± 0.02	0.07 ± 0.01	0.61294	*n.s.*	0.11 ± 0.02	0.16 ± 0.03	0.27052	*n.s.*	0.08 ± 0.02	0.13 ± 0.03	0.07656	*n.s.*	0.15 ± 0.03	0.19 ± 0.02	0.21731	*n.s.*	0.07 ± 0.01	0.15 ± 0.03	0.01386	*	0.25 ± 0.04	0.24 ± 0.02	0.84711	*n.s.*	0.10 ± 0.03	0.16 ± 0.02	0.07690	*n.s.*
6					0.09 ± 0.01	0.13 ± 0.01	0.01538	*					0.13 ± 0.02	0.19 ± 0.03	0.10466	*n.s.*					0.28 ± 0.05	0.28 ± 0.03	0.95595	*n.s.*				
7					0.10 ± 0.02	0.14 ± 0.02	0.14592	*n.s.*					0.19 ± 0.04	0.18 ± 0.02	0.71307	*n.s.*					0.29 ± 0.06	0.28 ± 0.03	0.89154	*n.s.*				
8					0.09 ± 0.01	0.14 ± 0.02	0.02968	*					0.16 ± 0.03	0.20 ± 0.03	0.33549	*n.s.*					0.33 ± 0.06	0.28 ± 0.02 (9)	0.38343	*n.s.*				
9					0.10 ± 0.01	0.16 ± 0.03	0.03855	*					0.15 ± 0.04	0.20 ± 0.03	0.27005	*n.s.*					0.32 ± 0.05	0.29 ± 0.02 (9)	0.58552	*n.s.*				
10	0.08 ± 0.02	0.07 ± 0.01	0.51521	*n.s.*	0.09 ± 0.01	0.17 ± 0.03	0.01022	*	0.06 ± 0.01	0.10 ± 0.02	0.07518	*n.s.*	0.13 ± 0.03	0.22 ± 0.03	0.02926	*	0.07 ± 0.02	0.11 ± 0.02	0.24150	*n.s.*	0.37 ± 0.07	0.29 ± 0.03 (9)	0.26821	*n.s.*	0.09 ± 0.03	0.13 ± 0.02	0.33308	*n.s.*
11					0.10 ± 0.01	0.15 ± 0.02	0.06192	*n.s.*					0.13 ± 0.02	0.22 ± 0.03	0.02770	*					0.33 ± 0.06	0.29 ± 0.02 (9)	0.47708	*n.s.*				
12					0.10 ± 0.01	0.20 ± 0.03	0.00911	**					0.20 ± 0.04	0.27 ± 0.04	0.23120	*n.s.*					0.38 ± 0.05	0.29 ± 0.02 (9)	0.11408	*n.s.*				
13					0.10 ± 0.01	0.15 ± 0.02	0.04615	*					0.18 ± 0.04	0.27 ± 0.04	0.09254	*n.s.*					0.41 ± 0.06	0.29 ± 0.03 (9)	0.10544	*n.s.*				
14					0.10 ± 0.02	0.15 ± 0.02	0.07556	*n.s.*					0.20 ± 0.04	0.28 ± 0.04	0.20092	*n.s.*					0.39 ± 0.07	0.30 ± 0.03 (9)	0.28746	*n.s.*				
15	0.07 ± 0.02	0.08 ± 0.01	0.94798	*n.s.*	0.10 ± 0.01	0.16 ± 0.02	0.02540	*	0.05 ± 0.01	0.10 ± 0.02	0.06003	*n.s.*	0.22 ± 0.06	0.26 ± 0.04	0.55776	*n.s.*	0.06 ± 0.01	0.08 ± 0.01	0.16912	*n.s.*	0.36 ± 0.06	0.29 ± 0.03 (9)	0.28205	*n.s.*	0.07 ± 0.03	0.15 ± 0.03	0.08962	*n.s.*
16					0.12 ± 0.03	0.20 ± 0.04	0.11505	*n.s.*					0.24 ± 0.06	0.27 ± 0.04	0.66963	*n.s.*					0.39 ± 0.06	0.32 ± 0.03 (9)	0.30110	*n.s.*				
17					0.12 ± 0.02	0.16 ± 0.03	0.20518	*n.s.*					0.30 ± 0.07	0.29 ± 0.05	0.86751	*n.s.*					0.39 ± 0.06	0.33 ± 0.03 (9)	0.29377	*n.s.*				
18					0.10 ± 0.02	0.15 ± 0.02	0.08249	*n.s.*					0.23 ± 0.05	0.32 ± 0.05	0.21038	*n.s.*					0.39 ± 0.04	0.32 ± 0.04 (9)	0.19948	*n.s.*				
19					0.10 ± 0.02	0.16 ± 0.02	0.06292	*n.s.*					0.22 ± 0.05	0.30 ± 0.05	0.28256	*n.s.*					0.41 ± 0.05	0.35 ± 0.03 (9)	0.34785	*n.s.*				
20	0.08 ± 0.02	0.07 ± 0.02	0.66748	*n.s.*	0.12 ± 0.03	0.19 ± 0.05	0.25520	*n.s.*	0.05 ± 0.01	0.09 ± 0.01	0.02564	*	0.31 ± 0.06	0.30 ± 0.05	0.86698	*n.s.*	0.05 ± 0.01	0.09 ± 0.01	0.03493	*	0.38 ± 0.04	0.39 ± 0.05 (9)	0.89233	*n.s.*	0.03 ± 0.00	0.13 ± 0.03	0.00618	**
21					0.11 ± 0.02	0.17 ± 0.03	0.16749	*n.s.*					0.28 ± 0.07	0.29 ± 0.05	0.90318	*n.s.*					0.36 ± 0.05	0.38 ± 0.05 (9)	0.79862	*n.s.*				
22					0.10 ± 0.02	0.17 ± 0.03	0.04869	*					0.29 ± 0.06	0.31 ± 0.05	0.76985	*n.s.*					0.47 ± 0.09	0.34 ± 0.03 (9)	0.23517	*n.s.*				
23					0.13 ± 0.02	0.16 ± 0.03	0.44323	*n.s.*					0.29 ± 0.05	0.31 ± 0.05	0.76264	*n.s.*					0.37 ± 0.05	0.38 ± 0.04 (9)	0.88195	*n.s.*				
24					0.10 ± 0.02	0.18 ± 0.03	0.03502	*					0.30 ± 0.06	0.33 ± 0.06	0.72237	*n.s.*					0.36 ± 0.05	0.36 ± 0.04 (9)	0.97353	*n.s.*				
25	0.06 ± 0.01	0.06 ± 0.01	0.89053	*n.s.*	0.12 ± 0.02	0.16 ± 0.03	0.28860	*n.s.*	0.06 ± 0.01	0.09 ± 0.02	0.13525	*n.s.*	0.32 ± 0.06	0.35 ± 0.06	0.66757	*n.s.*	0.04 ± 0.01	0.09 ± 0.01	0.00512	**	0.33 ± 0.05 (9)	0.35 ± 0.04 (9)	0.73108	*n.s.*	0.05 ± 0.01	0.11 ± 0.02	0.00519	**
26					0.13 ± 0.02	0.17 ± 0.02 (17)	0.20968	*n.s.*					0.31 ± 0.06	0.32 ± 0.05	0.87909	*n.s.*					0.35 ± 0.05	0.36 ± 0.05 (9)	0.93792	*n.s.*				
27					0.10 ± 0.01	0.15 ± 0.02	0.03092	*					0.33 ± 0.06	0.34 ± 0.05	0.85055	*n.s.*					0.39 ± 0.07	0.35 ± 0.05 (9)	0.68271	*n.s.*				
28					0.12 ± 0.03	0.17 ± 0.03	0.20599	*n.s.*					0.31 ± 0.07	0.33 ± 0.06	0.82584	*n.s.*					0.38 ± 0.06	0.32 ± 0.03 (9)	0.36452	*n.s.*				
29					0.14 ± 0.03	0.14 ± 0.02	0.94999	*n.s.*					0.34 ± 0.07	0.35 ± 0.06	0.84883	*n.s.*					0.39 ± 0.07	0.30 ± 0.02 (9)	0.22626	*n.s.*				
30	0.09 ± 0.02	0.07 ± 0.02	0.60614	*n.s.*	0.11 ± 0.02	0.16 ± 0.02 (17)	0.09773	*n.s.*	0.07 ± 0.01	0.09 ± 0.02	0.48890	*n.s.*	0.35 ± 0.09	0.37 ± 0.06	0.83477	*n.s.*	0.05 ± 0.01	0.11 ± 0.02	0.01089	*	0.42 ± 0.07	0.30 ± 0.04 (9)	0.18557	*n.s.*	0.03 ± 0.01	0.11 ± 0.02	0.00250	**
31					0.14 ± 0.03	0.19 ± 0.04	0.29622	*n.s.*					0.32 ± 0.08	0.33 ± 0.05	0.91267	*n.s.*					0.37 ± 0.07	0.37 ± 0.03 (9)	0.94632	*n.s.*				
32					0.12 ± 0.02	0.16 ± 0.03	0.26866	*n.s.*					0.33 ± 0.07	0.33 ± 0.06	0.99864	*n.s.*					0.32 ± 0.05	0.33 ± 0.03 (9)	0.83184	*n.s.*				
33					0.14 ± 0.03	0.19 ± 0.03 (17)	0.22109	*n.s.*					0.31 ± 0.07	0.34 ± 0.06	0.72651	*n.s.*					0.36 ± 0.07	0.32 ± 0.04 (9)	0.58983	*n.s.*				
34					0.14 ± 0.03	0.15 ± 0.02	0.95018	*n.s.*					0.34 ± 0.07	0.34 ± 0.05	0.95390	*n.s.*					0.36 ± 0.07	0.32 ± 0.02 (9)	0.52816	*n.s.*				
35	0.07 ± 0.02	0.05 ± 0.01	0.30559	*n.s.*	0.13 ± 0.03	0.17 ± 0.02	0.31976	*n.s.*	0.05 ± 0.01	0.07 ± 0.01	0.08009	*n.s.*	0.34 ± 0.07	0.33 ± 0.05	0.88404	*n.s.*	0.06 ± 0.01	0.06 ± 0.01	0.90635	*n.s.*	0.39 ± 0.06	0.35 ± 0.04 (9)	0.59954	*n.s.*	0.04 ± 0.01	0.08 ± 0.01	0.00572	**
36					0.10 ± 0.02	0.22 ± 0.05	0.04800	*					0.40 ± 0.08	0.37 ± 0.06	0.80550	*n.s.*					0.39 ± 0.08	0.28 ± 0.03 (9)	0.24154	*n.s.*				
37					0.15 ± 0.04	0.17 ± 0.02 (17)	0.69526	*n.s.*					0.34 ± 0.06	0.37 ± 0.06	0.67958	*n.s.*					0.38 ± 0.06	0.33 ± 0.03 (9)	0.49605	*n.s.*				
38					0.14 ± 0.03	0.19 ± 0.02	0.17710	*n.s.*					0.36 ± 0.07	0.34 ± 0.05	0.78057	*n.s.*					0.36 ± 0.06	0.35 ± 0.05 (9)	0.91158	*n.s.*				
39					0.12 ± 0.02	0.22 ± 0.03 (17)	0.00884	**					0.33 ± 0.07	0.37 ± 0.05	0.69848	*n.s.*					0.39 ± 0.06	0.33 ± 0.03 (9)	0.37765	*n.s.*				
40	0.06 ± 0.01	0.08 ± 0.02	0.32270	*n.s.*	0.18 ± 0.05	0.17 ± 0.02	0.85786	*n.s.*	0.05 ± 0.01	0.09 ± 0.01	0.03696	*	0.32 ± 0.07	0.36 ± 0.05	0.62491	*n.s.*	0.05 ± 0.01	0.09 ± 0.01	0.04088	*	0.35 ± 0.05	0.30 ± 0.03 (9)	0.42981	*n.s.*	0.04 ± 0.01	0.14 ± 0.02	0.00053	***
41					0.14 ± 0.03	0.24 ± 0.06	0.13815	*n.s.*					0.34 ± 0.08	0.34 ± 0.05	0.99496	*n.s.*					0.33 ± 0.05	0.32 ± 0.03 (9)	0.93616	*n.s.*				
42					0.13 ± 0.02	0.21 ± 0.03	0.04492	*					0.39 ± 0.09	0.35 ± 0.06	0.70800	*n.s.*					0.34 ± 0.04	0.32 ± 0.02 (9)	0.63338	*n.s.*				
43					0.15 ± 0.03	0.21 ± 0.02	0.14758	*n.s.*					0.34 ± 0.08	0.35 ± 0.05	0.97110	*n.s.*					0.33 ± 0.04	0.31 ± 0.04 (9)	0.76663	*n.s.*				
44					0.17 ± 0.04	0.19 ± 0.02	0.62643	*n.s.*					0.40 ± 0.10	0.29 ± 0.04	0.32646	*n.s.*					0.31 ± 0.04	0.32 ± 0.03 (9)	0.84532	*n.s.*				
45	0.08 ± 0.01	0.09 ± 0.02	0.58708	*n.s.*	0.14 ± 0.03	0.22 ± 0.03	0.07742	*n.s.*	0.04 ± 0.00	0.07 ± 0.01	0.03529	*	0.33 ± 0.07	0.32 ± 0.04	0.91559	*n.s.*	0.05 ± 0.01	0.07 ± 0.01	0.27464	*n.s.*	0.39 ± 0.07	0.30 ± 0.02 (9)	0.20797	*n.s.*	0.07 ± 0.03	0.08 ± 0.01	0.66641	*n.s.*
46					0.13 ± 0.03	0.18 ± 0.02	0.17217	*n.s.*					0.35 ± 0.08	0.34 ± 0.05	0.91178	*n.s.*					0.42 ± 0.06	0.32 ± 0.03 (9)	0.15861	*n.s.*				
47					0.16 ± 0.04	0.26 ± 0.04	0.10400	*n.s.*					0.34 ± 0.07	0.31 ± 0.04	0.75950	*n.s.*					0.41 ± 0.06	0.31 ± 0.03 (9)	0.19718	*n.s.*				
48					0.12 ± 0.02	0.21 ± 0.03	0.02804	*					0.35 ± 0.07	0.30 ± 0.04	0.50928	*n.s.*					0.36 ± 0.08	0.36 ± 0.05 (9)	0.98513	*n.s.*				
49					0.14 ± 0.04	0.21 ± 0.02	0.08022	*n.s.*					0.37 ± 0.08	0.31 ± 0.04	0.49889	*n.s.*					0.41 ± 0.07	0.30 ± 0.05 (9)	0.19850	*n.s.*				
50	0.09 ± 0.03	0.07 ± 0.02	0.65731	*n.s.*	0.15 ± 0.04	0.23 ± 0.03	0.09102	*n.s.*	0.06 ± 0.01	0.08 ± 0.01	0.17675	*n.s.*	0.38 ± 0.09	0.37 ± 0.05	0.96882	*n.s.*	0.04 ± 0.01	0.08 ± 0.02	0.11230	*n.s.*	0.39 ± 0.06	0.29 ± 0.02 (9)	0.15406	*n.s.*	0.04 ± 0.01	0.07 ± 0.01	0.06649	*n.s.*
51					0.17 ± 0.04	0.19 ± 0.02	0.69598	*n.s.*					0.31 ± 0.07	0.36 ± 0.04	0.53534	*n.s.*					0.34 ± 0.06	0.26 ± 0.03 (9)	0.24029	*n.s.*				
52					0.14 ± 0.03	0.25 ± 0.02	0.00891	**					0.37 ± 0.08	0.34 ± 0.04	0.72179	*n.s.*					0.36 ± 0.07	0.29 ± 0.03 (9)	0.39026	*n.s.*				
53					0.14 ± 0.04	0.23 ± 0.04 (17)	0.09568	*n.s.*					0.31 ± 0.06	0.30 ± 0.03	0.87978	*n.s.*					0.41 ± 0.06	0.33 ± 0.04 (9)	0.32318	*n.s.*				
54					0.14 ± 0.03	0.20 ± 0.03	0.15309	*n.s.*					0.34 ± 0.08	0.34 ± 0.05	0.99958	*n.s.*					0.41 ± 0.06	0.39 ± 0.05 (9)	0.82050	*n.s.*				
55	0.08 ± 0.02	0.06 ± 0.01	0.29928	*n.s.*	0.18 ± 0.05	0.22 ± 0.03	0.43397	*n.s.*	0.07 ± 0.01	0.07 ± 0.01	0.90889	*n.s.*	0.32 ± 0.07	0.32 ± 0.05	0.95697	*n.s.*	0.07 ± 0.02	0.08 ± 0.01	0.57291	*n.s.*	0.35 ± 0.07	0.25 ± 0.03 (9)	0.21672	*n.s.*	0.05 ± 0.01	0.10 ± 0.03	0.11495	*n.s.*
56					0.13 ± 0.04	0.23 ± 0.03 (17)	0.06926	*n.s.*					0.33 ± 0.07	0.30 ± 0.04	0.72772	*n.s.*					0.38 ± 0.05	0.33 ± 0.03 (9)	0.43235	*n.s.*				
57					0.15 ± 0.04	0.22 ± 0.03	0.17387	*n.s.*					0.30 ± 0.06	0.31 ± 0.04	0.91521	*n.s.*					0.39 ± 0.06	0.30 ± 0.03 (9)	0.22211	*n.s.*				
58					0.14 ± 0.03	0.24 ± 0.03	0.02391	*					0.35 ± 0.06	0.31 ± 0.04	0.61789	*n.s.*					0.38 ± 0.06	0.31 ± 0.05 (9)	0.34755	*n.s.*				
59					0.17 ± 0.05	0.22 ± 0.03 (17)	0.34959	*n.s.*					0.30 ± 0.06	0.36 ± 0.05	0.45855	*n.s.*					0.40 ± 0.07	0.31 ± 0.02 (9)	0.22382	*n.s.*				
60	0.08 ± 0.02	0.08 ± 0.02	0.73901	*n.s.*	0.14 ± 0.03	0.23 ± 0.03 (17)	0.04996	*	0.06 ± 0.01	0.08 ± 0.01	0.15781	*n.s.*	0.36 ± 0.07	0.27 ± 0.03	0.24871	*n.s.*	0.07 ± 0.02	0.07 ± 0.01	0.93290	*n.s.*	0.33 ± 0.06	0.33 ± 0.03 (9)	0.93435	*n.s.*	0.05 ± 0.01	0.10 ± 0.02	0.03194	*

Data are presented as mean $SD_{Latency}$ ± SEM of events (cf. 2.3.5) in 5-s (1 Hz and recoveries) or 1-s (challenges) bins (cf. Figure 27B). Numbers in brackets depict sample sizes (number of cells). Only events with eIPSCs amplitudes above threshold (= responded stimuli; cf. 2.3.5) were used for analysis. Note the reduced sample size in some conditions as some cells had too few events for SD calculation. The reduced sample sizes are indicated in brackets at the affected datasets. Testing for outliers and normal distribution was not performed. For significance levels see Table 1. SD = standard deviation, sign. = significance, *n.s.* = not significant

3.9. eIPSC decay times during sustained transmission at the MNTB-LSO synapse

Loss of GlyT1 is known to result in glycine accumulation in the synaptic cleft and a concomitant longer activation of GlyRs finally leads to prolonged decay times (Gomeza et al., 2003a; Eulenburg et al., 2018). In contrast to these observations, no decay time prolongation of spontaneous events was observed at the LSO (Figure 15). I therefore wanted to find out if this effect occurs after the release of a higher number of vesicles, achieved by stimulation of MNTB fibers. For analysis, decay times of events (eIPSCs above threshold) and with a good fit quality (cf. 2.3.5) were binned in 5-s (1 Hz and recoveries) or 1-s (challenges) bins. To examine decay time changes due to sustained synaptic transmission, differences between the first and the last bin of each condition were analyzed (3.9.1). For differences between WT and KO, data of each bin were compared to get a higher temporal resolution for decay time changes induced by the loss of GlyT1 (3.9.2). 200 Hz decay times could not be analyzed as the time between peak and the next stimulus artefact was shorter than the 37% decay time (cf. 2.3.5 and Figure 17C). Accordingly, decay time estimation could not be performed for 200 Hz eIPSCs.

3.9.1. Challenges induce decay time prolongations in both genotypes

In WT, decay times during 1 Hz did not change and remained at an average value of 1.80 ms (set as WT 100% value) with single cell data ranging from ~1.0 ms to ~3.4 ms (Figure 28A, Table 16). During 50 Hz and 100 Hz, decay times increased significantly in a time- and frequency-dependent manner ($p \leq 0.01166$ for both comparisons) to 1% and 12% longer decay times at the end, respectively, compared to 1 Hz. Conclusively, decay times at the end of 50 Hz stimulation were nearly at the same level as during 1 Hz. During recoveries, decay times were shorter as in 1 Hz already from the beginning on, and remained nearly constant throughout the 60 s with no significant change from the first to the last bin. Consequently, values at the end of recoveries were even smaller compared to 1 Hz (-5%, -4%, and -14% for rec50, rec100, and rec200, respectively). Markedly, also at the beginning of the challenges decay times were shorter as during 1 Hz. In KO (Figure 28B), the mean decay time during 1 Hz was 2.16 ms (set as 100% KO value) and therefore was longer as in WT. But similar to WT, decay times during 1 Hz did not change significantly, but markedly increased during 50 Hz and 100 Hz ($p \leq 0.03241$ for both comparisons) to 10% and 28% higher values compared to 1 Hz. Regarding recoveries, decay times remained longer as in 1 Hz and did not decline

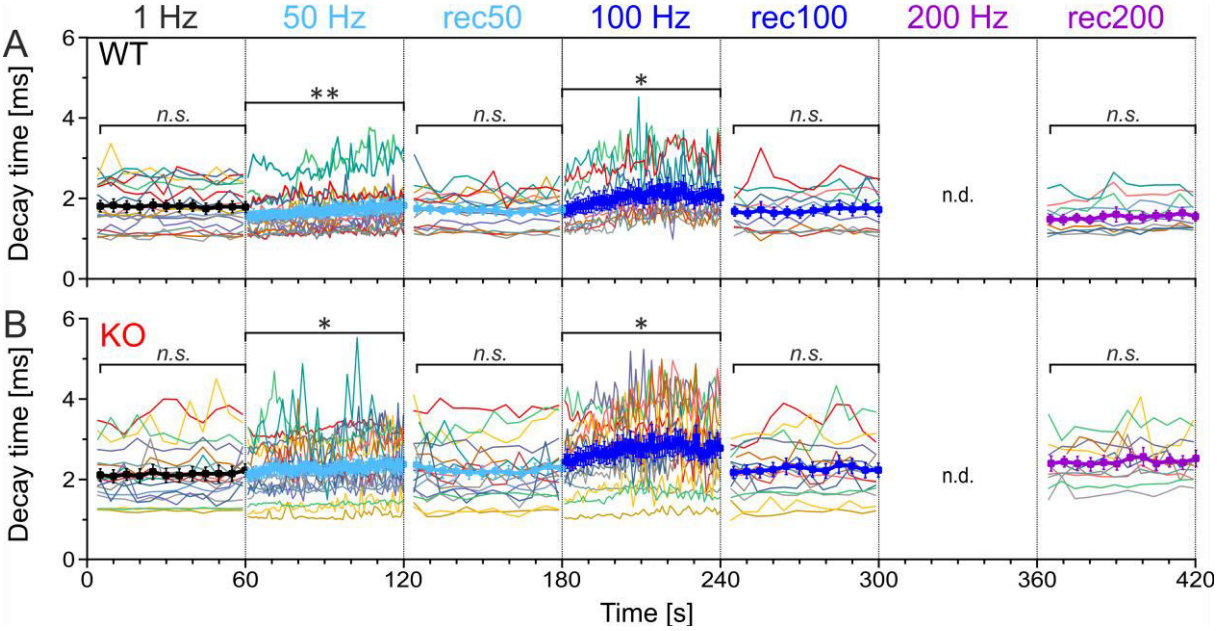

Figure 28: Frequency-dependent change of decay times in WT and KO

Decay times over time in WT (**A**) and KO (**B**). Decay times in 5-s (1 Hz and recoveries) or 1-s (challenges) bins were calculated and drawn for single cell data (thin lines) and for mean values (bold lines with data points). Only events with eIPSCs amplitudes above threshold and with a reliable calculation of decay time (cf. 2.3.5) were used for analysis. Significant differences were analyzed between the first and the last bins. Decay times of 200 Hz could not be obtained as superposition of eIPSCs was too strong. For details see Table 16. For comparison between WT and KO see Figure 29 and Table 17. For significance levels see Table 1.
n (cells) = 17/14/11/10 (WT) / 18/18/15/10 (KO), no testing for outlier or normal distribution was performed; *n.s.* = not significant, n.d. = not determined

Table 16: Decay time change

Condition		WT (17/14/11/10)			KO (18/18/15/10)		
		Decay time [ms]	p value	sign.	Decay time [ms]	p value	sign.
1 Hz	first bin	1.81 ± 0.14	0.54361	*n.s.*	2.10 ± 0.15	0.10731	*n.s.*
	last bin	1.78 ± 0.13			2.21 ± 0.16		
50 Hz	first bin	1.57 ± 0.11	0.00496	**	2.11 ± 0.16	0.03043	*
	last bin	1.82 ± 0.17			2.37 ± 0.19 (17)		
rec50	first bin	1.74 ± 0.15	0.75419	*n.s.*	2.37 ± 0.19	0.37922	*n.s.*
	last bin	1.71 ± 0.12			2.29 ± 0.20		
100 Hz	first bin	1.67 ± 0.14	0.01166	*	2.41 ± 0.22	0.03241	*
	last bin	2.02 ± 0.20			2.77 ± 0.24		
rec100	first bin	1.68 ± 0.12	0.56007	*n.s.*	2.25 ± 0.17	0.95433	*n.s.*
	last bin	1.72 ± 0.16			2.24 ± 0.17		
200 Hz	first bin	n.d.			n.d.		
	last bin	n.d.			n.d.		
rec200	first bin	1.48 ± 0.12	0.28126	*n.s.*	2.39 ± 0.19	0.11120	*n.s.*
	last bin	1.55 ± 0.12			2.51 ± 0.20 (9)		

Data are presented as mean of the first and the last bin ± SEM (cf. Figure 28), with 5-s bins for 1 Hz and recoveries, and 1-s bins for challenges. Numbers in brackets depict sample sizes (number of cells). Only events with eIPSCs amplitudes above threshold and with a reliable calculation of decay time (cf. 2.3.5) were used for analysis. As one KO cell at 50 Hz had too few events during the last bin, sample size is reduced at this condition (indicated in brackets). 200 Hz decay times could not be calculated as superposition of eIPSCs was too strong. Testing for outlier and normal distribution was not applied. For significance levels see Table 1. sign. = significance, *n.s.* = not significant, n.d. = not determined

significantly during the course, resulting in 6%, 3%, and 16% longer decay times at the end of rec50, rec100, and rec200, respectively, compared to 1 Hz. For data and individual p values see Table 16.

Conclusively, decay times during 1 Hz and recoveries did not change markedly in both genotypes. In contrast, a prolongation was observed during all applied challenges in WT as well as in KO. But are the longer decay times in KO significantly different from WT and did they exhibit a more severe prolongation? To analyze this, decay time data of WT and KO were directly compared (see next chapter.

3.9.2. 50 Hz stimulation leads to irreversibly increased decay times in KO

As shown in 3.9.1, KO events appeared to have longer decay times as WT events. When comparing WT and KO (Figure 29, Table 17), decay times in KO during 1 Hz were in average 0.43 ms (24%) longer as in WT, but a significant difference was only detected in 2/12 bins (17%; $p \leq 0.04055$ for both comparisons). During 50 Hz and 100 Hz KO decay times were significantly longer throughout the complete courses, with only few exceptions (98% and 85% significant comparisons, respectively). At the beginning of 50 Hz, KO events already depicted 35% longer decay times compared to WT ($p = 0.00680$), and remained at an increased value until the end with +30% ($p = 0.02249$). During 100 Hz, the difference was more pronounced, e.g. with 44% (at the beginning) and 37% (at the end) longer decay times in KO ($p \leq 0.01621$ for both comparisons). Comparably to challenges, the KO decay times during recoveries were significantly longer compared to WT in 100% (rec50 and rec200) or in 92% of comparisons (rec100). During rec50 and rec100, KO and WT decay times depicted a mean difference of 32%, which was more pronounced during rec200 with averaged 58% longer decay times in KO. For individual p values see Table 17.

Taken together, longer decay times occurred in KO throughout all analyzed challenges and recoveries. During 1 Hz, circumstances leading to a decay time increase appeared not yet to have an effect at this early part of the protocol. The faster stimulation at the beginning of 50 Hz quite likely led to decay time prolongation, which was more severe in KO. This resulted in a significant difference between the two genotypes, and was not compensated during the ensuing challenges and recoveries. Remarkably, the most pronounced decay time differences were observed during rec200 with up to 67% longer durations in KO.

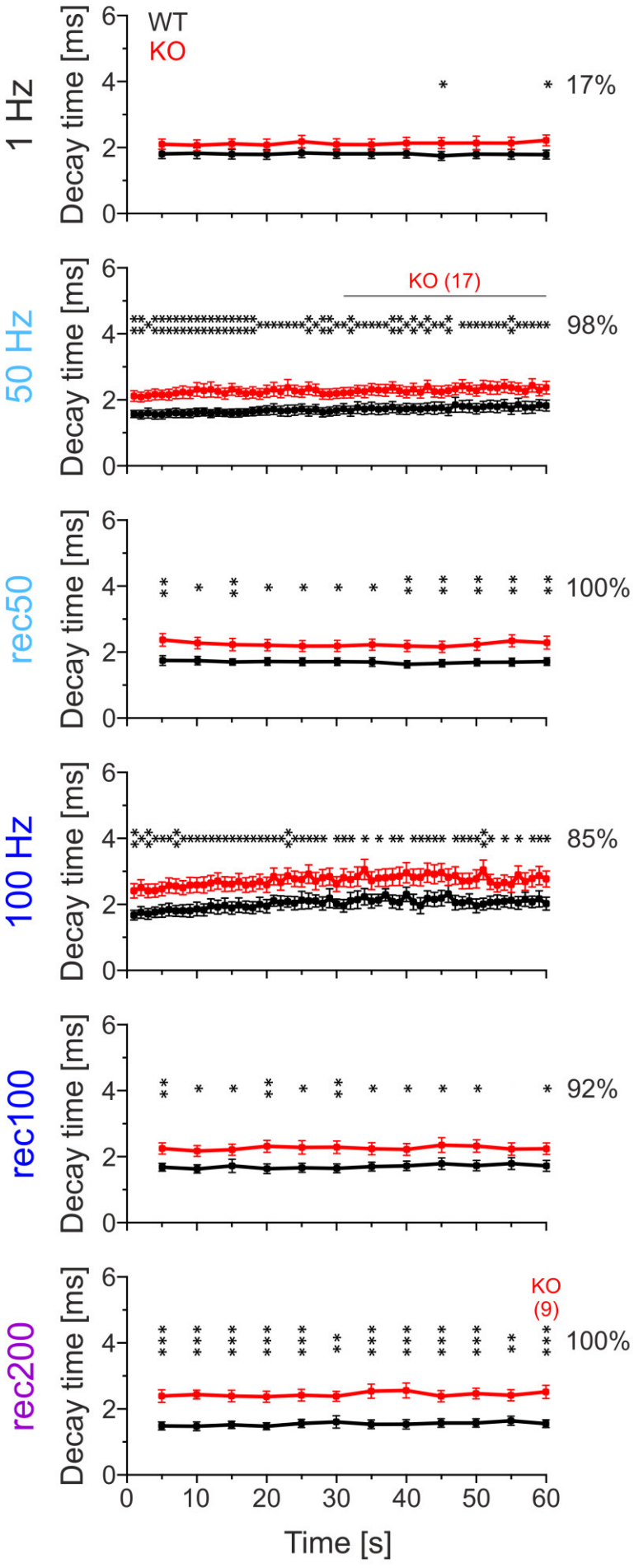

Figure 29: Decay times during challenges and recoveries are stronger prolonged as in WT
Overlays of the mean decay times shown in Figure 28. For 1 Hz and recovery situations decay times were binned in 5-s intervals, for challenge situations in 1-s intervals. Numbers on the right indicate percentage of significantly different bins. Note the reduced sample sizes in KO 50 Hz and rec200, as too few events occurred in a cell, respectively. For better visibility, not significant differences are not depicted. As in 200 Hz the eIPSCs mostly superimposed, the decay time at this stimulation frequency could not be examined. Only events with the following criteria were used for analysis: eIPSCs with amplitudes above threshold (= responded stimuli/ events) and reliable calculation of decay time (cf. 2.3.5). For details see Table 17 and for significance levels Table 1.
n (cells) at start =
17/14/11/10 (WT)
18/18/15/10 (KO)

Table 17: Decay time comparison between WT and KO

time	Decay time [ms]																							
	1 Hz				50 Hz				rec50				100 Hz				rec100				rec200			
	WT (17)	KO (18)	p value	sign.	WT (14)	KO (18)	p value	sign.	WT (14)	KO (18)	p value	sign.	WT (11)	KO (15)	p value	sign.	WT (11)	KO (15)	p value	sign.	WT (10)	KO (10)	p value	sign.
1					1.57 ± 0.11	2.11 ± 0.16	0.00680	**					1.67 ± 0.14	2.41 ± 0.22	0.00773	**								
2					1.55 ± 0.13	2.08 ± 0.15	0.00685	**					1.75 ± 0.18	2.51 ± 0.24	0.01333	*								
3					1.60 ± 0.15	2.12 ± 0.16	0.01232	*					1.71 ± 0.16	2.41 ± 0.21	0.00947	**								
4					1.55 ± 0.14	2.16 ± 0.16	0.00505	**					1.76 ± 0.16	2.41 ± 0.20	0.01107	*								
5	1.81 ± 0.14	2.10 ± 0.15	0.08500	*n.s.*	1.55 ± 0.14	2.15 ± 0.14	0.00299	**	1.74 ± 0.15	2.37 ± 0.19	0.00929	**	1.80 ± 0.19	2.47 ± 0.21	0.01562	*	1.68 ± 0.12	2.25 ± 0.17	0.00896	**	1.48 ± 0.12	2.39 ± 0.19	0.00038	***
6					1.59 ± 0.12	2.15 ± 0.17	0.00756	**					1.84 ± 0.19	2.57 ± 0.23	0.01450	*								
7					1.60 ± 0.14	2.20 ± 0.17	0.00679	**					1.80 ± 0.16	2.55 ± 0.22	0.00826	**								
8					1.58 ± 0.12	2.23 ± 0.19	0.00381	**					1.80 ± 0.18	2.50 ± 0.21	0.01255	*								
9					1.59 ± 0.13	2.21 ± 0.17	0.00506	**					1.80 ± 0.19	2.58 ± 0.24	0.01218	*								
10	1.83 ± 0.16	2.07 ± 0.16	0.15201	*n.s.*	1.62 ± 0.12	2.31 ± 0.21	0.00389	**	1.74 ± 0.13	2.27 ± 0.17	0.01296	*	1.86 ± 0.21	2.58 ± 0.22	0.01500	*	1.63 ± 0.13	2.17 ± 0.17	0.01113	*	1.47 ± 0.13	2.43 ± 0.13	0.00003	***
11					1.63 ± 0.12	2.28 ± 0.21	0.00553	**					1.83 ± 0.18	2.58 ± 0.24	0.01436	*								
12					1.58 ± 0.12	2.31 ± 0.23	0.00446	**					1.95 ± 0.21	2.64 ± 0.23	0.02244	*								
13					1.62 ± 0.12	2.25 ± 0.19	0.00646	**					1.91 ± 0.21	2.70 ± 0.25	0.01412	*								
14					1.60 ± 0.11	2.19 ± 0.17	0.00321	**					1.97 ± 0.22	2.61 ± 0.22	0.02834	*								
15	1.80 ± 0.14	2.11 ± 0.14	0.06438	*n.s.*	1.59 ± 0.12	2.31 ± 0.18	0.00192	**	1.70 ± 0.10	2.23 ± 0.19	0.00961	**	1.89 ± 0.19	2.61 ± 0.21	0.01143	*	1.72 ± 0.20	2.21 ± 0.17	0.03676	*	1.51 ± 0.11	2.39 ± 0.18	0.00026	***
16					1.60 ± 0.13	2.25 ± 0.15	0.00154	**					1.97 ± 0.22	2.69 ± 0.25	0.02514	*								
17					1.62 ± 0.11	2.18 ± 0.16	0.00448	**					1.92 ± 0.18	2.58 ± 0.22	0.01838	*								
18					1.64 ± 0.13	2.22 ± 0.17	0.00751	**					1.90 ± 0.18	2.61 ± 0.23	0.01375	*								
19					1.66 ± 0.13	2.18 ± 0.16	0.01166	*					1.99 ± 0.22	2.69 ± 0.23	0.02105	*								
20	1.79 ± 0.15	2.08 ± 0.18	0.11410	*n.s.*	1.68 ± 0.14	2.26 ± 0.18	0.01199	*	1.71 ± 0.12	2.21 ± 0.17	0.01609	*	1.94 ± 0.20	2.59 ± 0.23	0.02731	*	1.63 ± 0.15	2.31 ± 0.18	0.00560	**	1.47 ± 0.11	2.37 ± 0.17	0.00013	***
21					1.72 ± 0.16	2.32 ± 0.21	0.01978	*					2.11 ± 0.16	2.84 ± 0.26	0.01784	*								
22					1.66 ± 0.15	2.24 ± 0.18	0.01150	*					2.04 ± 0.22	2.66 ± 0.23	0.03557	*								
23					1.67 ± 0.17	2.37 ± 0.24	0.01617	*					2.08 ± 0.16	2.86 ± 0.24	0.00967	**								
24					1.68 ± 0.16	2.27 ± 0.17	0.01088	*					2.03 ± 0.20	2.77 ± 0.23	0.01594	*								
25	1.84 ± 0.14	2.18 ± 0.19	0.07901	*n.s.*	1.72 ± 0.15	2.24 ± 0.16	0.01564	*	1.71 ± 0.12	2.18 ± 0.17	0.01789	*	2.12 ± 0.27	2.75 ± 0.22	0.04132	*	1.66 ± 0.14	2.28 ± 0.20	0.01504	*	1.56 ± 0.12	2.41 ± 0.18	0.00045	***
26					1.65 ± 0.15	2.35 ± 0.19	0.00511	**					2.10 ± 0.24	2.91 ± 0.28	0.02283	*								
27					1.71 ± 0.15	2.30 ± 0.18	0.01013	*					2.10 ± 0.18	2.70 ± 0.26	0.04753	*								
28					1.62 ± 0.14	2.17 ± 0.15	0.00685	**					2.02 ± 0.20	2.80 ± 0.25	0.01502	*								
29					1.64 ± 0.14	2.17 ± 0.16	0.00959	**					2.18 ± 0.29	2.84 ± 0.26	0.05235	*n.s.*								
30	1.81 ± 0.14	2.09 ± 0.17	0.10841	*n.s.*	1.67 ± 0.14	2.19 ± 0.15	0.01008	*	1.71 ± 0.12	2.19 ± 0.17	0.01888	*	2.02 ± 0.14	2.61 ± 0.23	0.01772	*	1.64 ± 0.13	2.28 ± 0.19	0.00837	**	1.60 ± 0.19	2.38 ± 0.15	0.00235	**
31					1.73 ± 0.16	2.21 ± 0.16 (17)	0.02050	*					1.95 ± 0.19	2.81 ± 0.27	0.01238	*								
32					1.65 ± 0.15	2.21 ± 0.16 (17)	0.00915	**					2.11 ± 0.25	2.75 ± 0.23	0.03807	*								
33					1.76 ± 0.18	2.27 ± 0.16 (17)	0.02104	*					2.14 ± 0.27	2.84 ± 0.29	0.05030	*n.s.*								
34					1.72 ± 0.17	2.25 ± 0.18 (17)	0.02233	*					2.23 ± 0.25	3.05 ± 0.30	0.02869	*								
35	1.81 ± 0.14	2.09 ± 0.17	0.10988	*n.s.*	1.75 ± 0.18	2.32 ± 0.17 (17)	0.01551	*	1.70 ± 0.13	2.22 ± 0.17	0.01367	*	2.09 ± 0.21	2.71 ± 0.27	0.05039	*n.s.*	1.70 ± 0.13	2.24 ± 0.18	0.01765	*	1.53 ± 0.13	2.53 ± 0.21	0.00043	***
36					1.71 ± 0.17	2.29 ± 0.17 (17)	0.01024	*					2.13 ± 0.17	2.79 ± 0.25	0.02779	*								
37					1.73 ± 0.16	2.28 ± 0.18 (17)	0.01516	*					2.28 ± 0.18	2.80 ± 0.27	0.07597	*n.s.*								
38					1.78 ± 0.17	2.37 ± 0.17 (17)	0.00943	**					2.08 ± 0.20	2.82 ± 0.26	0.02159	*								
39					1.70 ± 0.14	2.27 ± 0.17 (17)	0.00850	**					2.05 ± 0.21	2.85 ± 0.28	0.02207	*								
40	1.82 ± 0.14	2.13 ± 0.18	0.08673	*n.s.*	1.72 ± 0.17	2.23 ± 0.17 (17)	0.02252	*	1.63 ± 0.11	2.18 ± 0.17	0.00799	**	2.30 ± 0.22	2.96 ± 0.31	0.05876	*n.s.*	1.72 ± 0.14	2.22 ± 0.18	0.02605	*	1.53 ± 0.14	2.56 ± 0.23	0.00060	***
41					1.74 ± 0.14	2.32 ± 0.18 (17)	0.00994	**					2.07 ± 0.23	2.82 ± 0.24	0.02077	*								
42					1.71 ± 0.17	2.22 ± 0.17 (17)	0.02255	*					1.96 ± 0.24	2.82 ± 0.26	0.01404	*								
43					1.74 ± 0.16	2.40 ± 0.19 (17)	0.00678	**					2.18 ± 0.23	2.96 ± 0.29	0.03034	*								
44					1.74 ± 0.19	2.25 ± 0.17 (17)	0.02787	*					2.15 ± 0.21	2.91 ± 0.29	0.02868	*								
45	1.75 ± 0.14	2.13 ± 0.17	0.04055	*	1.76 ± 0.17	2.24 ± 0.18 (17)	0.03294	*	1.66 ± 0.11	2.16 ± 0.17	0.00992	**	2.18 ± 0.23	2.96 ± 0.27	0.02551	*	1.78 ± 0.18	2.35 ± 0.22	0.03705	*	1.57 ± 0.13	2.38 ± 0.17	0.00068	***
46					1.69 ± 0.17	2.28 ± 0.16 (17)	0.00920	**					2.31 ± 0.26	2.82 ± 0.25	0.09125	*n.s.*								
47					1.85 ± 0.22	2.33 ± 0.18 (17)	0.05023	*n.s.*					2.05 ± 0.22	2.87 ± 0.27	0.01690	*								
48					1.80 ± 0.18	2.41 ± 0.20 (17)	0.01559	*					2.04 ± 0.18	2.70 ± 0.23	0.02409	*								
49					1.80 ± 0.19	2.34 ± 0.17 (17)	0.02171	*					2.10 ± 0.22	2.71 ± 0.23	0.03824	*								
50	1.80 ± 0.13	2.13 ± 0.21	0.09583	*n.s.*	1.73 ± 0.16	2.28 ± 0.17 (17)	0.01281	*	1.69 ± 0.11	2.23 ± 0.18	0.00819	**	1.95 ± 0.21	2.77 ± 0.28	0.01857	*	1.73 ± 0.16	2.32 ± 0.19	0.01482	*	1.57 ± 0.13	2.46 ± 0.16	0.00020	***
51					1.79 ± 0.17	2.40 ± 0.19 (17)	0.01218	*					2.00 ± 0.18	3.04 ± 0.30	0.00329	**								
52					1.81 ± 0.18	2.37 ± 0.20 (17)	0.02582	*					2.06 ± 0.19	2.68 ± 0.23	0.02867	*								
53					1.79 ± 0.18	2.35 ± 0.19 (17)	0.01914	*					2.07 ± 0.21	2.58 ± 0.21	0.05245	*n.s.*								
54					1.83 ± 0.17	2.42 ± 0.20 (17)	0.01857	*					2.09 ± 0.17	2.66 ± 0.23	0.03722	*								
55	1.79 ± 0.14	2.13 ± 0.18	0.07897	*n.s.*	1.73 ± 0.17	2.36 ± 0.17 (17)	0.00712	**	1.70 ± 0.12	2.34 ± 0.18	0.00456	**	2.12 ± 0.23	2.60 ± 0.23	0.08715	*n.s.*	1.79 ± 0.18	2.23 ± 0.19	0.05754	*n.s.*	1.64 ± 0.14	2.41 ± 0.17	0.00117	**
56					1.85 ± 0.19	2.33 ± 0.17 (17)	0.03657	*					2.04 ± 0.19	2.89 ± 0.27	0.01306	*								
57					1.77 ± 0.19	2.25 ± 0.17 (17)	0.03151	*					2.15 ± 0.21	2.69 ± 0.27	0.07466	*n.s.*								
58					1.77 ± 0.18	2.43 ± 0.20 (17)	0.01091	*					2.07 ± 0.17	2.78 ± 0.25	0.02142	*								
59					1.84 ± 0.16	2.29 ± 0.17 (17)	0.03508	*					2.16 ± 0.25	2.87 ± 0.28	0.04070	*								
60	1.78 ± 0.13	2.21 ± 0.16	0.02588	*	1.82 ± 0.17	2.37 ± 0.19 (17)	0.02249	*	1.71 ± 0.12	2.29 ± 0.20	0.00929	**	2.02 ± 0.20	2.77 ± 0.24	0.01621	*	1.72 ± 0.16	2.24 ± 0.17	0.02353	*	1.55 ± 0.12	2.51 ± 0.20 (9)	0.00026	***

For legend see next page.

Table 17: (continued) Decay time comparison between WT and KO
Data are presented as mean ± SEM of events in 5-s (1 Hz and recoveries) or 1-s (50 Hz and 100 Hz) bins (cf. Figure 29). Numbers in brackets depict sample sizes (number of cells). Only events with the following criteria were used for analysis: eIPSCs with amplitudes above threshold (= responded stimuli/events) and reliable calculation of decay time (cf. 2.3.5). Testing for outliers and normal distribution was not performed. As in 200 Hz the eIPSCs mostly superimposed, the decay time could not be assessed for this stimulation frequency. Note the reduced sample sizes in KO 50 Hz and rec200, as too few events occurred in a cell, respectively. The reduced sample sizes are indicated in brackets at the affected datasets. For significance levels see Table 1. sign. = significance, *n.s.* = not significant

3.10. Summary of principal findings

Taken together, on the one hand GlyT1 appears to play no major role during spontaneous neurotransmission. In line with this, basic properties regarding q, RRP, P_r, and eIPSC characteristics during 1 Hz stimulation were not altered in KO animals (Figure 21, Figure 16). On the other hand, when stimulating MNTB fibers with 50 Hz, MNTB-LSO neurotransmission in KO was impaired, indicated by significant prolonged decay times (Figure 29) and latencies (Figure 27). These increases could not be reversed during the ensuing recovery and were maintained or even further augmented in the next, more pretentious challenges and their recoveries. Nevertheless, GlyT1-lacking synapses were able to provide a WT-like $SD_{Latency}$ nearly throughout the complete stimulation protocol (Figure 27). Additionally, FDD and fidelity were comparable to WT until 200 Hz stimulation. But with this high stimulation frequency, the former withstanding could not be maintained, and eIPSCs were significantly stronger depressed (Figure 18) and fidelity was clearly reduced (Figure 20). A further analysis of q examining its changes during challenges and recoveries revealed another remarkable aspect: q at the end of challenges was reduced in KO but not in WT (Figure 22), which was not compensated with a higher m (Figure 23). Taken together, these observations indicate an importance for GlyT1 in proper synaptic function, particularly at high stimulation frequencies. For a graphical summary of the principal findings see Figure 30.

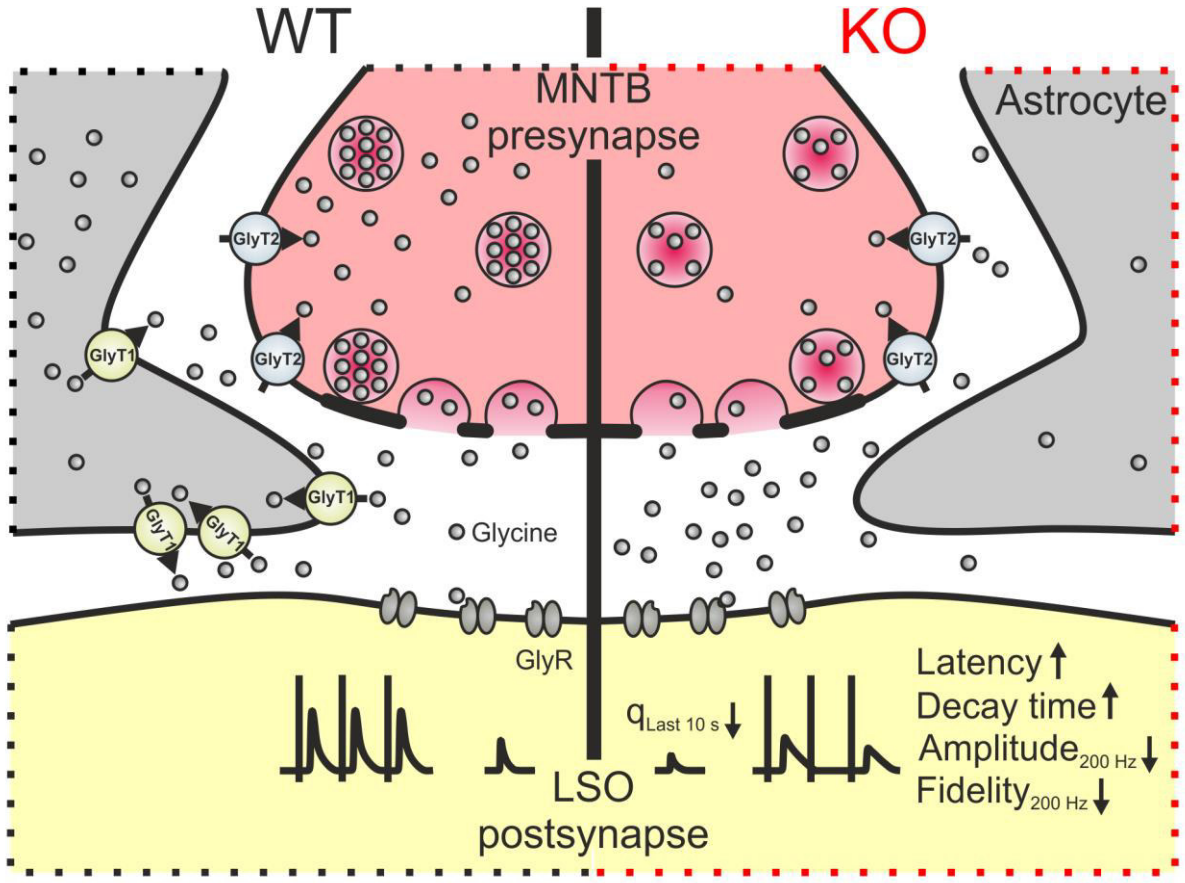

Figure 30: Graphical summary of principal findings
During stimulation with high frequencies, a great amount of glycine is released from the MNTB terminal into the synaptic cleft. At a KO synapse (right), glycine translocation into the astrocyte is most likely strongly diminished due to the loss of GlyT1, resulting in enhanced glycine accumulation compared to WT (left). Consequently, postsynaptic GlyRs should be longer activated at KO synapses during excess release of glycine, which would be indicated by longer decay times. Indeed, stimulation with 50 Hz resulted in more prominent prolonged decay times (cf. 3.9.2) and also led to stronger increased latencies (cf. 3.8.3). The decay time- and latency prolongations persisted throughout the complete ensuing stimulation protocol. Additionally, q was decreased during the last 10 s of 50 Hz and 100 Hz challenges compared to the initial q value (cf. **3.7.2**). As a further consequence of GlyT1 loss, a stronger amplitude depression (cf 3.5.1) and decline in fidelity (cf. 3.6.2) occurred in KO when stimulating with 200 Hz. These results indicate an involvement of GlyT1 in proper function of the MNTB-LSO synapse, especially during synaptic stress. MNTB = medial nucleus of the trapezoid body, LSO = lateral superior olive, GlyT1 = glycine transporter 1, GlyR = glycine receptor, q = quantal size

4. DISCUSSION

In the present study I addressed three issues indicating a putative impairment of synaptic transmission due to GlyT1 loss: Firstly, I analyzed changes of sIPSC properties with a focus on decay times. Secondly, I analyzed basic synaptic properties that underlie fast and temporally precise synaptic transmission. Thirdly, I unraveled the role of GlyT1 during sustained synaptic activation by analyzing the extent of FDD and changes in fidelity, decay time, and temporal precision. The major results as answers to the questions and hypotheses posed in 1.4 are as follows:

Hypotheses	Results
Due to glycine accumulation, GlyRs are longer activated, resulting in prolonged sIPSC decay times.	The loss of GlyT1 had no significant effect on spontaneous glycinergic transmission (Figure 15).
As GlyT1 is expressed only in astrocytes at inhibitory synapses, a loss does not impair presynaptic glycine uptake and therefore no change in basic synaptic properties is expected.	KO synapses had the same initial q and elicited similar eIPSCs during 1 Hz stimulation (Figure 16). At the beginning of challenges, WT and KO synapses did not differ in RRPs and P_rs (Figure 21).
The accumulation of excess glycine during sustained synaptic activation leads to longer decay times of eIPSCs, but fidelity and temporal precision are not impaired.	During 200 Hz stimulation, KO synapses exhibited a stronger depression with 67% smaller amplitudes as in WT (Figure 18), accompanied by a more severely reduced fidelity with only 25% of the fidelity observed in WT (Figure 20). A persistent latency and decay time prolongation was induced by the stimulation with 50 Hz, and remained significantly increased throughout the complete stimulation protocol. The differences accelerated to 60% longer decay times and 30% longer latencies, whereas $SD_{Latency}$ was only marginally changed (Figure 27, Figure 29). At the end of 50 Hz and 100 Hz challenges, q was decreased in KO synapses (Figure 22). This decrease was not rescued by a higher m (Figure 23).

4.1. General aspects of the GlyT1b/c mouse

Former GlyT1 KO models suffered from a high lethality (Gomeza et al., 2003a; Tsai et al., 2004; Eulenburg et al., 2010). The newly developed GlyT1b/c KO mouse (Eulenburg et al., 2018) enables measurements at mature synapses, as these animals are viable showing an expected birth rate and normal survival (Figure 13; cf. Schuster, 2015). The only discrepancy is the reduced gain in weight from P7 to P20, which is only a half of WT. This could be due to feeding impairment and respiration deficits that were found before in systemic GlyT1 KO (Gomeza et al., 2003a). Most importantly, KO brainstem tissue showed a strong reduction of the transporter (-84%, Figure 14). The remaining GlyT1 signal in western blots can be attributed to the isoform GlyT1a due to an incomplete shift from GlyT1a to GlyT1b/c. However, as no GlyT1 isoform-specific antibodies are available, this cannot be proved yet. A suspected compensatory upregulation of GlyT2 was excluded, because no difference between WT and KO was observed for GlyT2 expression (Figure 14). As GlyTs have the tendency to form dimers in intracellular membranes and monomers at the cell surface, both GlyTs were detected as double bands (Horiuchi et al., 2001; Bartholomaus et al., 2008). In summary, this mouse model is suitable for examining GlyT1 contribution to MNTB-LSO transmission at the mature synapse.

4.2. GlyT1 at the MNTB-LSO synapse is dispensable for glycine clearance under resting conditions

Previous findings determined GlyT1 as the most important transporter for glycine removal at glycinergic synapses and thus for terminating GlyR activation and subsequently IPSCs (Adams et al., 1995; Roux and Supplisson, 2000; Gomeza et al., 2003a; Eulenburg and Gomeza, 2010; Eulenburg et al., 2010; Kurolap et al., 2016). This was shown for example at hypoglossal motoneurons of neonatal GlyT1 KO mice that exhibited 64% longer sIPSC decay times compared to their WT littermates. Additionally, application of strychnine led to a 6-fold stronger change in holding current (I_{Hold}; Gomeza et al., 2003a). From these observations they concluded a persistent activation of strychnine-sensitive GlyRs by excess glycine, which is prevented in WT by GlyT1 activity. Similar findings were made after pharmacological inhibition of GlyT1 with 10 µM ORG24598 at lamina X neurons in rat spinal cord slices (Bradaia et al., 2004). The inhibitor induced decay time prolongation of sIPSCs (+133%) and increase in noise, accompanied by a slowly developing shift in I_{Hold}. Both effects were reversible by the application of strychnine, leading to the same conclusion as in Gomeza et al. (2003a) with

longer GlyR activation by a higher glycine concentration in the synaptic cleft. However, another study on dorsal horn neurons in spinal cord slices from adult mice found no sIPSC decay time prolongation after application of GlyT1 inhibitor N-[3-(40-fluorophenyl)-3-(40-phenylphenoxy)propyl] sarcosine (NFPS; Oyama et al., 2017). However, a missing effect could be also due to an insufficient inhibitor concentration. At a concentration of 100 nM, the dose in Oyama et al. (2017) compared to other studies was only a half or a fifth (Herdon et al., 2001; Lim et al., 2004, respectively), and hence could be too low to be effective. In our laboratory, even a NFPS concentration of 10 µM showed to be non-effective at the MNTB-LSO synapse (Kramer, 2012). Contradictory, other studies revealed concentrations below 100 nM to be sufficiently potent (Atkinson et al., 2001; Mallorga et al., 2003). So the question arises if the absence of an inhibitory effect on GlyT1 indicates a negligible contribution of GlyT1 to glycine homeostasis, a compensation of GlyT1 activity by other transporters, or an ineffective inhibition of the transporter. The latter can be only excluded by dose response curves of the pharmaceutical, which was not always performed. Furthermore, different morphologies of synaptic clefts or transporter concentrations could contribute to the varying drug effects on different synapses.

Based on the aforementioned studies, I hypothesized a prolongation of sIPSC decay times at the MNTB-LSO synapse in GlyT1b/c KO mice, which was not confirmed as WT and KO values were similar (Figure 15). In general, synapse properties of WT exhibited similar sIPSC properties when compared to another study in my group with adult animals (Weingarten, 2018), underlining the functionality of this mouse model. As no $GABA_AR$ blocker was applied in my study, one could speculate that a GABAergic component has influenced the measurements. However, at the mature MNTB-LSO synapse GABA was shown to have only modulatory effects via axonal or postsynaptic $GABA_ARs$ (Weisz et al., 2016; Fischer et al., 2019), whereas the primarily released transmitter is glycine (Moore and Caspary, 1983; Wenthold et al., 1987; Aoki et al., 1988; Kotak et al., 1998; Kim and Kandler, 2003; Nabekura et al., 2004). Underlining this, LSO inhibition in chinchilla was blocked by the application of strychnine, whereas application of the $GABA_AR$ antagonist bicuculline nearly had no effect (Moore and Caspary, 1983). Additionally, sustained activation of GlyRs during resting conditions caused by impaired glycine clearance can be excluded, as this would lead to a decreased R_M (Ghirardini et al., 2018) which was not observed in my study (Figure 8).

In comparison to the studies of Gomeza et al. (2003a) and Bradaia et al. (2004), showing a sIPSC decay time prolongation at spinal cord synapses after GlyT1 loss or inhibition, my results point to a distinct role of GlyT1 at the MNTB-LSO synapse. At glycinergic synapses, AP-independent exocytosis of a small amount of vesicles leads to a glycine release sufficient to elicit sIPSCs (Katz, 1971). In a sIPSC amplitude histogram, uni- or multiquantal release can be visualized, indicating a decreasing probability for the amount of synchronously released vesicles (Figure 11). In contrast to spinal cord synapses in the study of Bradaia et al. (2004), the amount of glycine exocytosed at the MNTB-LSO synapse during spontaneous transmission was not sufficient to cause prolonged decay times or transient GlyR activation. This could be either due to a compensation of GlyT1 loss by expression or increased activity of other transporters, or a stronger degree of diffusion. A compensation by other transporters in general is possible, as for example neuronal GlyT2 or alanine-serine-cysteine-1 (Asc-1) transporter, or astrocytic sodium-coupled neutral amino acid transporter (SNAT)1, SNAT2, SNAT5 and leucine-preferring amino acid transporter 2 (LAT2) are known to be able to transport glycine (Cubelos et al., 2005c; Safory et al., 2015; Lopez-Corcuera et al., 2017; Zafra et al., 2017). However, no increased expression was detected for GlyT2 (Figure 14). Altered expression levels of the other transporters still have to be analyzed. A possibly enhanced degree of diffusion could be due to a different spatial arrangement of MNTB-LSO synapses in comparison to spinal cord synapses. For example a lower degree of astrocytic enwrapping would allow a stronger diffusion out of the synaptic cleft (Clements, 1996; Danbolt, 2001; Chung et al., 2015; Tso and Herzog, 2015; Verkhratsky and Nedergaard, 2018). According to this, it was shown that astrocytes surround synapses more or less tightly in a region dependent manner (Theodosis et al., 2008), indicating different involvement in neurotransmitter homeostasis (Lippman et al., 2008). For example in the cerebellum, synapses are closely enwrapped by astrocytic processes, pointing to a crucial role for tight functional interactions between astrocytes and neurons (Theodosis et al., 2008). Similarly, astrocytic processes enriched with glutamate transporters occupy the fenestrations of the calyx of Held, which conceivably augments glutamate clearance (Ford et al., 2009; Joris and Trussell, 2018). Contrarily, less than 50% of the synapses in cortex and hippocampus were found to be tripartite synapses (Witcher et al., 2010) and therefore mainly diffusion or uptake by neurons is suggested to regulate transmitter concentrations in these regions (Eulenburg and Gomeza, 2010). This could be also the case for auditory brainstem synapses, enabling a high degree of

diffusion. In conclusion, uptake of glycine via other transporters and/or diffusion appears to be sufficient at the GlyT1-depleted MNTB-LSO tripartite synapse for maintaining glycine homeostasis during spontaneous transmission.

4.3. Basic synaptic properties and performance of the MNTB-LSO synapse during 1 Hz stimulation are not affected by the loss of GlyT1

Basic synaptic properties describe anatomical and functional specializations of a synapse and are mainly defined by the demands it has to fulfill. The basic conceptual framework for that was worked out by Katz and colleagues who determined three main factors: the RRP, P_r and q (Katz, 1971; Xu-Friedman, 2017). These three factors define the postsynaptic response with the equation PSC = N_{RRP} x P_r x q (Friauf et al., 2015). To ensure reliable transmission during sustained stimulation, the RRP has to comprise a sufficient number of vesicles, a high P_r, and efficient vesicle replenishment mechanisms that were shown to be very prominent at the MNTB-LSO synapse (Krachan et al., 2017). In the last decades, a contribution of astrocytes to presynaptic properties was suggested by several studies, pointing to an astrocytic involvement in proper synaptic function (Volterra and Meldolesi, 2005; Pannasch and Rouach, 2013). These findings imply that synaptic plasticity could be, to some extent, regulated by these glial cells. This could be mediated for example via the release of gliotransmitter (Allen and Barres, 2005; De Pitta et al., 2016) or by providing metabolic substrates to neurons (Pellerin and Magistretti, 2012). Indeed, in hippocampal slices, lactate supply by astrocytes to neurons was shown to be needed for sustained glutamatergic synapse activity (Rouach et al., 2008). Furthermore, transmitter from astrocytic sources were shown to increase RRP and P_r via activation of presynaptic receptors in autaptic hippocampal neuron cultures (Schwarz et al., 2017). However, the function of astrocyte-derived glycine in synaptic plasticity is still not resolved and remains to be elucidated.

In accordance to my hypothesis, initial RRPs and P_rs of WT and KO synapses were similar (Figure 21). This indicates that GlyT1 loss and therefore the absence of putatively released glycine at extrasynaptic sides or vice versa an increased extracellular glycine concentration nearby the synaptic cleft is not relevant for these parameters. With RRPs of 199 and 124 vesicles at the beginning of 50 Hz in WT and KO, respectively, WT data are in accordance with other studies estimating ~200 vesicles (Krachan et al., 2017). Furthermore, the similar RRP negates a disturbed microcircuit malformation during early postnatal development due to

GlyT1 loss, which in contrast was shown to occur in GlyT2 KO animals accompanied by a RRP reduction of 75% (Brill, 2018). The normal development of MNTB-LSO connection in the mouse model used in this study presumably can be dedicated to the isoform switch from GlyT1a to GlyT1b/c, as it should be accomplished around P14 (Schuster, 2015). Hence, the GlyT1b/c KO mouse provides a WT-like environment for refinement and maturation processes that should be accomplished until this age to a large extent (Kim and Kandler, 2003; Noh et al., 2010; Hirtz et al., 2012).

Similar to RRP values, P_rs of 17% for both WT and KO at the beginning of the 50 Hz stimulation were also comparable to Krachan et al. (2017) (Table S.11). RRP and P_r mainly determine PSC amplitudes and therefore synaptic strength (Lim et al., 1999; Neher, 2010; Kaeser and Regehr, 2017). Hence, the WT-like amplitudes of KO during 1 Hz stimulation (Figure 16) are another indicator for an absent GlyT1-mediated effect on these presynaptic properties. Furthermore, the 100% fidelity during this stimulation frequency in WT as well as in KO indicates that replenishment mechanisms presumably are not affected at this stimulation frequency (Figure 20). The unaltered behavior of KO synapses during 1 Hz stimulation is consistent with a pharmacological approach of our group, in which GlyT1 inhibition with 10 µM NFPS also had no effect on amplitudes during 1 Hz stimulation (Kramer, 2012). Regarding decay times during 1 Hz stimulation, a prolongation was observed only in 17% of comparisons (Figure 29), although the elicited currents were about 15-fold higher in WT and KO compared to spontaneous transmission, indicating a multiplicity of glycine in the synaptic cleft in comparison to spontaneous vesicle release. This contradicts my initial hypothesis of a substantial decay time prolongation due to glycine accumulation in the synaptic cleft and therefore longer GlyR activation (Clements, 1996; Gomeza et al., 2003a). But as decay times did not differ significantly in the majority of cases, I conclude that diffusion or activity of alternative glycine transporters is sufficient for glycine clearance during these conditions, as already speculated for spontaneous transmission (4.2). Conclusively, synaptic transmission during 1 Hz stimulation is not or only minimally impaired by the loss of GlyT1. Nevertheless, KO decay times in average were 24% longer, still pointing to the occurrence of a stronger glycine accumulation due to GlyT1 loss (Clements, 1996; Draguhn and Heinemann, 1996).

4.4. GlyT1 loss leads to impairment of the MNTB-LSO synapse during high activity

During MNTB-fiber stimulation with 50 Hz, the speculative high amount of released glycine in combination with the loss of GlyT1-mediated glycine uptake led to 30% longer decay times of KO eIPSCs compared to WT (Figure 29). As already mentioned, decay times of WT and KO were not significantly different during the first 1 Hz challenge. However, in KO they showed a tendency for acceleration, as indicated by a higher decay time ratio of the last and first ten events in KO, which did not occur in WT (WT: -1%; KO: +4%; Figure S.3). The significantly increased decay times during stimulation with 50 Hz persisted prolonged throughout the complete ensuing protocol including recoveries, augmenting to ~60% longer decay times in the recovery phase after 200 Hz stimulation.

A GlyT1-dependent decay time increase was also observed in other studies that analyzed effects on synaptic performance after genetic deletion or pharmacological inhibition of the transporter. At the MNTB-LSO synapse of juvenile mice, GlyT1 inhibition with 1 µM LY2365109 led to 24% longer eIPSC decay times at 1 Hz (Brill, 2014). In Bradaia et al. (2004), a blockade of GlyT1 with 10 µM ORG24598 at lamina X neurons in rat spinal cord also led to decay time prolongation of eIPSCs, but was more severe with 2.5-fold prolongation at only 0.2 Hz stimulation. In the latter study, also the decay times of sIPSCs were increased (~3.5-fold). Similarly, in Gomeza et al. (2003a), sIPSC decay times at GlyT1 KO hypoglossal motoneurons were prolonged (+54%). Although no stimulation experiment was performed, I assume that an increased decay time would also be visible on eIPSC level due to the higher amount of released glycine. Taken together, the discrepancy in affecting decay times of both sIPSCs and eIPSCs or of only eIPSCs, as in my study, may reflect brain region-dependent morphological and/or functional adaptations of the particular synapse type. At dorsal horn neurons in spinal cord slices from adult mice, for example, application of the GlyT1 inhibitor NFPS (100 nM) induced no decay time prolongation of sIPSCs but of eIPSCs (10 Hz) with 21% longer decay times (Oyama et al., 2017). However, as stated in 4.2, inhibition with 100 nM NFPS is suggested to be relatively low and hence may not reflect a complete abolishment of GlyT1 function. In spinal cord, glycine functions as a rheostat for spinal reflexes and pain perception (Bolon et al., 2013) and its contribution to excitation and inhibition has to be balanced properly. For example, an increase of glycine at inhibitory spinal cord synapses was shown to decrease excitability in nociceptive circuits, providing a possible tool to extenuate hyperalgesia via blockade of GlyTs (Winters et al., 2018). In contrast, glycine spillover to

excitatory synapses potentiated NMDAR activity and therefore could pathologically increase pain perception (Ahmadi et al., 2003). Hence, uncontrolled glycine diffusion has to be prevented as this would disturb the excitation-inhibition needed for normal pain perception. At the MNTB-LSO synapse, glycine spillover in contrast could provide an additional valuable tool for fine tuning of inhibitory and excitatory transmission and/or sharpening of isofrequency bands. E.g. in the case of glutamate, spillover from CN-LSO synapses to MNTB-LSO synapses was shown to decrease transmitter release via the activation of presynaptic metabotropic glutamate receptors (Nishimaki et al., 2007). However, as this effect was diminished by the third week after birth, it is possible that heterosynaptic action of transmitter loses its importance after maturation of auditory circuits. Concluding from the different findings of transmitter spillover effects at spinal cord and MNTB-LSO synapses, I would speculate that in spinal cord the prevention of glycine spillover is more important as in brainstem, indicated by the stronger pronounced decay time affection due to GlyT1 loss or inhibition.

Besides the transmitter concentration in the synaptic cleft (Twyman and Macdonald, 1991), the decay time of glycinergic synaptic events is determined by several factors, such as kinetics of GlyRs (Ali et al., 2000; Takahashi et al., 1992; Singer et al., 1998) and the rate of transmitter clearance from the synapse (Nerlich et al., 2014). GlyR activation and therefore Cl^- influx is terminated by decreasing extracellular glycine concentration due to uptake or diffusion, resulting in glycine dissociation from the receptor (Clements, 1996). If glycine does not dissociate fast enough, GlyRs are reactivated (Legendre, 1998). Additionally, it was shown that a higher glycine concentration leads to increased mean open times of GlyR channels (Twyman and Macdonald, 1991). A loss of GlyT1 therefore would result in a slower reduction of glycine concentration in the synaptic cleft and a consequently delayed dissociation of glycine from GlyR accompanied with GlyR reactivation and longer mean open times. As another important mechanism for shaping glycinergic IPSC decay times, GlyR desensitization was also shown to contribute to altered decay times (Clements, 1996). However, this aspect was proven to be negligible at the MNTB-LSO synapse, as it will be discussed as “mechanism I” in 4.4.1.

Summing up all these observations for decay time, I conclude that during 1 Hz, glycine accumulates stronger in KO MNTB-LSO synapses, but the 1 s between the stimuli is sufficient to prevent prolonged activation of GlyRs due to diffusion and/or uptake by other transporters,

e.g. GlyT2. During the ensuing 50 Hz stimulation, these mechanisms cannot compensate GlyT1 loss, as now there is only a fiftieth (20 ms) of the time left between the glycine release events. This leads to stronger glycine accumulation during challenges, which cannot be reversed in the course of recovery periods, and therefore results in sustained augmented decay times.

Another important factor for proper synaptic signaling is to ensure the transmission by releasing enough neurotransmitter and thereby eliciting a sufficiently high postsynaptic response even during sustained synaptic transmission (Krachan et al., 2017). If GlyT1 is knocked out, I assumed that no stronger depression of eIPSC amplitudes is observed as transmitter release should not be affected (cf. Figure 3). According to my hypothesis, KO amplitude courses exhibited a WT-like FDD until stimulating with 200 Hz (Figure 18). At this frequency, a significantly stronger amplitude reduction after 1 s (200 pulses) was observed in KO. At the end of the challenge, KO amplitudes had retained only 2% of their strength, whereas WT eIPSCs still exhibited 6%. The stronger depression in KO during 200 Hz is mirrored in the more severely weakened fidelity during 200 Hz (Figure 20). With a fidelity of 9% at the end of 200 Hz challenge, only one fourth of stimuli compared to WT (36%) is responded. Accordingly, 9% fidelity in KO at the end of 200 Hz resembles a severely reduced value and indicates that in KO in comparison to WT only a fourth of the stimuli are responded. However, when comparing FDD with fidelity, it has to be kept in mind that the values are not congruent. For example, with a 2-fold noise level of 10%, ten eIPSCs with 20% amplitude result in 20% mean amplitude and 100% fidelity; five eIPSCs with 35% amplitude plus five eIPSCs with 5% amplitude result in the same mean amplitude (20%) but only in 50% fidelity. Therefore fidelity is another important aspect to determine synapse performance. In general, WT values for FDD and fidelity are in accordance with other studies in our group that applied the same or similar stimulation protocols at the MNTB-LSO synapse (Table S.11).

The cause for amplitude depression during repeated stimulation can be dedicated to pre- and/or postsynaptic cues. The main mechanisms involved in STD and attenuation were found to be a reduced RRP, P_r, Ca^{2+} influx, and/or q, an insufficient RRP replenishment, and/or desensitization of postsynaptic receptors (cf. Figure 3, Friauf et al., 2015). Another cause for a stronger depression can be an increase in R_{In}, but as cells with >35% increase were excluded, this aspect can be negated in my study. During stimulation with high frequencies, RRP replenishment is a critical determinant for the extent of STD, as stimuli succeed in such a short time window that replenishment rates are too slow to maintain the initial RRP. However, in

comparison to other synapses, depression at the MNTB-LSO synapse is moderate and occurs over tens of seconds (Kramer et al., 2014; Friauf et al., 2015; Krachan et al., 2017). The depression reaches a steady state level depending on the constant replenishment rate that could achieve 561 or even 3500 vesicles/s (Krachan et al., 2017; Weingarten, 2018). This remarkably high rate is a major prerequisite for the MNTB-LSO synapse to maintain synaptic transmission also throughout sustained signaling of up to 1000 APs/s in vitro (Wu and Kelly, 1993) and 700 APs/s in vivo (Kopp-Scheinpflug et al., 2008). Hence, the applied stimulation frequencies are quite common to this system. As no stronger depression in KO was observed during 50 Hz and 100 Hz, KO synapses appear to be able to mediate RRP replenishment as in WT when IEIs are ≥10 ms. Additionally, the 60-s lasting recoveries are sufficient also for the KO synapse to reach initial RRP size and consequently to release the same number of vesicles at the beginning of challenges (Figure 21). In regard to the presumed higher glycine concentration in the synaptic cleft, GlyR desensitization could be one causal mechanism that contributes to reduced amplitudes (Legendre, 1998). However, GlyR desensitization at the MNTB-LSO synapse was found to be only minimally involved in amplitude depression (Fischer, 2016) and is further discussed as “mechanism I” in 4.4.1. More likely, a disturbed replenishment could to be causative for reduced eIPSC amplitudes and therefore reduced fidelity (Kaeser and Regehr, 2017). This would be indicative for an involvement of astrocytes in replenishment processes via their suggested function as a “glycine shuttle” (Roux and Supplisson, 2000; Aubrey et al., 2005; Eulenburg and Gomeza, 2010}), which is discussed as “mechanism III” in 4.4.3. Assuming a disturbed replenishment, the 5-ms IEIs during 200 Hz challenge could not provide enough time for WT-like replenishment, resulting in lower amount of released glycine and therefore in smaller eIPSC amplitudes. Interestingly, q in KO was significantly decreased at the end of 50 Hz and 100 Hz stimulation (-14%, -19%, respectively), which was not observed in WT (Figure 22). However, the reduction of q apparently was not as severe to lead to an increase of m (Figure 23) or to significantly smaller amplitudes as in WT (Figure 18). At the end of the 200 Hz challenge, q could not be estimated due to eIPSC summation, but presumably it is stronger decreased as during 50 Hz and 100 Hz challenge. Hence, the stronger reduction of q speculatively could be the cause for the significantly smaller eIPSC amplitudes and fidelity during 200 Hz. In general, q depends on vesicle size, vesicular transmitter concentration (Edwards, 2007) and postsynaptic receptor kinetics. The hypothesis that loss of GlyT1 function leads to a decrease in q due to lower

vesicular transmitter concentration and concomitantly reduced IPSC amplitudes was also speculated by Gomeza et al. (2003b) and Brill (2014). Contradicting this issue, it was suggested in a recent study that only sufficiently filled vesicles are released (Kurz, 2019). In this aspect, the reduction of q during challenges could also result from GlyR desensitization, which however, as mentioned before, was suggested to be not the underlying cause (for further discussion of this aspect see 4.4.1). Nevertheless, KO eIPSC amplitudes during recoveries were similar to WT (Figure 18). The only discrepancy was observed for fidelity at the beginning of recovery periods, as KO fidelity was still reduced to 95% (rec50, rec100) or 90% (rec200), whereas WT synapses immediately were able to respond to each stimulus (Figure 20). But how can KO synapses then achieve WT-like amplitudes at the beginning of recoveries? Single cell data reveal that single cell data of "weak" KO cells with small amplitudes were compensated by some cells with nearly 100% amplitudes. Nevertheless, disturbed increase in fidelity did only occur in KO and therefore could further underline a disturbance of replenishment processes somehow connected to GlyT1 loss. A reduced glycine supply via reverse function of GlyT1 (cf. 4.4.3) could be causative for reduced fidelity and amplitudes. But also activation of presynaptic GlyRs resulting in homosynaptic inhibition could be speculated. At neuromuscular junctions, for example, this process contributed to depression during prolonged stimulation, but only to a minimal degree (Malinowski et al., 1997). However, activation of presynaptic GlyR was found to depolarize the presynapse and thus facilitate transmitter release (Turecek and Trussell, 2001; Jeong et al., 2003; Kono and Hulsmann, 2016). Hence, this would result in higher KO eIPSC amplitudes and an ameliorated fidelity during challenges, which would be the opposite of the observed effects. But other studies in contrast revealed that activation of presynaptic GlyRs results in shunting inhibition (Casado and Ascher, 2009; Paulus and Rothwell, 2016), which could in this regard explain reduced amplitudes, fidelity, q, and prolonged latencies. For further discussion of this aspect see "mechanism III" (4.4.2).

In accordance to my initial hypothesis, WT and KO synaptic transmission exhibited similar high temporal precision during 1 Hz stimulation (Figure 27), a prominent feature for auditory brainstem synapses (Kandler and Friauf, 1995; Krachan et al., 2017). At this stimulation frequency, latencies and $SD_{Latency}$ of both genotypes were stable and in accordance with Muller (2019). The latency is mainly determined by the axonal conductance velocity, synchrony of vesicle release, m, and neurotransmitter receptor kinetics (Kaeser and Regehr,

2014; Ford et al., 2015; Krachan et al., 2017; Stange-Marten et al., 2017; Turecek and Regehr, 2019). During challenges, latencies and $SD_{Latency}$ of both genotypes increased in a time- and frequency-dependent manner (Figure 26), which is consistent to other studies (Krachan et al., 2017; Weingarten, 2018; Muller, 2019). This decline in temporal precision mainly was due to a reduction of m, which provides the basis of temporal precise synaptic transmission (Krachan et al., 2017). However, the molecular determinants of release kinetics remain poorly understood (Turecek and Regehr, 2019). Unexpectedly, the increase in latency was much severe in KO, resulting in significantly longer latencies just from the beginning of the 50 Hz stimulation on, and persisted prolonged throughout the complete ensuing protocol (Figure 27). At the end of challenges, the more severe latency increase resulted in ~30% longer latencies. Regarding rec100 and rec200, the difference was even higher with +35% at the end. In contrast to latency, the difference in $SD_{Latency}$ was less pronounced with only 15% significantly higher values. The time courses of both latency and $SD_{Latency}$ realized, that the latency increase during 50 Hz stimulation was accompanied with an occasionally stronger variation of $SD_{Latency}$. Conclusively, the KO synapse could not perform as precise as the WT synapse even at this relatively mild challenge situation. During 100 and 200 Hz stimulation, latencies were again longer, but in contrast, $SD_{Latency}$ was only different in the beginning. Therefore I suspect that KO synapses entered earlier a state of imprecision as WT synapses. During recoveries, KO synapses did not reverse the higher latency and hence were not able to achieve the same short latencies as during 1 Hz, which in contrast was observed for WT synapses. But what could be the reason for these sustained longer latencies? An altered axonal conductance velocity is likely to be excluded, as KO latencies during 1 Hz stimulation were similar to WT. The reduced number of released vesicles also cannot be causative, as amplitudes except during 200 Hz challenge and initial q were similar. Interestingly, the latency-increases nearly co-occurred with decay time prolongations (Figure 27, Figure 29). Could it then be that desensitized GlyRs ("mechanism I") are the underlying cause as they would enter their activatable state later as in WT? But why then latencies are also prolonged during recoveries, where q was shown to be the same as during 1 Hz stimulation and therefore indicate no GlyR desensitization at the end of recoveries? Therefore this aspect was rather not suspected to be the underlying cause (for detailed discussion of this point see 4.4.1). The other possibility is a deterioration of synchronous release. This was found to be determined by the RRP, VGCCs that open and close quickly upon arrival of the AP, a Ca^{2+} triggering mechanism

with fast on- and off-kinetics, and a tight spatial coupling between the Ca^{2+} channel, Ca^{2+} sensor, and primed vesicles (Kaeser and Regehr, 2014). However, the similarity of latencies during 1 Hz stimulation indicate that the KO synapse have the same prerequisites for temporal precision as the WT synapse. A possible parameter contributing to prolonged latencies is the shrinking number of available vesicles in the RRP. Longer latencies but similar $SD_{Latency}$ lead to the assumption that m in WT and KO is equal, but q is decreased and exocytosis is delayed, presumably indicating an impaired replenishment. Is it therefore possible that a loss of astrocytic glycine supply via GlyT1 leads to a delayed vesicle refilling and hence to a prolonged replenishment of the RRP? This would indicate an astrocytic-neuronal glycine shuttle, which is further discussed as "mechanism III" in 4.4.3. In contrast to a decrease in available glycine at extrasynaptic locations, the accumulation of glycine in the synaptic cleft could lead to a stronger presynaptic GlyR activation located nearby the synapse. If this would result in Cl^- influx and therefore mediate shunting inhibition, this could be another explanation for delayed and/or decreased vesicle exocytosis and is further discussed as "mechanism II" in 4.4.2.

In summary, the latency and decay time prolongations as well as the reduced fidelity and amplitudes during 200 Hz stimulation and the decreased q at the end of challenges indicate an impairment of proper and reliable performance of the MNTB-LSO synapse. However, before the first challenge, KO synapses are not distinguishable from WT synapses. Therefore it can be speculated that WT and KO synapses have the same basic properties, and that glycine clearance in the synaptic cleft during relatively weak stressing conditions can be mediated by alternate transporters or diffusion. This could not be maintained during challenge conditions, as decay times showed a stronger prolongation in KO. As expected, this most likely results from higher glycine concentrations in the synaptic cleft and thereby longer GlyR activation at the postsynapse, as transmitter clearance could not be performed as effectively as in WT. However, the change of latency, q, amplitudes, and fidelity cannot be explained by a sustained activation of postsynaptic GlyRs. I suspect that prolonged postsynaptic GlyR activation is accompanied by other mechanisms to varying degrees, providing explanations for one or more of the observed effects. The mechanisms are thought to be

I. postsynaptic GlyR desensitization (4.4.1)
II. enhanced presynaptic GlyR activation (4.4.2)
III. disturbed glycine shuttle (4.4.3)

and are illustrated in Figure 31. The probability how and to what degree these mechanisms could contribute to the observed changes in KO is discussed in the next sections.

4.4.1. Mechanism I - postsynaptic GlyR desensitization

Receptor desensitization is one mechanism that contributes to STD and affects all ionotropic receptors. It causes the receptor to be non-activatable although transmitter is present. However, there is a high variation in sensitivity and time course, mainly depending on transmitter kinetics in the synaptic cleft and on receptor kinetics (Jones and Westbrook, 1996). For example, AMPA, NMDA or $GABA_A$ receptors show fast desensitization processes in the range of one to hundreds of ms (Jones and Westbrook, 1995; Dingledine et al., 1999). By contrast, postsynaptic GlyRs composed of α1β subunits were shown to have a relatively slow desensitization (Akaike and Kaneda, 1989; Walstrom and Hess, 1994; Kungel and Friauf, 1997). When exposed to high ambient glycine concentrations as in the case of repetitive stimulation of glycinergic terminals, GlyT1 would efficiently remove glycine, preventing further receptor occupancy and desensitization. Therefore, ineffective clearance of transmitter molecules from the synaptic cleft would lead to their accumulation and thus to desensitization of postsynaptic receptors (Trussell et al., 1993; Friauf et al., 2015), resulting in the observed stronger decreased amplitudes in KO. Hence, the stronger amplitude depression during 200 Hz stimulation in KO (Figure 18) could be attributed to stronger GlyR desensitization. The reduced q values at the end of high-frequency challenges (Figure 22) might be a further evidence for this aspect (Krachan et al., 2017). A q reduction of 10% in WT was already observed in other studies (Krachan et al., 2017) and was therefore more severe as in my study with maximal 8%. Nevertheless, in KO the effect was 2.3-fold stronger with a reduction of 19% at the end of 100 Hz stimulation. However, postsynaptic GlyR desensitization was shown to contribute only marginally to synaptic depression at brainstem synapses (Gomeza et al., 2003a; Gomeza et al., 2003b; Krachan et al., 2017). For example, at hypoglossal motoneurons of a GlyT1 KO mouse, no reduction of glycinergic IPSCs upon increasing levels of extracellular glycine was observed (Gomeza et al., 2003a). Similarly, application of 10 µM glycine at the MNTB-LSO synapse did not induce a changed depression during 50 Hz stimulation (Eubler, 2013). These observations could be due to the relatively slow desensitization of GlyRs, leading to the suggestion that the time course and amplitude of glycinergic IPSCs will be little affected by desensitization. In zebrafish Mauthner cells, also no GlyR desensitization was found after paired-pulse

stimulation, which could provide another hint for the weak GlyR desensitization (Legendre, 1998). As a consequence, the inhibition evoked by glycinergic synapses will remain highly efficient during repetitive firing, provided that the frequency of presynaptic APs remains low enough that slow GlyR desensitization does not occur. Moreover, the low degree of desensitization at glycinergic events should act to reinforce the efficacy of inhibition (Legendre, 1998), important for the auditory system to ensure reliable transmission of persistent acoustic signals. At the calyx of Held, as example for an auditory synapse, it was found that glutamate-induced postsynaptic desensitization did not account for the synaptic depression during high frequency stimulation (Wang and Kaczmarek, 1998). As a further important characteristic for GlyR desensitization is the concomitant shortening of decay time, as a decreasing amount of receptors contribute to the postsynaptic event (Gu and Huang, 1998; Wang and Kaczmarek, 1998; Imboden et al., 2001). In my study, however, decay times were continuously prolonged after the first 1 Hz phase, further contradicting a stronger GlyR desensitization as a cause for reduced IPSC amplitudes in KO.

The degree of receptor desensitization is also determined by the subunit composition and receptor density at the postsynapse (Legendre, 2001; Legendre et al., 2002; Freche et al., 2011). Hence, a change of these parameters could also be responsible for the stronger amplitude depression and moreover to prolonged decay times. Such a difference could reflect an adaptation to an altered synaptic microenvironment with an increased extrasynaptic glycine concentration. However, these aspects can be excluded to a great extent. Neither in systemic nor in astrocyte-specific KO, as well as in the mouse used in my study, no change in postsynaptic GlyR density or GlyRα expression was detected (Gomeza et al., 2003a; Eulenburg et al., 2010; Schuster, 2015). Furthermore, an altered GlyR subunit expression or clustering most likely would also lead to differences of the initial q or of eIPSCs during 1 Hz stimulation, which was not observed. Therefore I conclude that the stronger reduction in amplitudes as well as the reduced q at the end of challenges rather reflect a presynaptic cause than GlyR desensitization.

4.4.2. Mechanism II - enhanced presynaptic GlyR activation

Presynaptic ligand-gated ion channels are known to mediate a relatively slow modulation of presynaptic exocytosis and plasticity (Malinowski et al., 1997; Danbolt, 2001; Turecek and Trussell, 2001; Xiong et al., 2014; Weisz et al., 2016). In contrast to synaptic GlyRs, presynaptic

receptors are α1 homomers (Jeong et al., 2003; Kubota et al., 2010; Hruskova et al., 2012; Xiong et al., 2014) and are not found in clusters but rather show a dispersed distribution (Hruskova et al., 2012). Upon activation by neurotransmitter spillover they were shown to mediate a slow modulation of neurotransmitter release (Turecek and Trussell, 2001; Jeong et al., 2003; Hruskova et al., 2012).

At the MNTB-LSO synapse, spillover of glutamate from the CN-LSO synapse decreases transmitter release via heterosynaptic activation of presynaptic metabotropic glutamate receptors (Nishimaki et al., 2007). However, less is known about the presynaptic modulation at the MNTB-LSO synapse induced by spilled over glycine. At KO synapses, the increased extracellular glycine concentration due to the lack of GlyT1 could lead to a stronger activation of GlyRs at the MNTB terminal nearby the synapse. The polarity of GlyR-mediated responses is predominantly determined by the concentration of Cl^- and V_{Rest}, with the Cl^- gradient mainly established by K^+-Cl^--co-transporter 2 (KCC2; Chamma et al., 2012). At the postsynapse, activation of GlyRs lead to Cl^- influx due to its low equilibrium potential, resulting in IPSCs. However, if the activation of presynaptic GlyRs at MNTB-terminals leads to Cl^- influx or efflux remains speculative, as the internal Cl^- concentration is unknown. If I presume a low internal Cl^- concentration, Cl^- influx into the presynapse occurs upon activation of the presynaptic GlyR. This would result in hyperpolarization and furthermore AP propagation is impeded, as Na^+ influx is compensated by Cl^- influx, a process which is known as shunting inhibition (Casado and Ascher, 2009; Paulus and Rothwell, 2016). However, studies at presynaptic GlyRs of other synapses could contradict the assumption of a low internal Cl^- concentration in MNTB-terminals. As the high Cl^- gradient between extracellular and intracellular compartment mainly is established by the action of KCC2 (Chamma et al., 2012), a low or absent expression of KCC2 would indicate a high intracellular Cl^- concentration. This could be consequently a hint for a possibly depolarizing action of activated GlyRs. For example, a low KCC2 expression was found in LSO neurons at early postnatal stages at the LSO (Friauf et al., 2011; Lee et al., 2016). This underlies a low Cl^- gradient in early development with the Cl^- equilibrium potential above V_{Rest}, and consequently glycinergic transmission at the MNTB-LSO synapse is excitatory. This was found to be important for the development of inhibitory synaptic contacts (Blaesse et al., 2006). Interestingly, KCC2 expression was found to be restricted to the somato-dendritic compartment and excluded from the axon (Hubner et al., 2001; Bartho et al., 2004; Szabadics et al., 2006). Conclusively, terminal Cl^- concentration could be higher than in the soma or in

dendrites, but Cl^- concentrations in synaptic terminals are hard to determine because of experimental limitations. However, at the calyx of Held this was possible due to its characteristic morphology, which revealed a four to five fold higher Cl^- concentration in terminals compared to the somata (Price and Trussell, 2006). Accordingly, presynaptic GlyRs were found to be depolarizing and had a facilitating effect on transmitter release. This is due to Cl^- efflux upon activation leading to nerve terminal depolarization and subsequent activation of VGCCs. The increasing Ca^{2+} concentration mediates vesicle release and therefore facilitation (Turecek and Trussell, 2001; Price and Trussell, 2006). Also the activation of TTX-sensitive Na^+ channels upon depolarization is speculated, leading to AP initiation and subsequent Ca^{2+} influx through VGCCs, resulting also in facilitation (Jeong et al., 2003). A promotive effect for vesicle release mediated by presynaptic GlyRs was also found at a glycinergic synapse. In spinal cord, glycine application led to an increase in sIPSC frequency (Jeong et al., 2003). As this effect was Ca^{2+} dependent and sIPSC amplitudes as well as decay times were not affected, they concluded that the facilitated transmitter release was mediated by presynaptic GlyR activation. This assumption is supported by a study that observed a decreased sIPSC frequency in spinal cord slices after point mutating the presynaptic α1 GlyR subunit (Xiong et al., 2014). Conclusively, the presynaptic GlyR at glycinergic spinal cord synapses was identified as a contributor to facilitation. However, it should be noted that depolarizing presynaptic currents may still be functionally inhibitory due to the electrical shunt of the membrane input resistance generated by opening of GlyRs (Staley and Mody, 1992), leading to Cl^- influx upon depolarization-induced Na^+ influx. Hence, presynaptic GlyRs are inhibitory when intracellular Cl^- concentration is low, but are also inhibitory at high intracellular Cl^- concentrations during AP-induced signaling, as Na^+ influx induces Cl^- influx, impeding AP propagation.

The shunting inhibition therefore provides a good mechanism to explain the stronger amplitude depression during 200 Hz (Figure 18) and the reduced fidelity (Figure 20), as incoming signals are attenuated or even diminished at single synapses. Furthermore, shunting inhibition could be an underlying cause for the prolonged latencies as incoming excitatory postsynaptic potentials (EPSPs) need longer to pass the threshold for AP generation. But how it can be explained that latencies are increased already from 50 Hz challenge on (Figure 27), but amplitudes are reduced just during 200 Hz stimulation? Regarding this, I would speculate that the stronger accumulation of extracellular glycine in KO during 50 Hz is sufficient for a

stronger and/or more numerous presynaptic GlyR activation as in WT. Accordingly, AP propagation in KO is more severely impaired, but the depolarization of the MNTB terminal is still sufficient to elicit the WT-like vesicle release. During 200 Hz stimulation, however, extracellular glycine has reached a concentration that activates such a high amount of presynaptic GlyRs that incoming APs are largely blocked. This would lead to failures and thus to decreased amplitudes and fidelity. The threshold for the critical extracellular glycine concentration appears to remain at some synapses until the ensuing recovery phase, indicated by the reduced fidelity at the beginning (Figure 20). A further consequence of a more pronounced GlyR activation at KO synapses could be an impaired replenishment. At goldfish bipolar cell terminals, an intracellular Cl^- increase led to slowed endocytosis (Hull and von Gersdorff, 2004). Assuming this for the MNTB-LSO synapse, a reduced replenishment rate in KO could be completely or in concert with shunting inhibition causative for the reduced amplitudes and fidelity. Furthermore, an impaired replenishment could also lead to decreased q observed at the end of challenges (Figure 22). As the change of q was estimated during the last 10 s of the stimulation period, the reserve and recycling pool are likely depleted. Hence, replenishment of the RRP has to be directly achieved by vesicle endocytosis and refilling, which is considered to be the rate-limiting step in synaptic transmission (Fernandez-Alfonso and Ryan, 2004; Sudhof, 2004), especially at high signaling frequencies. Hence, the reduced q could reflect an incomplete vesicle refilling due to delayed endocytosis.

In conclusion, a stronger shunting inhibition at MNTB terminals in KO due to the increased and/or prolonged activation of presynaptic GlyRs could provide a satisfactory explanation for reduced amplitudes, reduced fidelity, prolonged latencies, and decreased q at the end of challenges.

4.4.3. Mechanism III - disturbed glycine shuttle

It is assumed that astrocytes can play a role in replenishment processes as they are supposed to work as a “glycine shuttle” (Roux and Supplisson, 2000; Aubrey et al., 2005; Eulenburg and Gomeza, 2010). With GlyT1, astrocytes can take up glycine from locations with temporally high concentrations, e.g. the synaptic cleft, and mediate glycine release at extrasynaptic compartments with low concentrations via reversal function of GlyT1 (Supplisson and Roux, 2002; Aragon and Lopez-Corcuera, 2003). Consecutively, presynaptic GlyT2 which was shown to be highly involved in RRP replenishment (Spike et al., 1997; Legendre, 2001; Gomeza et al.,

2003b; Bradaia et al., 2004; Latal et al., 2010), takes up nearby glycine which is subsequently used for vesicle refilling (Rousseau et al., 2008). Concluding from a hypothetical involvement of GlyT1 in a glycine shuttle, a loss of this transporter would impair replenishment processes during situations with high demand for glycine. Indeed, q at KO synapses was frequency-dependently decreased at the end of challenges to ~84% (Figure 22). During 200 Hz stimulation, q probably would have further declined, eliciting the observed significantly smaller amplitudes as in WT (Figure 18) accompanied by an increased failure rate (Figure 20). As another consequence of an impaired replenishment and reduced m, temporal precision is likely to be deteriorated as these parameters were found to be strongly connected (Krachan et al., 2017). According to this, latencies, but not $SD_{Latency}$, were found to be altered at KO synapses (Figure 27).

Replenishment at the MNTB-LSO synapse is a highly efficient mechanism (Krachan et al., 2017) and, although still not completely clarified, endocytic membrane retrieval is suggested to be used for vesicle formation (Rizzoli and Betz, 2005). This is an energy-expensive process, but as the SOC and other auditory brainstem regions were found to consume the highest amount of energy among many brain regions (Sokoloff, 1977), this could be a hint that these costs are paid in respect to ensure a reliable and sustained signal transmission. Besides new vesicles, the provision of glycine for refilling is another important factor for vesicle replenishment. Due to higher metabolic costs of *de novo* glycine synthesis and a longer time until newly formed glycine is available, it is more likely that the synapse draws on glycine which is taken up from the extracellular space. This hypothesis is supported by studies with GlyT2 KO mice, showing the inability of synapses to compensate the lack of glycine uptake by *de novo* synthesis or substitution with GABA (Gomeza et al., 2003b; Latal et al., 2010)

In general, astrocytes are considered to be a major source for glycine (Shank and Aprison, 1970; Shibasaki et al., 2017), as they are known to take up glucose out of the blood, which can be further used for conversion into glycine. Interestingly, no glial glycine immunoreactivity was found in mixed cell cultures of spinal cord (Poyatos et al., 1997). Furthermore, even if glycine is the prevailing inhibitory neurotransmitter, immunostaining for GCS was the weakest in brainstem and spinal cord compared to other regions (Sato et al., 1991). Additionally, no functional GCS was expressed in cultured primary astrocytes from spinal cord (Sakata et al., 2001). The discrepancy of predominant glycine usage but only weak abundance of GCS and glycine in astrocytes could indicate the preference of recycling in

brainstem instead of *de novo* synthesis. In a system with high need for glycine, cleavage is rendered as rather uneconomic, as this would consequently require *de novo* synthesis accompanied by high metabolic costs and possibly longer time investment until transmitter availability. Therefore it would be advantageous to use abundant glycine by relocating the transmitter to the presynapse presumably via reverse function of astrocytic GlyT1 and subsequent uptake by presynaptic GlyT2. Supporting the idea of a possible functional interaction of both transporters, the distribution of GlyT1 and GlyT2 implies that they operate in concert within the area where both are present (Jursky and Nelson, 1996). At the MNTB-LSO synapse, it was even shown that these two transporters are located in close vicinity to each other (Figure 5), further indicating the abundance of an astrocyte-neuron glycine shuttle via GlyT1 and GlyT2. Indeed, a strong connection between astrocytic GlyT1 and neuronal function appears to exist as GlyT1 was only expressed by cultured astrocytes when they were in contact with neurons (Zafra et al., 1997a).

The assumption of a glycine shuttle via GlyT1 and GlyT2 is further supported by their different transport characteristics. GlyT1 can perform inward directed transport only until a relatively low intracellular glycine concentration of ~1-2 mM (Supplisson and Roux, 2002). In contrast, GlyT2 is not able to act in reverse mode but therefore it can establish and maintain a relatively high intracellular glycine concentration of 20-40 mM, which the presynapse needs for vesicle refilling (Supplisson and Roux, 2002). According to this, astrocytes could be rather used as a transitory glycine store during periods with high synaptic glycine concentrations and as a regulator of glycine concentrations at extracellular sites (Harsing and Matyus, 2013).

Concluding from the properties of GlyT1 and GlyT2 as well as from the indications that they function in concert, I would speculate the existence of a glycine shuttle at the MNTB-LSO tripartite synapse. During high-frequency neurotransmission, GlyT1 translocates glycine into the astrocyte because of the high extracellular glycine concentration, contributing to the termination of the IPSC and preventing glycine spillover (Roux and Supplisson, 2000). At extrasynaptic sites, glycine concentration is decreased, possibly because of GlyT2 which is highly active due to the accelerated glycine consumption in the presynapse. If the extracellular glycine concentration falls below GlyT1 equilibrium, GlyT1 works in reverse mode, letting glycine leak out of astrocytes (Supplisson and Roux, 2002; Aragon and Lopez-Corcuera, 2003). Subsequently, co-localized GlyT2 transports the released glycine into the presynapse to provide VIAAT with a sufficiently high glycine concentration needed for adequate vesicle

refilling. Therefore, astrocytes could be an important glycine source for the presynapse during excess release of glycine. When GlyT1 function is lost, GlyT2 is not sufficiently provided with glycine resulting in reduced vesicle refilling and therefore in decreased q and IPSC amplitudes. Furthermore, it could be possible that the disturbance of replenishment mechanisms leads to delayed vesicle release and consequently to the prolonged latencies.

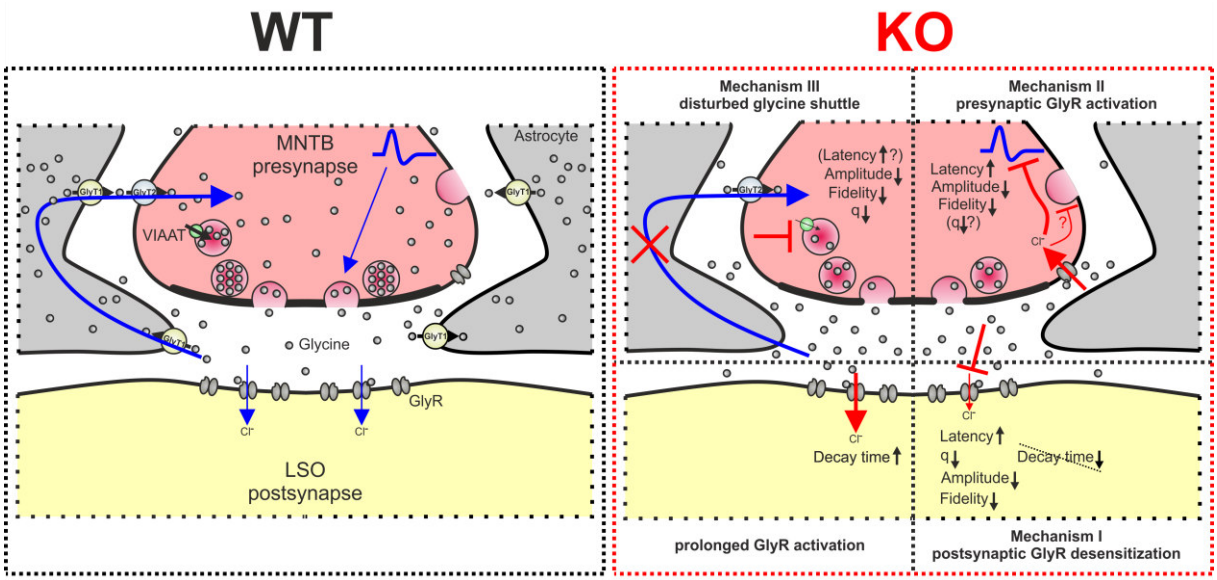

Figure 31: Hypothetical mechanisms that could be causative for the observed differences between WT and KO

At WT synapses (left), GlyR activation and ensuing Cl^- influx in the postsynapse is terminated by a decrease of glycine concentration via diffusion and subsequent uptake by astrocytic GlyT1. In vicinity to the synaptic cleft, GlyT1 transports glycine into the astrocyte due to the high extracellular glycine concentration. At KO synapses (right), loss of GlyT1 leads to glycine accumulation in the synaptic cleft, resulting in sustained activation of postsynaptic GlyRs and therefore in stronger prolonged decay times. A consequent desensitization of these receptors could be responsible for prolonged latencies and reduced q, amplitudes, and fidelity (mechanism I, cf. 4.4.1), but would also cause a shortening of decay times, which was not observed. This promotes the hypothesis that receptor desensitization is negligible at MNTB-LSO synapses. Another effect of the stronger glycine accumulation could be a stronger activation of presynaptic GlyRs located nearby the synaptic cleft (mechanism II, cf. 4.4.2). Concomitant Cl^- influx would lead to impairment of AP propagation via shunting inhibition, resulting in prolonged latencies, reduced amplitudes, and deteriorated fidelity. A disturbance of vesicle endocytosis can be discussed, as an increase in intracellular Cl^- was shown to negatively affect this process in another system. Altogether, presynaptic GlyR activation could delay replenishment, resulting in prolonged latencies and possibly in reduced q. A third hypothesis for the observed effects is the impairment of a proposed astrocytic-neuronal glycine shuttle (blue curved arrow; mechanism III, cf. 4.4.3). During excess release of glycine, the intracellular glycine concentration of astrocytes increases due to GlyT1 activity. At extrasynaptic sites, the glycine gradient with a low extracellular and a higher intracellular glycine concentration in astrocytes induces reverse function of GlyT1, leading to glycine release. Neuronal GlyT2, which is presumably opposed to astrocytic GlyT1, translocates extracellular glycine into the presynapse, increasing intraterminal glycine concentration needed for VIAAT to refill newly endocytosed vesicles. The loss of GlyT1 could therefore lead to impaired replenishment and eventually delayed vesicle exocytosis. Possible consequences are prolonged latencies and reduction of q, amplitudes, and fidelity, during periods with high consumption of glycine. As conclusion, these mechanisms could play in concert with varying degrees, leading to the observed impairment of synaptic transmission at the GlyT1-depleted MNTB-LSO synapse. GlyT = glycine transporter, GlyR = glycine receptor, VIAAT = vesicular inhibitory amino acid transporter, q = quantal size, MNTB = medial nucleus of the trapezoid body, LSO = lateral superior olive

4.5. Conclusion

In the last decades, the knowledge about astrocytic functions evolved from being only passive "glue" cells into cells with manifold functions. According to this, my study provides new insights into involvement of astrocytes in signal transmission at the MNTB-LSO synapse.

Interestingly, the synapse was able to compensate the depletion of GlyT1 during conditions with low amount of released glycine. However, during excess release of glycine, GlyT1 loss took effect, reflected by delayed, prolonged, and reduced inhibitory inputs to the LSO. The underlying mechanisms were not analyzed in this study, but provide discussion points that GlyT1 is not responsible only for glycine clearance from the synaptic cleft, but also for mediating glycine supply to neurons and presynaptic modifications (Figure 31).

As a further consequence, astrocytic GlyT1 loss at glycinergic synapses could also lead to a higher degree of glycine spillover to nearby glutamatergic synapses, where it was shown to potentiate NMDAR function (Ahmadi et al., 2003; Martina et al., 2004; Aubrey et al., 2005; Yee et al., 2006; Igartua et al., 2007; Singer et al., 2007; Harsing and Matyus, 2013) and/or facilitate transmitter release (Turecek and Trussell, 2001). In the LSO, postsynaptic NMDARs were found to play a prominent role for developmental refinement (Case and Gillespie, 2011), but shift to a rather balancing function in the mature system (Caspary and Faingold, 1989; Wu and Kelly, 1992; Wu and Fu, 1998).

As conclusion, the disturbed inhibitory transmission in a GlyT1-depleted LSO shown in this study could result in an impaired integration of inputs from the ipsi- and contralateral ear, which could be further deteriorated by the stronger influence on balancing NMDAR activity. Hence, ILD calculation would deliver falsified information to upstream auditory brain regions, resulting in disturbed sound source localization in GlyT1 KO animals. Thus, astrocytes contribute to proper function of the MNTB-LSO synapse and therefore are required for correct localization of high-frequency and sustained active sound sources.

4.6. Outlook

In my discussion, I proposed three mechanisms that could underlie the changes in the MNTB-LSO synapse of KO animals. Selected ideas for potential experiments to address these issues are listed below:

- Mechanism I: desensitization of postsynaptic GlyRs

  Postsynaptic GlyR desensitization was shown to contribute only marginally to synaptic depression at brainstem synapses (Gomeza et al., 2003a; Gomeza et al., 2003b; Krachan et al., 2017). Hence, the following proposed experiments could be performed to verify the exclusion of GlyR desensitization as cause for the impairment of synaptic transmission in KO:

  - Postsynaptic GlyRs are α1β heteromers. Ginkgolide B and C were shown to block heteromers more efficiently than homomers (Hawthorne et al., 2006). Applied to WT, a disturbance of synaptic transmission as in KO would indicate postsynaptic GlyR desensitization.
  - Wash-in of glycine to WT samples could be used to mimic glycine accumulation and concomitant stronger GlyR desensitization in KO. To exclude shunting inhibition, presynaptic GlyRs should be blocked with Picrotoxinin (see next paragraph).

- Mechanism II: enhanced activation of presynaptic GlyRs
  - Presynaptic GlyRs in the mature brain are supposed to be α1 homomers (Zeilhofer et al., 2018). Picrotoxinin was shown to have a stronger inhibitory effect on α homomers, as the β subunit appears to provide resistance (Pribilla et al., 1992). This inhibitor could be applied to KO to rescue a WT phenotype by preventing presynaptic shunting inhibition and its effects on synaptic transmission.
  - Pregnenolone (PREG) and dehydroxylcannabidiol (DH-CBD) were shown to potentiate homomeric α1 GlyRs without significantly altering postsynaptic GlyR activity (Maksay et al., 2001; Xiong et al., 2014). Hence, these drugs can be used in WT to mimic enhanced activation of presynaptic GlyRs.

- Mechanism III: disturbed glycine shuttle
  - Glycine can be radioactively labelled ([^{3}H]glycine). When [^{3}H]glycine is applied to the pipette solution, it can be transferred to an astrocyte in the LSO via patch-clamp. The administered [^{3}H]glycine likely enters adjacent astrocytes, as they are

known to form networks via gap junctions (Rouach et al., 2008; Pannasch and Rouach, 2013; Augustin et al., 2016; Wadle et al., 2018). During stimulation of MNTB-fibers, glycine-induced currents at astrocytes that predominantly originate from GlyT1 activity can be measured in LSO astrocytes (Stephan and Friauf, 2014). The 2:1 ratio of Na^+ and Cl^-, and the neutral net charge of glycine (isoelectric point: 5.97) at an intracellular pH of 7.2 in astrocytes (Verkhratsky and Nedergaard, 2018) elicits an inward (inward transport) or outward (reverse transport) current, depending on intra- and extracellular glycine concentrations. In WT astrocytes, I would expect a high sustained inward current at the beginning of challenges, which is sensitive to the GlyT1 inhibitor bitopertin (Armbruster et al., 2018). This would indicate an inwardly directed GlyT1 activity due to the high extracellular and low intracellular glycine concentration. The initial inward current could be reduced after some time, as the augmentation of intracellular glycine induces reverse function of GlyT1. In contrast, KO astrocytes should show no GlyT1-mediated currents, or only currents that are insensitive to bitopertin. After stimulation, brainstem slices can be histologically analyzed for [^{3}H]glycine as described in Ball and Brandon (1986) with GlyT2 as neuronal marker (Poyatos et al., 1997; Zeilhofer et al., 2005). Abundance of [^{3}H]glycine in neurons would prove the astrocytic origin of the intraneuronal glycine. In KO samples, [^{3}H]glycine should not be detected in neurons, as it is not transported out from astrocytes by GlyT1. However, if neuronal [^{3}H]glycine is present, this could indicate alternate astrocytic transport systems for glycine like SNAT1, SNAT2, SNAT5 and LAT2 (Cubelos et al., 2005c; Safory et al., 2015; Lopez-Corcuera et al., 2017; Zafra et al., 2017).

- Alternatively, neuronal [^{3}H]glycine originating from astrocytes could be estimated by using fluorescence-activated cell sorting (FACS) and a neuronal reporter mouse. This could be for example tdTomato^{Stopflx}Cre^{GlyT2}, which is already available in our group. Stimulation and administration of [^{3}H]glycine to astrocytes should be performed as mentioned above. Afterwards, tdTomato positive cells (= neurons) can be separated by using FACS. Ensuing analysis should reveal an abundance of [^{3}H]glycine in tdTomato-positive fraction of WT, but not of KO. In KO, [^{3}H]glycine is probably only detected in the tdTomato-negative fraction.

Finally, I want to address a disadvantage of the used mouse model. For the analysis of astrocytic GlyT1 function and its involvement in synaptic transmission, the systemic depletion of GlyT1 also affects neuronal GlyT1 present at glutamatergic synapses (Cubelos et al., 2005a; Cubelos et al., 2005b; Yee et al., 2006; Raiteri and Raiteri, 2010). Hence, side effects caused by neuronal GlyT1 depletion cannot be excluded. Another disadvantage could be a disturbance of development, as it was shown that complete KO of GlyT1 leads to a high lethality and therefore is crucially involved in postnatal development. This was solved by depletion of only isoform b and c, ensuring a quite normal development due to the expression of GlyT1a as the main GlyT1 isoform in early development. However, these KO mice gained only half the bodyweight as their WT littermates (Figure 13), which also indicates an impaired development and consequently synapses could be less mature. The use of an astrocyte-specific and temporally inducible GlyT1 KO would exclude these disadvantages. The GlyT1^{flx} tdTomato$^{CAG\text{-}Stopflx}$ Cre-ER-T2^{Glast} mouse (Mori et al., 2006; Madisen et al., 2010) allows an astrocyte specific KO, as Cre expression is regulated by glutamate aspartate transporter (Glast)-promoter activity. Additionally, the induction of the KO can be timed by the application of tamoxifen. With assistance by Vanessa Bräuler, I established a tamoxifen injection protocol that ensures reliable recombination of astrocytes, which can be used for future experiments (Bräuler, 2016).

5. REFERENCES

Abbott LF, Regehr WG (2004) Synaptic computation. Nature 431:796-803.

Abdi H (2007) The Bonferonni and Šidák Corrections for Multiple Comparisons. In: Encyclopedia of Measurement and Statistics (Salkind NJ, ed), pp 103-107. California, USA: SAGE Publications, Inc.

Adams RH, Sato K, Shimada S, Tohyama M, Puschel AW, Betz H (1995) Gene structure and glial expression of the glycine transporter GlyT1 in embryonic and adult rodents. J Neurosci 15:2524-2532.

Ahmadi S, Muth-Selbach U, Lauterbach A, Lipfert P, Neuhuber WL, Zeilhofer HU (2003) Facilitation of spinal NMDA receptor currents by spillover of synaptically released glycine. Science 300:2094-2097.

Akaike N, Kaneda M (1989) Glycine-gated chloride current in acutely isolated rat hypothalamic neurons. J Neurophysiol 62:1400-1409.

Ali DW, Drapeau P, Legendre P (2000) Development of spontaneous glycinergic currents in the Mauthner neuron of the zebrafish embryo. J Neurophysiol 84:1726-1736.

Allen NJ, Barres BA (2005) Signaling between glia and neurons: focus on synaptic plasticity. Curr Opin Neurobiol 15:542-548.

Altieri SC, Zhao T, Jalabi W, Maricich SM (2014) Development of glycinergic innervation to the murine LSO and SPN in the presence and absence of the MNTB. Front Neural Circuits 8:109.

Aoki E, Semba R, Keino H, Kato K, Kashiwamata S (1988) Glycine-like immunoreactivity in the rat auditory pathway. Brain Res 442:63-71.

Applegarth DA, Toone JR (2001) Nonketotic hyperglycinemia (glycine encephalopathy): laboratory diagnosis. Mol Genet Metab 74:139-146.

Aragon C, Lopez-Corcuera B (2003) Structure, function and regulation of glycine neurotransporters. Eur J Pharmacol 479:249-262.

Araque A, Parpura V, Sanzgiri RP, Haydon PG (1999) Tripartite synapses: glia, the unacknowledged partner. Trends Neurosci 22:208-215.

Armbruster A, Neumann E, Kotter V, Hermanns H, Werdehausen R, Eulenburg V (2018) The GlyT1 inhibitor bitopertin ameliorates allodynia and hyperalgesia in animal models of neuropathic and inflammatory pain. Front Mol Neurosci 10:438.

Aroeira RI, Sebastiao AM, Valente CA (2014) GlyT1 and GlyT2 in brain astrocytes: expression, distribution and function. Brain Struct Funct 219:817-830.

Ashida G, Carr CE (2011) Sound localization: Jeffress and beyond. Curr Opin Neurobiol 21:745-751.

Atkinson BN, Bell SC, De Vivo M, Kowalski LR, Lechner SM, Ognyanov VI, Tham CS, Tsai C, Jia J, Ashton D, Klitenick MA (2001) ALX 5407: a potent, selective inhibitor of the hGlyT1 glycine transporter. Mol Pharmacol 60:1414-1420.

Aubrey KR, Vandenberg RJ, Clements JD (2005) Dynamics of forward and reverse transport by the glial glycine transporter, GlyT1b. Biophys J 89:1657-1668.

Augustin V, Bold C, Wadle SL, Langer J, Jabs R, Philippot C, Weingarten DJ, Rose CR, Steinhauser C, Stephan J (2016) Functional anisotropic panglial networks in the lateral superior olive. Glia 64:1892-1911.

Ball AK, Brandon C (1986) Localization of 3H-GABA, -muscimol, and -glycine in goldfish retinas stained for glutamate decarboxylase. J Neurosci 6:1621-1627.

Bartho P, Payne JA, Freund TF, Acsady L (2004) Differential distribution of the KCl cotransporter KCC2 in thalamic relay and reticular nuclei. Eur J Neurosci 20:965-975.

Bartholomaus I, Milan-Lobo L, Nicke A, Dutertre S, Hastrup H, Jha A, Gether U, Sitte HH, Betz H, Eulenburg V (2008) Glycine transporter dimers: evidence for occurrence in the plasma membrane. J Biol Chem 283:10978-10991.

Beato M (2008) The time course of transmitter at glycinergic synapses onto motoneurons. J Neurosci 28:7412-7425.

Becker CM, Hoch W, Betz H (1988) Glycine receptor heterogeneity in rat spinal cord during postnatal development. EMBO J 7:3717-3726.

Beebe NL, Young JW, Mellott JG, Schofield BR (2016) Extracellular molecular markers and soma size of inhibitory neurons: evidence for four subtypes of GABAergic cells in the inferior colliculus. J Neurosci 36:3988-3999.

Beiderbeck B, Myoga MH, Muller NIC, Callan AR, Friauf E, Grothe B, Pecka M (2018) Precisely timed inhibition facilitates action potential firing for spatial coding in the auditory brainstem. Nat Commun 9:1771.

Ben Achour S, Pascual O (2010) Glia: the many ways to modulate synaptic plasticity. Neurochem Int 57:440-445.

Betz H, Kuhse J, Schmieden V, Laube B, Kirsch J, Harvey RJ (1999) Structure and functions of inhibitory and excitatory glycine receptors. Ann N Y Acad Sci 868:667-676.

Betz WJ (1970) Depression of transmitter release at the neuromuscular junction of the frog. J Physiol 206:629-644.

Blaesse P, Guillemin I, Schindler J, Schweizer M, Delpire E, Khiroug L, Friauf E, Nothwang HG (2006) Oligomerization of KCC2 correlates with development of inhibitory neurotransmission. J Neurosci 26:10407-10419.

Bolon B, Butt MT, Garman RH, Dorman DC (2013) Nervous System. In: Haschek and Rousseaux's Handbook of Toxicologic Pathology (Third Edition) (Haschek WM, Rousseaux CG, Wallig MA, eds), pp 2005-2093. Boston: Academic Press.

Borowsky B, Hoffman BJ (1998) Analysis of a gene encoding two glycine transporter variants reveals alternative promoter usage and a novel gene structure. J Biol Chem 273:29077-29085.

Borowsky B, Mezey E, Hoffman BJ (1993) Two glycine transporter variants with distinct localization in the CNS and peripheral tissues are encoded by a common gene. Neuron 10:851-863.

Boudreau JC, Tsuchitani C (1968) Binaural interaction in the cat superior olive S segment. J Neurophysiol 31:442-454.

Bradaia A, Schlichter R, Trouslard J (2004) Role of glial and neuronal glycine transporters in the control of glycinergic and glutamatergic synaptic transmission in lamina X of the rat spinal cord. J Physiol 559:169-186.

Bräuler V (2016) Tamoxifen induzierte tdTomato-Expression im auditorischen Hirnstamm bei Mäusen. University of Kaiserslautern, Bachelor thesis

Brill S (2014) Role of the astrocytic glycine transporter 1 in the synaptic transmission in the superior olivary complex. University of Kaiserslautern, Master thesis

Brill S (2018) Auditory brainstem neurons: synaptic plasticity and the relevance of glycine transporter 2 for vesicle replenishment. University of Kaiserslautern, PhD thesis

Caird D, Klinke R (1983) Processing of binaural stimuli by cat superior olivary complex neurons. Exp Brain Res 52:385-399.

Cant NB, Casseday JH (1986) Projections from the anteroventral cochlear nucleus to the lateral and medial superior olivary nuclei. J Comp Neurol 247:457-476.

Casado M, Ascher P (2009) Presynaptic Receptor Signaling. In: Encyclopedia of Neuroscience (Squire LR, ed), pp 1007-1015: Elsevier Ltd.

Case DT, Gillespie DC (2011) Pre- and postsynaptic properties of glutamatergic transmission in the immature inhibitory MNTB-LSO pathway. J Neurophysiol 106:2570-2579.

Caspary DM, Faingold CL (1989) Non-N-methyl-D-aspartate receptors may mediate ipsilateral excitation at lateral superior olivary synapses. Brain Res 503:83-90.

Chamma I, Chevy Q, Poncer JC, Levi S (2012) Role of the neuronal K-Cl co-transporter KCC2 in inhibitory and excitatory neurotransmission. Front Cell Neurosci 6:5.

Chen Z, Das B, Nakamura Y, DiGregorio DA, Young SM, Jr. (2015) Ca^{2+} channel to synaptic vesicle distance accounts for the readily releasable pool kinetics at a functionally mature auditory synapse. J Neurosci 35:2083-2100.

Chung WS, Allen NJ, Eroglu C (2015) Astrocytes control synapse formation, function, and elimination. Cold Spring Harb Perspect Biol 7:a020370.

Citri A, Malenka RC (2008) Synaptic plasticity: multiple forms, functions, and mechanisms. Neuropsychopharmacology 33:18-41.

Clements JD (1996) Transmitter timecourse in the synaptic cleft: its role in central synaptic function. Trends Neurosci 19:163-171.

Cubelos B, Gimenez C, Zafra F (2005a) Localization of the GLYT1 glycine transporter at glutamatergic synapses in the rat brain. Cereb Cortex 15:448-459.

Cubelos B, Gonzalez-Gonzalez IM, Gimenez C, Zafra F (2005b) The scaffolding protein PSD-95 interacts with the glycine transporter GLYT1 and impairs its internalization. J Neurochem 95:1047-1058.

Cubelos B, Gonzalez-Gonzalez IM, Gimenez C, Zafra F (2005c) Amino acid transporter SNAT5 localizes to glial cells in the rat brain. Glia 49:230-244.

Danbolt NC (2001) Glutamate uptake. Prog Neurobiol 65:1-105.

De Pitta M, Brunel N, Volterra A (2016) Astrocytes: Orchestrating synaptic plasticity? Neuroscience 323:43-61.

Denker A, Rizzoli SO (2010) Synaptic vesicle pools: an update. Front Synaptic Neurosci 2:135.

Dingledine R, Borges K, Bowie D, Traynelis SF (1999) The glutamate receptor ion channels. Pharmacol Rev 51:7-61.

Dobrunz LE, Stevens CF (1997) Heterogeneity of release probability, facilitation, and depletion at central synapses. Neuron 18:995-1008.

Draguhn A, Heinemann U (1996) Different mechanisms regulate IPSC kinetics in early postnatal and juvenile hippocampal granule cells. J Neurophysiol 76:3983-3993.

Dumoulin A, Rostaing P, Bedet C, Levi S, Isambert MF, Henry JP, Triller A, Gasnier B (1999) Presence of the vesicular inhibitory amino acid transporter in GABAergic and glycinergic synaptic terminal boutons. J Cell Sci 112 (Pt 6):811-823.

Dutertre S, Becker CM, Betz H (2012) Inhibitory glycine receptors: an update. J Biol Chem 287:40216-40223.

Edwards FA, Konnerth A, Sakmann B, Takahashi T (1989) A thin slice preparation for patch clamp recordings from neurones of the mammalian central nervous system. Pflugers Arch 414:600-612.

Edwards RH (2007) The neurotransmitter cycle and quantal size. Neuron 55:835-858.

Elmqvist D, Quastel DM (1965) A quantitative study of end-plate potentials in isolated human muscle. J Physiol 178:505-529.

Eubler K (2013) Die Wirkung von ambientem Glycin auf die glycinerge Transmission der MNTB-LSO Synapse. University of Kaiserslautern, Master thesis

Eulenburg V, Gomeza J (2010) Neurotransmitter transporters expressed in glial cells as regulators of synapse function. Brain Res Rev 63:103-112.

Eulenburg V, Armsen W, Betz H, Gomeza J (2005) Glycine transporters: essential regulators of neurotransmission. Trends Biochem Sci 30:325-333.

Eulenburg V, Retiounskaia M, Papadopoulos T, Gomeza J, Betz H (2010) Glial glycine transporter 1 function is essential for early postnatal survival but dispensable in adult mice. Glia 58:1066-1073.

Eulenburg V, Knop G, Sedmak T, Schuster S, Hauf K, Schneider J, Feigenspan A, Joachimsthaler A, Brandstatter JH (2018) GlyT1 determines the glycinergic phenotype of amacrine cells in the mouse retina. Brain Struct Funct 223:3251-3266.

Farley FW, Soriano P, Steffen LS, Dymecki SM (2000) Widespread recombinase expression using FLPeR (flipper) mice. Genesis 28:106-110.

Fedele E, Foster AC (1992) [^{3}H]glycine uptake in rat hippocampus: kinetic analysis and autoradiographic localization. Brain Res 572:154-163.

Felmy F, Künzel T (2014) Giant synapses in the central auditory system. In: e-Neuroforum, p 53.

Fernandez-Alfonso T, Ryan TA (2004) The kinetics of synaptic vesicle pool depletion at CNS synaptic terminals. Neuron 41:943-953.

Finlayson PG, Caspary DM (1989) Synaptic potentials of chinchilla lateral superior olivary neurons. Hear Res 38:221-228.

Fischer A (2016) Synaptic and extrasynaptic inhibition in the lateral superior olive and its relevance for short-term plasticity and postsynaptic processing. University of Kaiserslautern, PhD thesis

Fischer AU, Muller NIC, Deller T, Del Turco D, Fisch JO, Griesemer D, Kattler K, Maraslioglu A, Roemer V, Xu-Friedman MA, Walter J, Friauf E (2019) GABA is a modulator, rather than a classical transmitter, in the medial nucleus of the trapezoid body-lateral superior olive sound localization circuit. J Physiol 597:2269-2295.

Ford MC, Grothe B, Klug A (2009) Fenestration of the calyx of Held occurs sequentially along the tonotopic axis, is influenced by afferent activity, and facilitates glutamate clearance. J Comp Neurol 514:92-106.

Ford MC, Alexandrova O, Cossell L, Stange-Marten A, Sinclair J, Kopp-Scheinpflug C, Pecka M, Attwell D, Grothe B (2015) Tuning of Ranvier node and internode properties in myelinated axons to adjust action potential timing. Nat Commun 6:8073.

Freche D, Pannasch U, Rouach N, Holcman D (2011) Synapse geometry and receptor dynamics modulate synaptic strength. PloS one 6:e25122.

Friauf E, Hammerschmidt B, Kirsch J (1997) Development of adult-type inhibitory glycine receptors in the central auditory system of rats. J Comp Neurol 385:117-134.

Friauf E, Fischer AU, Fuhr MF (2015) Synaptic plasticity in the auditory system: a review. Cell Tissue Res 361:177-213.

Friauf E, Krachan EG, Muller NIC (2019) Lateral Superior Olive: Organization, Development, and Plasticity. In: The Oxford Handbook of the Auditory Brainstem (Kandler K, ed): Oxford University Press.

Friauf E, Rust MB, Schulenborg T, Hirtz JJ (2011) Chloride cotransporters, chloride homeostasis, and synaptic inhibition in the developing auditory system. Hear Res 279:96-110.

Friauf E, Aragon C, Lohrke S, Westenfelder B, Zafra F (1999) Developmental expression of the glycine transporter GLYT2 in the auditory system of rats suggests involvement in synapse maturation. J Comp Neurol 412:17-37.

Galarreta M, Hestrin S (1998) Frequency-dependent synaptic depression and the balance of excitation and inhibition in the neocortex. Nat Neurosci 1:587-594.

Ghirardini E, Wadle SL, Augustin V, Becker J, Brill S, Hammerich J, Seifert G, Stephan J (2018) Expression of functional inhibitory neurotransmitter transporters GlyT1, GAT-1, and GAT-3 by astrocytes of inferior colliculus and hippocampus. Mol Brain 11:4.

Gjoni E, Zenke F, Bouhours B, Schneggenburger R (2018a) Specific synaptic input strengths determine the computational properties of excitation-inhibition integration in a sound localization circuit. J Physiol 596:4945-4967.

Gjoni E, Aguet C, Sahlender DA, Knott G, Schneggenburger R (2018b) Ultrastructural basis of strong unitary inhibition in a binaural neuron. J Physiol 596:4969-4982.

Gomeza J, Hulsmann S, Ohno K, Eulenburg V, Szoke K, Richter D, Betz H (2003a) Inactivation of the glycine transporter 1 gene discloses vital role of glial glycine uptake in glycinergic inhibition. Neuron 40:785-796.

Gomeza J, Ohno K, Hulsmann S, Armsen W, Eulenburg V, Richter DW, Laube B, Betz H (2003b) Deletion of the mouse glycine transporter 2 results in a hyperekplexia phenotype and postnatal lethality. Neuron 40:797-806.

Grothe B, Pecka M, McAlpine D (2010) Mechanisms of sound localization in mammals. Physiol Rev 90:983-1012.

Gu Y, Huang LY (1998) Cross-modulation of glycine-activated Cl- channels by protein kinase C and cAMP-dependent protein kinase in the rat. J Physiol 506 (Pt 2):331-339.

Guastella J, Brecha N, Weigmann C, Lester HA, Davidson N (1992) Cloning, expression, and localization of a rat brain high-affinity glycine transporter. Proc Natl Acad Sci U S A 89:7189-7193.

Hamill OP, Marty A, Neher E, Sakmann B, Sigworth FJ (1981) Improved patch-clamp techniques for high-resolution current recording from cells and cell-free membrane patches. Pflugers Arch 391:85-100.

Hanley JG, Jones EM, Moss SJ (2000) GABA receptor rho1 subunit interacts with a novel splice variant of the glycine transporter, GlyT1. J Biol Chem 275:840-846.

Hansen KB, Yi F, Perszyk RE, Furukawa H, Wollmuth LP, Gibb AJ, Traynelis SF (2018) Structure, function, and allosteric modulation of NMDA receptors. J Gen Physiol 150:1081-1105.

Harsing LG, Jr., Matyus P (2013) Mechanisms of glycine release, which build up synaptic and extrasynaptic glycine levels: the role of synaptic and non-synaptic glycine transporters. Brain Res Bull 93:110-119.

Harvey RJ, Yee BK (2013) Glycine transporters as novel therapeutic targets in schizophrenia, alcohol dependence and pain. Nat Rev Drug Discov 12:866-885.

Harvey RJ, Carta E, Pearce BR, Chung SK, Supplisson S, Rees MI, Harvey K (2008) A critical role for glycine transporters in hyperexcitability disorders. Front Mol Neurosci 1:1.

Hawthorne R, Cromer BA, Ng HL, Parker MW, Lynch JW (2006) Molecular determinants of ginkgolide binding in the glycine receptor pore. J Neurochem 98:395-407.

Helfert RH, Bonneau JM, Wenthold RJ, Altschuler RA (1989) GABA and glycine immunoreactivity in the guinea pig superior olivary complex. Brain Res 501:269-286.

Herculano-Houzel S (2014) The glia/neuron ratio: how it varies uniformly across brain structures and species and what that means for brain physiology and evolution. Glia 62:1377-1391.

Herdon HJ, Godfrey FM, Brown AM, Coulton S, Evans JR, Cairns WJ (2001) Pharmacological assessment of the role of the glycine transporter GlyT-1 in mediating high-affinity glycine uptake by rat cerebral cortex and cerebellum synaptosomes. Neuropharmacology 41:88-96.

Hirtz JJ, Braun N, Griesemer D, Hannes C, Janz K, Lohrke S, Muller B, Friauf E (2012) Synaptic refinement of an inhibitory topographic map in the auditory brainstem requires functional Cav1.3 calcium channels. J Neurosci 32:14602-14616.

Horiuchi M, Nicke A, Gomeza J, Aschrafi A, Schmalzing G, Betz H (2001) Surface-localized glycine transporters 1 and 2 function as monomeric proteins in Xenopus oocytes. Proc Natl Acad Sci U S A 98:1448-1453.

Hruskova B, Trojanova J, Kulik A, Kralikova M, Pysanenko K, Bures Z, Syka J, Trussell LO, Turecek R (2012) Differential distribution of glycine receptor subtypes at the rat calyx of Held synapse. J Neurosci 32:17012-17024.

Hubner CA, Stein V, Hermans-Borgmeyer I, Meyer T, Ballanyi K, Jentsch TJ (2001) Disruption of KCC2 reveals an essential role of K-Cl cotransport already in early synaptic inhibition. Neuron 30:515-524.

Hull C, von Gersdorff H (2004) Fast endocytosis is inhibited by GABA-mediated chloride influx at a presynaptic terminal. Neuron 44:469-482.

Igartua I, Solis JM, Bustamante J (2007) Glycine-induced long-term synaptic potentiation is mediated by the glycine transporter GLYT1. Neuropharmacology 52:1586-1595.

Imboden M, De Saint Jan D, Leulier F, Korn H, Goblet C, Bregestovski P (2001) Isolation and characterization of an alpha 2-type zebrafish glycine receptor subunit. Neuroscience 103:799-810.

Jeffress LA (1948) A place theory of sound localization. J Comp Physiol Psychol 41:35-39.

Jenkins WM, Masterton RB (1982) Sound localization: effects of unilateral lesions in central auditory system. J Neurophysiol 47:987-1016.

Jeong HJ, Jang IS, Moorhouse AJ, Akaike N (2003) Activation of presynaptic glycine receptors facilitates glycine release from presynaptic terminals synapsing onto rat spinal sacral dorsal commissural nucleus neurons. J Physiol 550:373-383.

Johnson JW, Ascher P (1987) Glycine potentiates the NMDA response in cultured mouse brain neurons. Nature 325:529-531.

Jones MV, Westbrook GL (1995) Desensitized states prolong GABAA channel responses to brief agonist pulses. Neuron 15:181-191.

Jones MV, Westbrook GL (1996) The impact of receptor desensitization on fast synaptic transmission. Trends Neurosci 19:96-101.

Joris PX, Yin TC (1995) Envelope coding in the lateral superior olive. I. Sensitivity to interaural time differences. J Neurophysiol 73:1043-1062.

Joris PX, Yin TC (1998) Envelope coding in the lateral superior olive. III. Comparison with afferent pathways. J Neurophysiol 79:253-269.

Joris PX, Trussell LO (2018) The calyx of Held: a hypothesis on the need for reliable timing in an intensity-difference encoder. Neuron 100:534-549.

Jursky F, Nelson N (1995) Localization of glycine neurotransmitter transporter (GLYT2) reveals correlation with the distribution of glycine receptor. J Neurochem 64:1026-1033.

Jursky F, Nelson N (1996) Developmental expression of the glycine transporters GLYT1 and GLYT2 in mouse brain. J Neurochem 67:336-344.

Jursky F, Tamura S, Tamura A, Mandiyan S, Nelson H, Nelson N (1994) Structure, function and brain localization of neurotransmitter transporters. J Exp Biol 196:283-295.

Kaeser PS, Regehr WG (2014) Molecular mechanisms for synchronous, asynchronous, and spontaneous neurotransmitter release. Annu Rev Physiol 76:333-363.

Kaeser PS, Regehr WG (2017) The readily releasable pool of synaptic vesicles. Curr Opin Neurobiol 43:63-70.

Kandler K, Friauf E (1995) Development of glycinergic and glutamatergic synaptic transmission in the auditory brainstem of perinatal rats. J Neurosci 15:6890-6904.

Kandler K, Clause A, Noh J (2009) Tonotopic reorganization of developing auditory brainstem circuits. Nat Neurosci 12:711-717.

Kaplan EL, Meier P (1958) Nonparametric estimation from incomplete observations. J Am Stat Assoc 53:457-481.

Katz B (1971) Quantal mechanism of neural transmitter release. Science 173:123-126.

Kavalali ET (2006) Synaptic vesicle reuse and its implications. Neuroscientist 12:57-66.

Khimich D, Nouvian R, Pujol R, Tom Dieck S, Egner A, Gundelfinger ED, Moser T (2005) Hair cell synaptic ribbons are essential for synchronous auditory signalling. Nature 434:889-894.

Kim G, Kandler K (2003) Elimination and strengthening of glycinergic/GABAergic connections during tonotopic map formation. Nat Neurosci 6:282-290.

Kim G, Kandler K (2010) Synaptic changes underlying the strengthening of GABA/glycinergic connections in the developing lateral superior olive. Neuroscience 171:924-933.

Kim KM, Kingsmore SF, Han H, Yang-Feng TL, Godinot N, Seldin MF, Caron MG, Giros B (1994) Cloning of the human glycine transporter type 1: molecular and pharmacological characterization of novel isoform variants and chromosomal localization of the gene in the human and mouse genomes. Mol Pharmacol 45:608-617.

Kim SK, Nabekura J, Koizumi S (2017) Astrocyte-mediated synapse remodeling in the pathological brain. Glia 65:1719-1727.

Klein J, Moeschberger M (2003) Survival Analysis - Techniques for Censored and Truncated Data, 2nd Edition. New York: Springer-Verlag.

Kono Y, Hulsmann S (2016) Presynaptic facilitation of glycinergic mIPSC is reduced in mice lacking alpha3 glycine receptor subunits. Neuroscience 320:1-7.

Kopp-Scheinpflug C, Tolnai S, Malmierca MS, Rubsamen R (2008) The medial nucleus of the trapezoid body: comparative physiology. Neuroscience 154:160-170.

Kotak VC, Korada S, Schwartz IR, Sanes DH (1998) A developmental shift from GABAergic to glycinergic transmission in the central auditory system. J Neurosci 18:4646-4655.

Krachan EG, Fischer AU, Franke J, Friauf E (2017) Synaptic reliability and temporal precision are achieved via high quantal content and effective replenishment: auditory brainstem versus hippocampus. J Physiol 595:839-864.

Kramer F (2012) Die Leistungsfähigkeit einer glycinergen inhibitorischen Synapse im auditorischen Hirnstamm und die Beteiligung der Glycintransporter. University of Kaiserslautern, PhD thesis

Kramer F, Griesemer D, Bakker D, Brill S, Franke J, Frotscher E, Friauf E (2014) Inhibitory glycinergic neurotransmission in the mammalian auditory brainstem upon prolonged stimulation: short-term plasticity and synaptic reliability. Front Neural Circuits 8:14.

Kristensen AS, Andersen J, Jorgensen TN, Sorensen L, Eriksen J, Loland CJ, Stromgaard K, Gether U (2011) SLC6 neurotransmitter transporters: structure, function, and regulation. Pharmacol Rev 63:585-640.

Kubota H, Alle H, Betz H, Geiger JR (2010) Presynaptic glycine receptors on hippocampal mossy fibers. Biochem Biophys Res Commun 393:587-591.

Kungel M, Friauf E (1997) Physiology and pharmacology of native glycine receptors in developing rat auditory brainstem neurons. Brain Res Dev Brain Res 102:157-165.

Kurolap A, Armbruster A, Hershkovitz T, Hauf K, Mory A, Paperna T, Hannappel E, Tal G, Nijem Y, Sella E, Mahajnah M, Ilivitzki A, Hershkovitz D, Ekhilevitch N, Mandel H, Eulenburg V, Baris HN (2016) Loss of glycine transporter 1 causes a subtype of glycine encephalopathy with arthrogryposis and mildly elevated cerebrospinal fluid glycine. Am J Hum Genet 99:1172-1180.

Kurz C (2019) Was können glycinerge Synapsen in Abwesenheit des Glycin-Transporters 2 im auditorischen Hirnstamm leisten? University of Kaiserslautern, Diploma thesis

Latal AT, Kremer T, Gomeza J, Eulenburg V, Hulsmann S (2010) Development of synaptic inhibition in glycine transporter 2 deficient mice. Mol Cell Neurosci 44:342-352.

Laube B, Maksay G, Schemm R, Betz H (2002) Modulation of glycine receptor function: a novel approach for therapeutic intervention at inhibitory synapses? Trends Pharmacol Sci 23:519-527.

Lauer AM, Connelly CJ, Graham H, Ryugo DK (2013) Morphological characterization of bushy cells and their inputs in the laboratory mouse (Mus musculus) anteroventral cochlear nucleus. PloS one 8:e73308.

Lee H, Bach E, Noh J, Delpire E, Kandler K (2016) Hyperpolarization-independent maturation and refinement of GABA/glycinergic connections in the auditory brain stem. J Neurophysiol 115:1170-1182.

Legendre P (1998) A reluctant gating mode of glycine receptor channels determines the time course of inhibitory miniature synaptic events in zebrafish hindbrain neurons. J Neurosci 18:2856-2870.

Legendre P (2001) The glycinergic inhibitory synapse. Cell Mol Life Sci 58:760-793.

Legendre P, Muller E, Badiu CI, Meier J, Vannier C, Triller A (2002) Desensitization of homomeric alpha1 glycine receptor increases with receptor density. Mol Pharmacol 62:817-827.

Lim R, Alvarez FJ, Walmsley B (1999) Quantal size is correlated with receptor cluster area at glycinergic synapses in the rat brainstem. J Physiol 516 (Pt 2):505-512.

Lim R, Hoang P, Berger AJ (2004) Blockade of glycine transporter-1 (GLYT-1) potentiates NMDA receptor-mediated synaptic transmission in hypoglossal motorneurons. J Neurophysiol 92:2530-2537.

Lin KH, Oleskevich S, Taschenberger H (2011) Presynaptic Ca^{2+} influx and vesicle exocytosis at the mouse endbulb of Held: a comparison of two auditory nerve terminals. J Physiol 589:4301-4320.

Lippman JJ, Lordkipanidze T, Buell ME, Yoon SO, Dunaevsky A (2008) Morphogenesis and regulation of Bergmann glial processes during Purkinje cell dendritic spine ensheathment and synaptogenesis. Glia 56:1463-1477.

Lipstein N, Sakaba T, Cooper BH, Lin KH, Strenzke N, Ashery U, Rhee JS, Taschenberger H, Neher E, Brose N (2013) Dynamic control of synaptic vesicle replenishment and short-term plasticity by Ca^{2+}-calmodulin-Munc13-1 signaling. Neuron 79:82-96.

Liu QR, Nelson H, Mandiyan S, Lopez-Corcuera B, Nelson N (1992) Cloning and expression of a glycine transporter from mouse brain. FEBS Lett 305:110-114.

Liu QR, Lopez-Corcuera B, Mandiyan S, Nelson H, Nelson N (1993) Cloning and expression of a spinal cord- and brain-specific glycine transporter with novel structural features. J Biol Chem 268:22802-22808.

Logan WJ, Snyder SH (1972) High affinity uptake systems for glycine, glutamic and aspaspartic acids in synaptosomes of rat central nervous tissues. Brain Res 42:413-431.

Lopez-Corcuera B, Benito-Munoz C, Aragon C (2017) Glycine transporters in glia cells: structural studies. Adv Neurobiol 16:13-32.

Lorteije JA, Rusu SI, Kushmerick C, Borst JG (2009) Reliability and precision of the mouse calyx of Held synapse. J Neurosci 29:13770-13784.

Lottspeich F, Engels JW (2006) Bioanalytik, 2nd Edition: Spektrum Akademischer Verlag.

Lujan B, von Gersdorff H (2017) Tuning auditory synapses for resilience, reliability and precision. J Physiol 595:621-622.

Lynch JW (2004) Molecular structure and function of the glycine receptor chloride channel. Physiol Rev 84:1051-1095.

Madisen L, Zwingman TA, Sunkin SM, Oh SW, Zariwala HA, Gu H, Ng LL, Palmiter RD, Hawrylycz MJ, Jones AR, Lein ES, Zeng H (2010) A robust and high-throughput Cre reporting and characterization system for the whole mouse brain. Nat Neurosci 13:133-140.

Maksay G, Laube B, Betz H (2001) Subunit-specific modulation of glycine receptors by neurosteroids. Neuropharmacology 41:369-376.

Malinowski MN, Cannady SB, Schmit KV, Barr PM, Schrock JW, Wilson DF (1997) Adenosine depresses transmitter release but is not the basis for 'tetanic fade' at the neuromuscular junction of the rat. Neurosci Lett 230:81-84.

Mallorga PJ, Williams JB, Jacobson M, Marques R, Chaudhary A, Conn PJ, Pettibone DJ, Sur C (2003) Pharmacology and expression analysis of glycine transporter GlyT1 with [3H]-(N-[3-(4'-fluorophenyl)-3-(4'phenylphenoxy)propyl])sarcosine. Neuropharmacology 45:585-593.

Manis PB, Xie R, Wang Y, Marrs GS, Spirou GA (2012) The Endbulbs of Held. In: Synaptic Mechanisms in the Auditory System. Springer Handbook of Auditory Research (Trussell LO, Popper A, eds), pp 61-93. New York: Springer.

Martina M, Gorfinkel Y, Halman S, Lowe JA, Periyalwar P, Schmidt CJ, Bergeron R (2004) Glycine transporter type 1 blockade changes NMDA receptor-mediated responses and LTP in hippocampal CA1 pyramidal cells by altering extracellular glycine levels. J Physiol 557:489-500.

Marz S (2018) Interactome analysis of the glycine transporter 2. University of Kaiserslautern, PhD thesis

Meyer G, Kirsch J, Betz H, Langosch D (1995) Identification of a gephyrin binding motif on the glycine receptor beta subunit. Neuron 15:563-572.

Moore MJ, Caspary DM (1983) Strychnine blocks binaural inhibition in lateral superior olivary neurons. J Neurosci 3:237-242.

Mori T, Tanaka K, Buffo A, Wurst W, Kuhn R, Gotz M (2006) Inducible gene deletion in astroglia and radial glia--a valuable tool for functional and lineage analysis. Glia 54:21-34.

Muller NIC (2019) The influence of peripheral and central protein loss on synaptic wiring and performance of an inhibitory auditory brainstem circuit. Technical University of Kaiserslautern, PhD thesis

Nabekura J, Katsurabayashi S, Kakazu Y, Shibata S, Matsubara A, Jinno S, Mizoguchi Y, Sasaki A, Ishibashi H (2004) Developmental switch from GABA to glycine release in single central synaptic terminals. Nat Neurosci 7:17-23.

Neher E (2010) What is rate-limiting during sustained synaptic activity: vesicle supply or the availability of release sites. Front Synaptic Neurosci 2:144.

Nelson N (1998) The family of Na+/Cl- neurotransmitter transporters. J Neurochem 71:1785-1803.

Nerlich J, Keine C, Rubsamen R, Burger RM, Milenkovic I (2014) Activity-dependent modulation of inhibitory synaptic kinetics in the cochlear nucleus. Front Neural Circuits 8:145.

Nishimaki T, Jang IS, Ishibashi H, Yamaguchi J, Nabekura J (2007) Reduction of metabotropic glutamate receptor-mediated heterosynaptic inhibition of developing MNTB-LSO inhibitory synapses. Eur J Neurosci 26:323-330.

Noh J, Seal RP, Garver JA, Edwards RH, Kandler K (2010) Glutamate co-release at GABA/glycinergic synapses is crucial for the refinement of an inhibitory map. Nat Neurosci 13:232-238.

Olivares L, Aragon C, Gimenez C, Zafra F (1994) Carboxyl terminus of the glycine transporter GLYT1 is necessary for correct processing of the protein. J Biol Chem 269:28400-28404.

Olivares L, Aragon C, Gimenez C, Zafra F (1997) Analysis of the transmembrane topology of the glycine transporter GLYT1. J Biol Chem 272:1211-1217.

Oyama M, Kuraoka S, Watanabe S, Iwai T, Tanabe M (2017) Electrophysiological evidence of increased glycine receptor-mediated phasic and tonic inhibition by blockade of glycine transporters in spinal superficial dorsal horn neurons of adult mice. J Pharmacol Sci 133:162-167.

Pannasch U, Rouach N (2013) Emerging role for astroglial networks in information processing: from synapse to behavior. Trends Neurosci 36:405-417.

Pannasch U, Vargova L, Reingruber J, Ezan P, Holcman D, Giaume C, Sykova E, Rouach N (2011) Astroglial networks scale synaptic activity and plasticity. Proc Natl Acad Sci U S A 108:8467-8472.

Park TJ, Grothe B, Pollak GD, Schuller G, Koch U (1996) Neural delays shape selectivity to interaural intensity differences in the lateral superior olive. J Neurosci 16:6554-6566.

Paulus W, Rothwell JC (2016) Membrane resistance and shunting inhibition: where biophysics meets state-dependent human neurophysiology. J Physiol 594:2719-2728.

Pellerin L, Magistretti PJ (2012) Sweet sixteen for ANLS. J Cereb Blood Flow Metab 32:1152-1166.

Perea G, Araque A (2007) Astrocytes potentiate transmitter release at single hippocampal synapses. Science 317:1083-1086.

Pow DV, Hendrickson AE (1999) Distribution of the glycine transporter glyt-1 in mammalian and nonmammalian retinae. Vis Neurosci 16:231-239.

Poyatos I, Ponce J, Aragon C, Gimenez C, Zafra F (1997) The glycine transporter GLYT2 is a reliable marker for glycine-immunoreactive neurons. Brain Res Mol Brain Res 49:63-70.

Pramod AB, Foster J, Carvelli L, Henry LK (2013) SLC6 transporters: structure, function, regulation, disease association and therapeutics. Mol Aspects Med 34:197-219.

Pribilla I, Takagi T, Langosch D, Bormann J, Betz H (1992) The atypical M2 segment of the beta subunit confers picrotoxinin resistance to inhibitory glycine receptor channels. EMBO J 11:4305-4311.

Price GD, Trussell LO (2006) Estimate of the chloride concentration in a central glutamatergic terminal: a gramicidin perforated-patch study on the calyx of Held. J Neurosci 26:11432-11436.

Pusch M, Neher E (1988) Rates of diffusional exchange between small cells and a measuring patch pipette. Pflugers Arch 411:204-211.

Raiteri L, Raiteri M (2010) Functional 'glial' GLYT1 glycine transporters expressed in neurons. J Neurochem 114:647-653.

Raiteri L, Raiteri M, Bonanno G (2001) Glycine is taken up through GLYT1 and GLYT2 transporters into mouse spinal cord axon terminals and causes vesicular and carrier-mediated release of its proposed co-transmitter GABA. J Neurochem 76:1823-1832.

Raiteri L, Stigliani S, Siri A, Passalacqua M, Melloni E, Raiteri M, Bonanno G (2005) Glycine taken up through GLYT1 and GLYT2 heterotransporters into glutamatergic axon terminals of mouse spinal cord elicits release of glutamate by homotransporter reversal and through anion channels. Biochem Pharmacol 69:159-168.

Regehr WG (2012) Short-term presynaptic plasticity. Cold Spring Harb Perspect Biol 4:a005702-a005702.

Richerson GB, Wu Y (2003) Dynamic equilibrium of neurotransmitter transporters: not just for reuptake anymore. J Neurophysiol 90:1363-1374.

Rizzoli SO, Betz WJ (2005) Synaptic vesicle pools. Nat Rev Neurosci 6:57-69.

Rouach N, Koulakoff A, Abudara V, Willecke K, Giaume C (2008) Astroglial metabolic networks sustain hippocampal synaptic transmission. Science 322:1551-1555.

Rousseau F, Aubrey KR, Supplisson S (2008) The glycine transporter GlyT2 controls the dynamics of synaptic vesicle refilling in inhibitory spinal cord neurons. J Neurosci 28:9755-9768.

Roux MJ, Supplisson S (2000) Neuronal and glial glycine transporters have different stoichiometries. Neuron 25:373-383.

Safory H, Neame S, Shulman Y, Zubedat S, Radzishevsky I, Rosenberg D, Sason H, Engelender S, Avital A, Hülsmann S, Schiller J, Wolosker H (2015) The alanine-serine-cysteine-1 (Asc-1) transporter controls glycine levels in the brain and is required for glycinergic inhibitory transmission. EMBO reports 16:590-598.

Sakaba T, Neher E (2001) Calmodulin mediates rapid recruitment of fast-releasing synaptic vesicles at a calyx-type synapse. Neuron 32:1119-1131.

Sakata Y, Owada Y, Sato K, Kojima K, Hisanaga K, Shinka T, Suzuki Y, Aoki Y, Satoh J, Kondo H, Matsubara Y, Kure S (2001) Structure and expression of the glycine cleavage system in rat central nervous system. Brain Res Mol Brain Res 94:119-130.

Sanes DH (1990) An in vitro analysis of sound localization mechanisms in the gerbil lateral superior olive. J Neurosci 10:3494-3506.

Sato K, Yoshida S, Fujiwara K, Tada K, Tohyama M (1991) Glycine cleavage system in astrocytes. Brain Res 567:64-70.

Schneggenburger R, Sakaba T, Neher E (2002) Vesicle pools and short-term synaptic depression: lessons from a large synapse. Trends Neurosci 25:206-212.

Schuster S (2015) Generation and characterization of a GlyT1b/c *knock-in* mouse. Friedrich-Alexander-University Erlangen-Nürnberg, PhD thesis

Schwarz Y, Zhao N, Kirchhoff F, Bruns D (2017) Astrocytes control synaptic strength by two distinct v-SNARE-dependent release pathways. Nat Neurosci 20:1529-1539.

Shank RP, Aprison MH (1970) The metabolism in vivo of glycine and serine in eight areas of the rat central nervous system. J Neurochem 17:1461-1475.

Shibasaki K, Hosoi N, Kaneko R, Tominaga M, Yamada K (2017) Glycine release from astrocytes via functional reversal of GlyT1. J Neurochem 140:395-403.

Singer JH, Talley EM, Bayliss DA, Berger AJ (1998) Development of glycinergic synaptic transmission to rat brain stem motoneurons. J Neurophysiol 80:2608-2620.

Singer P, Boison D, Mohler H, Feldon J, Yee BK (2007) Enhanced recognition memory following glycine transporter 1 deletion in forebrain neurons. Behav Neurosci 121:815-825.

Smith KE, Borden LA, Hartig PR, Branchek T, Weinshank RL (1992) Cloning and expression of a glycine transporter reveal colocalization with NMDA receptors. Neuron 8:927-935.

Sokoloff L (1977) Relation between physiological function and energy metabolism in the central nervous system. J Neurochem 29:13-26.

Spangler KM, Warr WB, Henkel CK (1985) The projections of principal cells of the medial nucleus of the trapezoid body in the cat. J Comp Neurol 238:249-262.

Spike RC, Watt C, Zafra F, Todd AJ (1997) An ultrastructural study of the glycine transporter GLYT2 and its association with glycine in the superficial laminae of the rat spinal dorsal horn. Neuroscience 77:543-551.

Spirou GA, Berrebi AS (1997) Glycine immunoreactivity in the lateral nucleus of the trapezoid body of the cat. J Comp Neurol 383:473-488.

Spirou GA, Brownell WE, Zidanic M (1990) Recordings from cat trapezoid body and HRP labeling of globular bushy cell axons. J Neurophysiol 63:1169-1190.

Staley KJ, Mody I (1992) Shunting of excitatory input to dentate gyrus granule cells by a depolarizing GABAA receptor-mediated postsynaptic conductance. J Neurophysiol 68:197-212.

Stange-Marten A, Nabel AL, Sinclair JL, Fischl M, Alexandrova O, Wohlfrom H, Kopp-Scheinpflug C, Pecka M, Grothe B (2017) Input timing for spatial processing is precisely tuned via constant synaptic delays and myelination patterns in the auditory brainstem. Proc Natl Acad Sci U S A 114:E4851-E4858.

Stephan J, Friauf E (2014) Functional analysis of the inhibitory neurotransmitter transporters GlyT1, GAT-1, and GAT-3 in astrocytes of the lateral superior olive. Glia 62:1992-2003.

Sterenborg JC, Pilati N, Sheridan CJ, Uchitel OD, Forsythe ID, Barnes-Davies M (2010) Lateral olivocochlear (LOC) neurons of the mouse LSO receive excitatory and inhibitory synaptic inputs with slower kinetics than LSO principal neurons. Hear Res 270:119-126.

Sudhof TC (2004) The synaptic vesicle cycle. Annu Rev Neurosci 27:509-547.

Supplisson S, Bergman C (1997) Control of NMDA receptor activation by a glycine transporter co-expressed in Xenopus oocytes. J Neurosci 17:4580-4590.

Supplisson S, Roux MJ (2002) Why glycine transporters have different stoichiometries. FEBS Lett 529:93-101.

Szabadics J, Varga C, Molnar G, Olah S, Barzo P, Tamas G (2006) Excitatory effect of GABAergic axo-axonic cells in cortical microcircuits. Science 311:233-235.

Szoke K, Hartel K, Grass D, Hirrlinger PG, Hirrlinger J, Hulsmann S (2006) Glycine transporter 1 expression in the ventral respiratory group is restricted to protoplasmic astrocytes. Brain Res 1119:182-189.

Takahashi T, Momiyama A, Hirai K, Hishinuma F, Akagi H (1992) Functional correlation of fetal and adult forms of glycine receptors with developmental changes in inhibitory synaptic receptor channels. Neuron 9:1155-1161.

Theodosis DT, Poulain DA, Oliet SH (2008) Activity-dependent structural and functional plasticity of astrocyte-neuron interactions. Physiol Rev 88:983-1008.

Ting JT, Daigle TL, Chen Q, Feng G (2014) Acute brain slice methods for adult and aging animals: application of targeted patch clamp analysis and optogenetics. Methods Mol Biol 1183:221-242.

Titmus MJ, Korn H, Faber DS (1996) Diffusion, not uptake, limits glycine concentration in the synaptic cleft. J Neurophysiol 75:1738-1752.

Tollin DJ (2003) The lateral superior olive: a functional role in sound source localization. Neuroscientist 9:127-143.

Tollin DJ, Koka K, Tsai JJ (2008) Interaural level difference discrimination thresholds for single neurons in the lateral superior olive. J Neurosci 28:4848-4860.

Traynelis SF, Wollmuth LP, McBain CJ, Menniti FS, Vance KM, Ogden KK, Hansen KB, Yuan H, Myers SJ, Dingledine R (2010) Glutamate receptor ion channels: structure, regulation, and function. Pharmacol Rev 62:405-496.

Trussell LO, Zhang S, Raman IM (1993) Desensitization of AMPA receptors upon multiquantal neurotransmitter release. Neuron 10:1185-1196.

Tsai G, Ralph-Williams RJ, Martina M, Bergeron R, Berger-Sweeney J, Dunham KS, Jiang Z, Caine SB, Coyle JT (2004) Gene knockout of glycine transporter 1: characterization of the behavioral phenotype. Proc Natl Acad Sci U S A 101:8485-8490.

Tso MC, Herzog ED (2015) Was Cajal right about sleep? BMC Biol 13:67.

Turecek J, Regehr WG (2019) Neuronal regulation of fast synaptotagmin isoforms controls the relative contributions of synchronous and asynchronous release. Neuron 101:938-949.e934.

Turecek R, Trussell LO (2001) Presynaptic glycine receptors enhance transmitter release at a mammalian central synapse. Nature 411:587-590.

Twyman RE, Macdonald RL (1991) Kinetic properties of the glycine receptor main- and sub-conductance states of mouse spinal cord neurones in culture. J Physiol 435:303-331.

Verkhratsky A, Nedergaard M (2018) Physiology of astroglia. Physiol Rev 98:239-389.

Volterra A, Meldolesi J (2005) Astrocytes, from brain glue to communication elements: the revolution continues. Nat Rev Neurosci 6:626-640.

Wadle SL, Augustin V, Langer J, Jabs R, Philippot C, Weingarten DJ, Rose CR, Steinhäuser C, Stephan J (2018) Anisotropic panglial coupling reflects tonotopic organization in the inferior colliculus. Front Cell Neurosci 12.

Walstrom KM, Hess GP (1994) Mechanism for the channel-opening reaction of strychnine-sensitive glycine receptors on cultured embryonic mouse spinal cord cells. Biochemistry 33:7718-7730.

Wang LY, Kaczmarek LK (1998) High-frequency firing helps replenish the readily releasable pool of synaptic vesicles. Nature 394:384-388.

Warr WB (1966) Fiber degeneration following lesions in the anterior ventral cochlear nucleus of the cat. Exp Neurol 14:453-474.

Weingarten DJ (2018) Maturation of the auditory brainstem after hearing onset: Role of Ca^{2+} sensitivity and vesicle pool organization in reliable synaptic transmission. University of Kaiserslautern, PhD thesis

Weisz CJ, Rubio ME, Givens RS, Kandler K (2016) Excitation by axon terminal GABA spillover in a sound localization circuit. J Neurosci 36:911-925.

Wenthold RJ, Huie D, Altschuler RA, Reeks KA (1987) Glycine immunoreactivity localized in the cochlear nucleus and superior olivary complex. Neuroscience 22:897-912.

Whitehead KJ, Pearce SM, Walker G, Sundaram H, Hill D, Bowery NG (2004) Positive N-methyl-D-aspartate receptor modulation by selective glycine transporter-1 inhibition in the rat dorsal spinal cord in vivo. Neuroscience 126:381-390.

Wichmann C (2015) Molecularly and structurally distinct synapses mediate reliable encoding and processing of auditory information. Hear Res 330:178-190.

Winters BL, Rawling T, Vandenberg RJ, Christie MJ, Bhola RF, Imlach WL (2018) Activity of novel lipid glycine transporter inhibitors on synaptic signalling in the dorsal horn of the spinal cord. Br J Pharmacol 175:2337-2347.

Witcher MR, Park YD, Lee MR, Sharma S, Harris KM, Kirov SA (2010) Three-dimensional relationships between perisynaptic astroglia and human hippocampal synapses. Glia 58:572-587.

Wu SH, Kelly JB (1992) NMDA, non-NMDA and glycine receptors mediate binaural interaction in the lateral superior olive: physiological evidence from mouse brain slice. Neurosci Lett 134:257-260.

Wu SH, Kelly JB (1993) Response of neurons in the lateral superior olive and medial nucleus of the trapezoid body to repetitive stimulation: intracellular and extracellular recordings from mouse brain slice. Hear Res 68:189-201.

Wu SH, Kelly JB (1994) Physiological evidence for ipsilateral inhibition in the lateral superior olive: synaptic responses in mouse brain slice. Hear Res 73:57-64.

Wu SH, Fu XW (1998) Glutamate receptors underlying excitatory synaptic transmission in the rat's lateral superior olive studied in vitro. Hear Res 122:47-59.

Xiong W, Chen SR, He L, Cheng K, Zhao YL, Chen H, Li DP, Homanics GE, Peever J, Rice KC, Wu LG, Pan HL, Zhang L (2014) Presynaptic glycine receptors as a potential therapeutic target for hyperekplexia disease. Nat Neurosci 17:232-239.

Xu-Friedman MA (2017) Measuring the basic physiological properties of synapses. Cold Spring Harb Protoc 2017.

Xu-Friedman MA, Harris KM, Regehr WG (2001) Three-dimensional comparison of ultrastructural characteristics at depressing and facilitating synapses onto cerebellar Purkinje cells. J Neurosci 21:6666-6672.

Yee BK, Balic E, Singer P, Schwerdel C, Grampp T, Gabernet L, Knuesel I, Benke D, Feldon J, Mohler H, Boison D (2006) Disruption of glycine transporter 1 restricted to forebrain neurons is associated with a procognitive and antipsychotic phenotypic profile. J Neurosci 26:3169-3181.

Yu WM, Goodrich LV (2014) Morphological and physiological development of auditory synapses. Hear Res 311:3-16.

Zafra F, Gimenez C (2008) Glycine transporters and synaptic function. IUBMB life 60:810-817.

Zafra F, Poyatos I, Gimenez C (1997a) Neuronal dependency of the glycine transporter GlyT1 expression in glial cells. Glia 20:155-162.

Zafra F, Aragon C, Gimenez C (1997b) Molecular biology of glycinergic neurotransmission. Mol Neurobiol 14:117-142.

Zafra F, Aragon C, Olivares L, Danbolt NC, Gimenez C, Storm-Mathisen J (1995) Glycine transporters are differentially expressed among CNS cells. J Neurosci 15:3952-3969.

Zafra F, Ibanez I, Bartolome-Martin D, Piniella D, Arribas-Blazquez M, Gimenez C (2017) Glycine transporters and its coupling with NMDA receptors. Adv Neurobiol 16:55-83.

Zeilhofer HU, Acuna MA, Gingras J, Yevenes GE (2018) Glycine receptors and glycine transporters: targets for novel analgesics? Cell Mol Life Sci 75:447-465.

Zeilhofer HU, Studler B, Arabadzisz D, Schweizer C, Ahmadi S, Layh B, Bosl MR, Fritschy JM (2005) Glycinergic neurons expressing enhanced green fluorescent protein in bacterial artificial chromosome transgenic mice. J Comp Neurol 482:123-141.

Zucker RS, Regehr WG (2002) Short-term synaptic plasticity. Annu Rev Physiol 64:355-405.

6. INDEX OF ABBREVIATIONS

ACSF	artificial cerebrospinal fluid
AMPAR	α-amino-3-hydroxy-5-methyl-4-isoxazolepropionic acid receptor
AP	action potential
Asc-1	alanine-serine-cysteine-1
AVCN	anterior ventral cochlear nucleus
BB	blocking buffer
CC	current clamp
CN	cochlear nucleus
CNQX	6-cyano-7-nitroquinoxaline-2,3-dione
CNS	central nervous system
EDTA	ethylenediaminetetraacetic acid
eIPSC	evoked IPSC
EPSC	excitatory PSC
FDD	frequency-dependent depression
Flp	flippase
Frt	Flp (flippase) recombinase targeting sequence
GBC	globular bushy cell
GCS	glycine cleavage system
GlyR	glycine receptor
GlyT1/2	glycine transporter 1/2
HT	heterozygous
IEI	interevent-interval
IHC	inner hair cells
ILD	interaural level difference
IPSC	inhibitory PSC
ITD	interaural time difference
KCC2	K^+-Cl^--co-transporter 2
KO	knockout
LSO	lateral superior olive
LucR	renilla luciferase
m	quantal content
MNTB	medial nucleus of the trapezoid body

MSO	medial superior olive
NEO	neomycin resistance cassette
NFPS	N-[3-(40-fluorophenyl)-3-(40-phenylphenoxy)propyl] sarcosine
NMDAR	N-methyl-D-aspartate receptor
P	postnatal day
PCR	polymerase chain reaction
P_r	release probability
PSC	postsynaptic current
q	quantal size
R_{In}	input resistance
R_M	membrane resistance
RRP	readily releasable pool
R_S	series resistance
SBC	spherical bushy cell
SD	standard deviation
SHMT	serine hydroxymethyltransferase
sIPSC	spontaneous IPSC
SNAT	sodium-coupled neutral amino acid transporter
SOC	superior olivary complex
STD	short-term depression
STF	short-term facilitation
STP	short-term plasticity
VC	voltage clamp
VGCC	voltage-gated calcium channel
VIAAT	vesicular inhibitory amino acid transporter
V_{Rest}	resting membrane potential
WT	wildtype

7. SUPPLEMENTARY FIGURES AND TABLES

Table S.1: Cells used for eIPSC analysis with color code and membrane properties

Cell ID	Color code	V_{Rest}	R_M	R_{In}	R_{In} change		
				1 Hz	rec50	rec100	rec200
	Q11 Candy	[mV]	[MΩ]	[MΩ]	[%]	[%]	[%]
WT							
15033306_wt_S1-C1		-75.0	36.0	46.8			
15033306_wt_S1-C2		-74.0	45.0	57.2			
15035407_wt_S1-C3		-73.0	38.0	47.2			
15045108_wt_S2-C2		-70.0	40.0	56.2	8	19	21
15063105_wt_S2-C1		-72.0	20.0	33.7	-1		
15063105_wt_S2-C2		-68.0	7.0	23.8	-5	-13	-20
15063105_wt_S2-C3		-72.0	29.0	38.0	-7	-7	-8
15063105_wt_S2-C4		-71.0	18.0	36.2	-2	-1	-5
15065103_wt_S1-C1		-69.0	14.0	20.5	-1	-8	-9
15069208_wt_S2-C1		-74.0	32.0	59.9	15	13	13
15069208_wt_S2-C3		-62.0	28.0	39.3	-12	-5	7
15069208_wt_S2-C4		-70.0	50.0	64.3	-2		
15069208_wt_S2-C5		-71.0	67.0	77.2	18	17	19
15069209_wt_S2-C2		-64.0	10.0	22.7	-6	-8	-7
15069209_wt_S2-C3		-67.0	41.0	48.8	-1		
15073208_wt_S1-C2		-67.0	49.0	67.5	-10	-2	
15073208_wt_S1-C3		-72.0	41.0	45.4	-13	-14	-16
	n	**17**	**17**	**17**	**14**	**11**	**10**
	Mean	**-70.1**	**33.2**	**46.2**	**-1**	**-1**	**-1**
	SEM	**0.9**	**3.9**	**4.0**	**2**	**4**	**5**
KO							
15033205_ki_S1-C2		-69.0	50.0	62.0	-7	-35	
15039106_ki_S1-C1		-73.0	17.0	28.7	-6	-6	-9
15039106_ki_S1-C2		-76.0	51.0	65.2	2	-7	27
15039107_ki_S1-C1		-73.0	67.0	77.5	-4	-5	11
15049104_ki_S1-C1		-66.0	34.0	67.6	8	6	5
15049104_ki_S1-C2		-63.0	9.0	22.8	-7	-11	-7
15049104_ki_S1-C3		-73.0	37.0	44.2	5	7	1
15053304_ki_S3-C2		-75.0	41.0	67.8	-16		
15055206_ki_S1-C1		-72.0	23.0	47.0	-9	-15	-15
15055207_ki_S1-C2		-73.3	26.1	51.4	-10		
15059203_ki_S1-C2		-72.0	47.0	53.6	-3		
15059203_ki_S2-C3		-75.0	70.0	84.2	7	-6	1
15059203_ki_S2-C6		-81.0	67.0	62.1	-16	-9	
15061101_ki_S1-C3		-72.0	50.0	65.7	-4	-1	-3
15061101_ki_S1-C4		-68.0	12.0	22.7	1	4	
15065101_ki_S1-C3		-71.0	33.0	43.5	1	-3	
15073213_ki_S1-C2		-67.0	17.0	26.0	-1	-2	
15073213_ki_S1-C3		-73.0	26.0	33.8	-11	-7	-9
	n	**18**	**18**	**18**	**18**	**15**	**10**
	Mean	**-71.8**	**37.6**	**51.4**	**-4**	**-6**	**0**
	SEM	**1.0**	**4.5**	**4.5**	**2**	**3**	**4**
	p value (WT/KO)	**0.19274**	**0.46773**	**0.38653**	**0.37798**	**0.24259**	**0.89916**
	sign.	***n.s.***	***n.s.***	***n.s.***	***n.s.***	***n.s.***	***n.s.***

List of cells used for eIPSC analysis with their membrane properties and the normalized change of R_{In}. The color code shown here was used for illustration of single cell data in eIPSC figures. The cells additionally marked with yellow were used as example cells (WT§ and KO§). R_{In} was calculated at the end of the depicted stimulation episodes. V_{Rest} = membrane potential during resting conditions, R_M = membrane resistance, R_{In} = input resistance

Table S.2: Survival probability

Age	WT	HT	KO
P0	100% (133)	99% (231/1)	99% (105/1)
P1	99% (132/1)		95% (104/4)
P2			93% (100/2)
P5	98% (131/1)	98% (228/1)	
P8	98% (130/1)		
P11	97% (129/1)		
P13	96% (127/1)		
P17			92% (84/1)
P19	95% (95/1)		
P30			
P38		94% (52/2)	no data
P50			

Survival probability until P50 of WT, HT and KO, obtained from Kaplan-Meier estimate (cf. Figure 13). Data are presented as the survival probability at the indicated age with n and the number of natural deaths in brackets.

Table S.3: GlyT1 and GlyT2 content in brainstem - arbitrary units

Genotype:	WT (12)	KO (12)	p value	significance
GlyT1 [a.u.]	7.8 ± 2.4 (11)	1.2 ± 0.5 (11)	1.2×10^{-6}	***
GlyT2 [a.u.]	73.7 ± 56.2	59.2 ± 33.4	0.22511	*n.s.*

Data are presented as mean ± SEM of the GlyT1 and GlyT2 antibody signal, respectively, obtained from western blotting (cf. Figure 14). Numbers in brackets depict sample sizes (number of tissues). Outlier-tests were positive for GlyT1 data in both genotypes. The reduced sample sizes are depicted in brackets at the affected datasets. For significance levels see Table 1. *n.s.* = not significant

Table S.4: Failures and fidelity of WT and KO example cells

Condition	total failures		total fidelity	
	WT§	KO§	WT§	KO§
	[n]	[n]	[%]	[%]
50 Hz	0	0	100	100
rec50	0	0	100	100
100 Hz	22	1	100	100
rec100	0	0	100	100
200 Hz	1757	2333	85	81
rec200	0	0	100	100

Number of failures and consequent fidelity of the two example cells for WT and KO (WT§, KO§), respectively (cf. Figure 17)

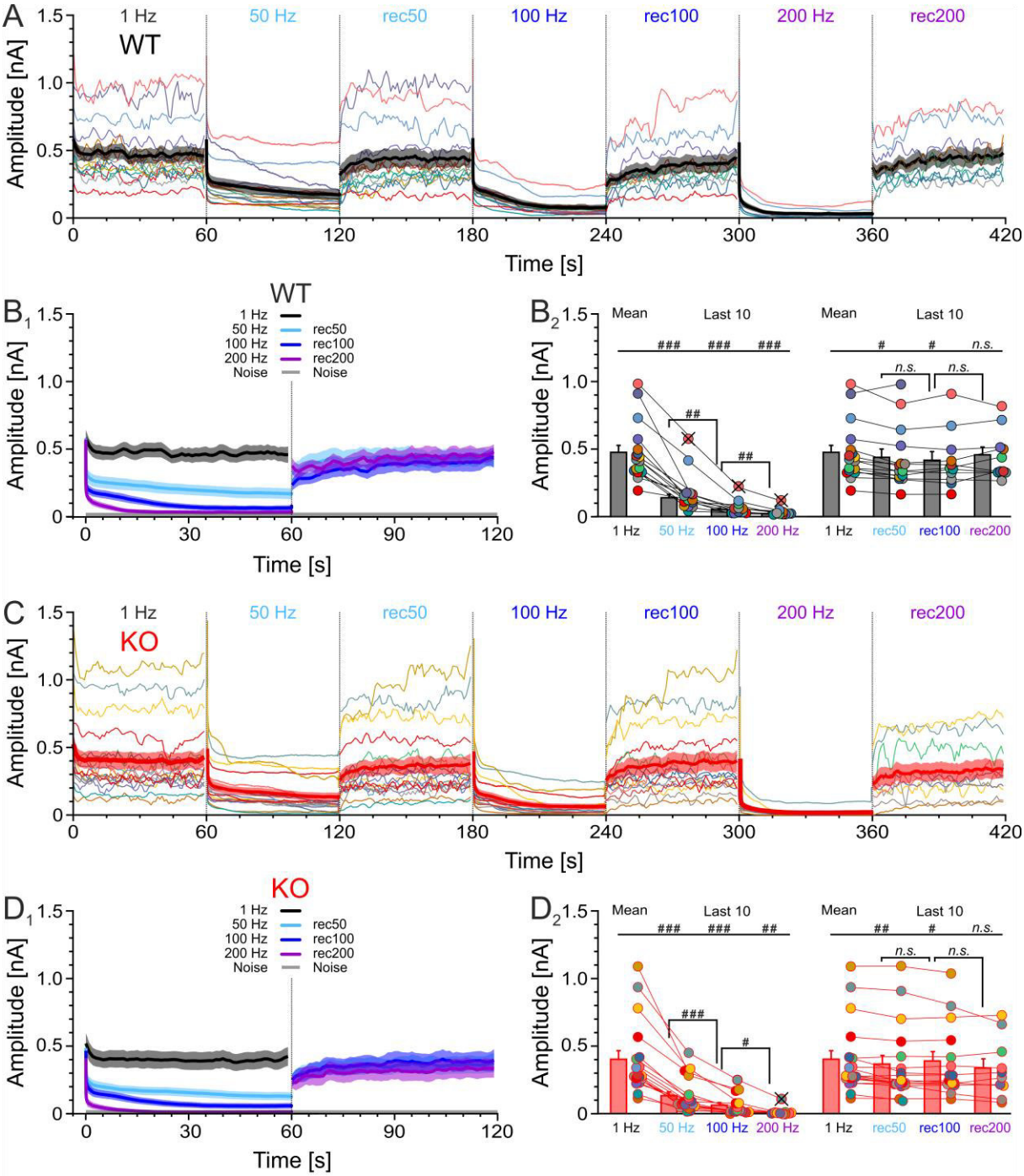

Figure S.1: FDD and recovery of WT and KO (absolute values)

A,C, FDD and recovery in absolute amplitudes of WT (A) and KO (C). **B_1,D_1**, Overlay of the mean courses of WT (B_1) and KO (D_1) shown in A and C, respectively. For clarity, the courses in A, C, B_1 and D_1 were smoothed with a moving average of 5% of the data points. **B_2,D_2**, Analysis of FDD (left) and recovery (right) with the mean amplitude during 1 Hz stimulation and the mean amplitude of the last ten eIPSCs of a challenge/recovery (failures included). Testing of significance was applied for the challenge/recovery data to the 1 Hz situation and additionally to the preceding challenge/recovery with *post hoc* Šidák correction. Note the reduced n in B_2 and D_2 due to outlier testing. Outliers are indicated with a cross-marked circle. For details see Table S.5 and for significance levels Table 1. n(cells) = 17/14/11/10(WT) / 18/18/15/10(KO), outliers included

Table S.5: FDD and recovery of WT and KO (absolute values)

Condition	WT (17/14/11/10)					KO (18/18/15/10)				
	Amplitude [pA]	p value (to 1 Hz)	sign. (k = 6)	p value (to prec.)	sign. (k = 2)	Amplitude [pA]	p value (to 1 Hz)	sign. (k = 6)	p value (to prec.)	sign. (k = 2)
1 Hz	474.6 ± 51.9					404.9 ± 63.6				
50 Hz	139.0 ± 25.9 (13)	0.00002	###			135.6 ± 29.5	3.1×10^{-6}	###		
100 Hz	53.8 ± 9.9 (10)	0.00002	###	0.00468	##	66.2 ± 19.6	0.00001	###	0.00042	###
200 Hz	22.1 ± 4.3 (9)	0.00001	###	0.00296	##	7.4 ± 1.6 (9)	0.00074	##	0.01542	#
rec50	438.0 ± 61.5	0.00328	#			369.0 ± 64.4	0.00105	##		
rec100	416.8 ± 63.3	0.0018	#	0.30993	*n.s.*	392.3 ± 69.1	0.00346	#	0.19041	*n.s.*
rec200	456.4 ± 57.9	0.10272	*n.s.*	0.46985	*n.s.*	339.2 ± 69.1	0.11919	*n.s.*	0.46296	*n.s.*

Data (cf. Figure S.1) are presented as mean ± SEM of all eIPSCs (1 Hz) or of the last ten eIPSCs (all other conditions). Numbers in brackets depict sample sizes (number of cells). Outlier tests were positive for some conditions. The reduced sample sizes are indicated in brackets at the affected datasets. Due to multiple comparisons, the critical α value was *post hoc* Šidák corrected. The number of comparisons (k) is indicated on top. For significance levels see Table 1. prec. = preceding, sign. = significance, *n.s.* = not significant

Table S.6: $q_{Last\ 10\ s}$ compared to initial q (absolute values)

Initial q:	WT (17/14/11/10) 23.4 ± 0.9 [pA]							KO (18/18/15/10) 23.3 ± 1.0 [pA]							WT/KO	
Condition	$q_{Last\ 10\ s}$ [pA]	to initial q			to preceding q			$q_{Last\ 10\ s}$ [pA]	to initial q			to preceding q			p value	sign.
		p value	k	sign.	p value	k	sign.		p value	k	sign.	p value	k	sign.		
1 Hz	21.8 ± 1.3	0.15666	5	*n.s.*				21.8 ± 1.2	0.16826	5	*n.s.*				0.99769	*n.s.*
50 Hz	21.4 ± 1.1	0.12067	5	*n.s.*	0.51111	2	*n.s.*	20.8 ± 1.0 (17)	0.00247	5	#	0.19502	2	*n.s.*	0.66739	*n.s.*
rec50	22.5 ± 1.3	0.53236	5	*n.s.*	0.09165	2	*n.s.*	22.4 ± 1.0 (17)	0.12797	5	*n.s.*	0.05052	2	*n.s.*	0.90741	*n.s.*
100 Hz	20.1 ± 1.2	0.10592	5	*n.s.*	0.07608	2	*n.s.*	19.1 ± 1.4 (12)	0.00200	5	##	0.00766	2	#	0.59776	*n.s.*
rec100	21.5 ± 1.5	0.67867	5	*n.s.*	0.06905	2	*n.s.*	22.8 ± 1.1 (14)	0.48721	5	*n.s.*	0.00032	2	###	0.50601	*n.s.*
200 Hz	n.d.							n.d.							n.d.	
rec200	n.d.							n.d.							n.d.	

Data are presented as mean ± SEM (cf. Figure 22). Numbers in brackets depict sample sizes (number of cells). Due to outliers and due to cells with too few sIPSCs to determine q, the sample sizes are reduced in some conditions, indicated in brackets at the affected datasets. q in 200 Hz and rec200 was not determined. Due to multiple comparisons the critical α value was *post hoc* Šidák corrected for comparison with the initial q and with the preceding q. The number of comparisons (k) is indicated. For significance levels see Table 1. For values normalized to initial q see Table 10. q = quantal size, prec. = preceding, sign. = significance, *n.s.* = not significant, n.d. = not determined

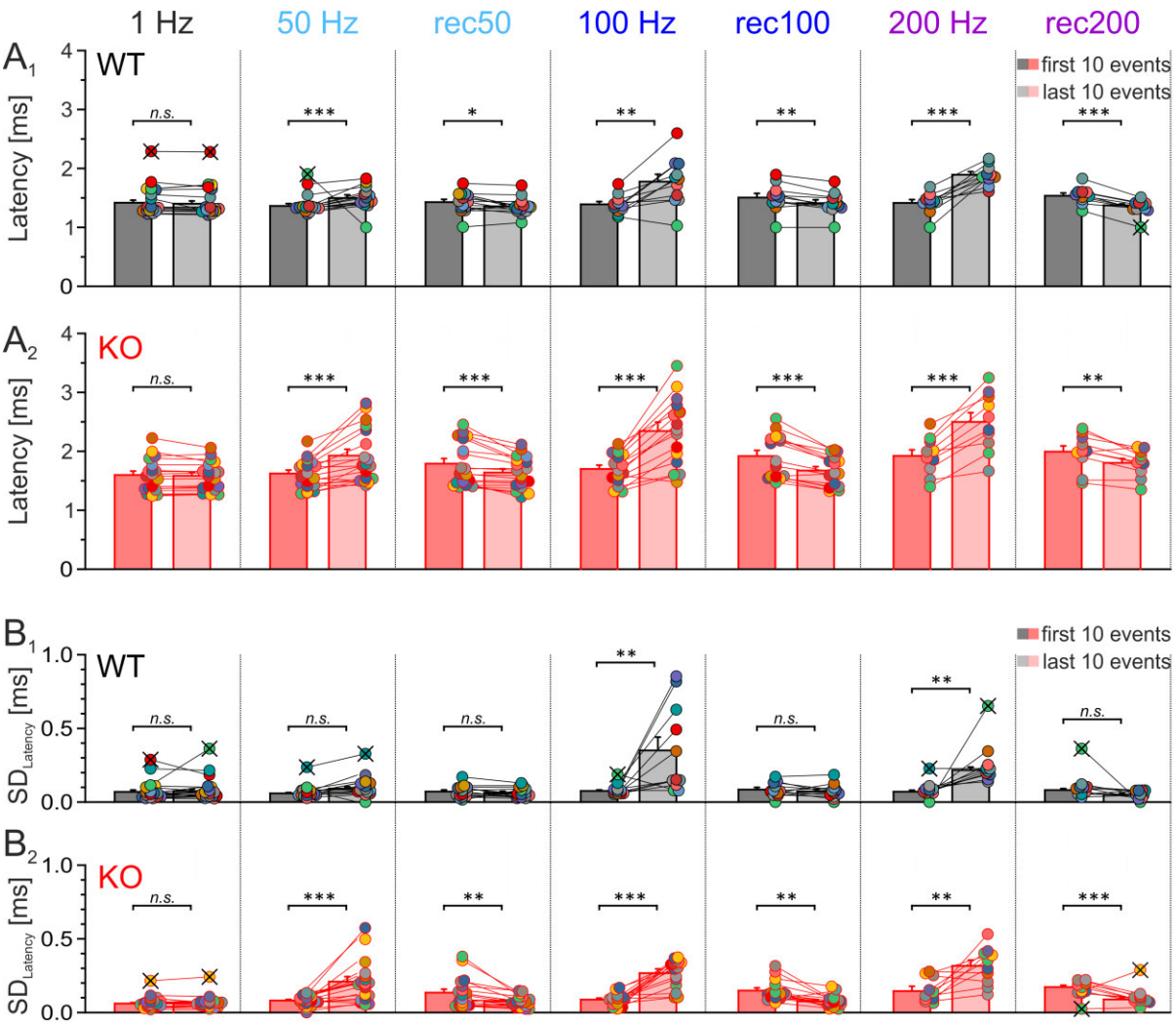

Figure S.2: Latency and $SD_{Latency}$ of the first and last 10 events

A, Comparison of the latencies of the first and last 10 events in WT (**A_1**) and KO (**A_2**). Only events with eIPSCs amplitudes above threshold (= responded stimuli/events; cf. 2.3.5) were used for analysis. **B,** Comparison of the $SD_{Latency}$ of the first and last 10 events in WT (**B_1**) and KO (**B_2**). Outliers are indicated with cross-marked circles. For details and comparison between WT and KO see Table S.7 (Latency) and Table S.8 ($SD_{Latency}$). For significance levels see Table 1. n (cells) = 17/14/11/10 (WT) / 18/18/15/10 (KO), outliers and cells with too few events included. *n.s.* = not significant

Table S.7: Latency comparison between first 10 events and last 10 events

Condition		WT (17/14/11/10)			KO (18/18/15/10)			WT/KO	
		Latency [ms]	p value	sign.	Latency [ms]	p value	sign.	p value	sign.
1 Hz	first 10	1.42 ± 0.04 (16)	0.32123	*n.s.*	1.60 ± 0.07	0.31178	*n.s.*	0.03415	*
	last 10	1.40 ± 0.05 (16)			1.58 ± 0.06			0.02034	*
50 Hz	first 10	1.37 ± 0.04 (13)	0.00030	***	1.63 ± 0.06	0.00043	***	0.00080	***
	last 10	1.50 ± 0.05			1.93 ± 0.11			0.00162	**
rec50	first 10	1.43 ± 0.05	0.03027	*	1.79 ± 0.09	0.00096	***	0.00122	**
	last 10	1.36 ± 0.04			1.64 ± 0.06			0.00069	***
100 Hz	first 10	1.39 ± 0.05	0.00311	**	1.70 ± 0.07	0.00002	***	0.00169	**
	last 10	1.78 ± 0.12			2.34 ± 0.15			0.01123	*
rec100	first 10	1.51 ± 0.07	0.00646	**	1.92 ± 0.10	0.00020	***	0.00333	**
	last 10	1.41 ± 0.06			1.67 ± 0.07			0.00860	**
200 Hz	first 10	1.42 ± 0.06	0.00006	***	1.93 ± 0.10	0.00011	***	0.00037	***
	last 10	1.89 ± 0.05			2.50 ± 0.16			0.00373	**
rec200	first 10	1.54 ± 0.05	0.00003	***	1.99 ± 0.10	0.00466	**	0.00102	**
	last 10	1.37 ± 0.02 (9)			1.81 ± 0.07			0.00019	***

Data are presented as mean of the first and the last 10 events ± SEM (cf. Figure S.2A). Numbers in brackets depict sample sizes (number of cells). Only events with eIPSCs amplitudes above threshold (= responded stimuli/events; cf. 2.3.5) were used for analysis. Comparison was performed between the first and last 10 events for WT and KO separately, and between the corresponding 10 events of WT and KO. Reduced sample sizes due to outliers and to cells with too few sIPSCs corresponding to the criteria are indicated in brackets at the affected datasets. For significance levels see Table 1. sign. = significance, *n.s.* = not significant

Table S.8: $SD_{Latency}$ comparison between first 10 events and last 10 events

Condition		WT (17/14/11/10)			KO (18/18/15/10)			WT/KO	
		$SD_{Latency}$ [ms]	p value	sign.	$SD_{Latency}$ [ms]	p value	sign.	p value	sign.
1 Hz	first 10	0.07 ± 0.01 (16)	0.86188	*n.s.*	0.06 ± 0.01 (17)	0.65391	*n.s.*	0.60072	*n.s.*
	last 10	0.07 ± 0.01 (16)			0.06 ± 0.00 (17)			0.31657	*n.s.*
50 Hz	first 10	0.06 ± 0.01 (13)	0.05776	*n.s.*	0.08 ± 0.01	0.00060	***	0.11205	*n.s.*
	last 10	0.09 ± 0.01 (13)			0.21 ± 0.03			0.00461	**
rec50	first 10	0.07 ± 0.01	0.46652	*n.s.*	0.14 ± 0.02	0.00404	**	0.02106	*
	last 10	0.06 ± 0.01			0.08 ± 0.01			0.38884	*n.s.*
100 Hz	first 10	0.07 ± 0.01 (10)	0.00968	**	0.09 ± 0.01	0.00001	***	0.39892	*n.s.*
	last 10	0.35 ± 0.09			0.27 ± 0.03			0.40157	*n.s.*
rec100	first 10	0.08 ± 0.01	0.35319	*n.s.*	0.15 ± 0.02	0.00163	**	0.01712	*
	last 10	0.07 ± 0.02			0.08 ± 0.01			0.80670	*n.s.*
200 Hz	first 10	0.07 ± 0.01 (9)	0.00187	**	0.15 ± 0.03	0.00912	**	0.01289	*
	last 10	0.22 ± 0.02 (9)			0.32 ± 0.04			0.04659	*
rec200	first 10	0.08 ± 0.01 (9)	0.07071	*n.s.*	0.17 ± 0.01 (9)	0.00007	***	0.00002	***
	last 10	0.05 ± 0.01			0.09 ± 0.01 (9)			0.01009	*

Data are presented as mean of the first and the last 10 events ± SEM (cf. Figure S.2B). Numbers in brackets depict sample size (number of cells). Only events with eIPSCs amplitudes above threshold (= responded stimuli/events; cf. 2.3.5) were used for analysis. Comparison was performed between the first and last 10 events for WT and KO separately, and between the corresponding 10 events of WT and KO. Reduced sample sizes due to outliers and to cells with too few sIPSCs corresponding to the criteria are indicated in brackets at the affected datasets. For significance levels see Table 1. sign. = significance, *n.s.* = not significant

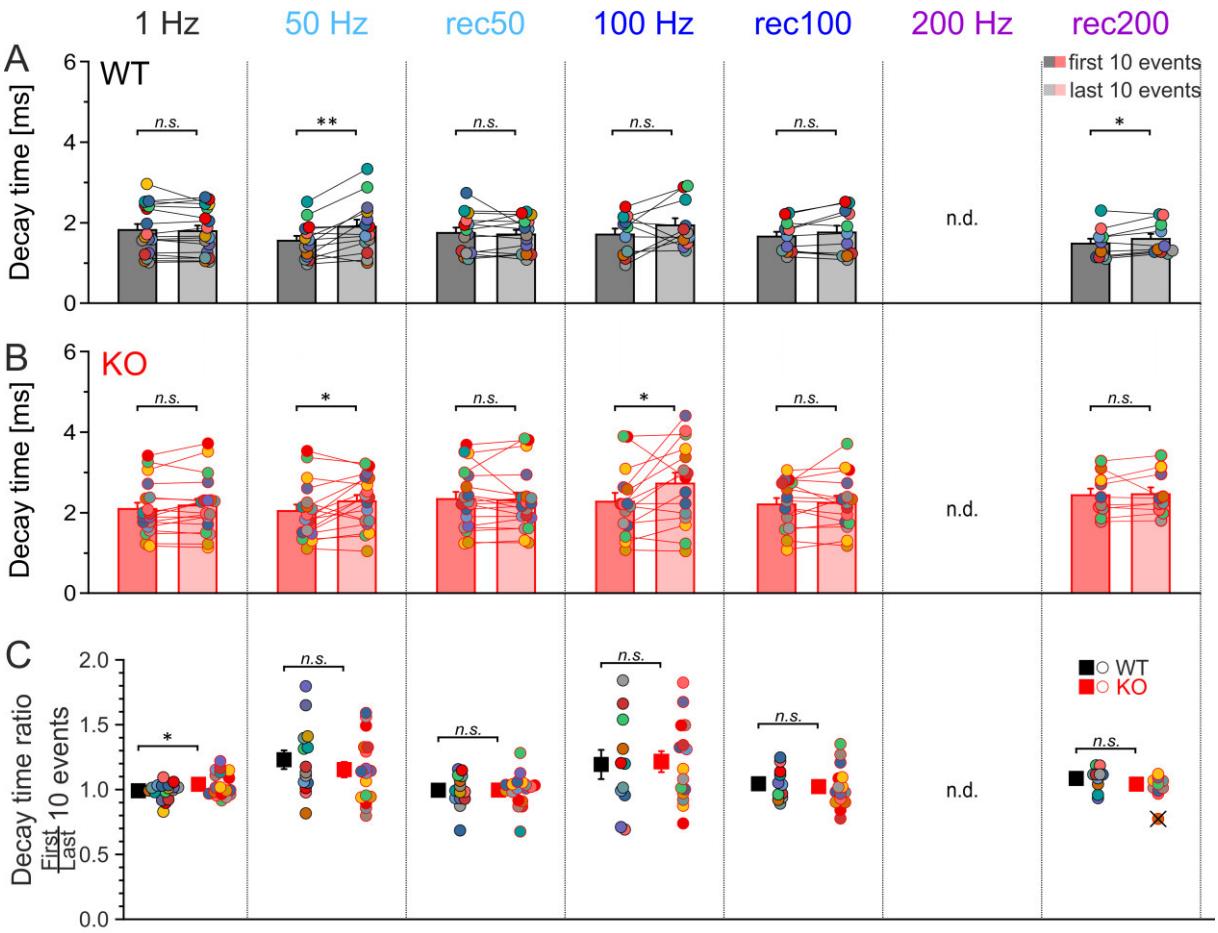

Figure S.3: Decay time of the first and last 10 events

Comparison of the decay times of the first and last 10 events in WT (**A**) and KO (**B**). **C,** Ratios of the last and first 10 events, compared between WT and KO. Only events with eIPSCs amplitudes above threshold (= responded stimuli/events) and with $R^2 \leq 0.8$ for the decay time fit (for criteria see 2.3.5) were used for analysis. For details see Table S.9 and Table S.10. n (cells) = 17/14/11/10 (WT) / 18/18/15/10 (KO), outliers and cells with too few events included. *n.s.* = not significant, n.d. = not determined

Table S.9: Decay time comparison between first 10 events and last 10 events

Condition		WT (17/14/11/10)			KO (18/18/15/10)			WT/KO	
		Decay time [ms]	p value	sign.	Decay time [ms]	p value	sign.	p value	sign.
1 Hz	first 10	1.82 ± 0.15	0.47006	*n.s.*	2.09 ± 0.16	0.08994	*n.s.*	0.10452	*n.s.*
	last 10	1.79 ± 0.14			2.18 ± 0.17			0.04214	*
50 Hz	first 10	1.55 ± 0.12	0.00502	**	2.04 ± 0.16	0.04431	*	0.01371	*
	last 10	1.90 ± 0.18			2.28 ± 0.16			0.05837	*n.s.*
rec50	first 10	1.74 ± 0.13	0.61534	*n.s.*	2.34 ± 0.18	0.77282	*n.s.*	0.00796	**
	last 10	1.71 ± 0.11			2.31 ± 0.19			0.00464	**
100 Hz	first 10	1.70 ± 0.15	0.19187	*n.s.*	2.27 ± 0.22	0.03719	*	0.02873	*
	last 10	1.93 ± 0.18			2.72 ± 0.27			0.01644	*
rec100	first 10	1.65 ± 0.12	0.1461	*n.s.*	2.21 ± 0.16	0.7093	*n.s.*	0.00721	**
	last 10	1.75 ± 0.17			2.24 ± 0.18			0.03406	*
200 Hz	first 10	n.d.			n.d.			n.d.	
	last 10	n.d.			n.d.			n.d.	
rec200	first 10	1.48 ± 0.12	0.0284	*	2.43 ± 0.16	0.78743	*n.s.*	0.00090	***
	last 10	1.59 ± 0.13			2.46 ± 0.17			0.00033	***

Data are presented as mean of the first and the last 10 events ± SEM (cf. Figure S.3A,B). Numbers in brackets depict sample size (number of cells). Only events with eIPSCs amplitudes above threshold (= responded stimuli/events) and with $R^2 \leq 0.8$ for the decay time fit (for criteria see 2.3.5) were used for analysis. Comparison was performed between the first and last 10 events for WT and KO separately, and between the corresponding 10 events of WT and KO. Reduced sample sizes due to outliers and to cells with too few sIPSCs corresponding to the criteria are indicated in brackets at the affected datasets. For significance levels see Table 1. sign. = significance, *n.s.* = not significant, n.d. = not determined

Table S.10: Decay time ratios of the last and first 10 events

Condition	$\frac{\text{Last 10}}{\text{First 10}}$ events			
	WT (17/14/11/10)	KO (18/18/15/10)	p value	sign.
1 Hz	0.99 ± 0.02	1.04 ± 0.02	0.03780	*
50 Hz	1.23 ± 0.07	1.15 ± 0.06	0.20835	*n.s.*
rec50	0.99 ± 0.03	1.00 ± 0.03	0.49076	*n.s.*
100 Hz	1.19 ± 0.11	1.22 ± 0.08	0.43576	*n.s.*
rec100	1.04 ± 0.04	1.02 ± 0.04	0.35235	*n.s.*
200 Hz	n.d.	n.d.		
rec200	1.09 ± 0.03	1.04 ± 0.02 (9)	0.09496	*n.s.*

Data are presented as ratio of the last and the first 10 events ± SEM (cf. Figure S.3C). Numbers in brackets depict sample size (number of cells). Only events with eIPSCs amplitudes above threshold (= responded stimuli/events) and with $R^2 \leq 0.8$ for the decay time fit (for criteria see 2.3.5) were used for analysis. The reduced sample size of KO rec200 due to an outlier is indicated in brackets at the affected dataset. For significance levels see Table 1. sign. = significance, *n.s.* = not significant, n.d. = not determined

Table S.11: Comparative study

Study		RRP (50 Hz) [vesicles]	P_r (50 Hz) [%]	amplitude (200 Hz) [%]	fidelity (200 Hz) [%]
GlyT1b/c WT	**(P20)**	**199**	**17**	**6**	**36**
GlyT1b/c KO	**(P20)**	**124**	**17**	**2**	**9**
Krachan et al. (2017)	(P11)	200	16	7	45
Kramer et al. (2014)	(P19)	X	X	6	22
Muller (2019)	(P38)	321 (100 Hz)	17 (100 Hz)	8	31

Comparison of 50 Hz RRP and P_r data as well as amplitudes and fidelity at the end of 200 Hz with values obtained in our group. Compared studies performed the same or a similar stimulation protocol. Please note the different mouse ages, as analyzed parameters are developmentally regulated. X indicates not analyzed parameters. RRP = readily releasable pool, P_r = release probability

8. CURRICULUM VITAE

WORK EXPERIENCE

01/2016 - 03/2019 **University of Kaiserslautern, Germany**	**Neurobiologist / Research assistant** Analysis of synaptic transmission in an astrocytic knockout mouse model, teaching
10/2010 - 12/2015 **Max Planck Institute for Medical Research, Heidelberg, Germany**	**Project co-ordinator / Research assistant** Neuron skeletonizing and synapse characterization in Area X of songbird, supervision of students
09/2007 - 03/2012 **i.a. ATOS Clinic Heidelberg, Germany**	**Physical therapist** Therapy of orthopedic, post-operative, neurological, immobilized, or chronically ill patients, back therapy training

EDUCATION

01/2016 - 08/2019 **Animal Physiology Group of Prof. Dr. Friauf, University of Kaiserslautern, Germany**	**Research on dissertation** Focus: neurobiology, patch-clamp technique, astrocytes, synaptic transmission Thesis title: "Impact of glycine transporter 1 knockout on inhibitory neurotransmission in the lateral superior olive"
09/2012 - 11/2014 **Ruprecht-Karls-University, Heidelberg, Germany**	**Master program "Molecular Bioscience - Neuroscience"** Focus: neurobiology, immunohistochemistry, astrocytes, immune cells, Alzheimer's disease Thesis title: "The Role of astrocytic gangliosides in Alzheimer's disease"
09/2009 - 08/2012 **Ruprecht-Karls-University, Heidelberg, Germany**	**Bachelor program "Biowissenschaften"** Focus: developmental neurobiology, retina Thesis title: "Function of a microtubule-associated protein for the growth of retinal axons and the morphology of the growth cone"
09/2004 - 07/2007	**State examination in physical therapy** Vocational School for Physiotherapy, Würzburg, Germany
08/1995 - 06/2004	**Qualification for university entrance (Abitur)** Matthias-Grünewald Gymnasium, Tauberbischofsheim, Germany

Julia Hammerich

PERSONAL PROFILE

Engaged team player with interest in science and administration, who offers funded experience in various biological techniques and a medical background.

My side interests are reading, spinning, board games, diving, and badminton.

Kaiserslautern, 22.08.2019

SPECIAL SKILLS

METHODS

- Electrophysiology (patch-clamp technique)
- Immunohistochemistry, ELISA, Western blot, PCR
- EM data analysis
- cell culture (mouse primary astrocytes, human glioblastoma cells), spheroid technique
- MACS, FACS
- viral gene transfer
- microscopy (confocal, life imaging)

SOFTWARE

MS Office	■■■■■■	Origin	■■■■■□
Corel	■■■■■■	Patchmaster	■■■■□□
Endnote	■■■■■■	MiniAnalysis	■■■□□□
Fiji	■■■■■□		

LANGUAGES

German	■■■■■■	French	■■■□□□
English	■■■■■■	Spanish	■□□□□□

PUBLICATION

Ghirardini E, Wadle SL, Augustin V, Becker J, Brill S, **Hammerich J**, Seifert G, Stephan J (2018). "Expression of functional inhibitory neurotransmitter transporters GlyT1, GAT-1, and GAT-3 by astrocytes of inferior colliculus and hippocampus." Molecular brain 11(1): 4.

SELECTED POSTER PRESENTATIONS AND TALKS

Hammerich J, Stephan J (2018). Knock-out of astrocytic GlyT1b/c interferes with proper MNTB-LSO signaling. ARO 41st Midwinter Meeting. San Diego, USA (Poster)

Hammerich J, Stephan J (2017). Influence of astrocytic GlyT1b/c on synaptic transmission at MNTB-LSO synapses. Midterm meeting DFG Priority Program 1608. Frauenchiemsee, Germany (Poster)

Hammerich J, Ghirardini E, Augustin V, Becker J, Brill S, Stephan J (2017). Inhibitory neurotransmitter transporters and receptors in astrocytes of the inferior colliculus and the hippocampus. 12th Meeting of the German Neuroscience Society (NWG). Göttingen, Germany (Poster)

Hammerich J (2016). Glycine and GABA transporters in astrocytes of the auditory system. Midterm meeting DFG Priority Program 1608, Delmenhorst, Germany (Talk)

TEACHING / SUPERVISION / RESPONSIBILITIES

2016-2019	Annual practical course in animal physiology: cardiac- and skeletal muscle
2016-2018	Annual seminar in fundamental neurobiology: genetically modified organisms, good laboratory practice, literature research, fraud in science
2016-2018	Instruction of students to microscopy
2016	Bräuler, V. (2016). Tamoxifen induzierte tdTomato-Expression im auditorischen Hirnstamm bei Mäusen. Department of Biology, University of Kaiserslautern
2016-2019	Responsibility for animal breeding (mouse lines of the Animal Physiology Group) Responsibility for microscope and binocular (Animal Physiology Group)

9. ACKNOWLEDGEMENT

An dieser Stelle möchte ich mich bei allen Personen danken, die zum Gelingen dieser Dissertation beigetragen haben.

Mein Dank geht dabei insbesondere an meinen Doktorvater Prof. Dr. Eckhard Friauf. Danke, dass ich in deiner Abteilung meine Doktorarbeit anfertigen konnte sowie für deine fordernde aber auch gleichermaßen fördernde Art, die ich sehr bewundere. Zudem weiß ich sehr zu schätzen, dass du der Betreuung und Gestaltung meines Projektes großen Freiraum gegeben hast. Einen großen Dank dafür.

Auch bei Dr. Jonathan Stephan, meinem Betreuer, möchte ich mich besonders bedanken. Ich danke dir, dass du mir die Möglichkeit gegeben hast, in diesem interessanten Projekt mitzuwirken, das für mich unter folgendem Übertitel steht: *ASTROCYTES ARE AWESOME*! Kannst du dir DAVON nicht mal ein T-Shirt besorgen? Danke auch für die vielen interessanten und bereichernden Gespräche, sowie dein großes Vertrauen in mein selbstständiges Arbeiten. Was ich dir zudem nie vergessen werde: deine Rücksichtnahme in Zeiten, in denen anderes kurz mal wichtiger war als die Doktorarbeit.

Weiterer Dank geht an PD Dr. Eulenburg. Danke dir, Volker, für die Übernahme des Zweitgutachtens und für die Bereitstellung der GlyT1b/c KO Maus. An die zwei Tage bei dir im schönen Leipzig erinnere ich mich sehr gern zurück. Die Diskussionen über meine Daten und Schlussfolgerungen haben meine Doktorarbeit sehr bereichert!

Danke auch an Prof. Dr. Stefan Kins, der sich bereiterklärt hat, den Vorsitz meiner Prüfungskommission zu übernehmen.

Ein großes Dankeschön geht zudem an alle aktuellen und ehemaligen Mitglieder der AG Tierphysiologie und AG Neuronale Netzwerke. Ohne die Hilfe von so manchem von euch beim Erlernen und Verstehen der Elektrophysiologie sowie bei der Auswertung wäre die Doktorarbeit jetzt wohl noch lange nicht abgeschlossen. Ganz besonders möchte ich mich bei folgenden Personen bedanken:

- Sabrina Marz für die Hilfe bei den Western Blots
- Alexander Fischer für Squid, das mir viel Klick-Frustration erspart hat

- Dennis Weingarten: Danke für das Feedback zu meiner Diskussion sowie für deine ruhige und verständnisvolle Art. Bleib so wie du bist.
- Elisa Krächan: Dein großes Herz, deine Ehrlichkeit und dein Zuspruch in schwierigen Phasen haben mir viel Kraft gegeben und mich ab und zu auch mal wieder richtig eingenordet. Ein großes Dankeschön dafür! Ich kann mir nicht vorstellen, wie die Zeit hier ohne dich gewesen wäre.
- Ralph Reiss für die Western Blots und die Durchführung der Genotypisierung meiner Mäuse.
- Tina Kehrwald für die Proteinfärbungen und die ein oder andere gemeinsame Kaffeepause, bei denen ich vor allem in der Schreibphase etwas abschalten konnte
- Kornelia Ociepka: An vielen langen PC-Tagen warst du mein Lichtblick. Danke für dein immer offenes Ohr und deine Herzlichkeit. Das hat mir vor allem in der Endphase der Doktorarbeit sehr geholfen und mir Kraft gegeben. DANKE!

Und last but not least: Ein großes Dankeschön auch an meine Eltern Gabi und Anton, sowie an meine Geschwister Matthias mit Renate und Maja, und Heike.

- Mama und Papa: Ohne eure Unterstützung hätte ich diesen Weg nicht einschlagen können. Ich danke euch für euer in mich gesetztes Vertrauen und den Rückhalt, den ihr mir gegeben habt, und dass ich immer zu euch kommen kann, wenn ich etwas Nestwärme brauche.
- Matthias mit Anhang: Danke für eure motivierenden Worte und den Zuspruch, den ihr mir gegeben habt, und auch für die Ablenkung an so manchen Tagen in Frankfurt/Distelhausen
- Heike: Meine kleine große Schwester, vielen Dank auch an dich! Ich weiß nicht, wie ich die letzten Monate ohne dich überstanden hätte, und das ist nicht nur eine Floskel! Ich bin so dankbar, dass es dich gibt!